



McColl, Jill Louise (2016) *Climate variability of the past 1000 years in the NW Pacific: high resolution, multi-biomarker records from Lake Toyoni*. PhD thesis.

<http://theses.gla.ac.uk/7793/>

Copyright and moral rights for this work are retained by the author

A copy can be downloaded for personal non-commercial research or study, without prior permission or charge

This work cannot be reproduced or quoted extensively from without first obtaining permission in writing from the author

The content must not be changed in any way or sold commercially in any format or medium without the formal permission of the author

When referring to this work, full bibliographic details including the author, title, awarding institution and date of the thesis must be given

Glasgow Theses Service
<http://theses.gla.ac.uk/>
theses@gla.ac.uk

Climate variability of the last 1000 years in the NW Pacific: high resolution, multi-biomarker records from Lake Toyoni

Jill Louise McColl

BSc. (Hons) University of Highlands and Islands

Submitted in fulfilment of the requirements for the
Degree of Doctor of Philosophy

School of Geographical and Earth Sciences
College of Science and Engineering
University of Glasgow

September 2016

This PhD is dedicated in loving memory of my Papi:

Alan Gracie

(1929-2014)

Abstract

The East Asian Monsoon (EAM) is an active component of the global climate system and has a profound social and economic impact in East Asia and its surrounding countries. Its impact on regional hydrological processes may influence society through industrial water supplies, food productivity and energy use. In order to predict future rates of climate change, reliable and accurate reconstructions of regional temperature and rainfall are required from all over the world to test climate models and better predict future climate variability.

Hokkaido is a region which has limited palaeo-climate data and is sensitive to climate change. Instrumental data show that the climate in Hokkaido is influenced by the East Asian Monsoon (EAM), however, instrumental data is limited to the past ~150 years. Therefore down-core climate reconstructions, prior to instrumental records, are required to provide a better understanding of the long-term behaviour of the climate drivers (e.g. the EAM, Westerlies, and teleconnections) in this region.

The present study develops multi-proxy reconstructions to determine past climatic and hydrologic variability in Japan over the past 1000 years and aid in understanding the effects of the EAM and the Westerlies independently and interactively. A 250-cm long sediment core from Lake Toyoni, Hokkaido was retrieved to investigate terrestrial and aquatic input, lake temperature and hydrological changes over the past 1000-years within Lake Toyoni and its catchment using X-Ray Fluorescence (XRF) data, alkenone palaeothermometry, the molecular and hydrogen isotopic composition of higher plant waxes ($\delta D_{(HPW)}$).

Here, we conducted the first survey for alkenone biomarkers in eight lakes in the Hokkaido, Japan. We detected the occurrence of alkenones within the sediments of Lake Toyoni. We present the first lacustrine alkenone record from Japan, including genetic analysis of the alkenone producer. C_{37} alkenone concentrations in surface sediments are $18\mu\text{g } C_{37} \text{ g}^{-1}$ of dry sediment and the dominant alkenone is $C_{37:4}$. 18S rDNA analysis revealed the presence of a single alkenone producer in Lake Toyoni and thus a single calibration is used for reconstructing lake temperature based on alkenone unsaturation patterns. Temperature reconstructions over the past 1000 years suggest that lake water temperatures

varies between 8 and 19°C which is in line with water temperature changes observed in the modern Lake Toyoni. The alkenone-based temperature reconstruction provides evidence for the variability of the EAM over the past 1000 years. The $\delta D_{(HPW)}$ suggest that the large fluctuations ($\sim 40\%$) represent changes in temperature and source precipitation in this region, which is ultimately controlled by the EAM system and therefore a proxy for the EAM system. In order to complement the biomarker reconstructions, the XRF data strengthen the lake temperature and hydrological reconstructions by providing information on past productivity, which is controlled by the East Asian Summer monsoon (EASM) and wind input into Lake Toyoni, which is controlled by the East Asian Winter Monsoon (EAWM) and the Westerlies.

By combining the data generated from XRF, alkenone palaeothermometry and the $\delta D_{(HPW)}$ reconstructions, we provide valuable information on the EAM and the Westerlies, including; the timing of intensification and weakening, the teleconnections influencing them and the relationship between them. During the Medieval Warm Period (MWP), we find that the EASM dominated and the EAWM was suppressed, whereas, during the Little Ice Age (LIA), the influence of the EAWM dominated with time periods of increased EASM and Westerlies intensification. The El Niño Southern Oscillation (ENSO) significantly influenced the EAM; a strong EASM occurred during El Niño conditions and a strong EAWM occurred during La Niña. The North Atlantic Oscillation, on the other hand, was a key driver of the Westerlies intensification; strengthening of the Westerlies during a positive NAO phase and weakening of the Westerlies during a negative NAO phase. A key finding from this study is that our data support an anti-phase relationship between the EASM and the EAWM (e.g. the intensification of the EASM and weakening of the EAWM and vice versa) and that the EAWM and the Westerlies vary independently from each other, rather than coincide as previously suggested in other studies.

Table of Contents

Abstract.....	iii
List of Tables.....	xi
List of Figures.....	xii
Acknowledgments.....	xvii
Author's Declaration.....	xx
Definitions and abbreviations.....	xxi
1.....	1
1.1 Motivation.....	1
1.1.1 The importance of climate reconstructions over the past 1000 years	1
1.1.2 Reconstructing East Asian Monsoon in Northern Japan.....	2
1.2 Lake Toyoni as a palaeo-climate archive.....	4
1.3 Climate and environmental proxies.....	4
1.3.1 <i>n</i> -alkanes.....	5
1.3.2 Alkenones.....	8
1.3.3 Elemental composition of lacustrine sediments.....	11
1.4 Objectives.....	12
1.5 Thesis organisation.....	12
2.....	15
2.1 Instrumental data.....	15
2.2 Climate drivers in Hokkaido.....	16
2.2.1 East Asian Monsoon (EAM).....	17
2.2.1.1 East Asian Summer Monsoon (EASM).....	18
2.2.1.2 East Asian Winter Monsoon (EAWM).....	21
2.2.2 Arctic Oscillation (AO).....	24
2.2.2.1 AO and the EASM.....	27
2.2.2.2 AO and the EAWM.....	28
2.2.2.3 AO and the Westerlies.....	28
2.2.3 Pacific Decadal Oscillation (PDO).....	29
2.2.3.1 PDO and the EASM.....	33
2.2.3.2 PDO and the EAWM.....	33
2.2.4 ENSO.....	33
2.2.4.1 ENSO and the EASM.....	37
2.2.4.2 ENSO and the EAWM.....	38
3.....	40
3.1 Location.....	40
3.1.1 Lake survey.....	40
3.1.2 Site description.....	41
3.1.3 Water probe data.....	43

3.1.3.1	Geology	46
3.2	Core collection.....	47
3.3	Age model	47
3.3.1	TY11	47
3.3.2	TY09	48
3.3.3	Lithological description.....	50
3.3.4	X-ray Fluorescence (XRF) and magnetic susceptibility (MS).....	50
3.3.4.1	Normalising data.....	51
3.3.5	Particle size analysis (PSA).....	51
3.3.6	Organic C/N ratio.....	52
3.3.7	rDNA haptophyte identification	52
3.3.7.1	Surface sediment collection	52
3.3.7.2	Extraction.....	53
3.3.7.3	Amplification and sequencing	53
3.3.7.4	Bioinformatics and phylogenetic reconstructions.....	54
3.3.8	Lipid analysis	55
3.3.8.1	Extraction.....	56
3.3.8.2	Column chromatography.....	56
3.3.9	Gas chromatography and mass spectroscopy	57
3.3.10	Vegetation samples	58
3.3.11	Compound specific hydrogen isotopes	58
4.....		59
4.1	Introduction	59
4.1.1	Human controls on environmental change during the past 1000 years in Hokkaido, Japan	59
4.1.2	Environmental controls on productivity in Lake Toyoni.....	60
4.1.3	Climatic significance of the proxy indices in the sedimentary record of Lake Toyoni.....	64
4.1.3.1	Magnetic susceptibility as a proxy for tephra layers, anoxic conditions and transportation processes.....	64
4.1.3.2	Rb/Sr ratio as a chemical weathering proxy.....	66
4.1.3.3	Inc/Coh ratio as a proxy for OM content of sediments.....	67
4.1.3.4	C/N ratio as a proxy for the source of OM	67
4.1.3.5	<i>n</i> -Alkane biomarkers as a proxy for source of OM	68
4.1.3.6	Si/Rb as a proxy for diatom productivity	71
4.1.3.7	Aims	72
4.2	Results	74
4.2.1	Core description	74
4.2.2	MS.....	74
4.2.3	Rb/Sr	74

4.2.4	Inc/Coh.....	75
4.2.5	C/N ratios.....	75
4.2.6	<i>n</i> -Alkanes	77
4.2.7	CPI	77
4.2.8	ACL.....	77
4.2.9	Paq.....	77
4.2.10	Si/Rb	77
4.3	Discussion	79
4.3.1	Productivity during the MWP (955-1300AD).....	79
4.3.1.1	Productivity LIA (1300-1850AD).....	82
4.3.1.2	Productivity recorded in short core TY11	86
4.3.2	Possible forcing mechanisms.....	88
4.3.2.1	Solar irradiance	88
4.3.2.2	PDO	89
4.4	Conclusions	94
5.....		96
5.1	Introduction	96
5.1.1	Global and regional wind circulation patterns	97
5.1.1.1	Westerlies.....	97
5.1.1.2	The EAWM.....	97
	Environmental conditions at the dust source region.....	98
5.1.2	Proxies for dust input into Lake Toyoni	99
5.2	Results	101
5.2.1	PSA.....	101
5.2.2	Ti/Rb	101
5.2.3	Magnetic susceptibility (MS)	101
5.3	Discussion	103
5.3.1	Grain-size and dust input (Ti/Rb ratio) as a proxy for global and regional wind systems	103
5.3.2	MWP (~1000-1300AD).....	103
5.3.3	LIA (~1300-1800AD).....	105
5.3.3.1	EAWM intensification during the LIA.....	106
5.3.3.2	Westerlies intensification during the LIA	109
5.3.3.3	EAWM weakening during the LIA	110
5.3.4	>1800AD.....	111
	Dust input into Lake Toyoni as a proxy for environmental changes in dust source regions	111
5.3.4.1	Climate in the Taklimakan Desert (Westerlies source region) .	111
5.3.4.2	Climate in the Gobi Desert (EAWM source region).....	112

5.3.5	Potential climate drivers	116
5.3.5.1	ENSO	117
5.3.5.2	PDO	117
5.3.5.3	NAO/AO	117
5.4	Conclusions	120
6.	121
6.1	Introduction	121
6.2	Results	123
6.2.1	18S rDNA Haptophyte Identification	123
6.2.2	Full-length 18S rRNA gene-based phylogeny.....	123
6.2.3	Partial length 18S rDNA gene-based phylogeny	124
6.2.4	Alkenone Distribution at Lake Toyoni	124
6.3	Discussion	128
6.3.1	Haptophyte DNA amplification and diversity in Lake Toyoni.....	128
6.3.2	Haptophyte identification	129
6.3.3	Alkenone occurrence	133
6.3.4	Alkenone distribution	133
6.3.5	Paleotemperature implications.....	136
6.4	Conclusions	139
7.	140
7.1	Introduction	140
7.1.1	Objectives of research	143
7.2	Results	144
7.3	Discussion	145
7.3.1	Application of the D’Andrea et al (2011) temperature calibration in Lake Toyoni	145
7.3.2	Alkenone-based temperature reconstructions: comparison with EAM records	147
7.3.2.1	Comparison with EASM records	151
7.3.2.2	Comparison with the EAWM	156
7.3.2.3	Summary	158
7.3.3	Alkenone-based temperature reconstructions: comparison with NAO/AO reconstruction	159
	Alkenone-based temperature reconstructions: comparison with Asian temperature records	160
7.3.3.1	Medieval warm period 1050-1300AD	168
7.3.3.2	Little Ice Age 1300-1850AD.....	170
7.3.3.3	>1850AD	174
7.3.4	Famines in Japan over the past 1000 years.....	175
7.4	Conclusions	177

8.....	178
8.1 Introduction	178
8.1.1 Leaf wax <i>n</i> -alkane δD as a recorder of δD of precipitation	179
8.1.2 Environmental controls on the δD values of terrestrial leaf waxes in Hokkaido, Japan.....	180
8.1.3 Aims	181
8.2 Background	184
8.2.1 Source of precipitation in Hokkaido, Japan	184
8.2.2 Temporal and spatial pattern of modern-day precipitation δD in Hokkaido, Japan.....	186
8.2.3 Interpretation of the δD_{HPW}	189
8.2.3.1 Sub-tropical maritime air-mass (high δD values).....	190
8.2.3.2 Sub-polar maritime air-mass (low δD values).....	191
8.2.3.3 Sub-polar continental air-mass (low δD values).....	192
8.2.4 Summary	193
8.3 Results	194
8.3.1 δD values of vegetation samples	194
8.3.2 δD values of down-core <i>n</i> -alkanes	195
8.4 Discussion	196
8.4.1 δD_{HPW} in the catchment surrounding Lake Toyoni.....	196
8.4.2 Apparent fractionation between precipitation and leaf wax	198
8.4.3 δD_{HPW} as a proxy for EAM variability	200
8.4.3.1 Solar activity and the EAM	200
8.4.3.2 Teleconnections	203
8.4.4 Hydrological variability in Hokkaido during the MWP and LIA	206
8.4.4.1 δD_{HPW} during the MWP	206
8.4.4.2 δD_{HPW} during the LIA	207
8.4.5 Post 1800 AD	210
8.4.6 Short core TY11	210
8.4.7 Relationship between the EASM and the EAWM.....	212
8.5 Conclusions	215
9.....	217
9.1 Summary	217
9.2 Dominant climate modes over the past 1000 years	219
9.2.1 Climate modes during the MWP (1050-1360AD)	219
9.2.2 Climate modes during the LIA (1360-1850AD)	219
9.2.2.1 Early LIA (1360-1580AD)	219
9.2.2.2 Late LIA (1600-1850AD).....	220
9.2.3 Climate modes >1850AD	221

9.3	Potential climate drivers of EASM intensification	225
9.3.1	The EASM and the NAO/AO	225
9.3.2	The EASM and the PDO	225
9.3.3	The EASM and ENSO	226
9.3.4	The intensification of the EASM and global climate variability	227
9.4	Potential climate drivers of EAWM intensification	229
9.4.1	Impacts of the NAO/AO	229
9.4.2	Impacts of ENSO	230
9.4.3	The intensification of the EAWM and global climate variability	231
9.5	Potential climate drivers of Westerlies intensification	233
9.5.1	Impact of the NAO/AO	233
9.5.2	Impact of ENSO	235
9.5.3	The Westerlies and global climate variability	235
9.6	Combined impacts of the NAO/AO and ENSO	239
9.7	Solar irradiance and climate variability in Hokkaido	240
9.8	Conclusions	244
10	246
10.1	Chapter 4: Decadal-resolved terrestrial and biological input into Lake Toyoni. 248	
10.2	Chapter 5: Assessing the contribution of dust from global (Westerlies) and regional (EAWM) wind patterns.....	249
10.3	Chapter 6: 18S rDNA analysis of the alkenone producer(s) in Lake Toyoni 250	
10.4	Chapter 7: Alkenone-based temperature reconstructions from Lake Toyoni 250	
10.5	Chapter 8: Hydrogen isotopic composition of higher plant waxes in the catchment and down-core sedimentary records of Lake Toyoni.....	251
10.6	Future work	253
10.7	Concluding remarks	254
	List of references.....	256

List of Tables

Table 1-1: alkenones and their shorthand notation	9
Table 2-1: Summary table detailing the average temperature, precipitation and snowfall change during strong/weak EASM/EAWM years, the positive and negative phase of the AO/NAO and the PDO and also during El Niño and La Niña years. Average annual values between 1958 and 2014 provided in bold.	39
Table 3-1: Lakes surveyed in Hokkaido for alkenones in 2008.	41
Table 3-2: Age model of core TY09	49
Table 4-1: Summary table of the different climatic influences (EAM and PDO) on the processes involved in Lake Toyoni.	72
Table 4-2: Lithofacies and visual description of the core.	75
Table 6-1: <i>Closest BLAST hits to OTUs</i>	125
Table 6-2: The range of primers used to target haptophyte rDNA.	126
Table 6-3: Number of base pairs targeted and successful/unsuccessful PCR with different primer combinations..	126
Table 6-4: Alkenone trends among haptophyte algae.....	127
Table 8-1: δD values of <i>n</i> -alkanes extracted from leaf samples in the catchment of Lake Toyoni (SD=standard deviation)	194
Table 8-2: Pearson correlations between $\delta D C_{27}$, $\delta D C_{29}$ and $\delta D C_{31}$	195
Table 9-1: Summary table of the key drivers of the EASM, EAWM and Westerlies intensification in Hokkaido, Japan.....	243

List of Figures

Figure 1-1: Diagram of Lake Toyoni and they key proxies (e.g. higher plant waxes and alkenones) used in this study. Wind and run-off input into Lake Toyoni are key processes in this lake, which can be studying using XRF elemental data.	5
Figure 2-1: Weather station data from Hiroo weather station (averaged between 1958-2014).....	16
Figure 2-2: Seasonal changes in the wind system of the EAM.....	18
Figure 2-3: Monthly temperature averages during strong EASM (small dashed line) and weak EASM (large dashed line) years compared with average (1958-2014) monthly temperature values (solid line).	20
Figure 2-4: Monthly rainfall averages during strong EASM (small dashed line) and weak EASM (large dashed line) years compared with average (1958-2014) monthly rainfall values (solid line).	20
Figure 2-5: Monthly temperature averages during strong EAWM (small dashed line) and weak EAWM (large dashed line) years compared with average (1958-2014) monthly temperature values (solid line).	22
Figure 2-6: Monthly rainfall averages during strong EAWM (small dashed line) and weak EAWM (large dashed line) years compared with average (1958-2014) monthly rainfall values (solid line).	23
Figure 2-7: Monthly snowfall averages during strong EAWM (small dashed line) and weak EAWM (large dashed line) years compared with average (1958-2014) monthly snowfall values (solid line).	23
Figure 2-8: Variations in the phase of the AO since 1950 from from NOAA’s Centre for weather and climate prediction (2016).	25
Figure 2-9: Monthly temperature averages during strong positive (small dashed line) and negative (large dashed line) AO years compared with average (1958-2014) monthly temperature values	26
Figure 2-10: Monthly rainfall averages during strong positive (small dashed line) and negative (large dashed line) AO years compared with average (1958-2014) monthly rainfall values.	26
Figure 2-11: Monthly snowfall averages during strong positive (small dashed line) and negative (large dashed line) AO years compared with average (1958-2014) monthly snowfall values. No snowfall occurs in June, July, August and September.	27
Figure 2-12: sea surface temperature differences during the positive and negative phase of the PDO (Figure adapted from; Goddard, 2014).....	30
Figure 2-13: Variations in the phase of the PDO since 1990 by Mantua et al., (1997).	31

Figure 2-14: Monthly temperature averages during negative (small dashed line) and positive (large dashed line) PDO years compared with average (1958-2014) monthly temperature values (solid line).	31
Figure 2-15: Monthly precipitation averages during negative (small dashed line) and positive (large dashed line) PDO years compared with average (1958-2014) monthly precipitation values (solid line).	32
Figure 2-16: Monthly snowfall averages during negative (small dashed line) and positive (large dashed line) PDO years compared with average (1958-2014) monthly snowfall values (solid line).	32
Figure 2-17: Monthly temperature averages during El Niño (small dashed line) and La Niña (large dashed line) years compared with average (1958-2014) monthly temperature values (solid line).	35
Figure 2-18: Monthly precipitation averages during El Niño (small dashed line) and La Niña (large dashed line) years compared with average (1958-2014) monthly precipitation values (solid line).	36
Figure 2-19: Monthly snowfall averages during El Niño (small dashed line) and La Niña (large dashed line) years compared with average (1958-2014) monthly snowfall values (solid line).	36
Figure 2-20: Monthly precipitation averages during the summer following El Niño (small dashed line) and El Niño developing (large dashed line) years compared with average (1958-2014) monthly precipitation values (solid line).	38
Figure 3-1: Location of lakes surveyed in 2008	40
Figure 3-2: Location of Lake Toyoni, Hokkaido, Japan.	42
Figure 3-3: Pictures of Lake Toyoni and the catchment area.....	42
Figure 3-4: Water temperature against depth between April and November. ...	44
Figure 3-5: A: Comparison between surface water column temperature and air temperature. B: Scatter plot between lake surface temperature and air temperature.....	44
Figure 3-6: Dissolved oxygen against depth between April and November.	45
Figure 3-7: pH against depth between April and November	45
Figure 3-8: Geology of Lake Toyoni.....	46
Figure 3-9: Pu dating of TY11.....	48
Figure 3-10: Age depth model for TY09	50
Figure 3-11: DNA sample procedure	53
Figure 3-12: BECS sample procedure for organic lipid analysis.	55

Figure 4-1: Diagram outlining the key processes influencing Lake Toyoni.	73
Figure 4-2: Magnetic susceptibility and lithofacies changes in the down-core sedimentary record.	76
Figure 4-3: Variations in productivity over the past 1000 years in Lake Toyoni..	78
Figure 4-4: Variations in molecular composition of <i>n</i> -alkanes over the past 1000 years.....	79
Figure 4-5: Variations in C/N ratios and the molecular composition of <i>n</i> -alkanes (ACL, CPI and Paq) in short core TY11.	85
Figure 4-6: Variations in the Rb/Sr ratios and temperature records from Asia...	87
Figure 4-7: Variations in lake productivity compared with solar irradiance (W/m ²) and the PDO index.	92
Figure 4-8: Comparison of monsoonal precipitation variations (as inferred from Inc/Coh ratio; bottom graph) over the past 1000 years with solar irradiance (Bard et al., 2000) and EAM record of Hu et al. (2008)..	93
Figure 5-1: Map of the locations of the Taklamakan Desert in northwestern China (source region of the Westerlies) and also the Gobi Desert in northern and northwestern China as well as southern Mongolia (source region of the EAWM).	99
Figure 5-2: Proxies for aeolian input and transport mechanisms into Lake Toyoni	102
Figure 5-3: Variations in the aeolian input into Lake Toyoni and the SibH intensity	105
Figure 5-4: Relationship between winter temperatures and dust input into Lake Toyoni..	108
Figure 5-5: Variations in the Westerlies, the EAWM and the EASM over the past ~1000 years.).....	109
Figure 5-6: comparison of dust input into Lake Toyoni via the Westerlies and environmental conditions in the Taklimakan Desert (the source region for dust transported via the Westerlies).	114
Figure 5-7: comparison of dust input into Lake Toyoni via the EAWM and environmental conditions in the Gobi Desert (the source region for dust transported via the EAWM).....	115
Figure 5-8: Variations in the aeolian record compared with the PDO index by Macdonald and Case (2009) (top graph; please note that the axis has been inversed) and the NAO index by Trouet et al. (2009) (Middle graph).....	119
Figure 6-1: A consensus Bayesian phylogenetic tree depicting 18S rRNA gene-inferred relationships among haptophyte algae using only full length sequences.	131

Figure 6-2: A consensus Bayesian phylogenetic tree depicting 18S rRNA gene-inferred relationships among haptophyte algae using partial length sequences..	132
Figure 6-3: Comparison of molecular composition of lacustrine alkenones from Lake Toyoni and Greenland lakes..	135
Figure 6-4: Temperature calibration developed for Greenland lake using a combination of in-situ water filter samples from Braya Sø collected during summer 2007 (red diamonds) and 2009 (blue squares) and a previously published calibration from Europe (black circles) by Zink et al (2001).	137
Figure 7-1: Alkenone-based temperature reconstruction reflecting averaged temperature values from the ice-free seasons (spring and summer) over the past 1000 years from Lake Toyoni	145
Figure 7-2: Standardised alkenone-based temperatures over the past 1000 years. Values above and below 1.3 °C are out with the mean standard calibration error.	146
Figure 7-3: Comparison of the alkenone-based temperature record with EASM records..	151
Figure 7-4: SST and salinity records from the Japan Sea compared with solar irradiance over the past 1300 years.	155
Figure 7-5: Comparison of the alkenone-based temperature records with winter temperature reconstruction from Japan	158
Figure 7-6: Alkenone-based temperature record compared to the NAO Index (Trouet et al., 2009)..	160
Figure 7-7: Comparison of the alkenone-based temperature variations over the past 1000 years with Asian temperature records. A: a combination of temperature reconstructions in Asia by Shi et al. (2015). B: a combination of temperature reconstructions in China using statistical software by Ge et al. (2013). C: the alkenone-based temperature variations over the past 1000 years (present study)	163
Figure 7-8: Comparison of the alkenone-based temperature record with palaeoclimate records from Japan	164
Figure 7-9: Relationship between temperature and famine points in Japan. The top graph is the famine point plot from Saito (2010) per half century. The bottom graph is the average alkenone-based temperature per half century.	176
Figure 8-1: North-South transect of the monthly average temperature and δD_{PRECIP} developed using temperature data from meteorological site and the corresponding δD_{PRECIP} from the OIPC.)	183
Figure 8-2: Map of Japan and the air-masses influencing Hokkaido..	185

Figure 8-3: The monthly deuterium excess values (top graph) and the correlation between deuterium excess and RH (%) from Lake Toyoni, Southern Hokkaido..	186
Figure 8-4: Monthly air temperature data from Hiroo weather station (averaged 1958-2014) and δD_{PRECIP} from OCIP.....	188
Figure 8-5: Scatter plot of monthly air temperature data from Hiroo weather station (averaged 1958-2014) and δD_{PRECIP} from OCIP.....	188
Figure 8-6: A surface weather chart from 21 st July 1993 in Japan based on the NCEP/NCAR reanalyses (Figure from: Nakamura and Fukamachi, 2004)..	192
Figure 8-7: Variations in the $\delta D_{C_{27}}$, $\delta D_{C_{29}}$ and $\delta D_{C_{31}}$ over the past 1000 years from Lake Toyoni, Japan	196
Figure 8-8: The fractionation corrected (-130‰) δD_{HPW} values to show the δD_{PRECIP} over the past 1000 years in Hokkaido, Japan.	199
Figure 8-9: Variations in δD_{HPW} compared with the APO index and solar irradiance over the past 1000 years.	203
Figure 8-10: Variations in the δD_{HPW} record compared with teleconnections; A. PDO index by Macdonald and Case (2009) (scale inverted), B. the NAO index by Trouet et al. (2009), C. ENSO Index by Yan et al. (2011), D. the down-core variations in the δD_{HPW} values (present study). s.	205
Figure 8-11: Variations in the $\delta D_{C_{29}}$ from short core (TY11) from Lake Toyoni, Japan.	212
Figure 8-12: Comparison of the normalised δD_{HPW} variations over the past 1000 years with EASM records.....	214
Figure 8-13: Comparison of the δD_{HPW} variations over the past 1000 years with the intensity of the SibH	215
Figure 9-1: Multi-proxy climate reconstructions from Lake Toyoni over the past 1000 years.	223
Figure 9-2: Downcore variations in C/N, ACL, CPI, P(aq) and δD_{HPW} from TY11.	224
Figure 9-3: Variations in δD_{HPW} compared with global climate modes.....	237
Figure 9-4: Variations in δD_{HPW} compared with global climate reconstructions	238
Figure 9-5: Schematic diagram of the combined influence of ENSO and the NAO/AO	240

Acknowledgments

This research has been funded by the National Environmental Research Council (NERC). Field work would not have been possible without the support of Sasakawa Foundation and the University of Glasgow travel fund and lab work at Hokkaido University and Tsukuba University in Japan would not be possible without the support of the Japanese Society of the Promotion of Science (JSPS). My attendance at conferences during my PhD has been financially supported by conference support fund within the Geographical and Earth Sciences departments, University of Glasgow. The completion of this PhD would not have been possible without the input and support from a number of people to whom I am extremely grateful.

Firstly, a special thank-you to my supervisors Dr. Jaime Toney and Dr. Vernon Pheonix, Dr. James Bendle, Dr. Andrew Henderson and Dr. Osamu Seki. Jaime, thanks for all your help and guidance throughout this research. In particular, thank-you for all the time and effort you put into edits and going over (and over) my practice talks for conferences. Field-work in Japan was an absolute highlight of my PhD, thanks for accompanying me to Lake Toyoni and helping with data collection. Everything you have done has helped me progress throughout my PhD and I appreciate it. Vern, thanks for being on hand in meetings and making sure I stay on track for completing my PhD. Your advice has been invaluable to me. James, although you weren't involved as a primary supervisor for long, I would like to say a massive thank-you for giving me such a wonderful opportunity and also for continuing to be involved with this project, even after your move. Andrew, thanks for all your help with the XRF scanning and for support at conferences and looking over radiocarbon grant proposal. Osamu, thanks for all your help with field and lab work in Japan. Thanks also for all your help during my 3 month stay in Japan doing lab work and for continuing to run samples for me when I returned home to Scotland. James/Andrew/Osamu, thanks for all the initial work you completed on this project; including the survey of lakes, the collection of the sediment core from Lake Toyoni and securing funding for the project. This project would not have been possible without all your hard work.

My journey into doing a PhD ultimately started at the Scottish Association for marine Science (SAMS), where I completed my undergraduate. Thanks to all of the inspiring lecturers along the way. Since my undergraduate at SAMS, I have had continued support from SAMS. Thanks to Dr. Richard Abel for assistance on the C/N prep and also for running the samples for me (Chapter 4). Christine Campbell is also thanked for supplying algae samples from culture collection of algae and protozoa (CCAP) for testing primers in Chapter 6. Jill, Anne and Julie are thankse for all their assistance in DNA analysis (Chapter 6).

BECS members, whom have listened and questioned me during countless talks about my research and whom have made working long hours in the lab more bearable. In particular, I would like to thanks to Antonio. Thanks for all your help with PAST, GC problems, supplying good papers to read, and for the coffee, cake and wine (“drink all the wine”!). Having you part of the group has been inspirational and I can’t thank you enough. In addition to lab-group meetings, I would also like to say a special thanks to the members of Geo-Bio (Andy, Maggie, Nick and Susan to name a few): thanks for all the support and encouragement with my PhD.

Thanks also to all the support staff in the Geographical and Earth Sciences department; Robert, John, Kenny, Margaret and Jackie. This department would be lost without you all.

To my fellow postgrads, we have had a lot of highs and lows in that office and I couldn’t imagine spending the past four years with anyone else: Heather, Hazel, Kirsty, Penne, Rebecca, Eric, Heidi, Mark, Callum, Crystal, Caroline, Charlotte, Sarah, Kazia, Phil and Daisy. Heather, I’m not sure I could have done this without you. Thanks for being the friendly face in the office when I started. You were my first friend in Glasgow and have always being on hand for a cuppa and a well needed chat-thanks for everything. Hazel, the best conference partner anyone could ask for. San Francisco and Vienna would not have been the same without you! Your life experience and love of the environment has inspired me. Thanks for being as excited about the small things in life as me! Kristy, you have been in my life throughout undergrad and postgrad, thanks for everything including the wine nights, which were always a well needed distraction.

Rebecca, thanks for always having a room for me when I come to Glasgow for meetings and for all your support.

A special thanks to my best friends in Oban, “the wolfpack”: Lynsey, Mairi, Nicola, Suz, Joan, Eilidh, Eilidh and Hannah. Thanks for all the support, encouragement and friendship over the years. Thanks for the nights in, nights out, the weekends away and not forgetting West Highland Way! Nicola and Hannah, thanks also for being amazing flat mates- we have had so many good times living together. I would also like to thank Jamie. You have been such a good friend to me in the 7 years we have known each other. Thanks for our weekly phone calls and for all the good times in between.

I’d also like to thanks to all the staff at Markie Dans for all your support and providing an escape from my PhD. Thanks for the new friendships I have made and the old ones I rediscovered. Steven, I was certainly not looking for a relationship when I moved home to write up my thesis, however, I am so happy you came back into my life. Thanks for your patience and being there for when I needed a distraction. Thanks for our trip to Copenhagen, I love that you are as excited about travelling and seeing the world as I am, and I hope we continue to have many more adventures together.

Last, but most certainly not least, I would like to express my gratitude to my amazing family: Dad, Mum, Lisa, Granny Gracie, Papa Malloy, Granny Malloy. Mum and Dad, thanks for all your financial and emotional support; my success would be nothing without this support I have received from you both. Lisa, you are not just my wee sister, you are my best friend. I couldn’t of gotten through this without your love, support, encouragement and patience. To my grandparents, thanks for always being proud of me and I hope I continue to make you proud in the future. This thesis is dedicated to all of you, and in particular, in loving memory of my Papi: Alan Gracie.

Author's Declaration

I declare that this thesis, except where acknowledged to others, represents my own work carried out in the School of Geographical and Earth Sciences, University of Glasgow, the Scottish Association for Marine Science and Hokkaido University. The research presented here has not been submitted for any other degree at the University of Glasgow, nor at any other institution. Any published or unpublished work by other authors has been given full acknowledgement in the text.

Jill Louise McColl

Definitions and abbreviations

ACA	Arid Central Asia
ACL	Average Chain Length
AD	Anno Domini
AO	Arctic Oscillation
APO	Asian-Pacific Oscillation
BLAST	Basic Local Alignment Search Tool
BP	Before present
bp	basepair
Bsi	Biogenic Silica
C/N	Carbon/Nitrogen
Cal.BP	calibrated (1000) years before present (present (0 BP) = 1950 AD)
CO ₂	Carbon Dioxide
CPI	Carbon Preference Index
CPI	carbon preference index
CWP	Current Warm Period
DCM	Dichloromethane
DNA	Deoxyribonucleic Acid
EAM	East Asian Monsoon
EASJ	East Asian Subtropical Jet
EASM	East Asian Summer Monsoon
EAWM	East Asian Winter Monsoon
ECS	Elemental Combustion System
ENSO	El Nino Southern Oscillation
FID	Flame Ionization Detector
GC	Gas-Chromatograph
GC-FID	Gas Chromatograph Flame Ionization Detector
GC-MS	Gas Chromatograph Mass Spectrometry
GHG	Greenhouse Gases
GNIP	Global Network of Isotopes in Precipitation
HPW	Higher plant waxes
Inc/Coh	Incoherent/Coherent
JJA	June, July, August
JSPS	Japanese Society for the Promotion of Science
LCAs	Long-Chain Alkenones
LGM	Last Glacial Maximum
LIA	Little Ice Age
LST	Lake Surface Temperature
MAP	Mean Annual Precipitation

MAT	Mean Annual air Temperature
MCMC	Markov Chain Monte Carlo
MeOH	Methanol
MJJ	May, June, July
MS	Mass Spectrometer
MS	Magnetic Susceptibility
MSCL	Multisenor Core Logger
MWP	Medieval Climate Anomaly
NAO	North Atlantic Oscillation
NCEP	National Centers for Environmental Prediction
NERC	National Environmental Research Council
NIES	National Institute for Environmental Science
NOAA	National Oceanic and Atmospheric Administration
NPSH	North Pacific Subtropical High
OH	Okhotsk High
OIPC	Online Isotopes in Precipitation Calculator
OM	Organic Matter
P(aq)	Proportion Aquatic
PCR	Polymerase Chain Reaction
PDO	Pacific Decadal Oscillation
PSA	Particle Size Analysis
rDNA	ribosomal Deoxyribonucleic Acid
RH	Relative Humidity
RPM	Rounds Per Minute
RT	Retention Time
SAMS	Scottish Association for Marine Science
SibH	Siberian High
SLP	Sea Level Pressure
SOI	Southern Oscillation Index
SST	Sea Surface Temperature
SUERC	Scottish Universities Environmental Research Centre
TAF	Total Acid Fraction
TLE	Total Lipid Extract
TN	Total Nitrogen
TNF	Total Neutral Fraction
TOC	Total Organic Carbon
TON	Total Organic Nitrogen
UK	Unsaturation Ketone index
UK37	Alkenone unsaturation index
UK'37	(modified) Alkenone unsaturation index
VPDB	Vienna Pee Dee Belemnite

VSMOW	Vienna Standard Mean Ocean Water
XRF	X-ray Fluorescence
$\delta^{13}\text{C}$	Stable Carbon Isotope Ratio
$\delta^{18}\text{O}$	Stable Oxygen Isotope Ratio
δD	Stable Hydrogen Isotope Ratio (D = Deuterium)
$\delta\text{D}_{\text{HPW}}$	Stable Hydrogen Isotope Ratio of Higher Plant Wxes
$\delta\text{D}_{\text{PRECIP}}$	Stable Hydrogen Isotope Ratio of Precipitation

1

Introduction

1.1 Motivation

1.1.1 The importance of climate reconstructions over the past 1000 years

In the past 1000 years, the Earth's climate has fluctuated as a result of natural forcing (e.g. volcanic and solar changes) (Crowley, 2000), which have resulted in two globally recognised climate events; the Medieval Warm Period (MWP) and the Little Ice Age (LIA). However, in recent times, the rate and magnitude of climate change cannot be explained by natural variability alone. Anthropogenic forcing, through the release of green-house gases by human activities, has been attributed to the recent rise in temperature (IPCC, 2013). These greenhouse gases will continue to rise and are superimposed on natural climate variability. To understand how regional climate has and will respond to anthropogenic forcing, we need to analyse climate change prior to 1850AD. Climate reconstructions from the past 1000 years are particularly important, because they encompass a period of natural climate forcing (prior to 1850AD) into a period of extreme anthropogenic forcing (post 1850AD). Although there is considerable uncertainty about what measures humans will put in place to abate further climate change, it is clear that the Earth will continue warming and the legacy of CO₂ that is currently in the atmosphere will continue to pose consequences for climate. In order to understand future climate change better, it is therefore necessary to have an understanding of how and why the natural climate has varied in the past.

Projecting future climate change is achieved by using climate models and the accuracy of climate models relies on using past climate reconstructions for validation (Li et al., 2010). The accuracy of models is important for projecting future climate in response to different scenarios of greenhouse gas concentrations and thus for quantifying climate change over the next century (Li et al., 2010). Climate reconstructions, particularly over the past 1000 years, are therefore imperative for understanding natural climate variability as a baseline and in-turn to better project future climate variability.

1.1.2 Reconstructing East Asian Monsoon in Northern Japan

In particular, variables such as temperature and precipitation are important to understand at the regional scale. In East Asia, temperature and precipitation are controlled by the strength of the East Asian Monsoon (EAM), which has two components; a winter component (EAWM) and a summer component (EASM). The EAM is characterised by the annual reversal of the meridional wind system due to the thermal contrast between the Pacific Ocean and the Asian continent (Wang et al., 2001). The intensity of the EASM and the EAWM is driven by the intensity of the North Pacific sub-tropical High (NPSH) (Zhou et al., 2009b, Wang et al., 2013a) and the Siberian High (SibH) (Ding, 1990, Zhang et al., 1997, Wu et al., 2006a, Gong et al., 2001), respectively. The EAM is connected to the global climate system as it influences, and is influenced by ENSO (e.g. Wang et al., 2003, Zhang et al., 1996, Hong et al., 2005) and changes in the North Atlantic (Liu et al., 2013c, Wang et al., 2001). As a result, investigating how the monsoon has behaved in the past, and the driving forces behind this variability, are required for a better understanding of future climate variability.

In addition to the global climate system, the EAM also has profound social and economic impacts in East Asia and its surrounding countries. Severe damage has been caused to the region's water resources, as well as, agricultural and industrial production due to the variability of the EAM. For example, the economic loss due to droughts and floods can reach over 200 billion yuan (21 billion pounds) (Huang et al., 1999, Huang and Zhou, 2002). Monsoon failure can also have a devastating impact on droughts in East Asian countries. For example, in the summer of 1994, the EAM failed and caused massive droughts, particularly in the southern half of Korea, Japan, and central China (World Meteorological

Organization 1995). The cause for monsoon failure is not fully understood and more research into past monsoon failure events, along with the mechanisms responsible for monsoon failure, are imperative.

The combination of the scientific and societal importance of the EAM is a key reason for investigating the variability of monsoon over the past 1000 years. High-resolution records from a variety of archives (e.g. stalagmites, lake sediments, marine sediments) from East Asia have documented the variability of the intensity of the EAM over the past 1000 years (Yamada et al., 2016, Hu et al., 2008, Yamada et al., 2010, Lee and Park, 2015). Although there are some general similarities in the variability of the EAM between these records, there are also large inconsistencies in the magnitude and timing of the strengthening and weakening of the EAM between the various reconstructions. Significantly, there are even inconsistencies between different stalagmites within the same cave (Dykoski et al., 2005, Wang et al., 2005). Recently, it has also been suggested that the source of the water vapour recorded in the ^{18}O values of stalagmites East Asia (southern and northwestern China) reflect the Indian summer monsoon (ISM) area (Yang et al., 2014), rather than the EASM, as previously reported. In addition, the relationship between the EASM and the EAWM is currently poorly understood. Some researchers' suggest that the EASM and the EAWM are inversely connected, e.g. a strong EASM occurs when the EAWM weakens and vice versa (Liu et al., 2009b, Sagawa et al., 2014). Whilst others suggest that there is no inverse relationship between the EASM and the EAWM, e.g. a strong EASM and strong EAWM occur together and a weak EASM and weak EAWM occur together (Yan et al., 2011b).

Although the climate in Hokkaido is mainly driven by the EAM, the Westerlies also influence climate in this region. The Westerlies transport cold, dry air-mass to Hokkaido (Fukusawa, 1999). The variability of the impact of the Westerlies over the past 1000 years in Japan is limited (Fukusawa, 1999). Often the intensification of the Westerlies is associated with the EAWM in Japan (e.g. Yamada, 2004, Yamada and Fukusawa, 1999). Therefore multi-proxy records from EAM-dominated regions, which are isolated from the interference of the ISM are required to investigate the (1) magnitude and the timing of the variability of the EAM, (2) the driving mechanisms of the EAM (3) the relationship between the

EASM and the EAWM and (4) the relationship between the EAM and the Westerlies, over the past 1000 years.

1.2 Lake Toyoni as a palaeo-climate archive

Natural archives such as lacustrine sediments, speleothems, tree-rings, ice cores or loess can be utilised to reconstruct past climate variability. Lacustrine sediments are advantageous because they provide unique and continuous sedimentary archives and they also have high sediment rates, which facilitate high-resolution climate records (Castañeda and Schouten, 2011). As a result, lake sediments provide valuable palaeo-climate reconstructions (Castañeda and Schouten, 2011). Lacustrine sediments from numerous lakes, using various proxies, provide detailed information of past changes in climate and the environment. In particular, Lake Toyoni represents a key natural archive to reconstruct past climate variability because the lake is situated at the boundary of the northern edge of the EASM (34-44°N; Xu et al., 2010b) making it sensitive to the enhancement of the EASM (Schöne et al., 2004).

1.3 Climate and environmental proxies

Instrumental records provide the most reliable information to understanding natural climate variability. However, the short length of human instrumental records (ca. 150 years) does not provide us with a long enough time-series to provide a natural baseline from which human induced changes deviate. Prior to instrumental records, we must rely on climate reconstructions using proxies. Proxies of climate can either be from historical documents (historical proxies) or from natural recorders of climate (natural proxies).

Molecular organic proxies are a common tool in the reconstruction of past biological assemblages, climate and environmental conditions (review by Castañeda and Schouten, 2011). Biomarkers, or chemical fossils, are specific organic compounds indicating the existence, past or present, of living organisms (Castañeda and Schouten, 2011). Analysis of biomarkers preserved in lake sediments can provide a wealth of information (Castañeda and Schouten, 2011) as they provide an indicator of environmental conditions at the time of

deposition (Eglinton and Eglinton, 2008) and they are easy to analyse. Due to these strengths, the use of lipid biomarkers for climate reconstruction is becoming increasingly established in the lacustrine environment (Castañeda and Schouten, 2011). The following sections provide an overview of the biomarkers used in this PhD research.

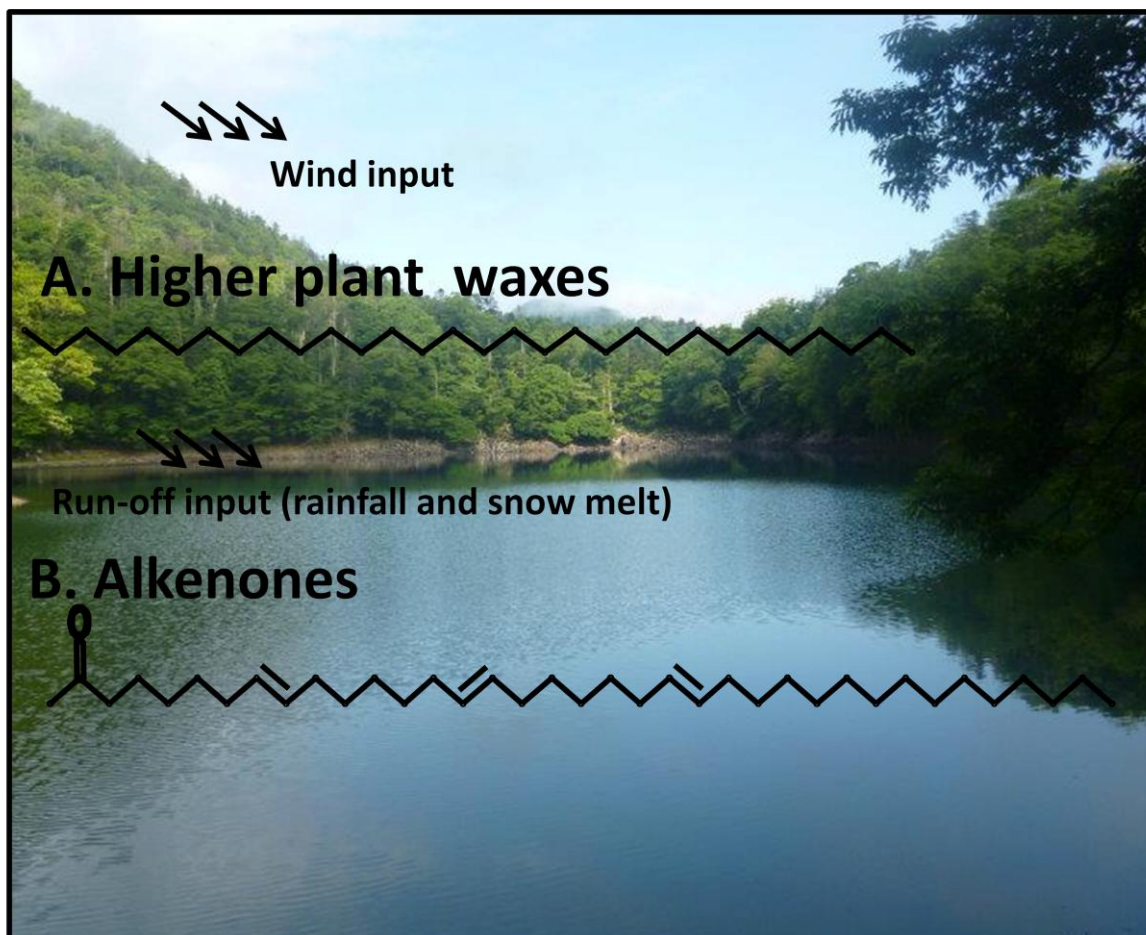


Figure 1-1: Diagram of Lake Toyoni and they key proxies (e.g. higher plant waxes and alkenones) used in this study. Wind and run-off input into Lake Toyoni are key processes in this lake, which can be studying using XRF elemental data.

1.3.1 *n*-alkanes

n-Alkanes (*n*-alkanols and *n*-alkanoic acids) are stable organic compounds that are generally well preserved in sediments. *n*-Alkanes are relatively easy to extract and all hydrogen atoms in *n*-alkanes are carbon-bound and therefore non-exchangeable, at least at lower temperatures (Schimmelmann et al., 1999). *n*-Alkanes originate from different biological sources. The long-chain homologues (C₂₇-C₃₅) are derived from terrestrial higher plants waxes (Eglinton and Hamilton,

1967; Figure 1-1). Whereas the short chain homologues (C_{17} - C_{21} *n*-alkanes) are derived from aquatic algae (Giger et al., 1980, Cranwell et al., 1987). In between are the mid-chain homologues (C_{23} , C_{24} and/or C_{25} *n*-alkanes), which are produced by submerged aquatic macrophytes (Ficken et al., 2000).

Terrestrial plants waxes are synthesised on plant leaf surfaces (Sachse et al., 2012), which protect the leaf surfaces (Eglinton and Hamilton, 1967). They protect the leaf from water loss (Cameron et al., 2006; Daly, 1964) and insect damage (Eglinton and Hamilton, 1967). Leaf wax *n*-alkanes are removed by rain and wind and subsequently transported to the lacustrine sediments via water (Castañeda and Schouten, 2011) or wind erosion (Hou et al., 2007).

The molecular compositions of *n*-alkanes provide a number of *n*-alkane based indices; for example, the carbon preference index (CPI index), Average Chain Length (ACL) and the proportion aquatic (Paq). The CPI index gives information of the extent of odd over even carbon number predominance (Bray and Evans, 1961). It is calculated using the following equation developed by Bray and Evans (1961; Equation 1). *n*-Alkanes produced by higher plants have a strong odd over even carbon number predominance (expressed as the CPI). In contrast, algal *n*-alkanes do not contain the strong odd over even carbon number predominance. Variations in the CPI index provides information on the biological origin of the source (e.g. Simoneit et al., 1979). For example, high CPI values (>3) results from a strong odd/even predominance which is a characteristics of higher plant wax *n*-alkanes. In contrast, *n*-alkanes from bacteria and algae show a weak odd/even predominance and give low CPI values (~1) (Cranwell et al., 1987).

$$CPI = \frac{1}{2} \left(\frac{C_{25} + C_{27} + C_{29} + C_{31} + C_{33}}{C_{24} + C_{26} + C_{28} + C_{30} + C_{32}} \right) + \left(\frac{C_{25} + C_{27} + C_{29} + C_{31} + C_{33}}{C_{24} + C_{26} + C_{28} + C_{30} + C_{32} + C_{34}} \right)$$

Equation 1: Carbon preference index (CPI). C_x represents the abundance of an *n*-alkane with a particular number of carbons in its chain (Bray and Evans, 1961).

Average chain length values indicate the dominant odd-chained *n*-alkane. The ACL value of a sample is calculated for the most abundant odd chained *n*-alkanes

of a homologous series using the equation below (Equation 2; Schefuß et al., 2003). Variations in the ACL of *n*-alkanes of terrestrial higher plants occur in response to plant stresses (e.g. temperature and/or aridity) (Gagosian and Peltzer, 1986, Kawamura et al., 2003) and vegetation type (Cranwell, 1973). By investigating the ACL index in lacustrine sediments, palaeo-temperature, palaeo-aridity conditions, as well as vegetation change can be inferred.

$$ACL = \frac{\sum(X_i \cdot C_i) n}{(C_i)n}$$

Equation 2: Average chain length (ACL); X_i represents the *n*-alkane and C_i the concentration of the *n*-alkane.

The *Paq* index was developed to reflect the relative contribution of aquatic macrophytes and emergent aquatic and terrestrial plants (Ficken et al., 2000). It is calculated using the following equation developed by Ficken et al. (2000; Equation 3). According to Ficken et al (2000), *Paq* values greater than 0.4 indicate the dominance of submerged and floating macrophytes (Ficken et al., 2000). By investigating the *Paq* index in lacustrine sediments, the contribution of *n*-alkanes from submerged/floating plants can be inferred.

$$Paq = \frac{(C_{23} + C_{25})}{(C_{23} + C_{25} + C_{29} + C_{31})}$$

Equation 3: Proportion aquatic (*Paq*). C_x represents the abundance of an *n*-alkane with a particular number of carbons in its chain (Ficken et al., 2000).

In addition to the molecular composition of *n*-alkanes, the hydrogen isotopic composition of *n*-alkanes derived from higher plant waxes (δD_{HPW}) are analysed using an isotope ratio mass spectrometry (IRMS). The δD_{HPW} provide a powerful tool for investigating hydrological change (e.g. Hou et al., 2008, Sachse et al., 2006) because the δD of terrestrial and aquatic *n*-alkanes records the isotopic signal of their environmental water; e.g. rainwater, groundwater, and snow-melt, which are all derived from precipitation. Previous studies have found that the δD of precipitation (δD_{PRECIP}) is a key control on the δD_{HPW} values (Sauer et al., 2001, Sessions, 2006, Hou et al., 2008), therefore; the δD_{HPW} can be used to

reconstruct changes in δD_{PRECIP} over a given period of time (e.g. Schefuss et al., 2005, Pagani et al., 2006). In general, the δD_{PRECIP} reflects a variety of hydrological and climate processes including temperature, precipitation amount, altitude, latitude, and moisture source (Dansgaard, 1964). Knowledge of the controls of the δD_{PRECIP} at the study site is important for interpreting the δD_{HPW} from palaeo-climate archives. Therefore prior to using D_{HPW} to reconstruct hydrological variability, it is important to identify the controls on the δD_{PRECIP} in Hokkaido.

1.3.2 Alkenones

Long chain alkenones are a class of C_{35} - C_{40} unsaturated ketones produced by members of the division Haptophyceae. The producer of alkenones in the marine environment is dominated by calcifying haptophytes *Emiliania huxleyi* and *Gephyrocapsa oceanica* in the open ocean (de Leeuw et al., 1980, Volkman et al., 1995) and by non-calcifying species *Isochrysis galbana* and *Chrysothila lamellosa* in the coastal marine setting (Marlowe et al., 1984). However, in lacustrine environments, the diversity of haptophytes producing alkenones varies according to their ecology and environment.

Alkenones are of interest because analysis of these compounds provides a method for quantitative reconstruction of past water temperature based on the degree of unsaturation in the ketone molecule (e.g. Prahl and Wakeham, 1987, Brassell et al., 1986, Herbert et al., 2003). The most abundant alkenones produced, are those with chain lengths of 37 and 38 carbon atoms with two, three or four double bonds (Table 1.1). The carbonyl functional group is either located at the second or third carbon in the chain. The relative abundances of $C_{37:2}$, $C_{37:3}$ and $C_{37:4}$ alkenones within the synthesising haptophyte species changes with growth temperature (Brassell et al., 1986, Prahl and Wakeham, 1987). When the temperature is warmer, the relative abundance of more unsaturated alkenones decreases resulting in high U_{37}^K values. This relationship has led to the formulation of the alkenone unsaturation index (U_{37}^K ; Equation 4a) by Brassell et al. (1986). Subsequent research showed that in the marine environments there was no empirical benefit to including the tetra-unsaturated ketone in the paleo-temperature equation because this alkenone is not abundant outside polar and sub-polar regions (Prahl and Wakeham, 1987). The $U_{37}^{K'}$ Index

was suggested (Prahl and Wakeham, 1987) and has been widely adopted (Equation 4b). Calibration equations are used to convert U_{37}^K and $U_{37}^{K'}$ values into water temperatures resulting in quantitative reconstructed past water temperature.

Table 1-1: alkenones and their shorthand notation

<i>Shorthand notation</i>	<i>IUPAC nomenclature</i>
C37:4Me	heptatriaconta-8E,15E,22E,29E-tetraen-2-one
C37:3Me	heptatriaconta-8E,15E,22E-trien-2-one
C37:2Me	heptatriaconta-15E,22E-dien-2-one
C38:4Et	octatriaconta-9E,16E,23E,30E-tetraen-3-one
C38:4Me	octatriaconta-9E,16E,23E,30E-tetraen-2-one
C38:3Et	octatriaconta-9E,16E,23E-trien-3-one
C38:3Me	octatriaconta-9E,16E,23E-trien-2-one
C38:2Et	octatriaconta-16E,23E-dien-3-one
C38:2Me	octatriaconta-16E,23E-dien-2-one
C39:4	nonatriaconta-10E,17E,24E,31E-tetraen-one
C39:3	nonatriaconta-10E,17E,24E-trien-one
C39:2	nonatriaconta-17E,24E-trien-one

$$U_{37}^K = \frac{(C_{37:2} - C_{37:4})}{\sum(C_{37:2}:C_{37:3}:C_{37:4})} \quad U_{37}^{K'} = \frac{(C_{37:2})}{\sum(C_{37:2}:C_{37:3})}$$

Equation 4: A: U_{37}^K calibration equation (Brassell et al., 1986). B: $U_{37}^{K'}$ calibration equation (Prahl and Wakeham, 1987).

The global $U_{37}^{K'}$ core top calibration equation produced by Conte et al., (2006) was developed using 742 samples from around the world. The use of this calibration makes it possible to reconstruct SST using marine sediments from any location in the world. Whereas the temperature calibration used in lacustrine settings depend on the alkenone-producer(s) present within the lake.

Although the alkenone producers in the marine environment are well constrained, the alkenone producer(s) in a given lake depends on their ecology and environment. In addition, there can be several alkenone-producers in one given lake (Theroux et al., 2010). Alkenone producers in lacustrine environments are similar to the haptophyte species *Isochrysis galbana* (Coolen et al., 2004a)

and *Chrysothila lamellosa* (Sun et al., 2007). In addition, several novel alkenone producers, which have not been fully classified taxonomically, have also been discovered (D'Andrea et al., 2006). Recently, there have been several key studies using environmental genomics to identify the alkenone-produce(s) in lakes (e.g., D'Andrea et al., 2006, Randlett et al., 2014) using the 18S molecular marker. The 18S molecular marker is present in all eukaryotes (Olsen et al., 1986, Woese, 1987) and therefore provides species level taxonomic resolution (Sogin et al., 1986, Edvardsen et al., 2000).

The identification of the alkenone-producer(s) in lakes prior to reconstructing temperature is important in order to choose the correct calibration as different alkenone-producers have the potential to produce different temperature calibrations, individual alkenone-containing lakes require unique calibration datasets dependent on species of haptophyte algae present (Chu et al., 2005, D'Andrea et al., 2006). Therefore prior to alkenone-based temperature reconstructions in lacustrine settings, it is important to identify the alkenone-producer(s) within the lake and determine the response of haptophyte species to temperature. There has been several studies which have successfully produced temperature calibrations for lakes based on a number of different calibration methods. The main site-specific temperature calibration methods are; examining surface sediments (Zink *et al.*, 2001; Chu *et al.*, 2005), isolation and culturing of alkenone producer(s) to create an experimental calibration (Sun *et al.*, 2007) and also filtering water column samples over an extended time period (Toney *et al.*, 2010; D'Andrea *et al.*, 2011) to produce an in-situ calibration. Zink *et al.* (2001) established a temperature calibration by examining surface sediments from a transect of lakes in Germany. During this study the best correlation existed between the $U^{K'}_{37}$ Index and the summer average lake surface temperature ($r^2 = 0.90$). This calibration approach makes large assumptions that all lakes sampled contain the same haptophyte species or that different species have the same relationship to temperature. Chu *et al.* (2005) also adopted this calibration method and examined 37 surface sediments of lakes in China. This study found a good correlation between $U^{K'}_{37}$ and mean annual air temperature (MAAT) ($r^2 = 0.83$). Toney *et al.* (2010) provide an *in-situ* calibration for $U^{K'}_{37}$ for Lake George, ND covering a temperature range from 2°C to 22°C. The in-situ calibration was derived from sampling temperature and LCA signatures from the lake water column at different depths during the haptophyte bloom to establish the

relationship between temperature and alkenone signature. They found a significant relationship between the U_{37}^K Index and water temperature ($r^2 = 0.75$) but in contrast to other studies, they found no relationship between U_{37}^K and water temperature ($r^2 = 0.14$). D'Andrea *et al* (2011) developed a temperature calibration for Lakes in Kangerlussuaq, West Greenland based on U_{37}^K of filtered alkenones and *in situ* temperature. They combined the results with Zink *et al* (2001) to extend the narrow temperature range. On the other hand, Sun *et al* (2007) collected and isolated *Chrysothila lamellosa* from an inland saline Lake in China. They created a culture-based calibration using the U_{37}^K Index that correlated with growth temperature varying from 10°C to 22°C.

Although it is evident that alkenones produced by haptophytes have a unique relationship with temperature, it is still not known why haptophytes produce alkenones and hence why the variations in alkenone ratios are related to temperature. Some early studies have suggested that alkenones are membrane lipids, which are produced for fluidity and rigidity (Prahl *et al.*, 1988). This would also explain why the unsaturation ratio of alkenones are related to temperature; e.g. increased unsaturation at lower temperatures would decrease the melting point of the lipids and hence keep membranes fluid. However, other studies have suggested that alkenones are not membrane lipids and instead are produced for buoyancy (Fernández *et al.*, 1994, Epstein *et al.*, 2001) or energy storage (Pond and Harris, 1996, Epstein *et al.*, 2001, Eltgroth *et al.*, 2005). On the other hand, the function of alkenones may not be related to the relationship between temperature and unsaturation. Instead, the temperature dependence of alkenone unsaturation may reflect different biochemical pathways (Epstein *et al.*, 2001). Epstein *et al.* (2001) suggested that the synthesis and degradation of alkenones may require different enzymes with different temperature optima.

1.3.3 Elemental composition of lacustrine sediments

In order to compliment the biomarker proxies, bulk elemental compositions via X-ray Fluorescence (XRF) scanning and carbon/nitrogen (C/N) ratios provide an insight into terrestrial and biological processes influencing the sedimentary record, which in-turn strengthens palaeo-climate reconstructions. XRF scanning offers a method for providing quick, non-destructive, high-resolution palaeo-climate records (Croudace *et al.*, 2006) to investigate changes in terrestrial input and

productivity within the lake and its catchment. The C/N ratio is used to assess the relative contributions of terrestrial and aquatic OM in lake sediments (Meyers, 1997). The C/N ratio of bulk sediments changes with respect to the concentration cellulose in the plant sources of OM (Meyers and Ishiwatari, 1993a). Nonvascular aquatic plants or algae have low concentrations of cellulose and typically have a C/N ratio between 4 and 10. In comparison, land plants contain high concentrations of cellulose and have C/N ratios ≥ 20 (Meyers, 1994). The C/N ratio found in the bulk sediments of lakes mostly reflects a mix of both aquatic and terrestrial sources of OM (Meyers, 1994). XRF scanning and C/N ratios therefore provides a wealth of information on terrestrial and biological input into the lake.

1.4 Objectives

The key objective of this thesis therefore was to reconstruct past climatic and hydrologic variability in East Asia using a multi-proxy approach from Lake Toyoni. This variability is controlled by the two key atmospheric systems; the Westerlies and the EAM, so the present study develops multi-proxy reconstructions to determine past climatic and hydrologic variability in Japan over the past 1000 years and aid in understanding the effects of the Westerlies and the EAM independently and interactively. The hypothesis being tested is:

The climate in Northern Japan was strongly influenced by the intensity of the EAM (EASM and the EAWM) and the Westerlies over the past 1000 years.

1.5 Thesis organisation

This thesis is organised into 9 Chapters:

- Chapter 2: “*Climate drivers in Hokkaido, Japan*”, aims to identify how natural climate drivers (e.g. the East Asian Monsoon [EAM], the Pacific Decadal Oscillation [PDO], the Arctic Oscillation [AO] and El Nino Southern Oscillation [ENSO]) in this region currently influence modern climate (e.g. temperature, rainfall and snowfall) at our study site. Modern data (1958-2014) was used from Hiroo weather station (25km from study site).

- Chapter 3: ***“Site location and methods”***, reports on the study site and the methods used in this PhD research.
- Chapter 4: ***“Decadal-resolved terrestrial and biological input into Lake Toyoni”***, aims to reconstruct EAM variability in Lake Toyoni using productivity proxies: Magnetic Susceptibility (proxy for magnetite preservation), Si/Rb (proxy for diatom productivity), Inc/Coh (proxy for OM), and molecular composition of *n*-alkanes; CPI, ACL and Paq (proxies for source of *n*-alkanes, temperature and productivity, respectively).
- Chapter 5: ***“Assessing the contribution of global and regional wind patterns”***, aims to reconstruct wind input into Lake Toyoni to infer changes in the EAWM and the Westerlies. The contribution of dust (transported to Hokkaido via the Westerlies and the EAWM) into Lake Toyoni was determined by the Ti/Rb proxy. The contribution from the Westerlies and the EAWM was separated based on the fine and coarse grain size of the dust, respectfully.
- Chapter 6: ***“18S rDNA analysis of the alkenone-producer(s) in lake Toyoni, Japan”***, aims to identify the alkenone producer(s) in Lake Toyoni using 18S rDNA analyses of planktonic, phototrophic algae that are preserved in the surface sediment and examine alkenone distribution variability between Lake Toyoni and other known haptophyte algae species.
- Chapter 7: ***“Alkenone-based temperature reconstruction from Lake Toyoni”***, aims to reconstruct water temperatures (which correspond to changes in air temperature) over the past 1000 years. The study site is located in the northern boundary of the EASM and the air temperature is currently strongly influenced by the variability of the EASM. Therefore reconstructions of temperature from this region will provide information on the intensity of the EASM.
- Chapter 8: ***“Hydrogen isotopic composition of higher plant waxes in the catchment and down-core sedimentary records of Lake Toyoni”***, aims to (1) determine the parameters controlling the hydrogen isotopic

composition of *n*-alkanes in the catchment of Lake Toyoni and (2) reconstruct hydrological variability (driven mainly by the EAM system) in Hokkaido, Japan.

- Chapter 9 “***Synthesis***” aims to bring together all results to provide a multi-proxy EAM reconstruction from Lake Toyoni and determine past climatic and hydrologic variability in Japan over the past 1000 years to (1) aid in understanding the effects of the Westerlies and the EAM independently and interactively (2) determine the factors driving changes in the EAM and the Westerlies and (3) define the link between global and East Asian climate variability.
- Chapter 10 “***Conclusions and future work***” provides a summary of the main results and provides some suggestions for future work.

Climate drivers in Hokkaido, Japan

2.1 Instrumental data

Weather station data from Hiroo meteorological station (42°17'02"N, 143°19'09"E; elevation of 24m; 1958-2014), which is the closest station to the sampling site, is used to determine average monthly and annually temperature (°C), rainfall (mm), snowfall (cm) and relative humidity (%) at our study site (Figure 2-1). The average (1958-2014) annual mean temperature is 6.8°C (ranges between 5.7 and 8°C). The warmest month is August (18.5°C; ranges between 15.4 and 21.9°C) and the coldest month is January (-4.8°C; ranges between -8.2 and -2.1°C). The average (1958-2014) annual rainfall is 1723mm (ranges between 1051 and 2431mm). The wettest month is September (249mm; ranges between 201 and 308mm) and the driest month is February (64mm; ranges between 57 and 297mm). The average (1958-2014) annual snowfall is 318.9cm (ranges between 145 and 566cm). There is no snowfall between June and October. The most snowfall falls in January (91.1cm; ranges between 20 and 198cm) and the lowest amount falls in May (2.9cm; ranges between 0 and 11cm). Relative humidity at our site is relatively high all year round. The annual average is 74.3% (ranges between 71 and 78%). The highest values occur in July (89.0%; ranges between 82 and 96%) and the lowest values occur in December (63%; ranges between 52 and 72%).

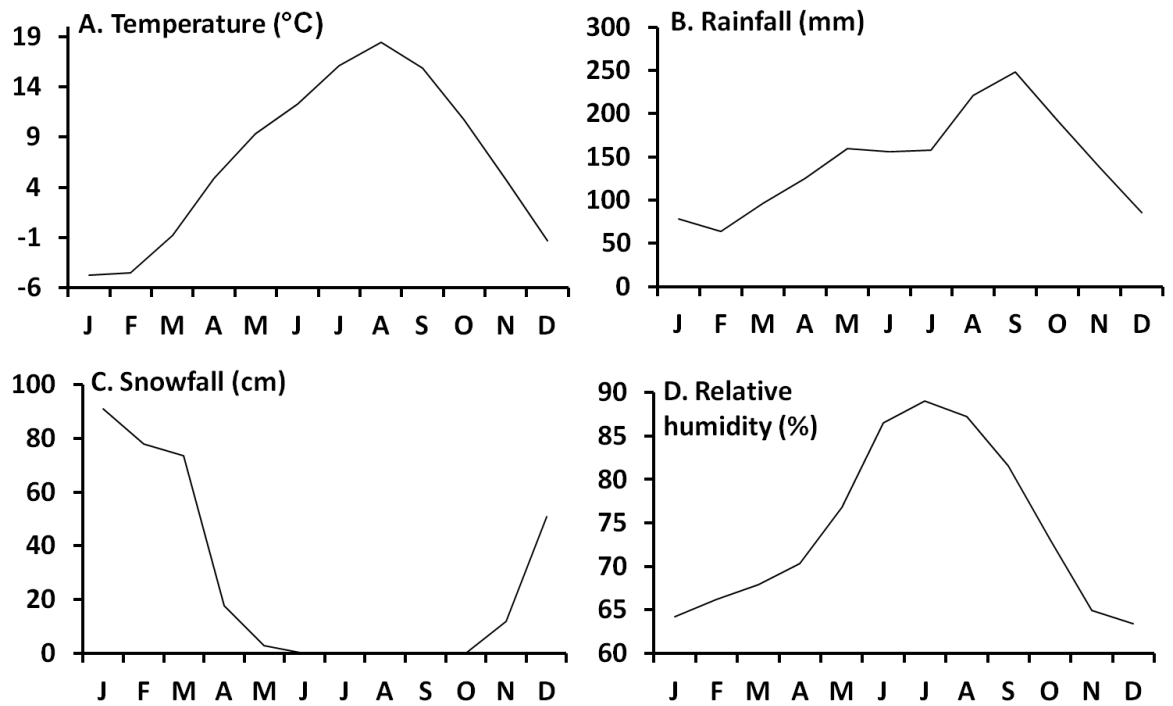


Figure 2-1: Weather station data from Hiroo weather station (averaged between 1958-2014). A. Temperature ($^{\circ}\text{C}$), B. Rainfall (mm), C. Snowfall (cm) and D. relative humidity (%). Months are on the X-axis. Climate drivers in Hokkaido

2.2 Climate drivers in Hokkaido

The climate (temperature, rainfall and snowfall) in Hokkaido is ultimately controlled by seasonal variations in the East Asian Monsoon (EAM) (D'Arrigo et al., 2001, Davi et al., 2002, Tsuji et al., 2008, Igarashi et al., 2011). Various teleconnections also influence Hokkaido, which in turn also influence the intensity of the EAM. The teleconnections that influence Hokkaido are the inter-annual patterns of the El Niño Southern Oscillation (ENSO) (Davi et al., 2002) and the decadal-to-centennial scale variations relating to the Pacific Decadal Oscillation (PDO) (Davi et al., 2002, Tsuji et al., 2008) and Arctic Oscillation (AO) (Tsuji et al., 2008). In this section, the influence of the EAM at Lake Toyoni will be examined by comparing strong and weak EAM years to the weather station data. In addition, we examine the influence of teleconnections at this site, and any influence teleconnections have on the EAM.

2.2.1 East Asian Monsoon (EAM)

The EAM comprising the summer (EASM) and winter (EAWM) sub-system, is characterised by the annual reversal of the meridional wind system (Figure 2-2) due to the thermal contrast between the Pacific Ocean and the Asian continent (Wang et al., 2001). The EAM exerts a strong control on the climate (e.g. temperature, rainfall and snowfall) in Hokkaido (D'Arrigo et al., 2001, Davi et al., 2002, Tsuji et al., 2008, Igarashi et al., 2011). Significantly, Lake Toyoni (42°N) is situated at the boundary of the northern edge of the EASM (34-44°N; Xu et al., 2010b) making it sensitive to the enhancement of the EASM (Schöne et al., 2004). The boundary of the northern edge of the EASM is the location where the warm tropical air meets the cold polar air-mass, termed the polar front. When the Pacific High intensifies the polar front is located further north than usual and as a result there is an increased influence from the tropical maritime air-mass from the Pacific Ocean to Hokkaido. When the polar front is located further south there is a reduction in the influence of the Pacific Ocean and an increased influence from the sub-polar maritime air-mass to Hokkaido. Although much research has focussed on the past variations and controls of the EAM, further research on the magnitude of the EAM and its relationship with other components of the global climate system are required, particularly over the past 1000 years, which has had limited research conducted. In addition, with multiple climate systems impacting regional climate here, we aim to distinguish the various drivers where possible. Our knowledge of the EAM will also be greatly improved with additional records from different regions of the EAM domain. This site is therefore a key location for expanding our knowledge on the variability of the EAM over the past 1000 years.

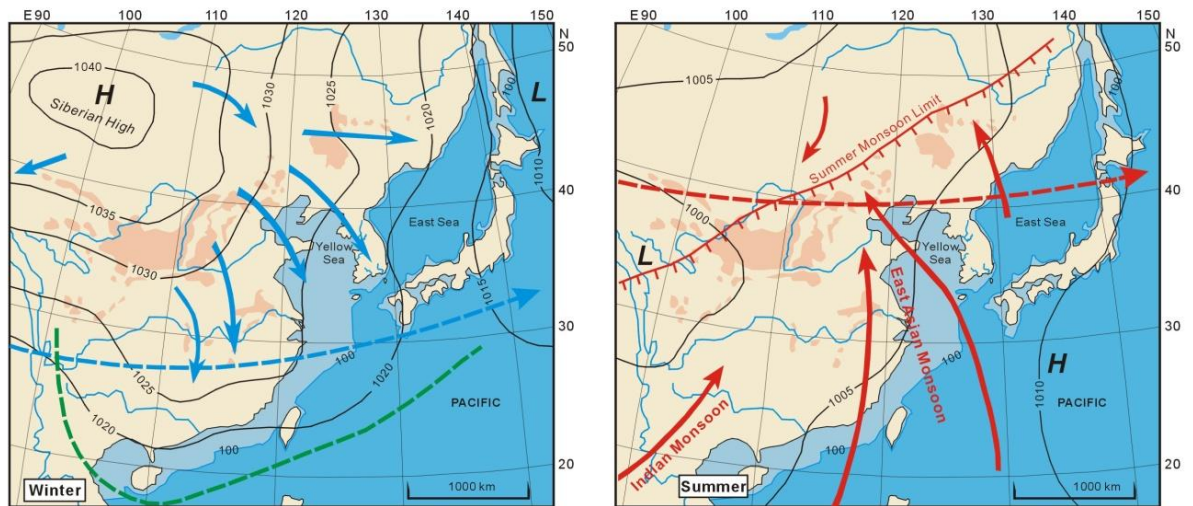


Figure 2-2: Seasonal changes in the wind system of the EAM. During winter a high pressure system develops over the Asian continent and the wind blows cold air-mass from the Asian continent towards the Pacific Ocean. In summer, a high pressure system develops over the Pacific Ocean and the wind blows warm air-mass towards the Asian continent (Figure from: Yi, 2011). Blue and red solid arrows indicate the dominant vectors of surface winds in winter and summer, respectively. Blue and red dashed arrows indicate the mean location of the East Asian jet stream in winter and summer, respectively. Green dashed arrow indicates the southern limit of cold surges in winter.

2.2.1.1 East Asian Summer Monsoon (EASM)

Monsoon circulation occurs because the land responds to seasonal changes in solar radiation faster than the ocean. In summer, strong solar radiation heats the land much more intensely than the ocean, which causes air to warm, expand and rise over the continents creating an area of low pressure at the surface. At the same time, a high pressure system develops in the northwest sub-tropical Pacific (the North Pacific sub-tropical High [NPSH]). The difference in pressure between the land and the ocean promotes the transport of moist air from the Pacific Ocean towards this low pressure region, which also warms and rises and contributes to monsoonal summer rainfall (April to September) (Seki et al., 2012). Hence, warm and wet conditions are experienced during summer in East Asia as a result of the EASM.

The influence of the EASM on climate in Hokkaido is demonstrated in modern (1958-2015) weather station data (Figure 2-3 and Figure 2-4). Zhou et al (2009a) defined strong EASM years in the period between 1958-2000 are 1958, 1959, 1960, 1961, 1962, 1963, 1964 and weak EASM years are 1980, 1986, 1991, 1996, 1997 (Zhou et al., 2009a). Strong EASM and weak EASM years are shown in Figure 2-3 (temperature) and Figure 2-4 (rainfall). When comparing strong and weak

EASM years to averaged temperature and rainfall data from Hiroo weather station, we find that temperatures during strong EASM years (6.8°C) are consistent with averaged temperature values (6.8°C). However, we find that during weak EASM years, the temperatures during August are significantly lower by about 2°C lower than averaged values. In comparison to temperature, rainfall values vary significantly depending on strong and weak EASM years. For example, averaged annual rainfall values between 1958 and 2014 are 1723mm. During strong EASM years, rainfall increases to 1849mm and during weak EASM years, rainfall decreases to 1608mm. Particularly noticeable are the months where rainfall increases (decreases) during strong (weak) EASM years in June and August, which is associated with the early monsoon rainy season.

There are two rainy seasons associated with the EASM in Japan. The first is called Baiu and is associated with the northward travelling rain-belt (Qian et al., 2002a). The northward movement of the rainband is closely associated with the northward shift of the NPSH (Huang et al., 2005, Huang et al., 2003, Lu and Kim, 2004). This rainy season occurs in the month of June (Lee, 1974, Sampe and Xie, 2010). The Baiu rain-band usually occurs between $30\text{-}40^{\circ}\text{N}$ (Sampe and Xie, 2010) and therefore Lake Toyoni (42°N) is usually unaffected by this monsoonal rainfall. This is demonstrated in the average monthly rainfall values in Figure 2-1, which show low rainfall in June. However, we find that when there is a strong EASM, rainfall in June increases at our site, suggesting that the Baiu rainy season extends further north (Figure 2-4). Rainfall increased from 1723mm (averaged between 1958 and 2014) to 1849mm during strong EASM years.

The second rainy season is called Shurin and this is a southward travelling rain-belt (Qian et al., 2002a). Shurin occurs in August and September (Kimura, 1966). The NPSH, which is associated with the EASM migrates to its annual northernmost position in August. The Shurin rainy season in Japan is complex because it is also the timing of the typhoon season (Lee, 1974, Nogami et al., 1980, Ho et al., 2004). As a result of monsoon and typhoon rainfall, autumn has the highest amount of rainfall. We find that rainfall increases in August during both strong and weak EASM years. Rainfall during September is lower than average in September during strong EASM and higher than average during weak EASM. However, in both strong and weak EASM years, most rainfall occurs during August and September (during the Shurin rainy season). The key difference

between strong and weak EASM years is the influence of Baiu (June) rainfall in this region.

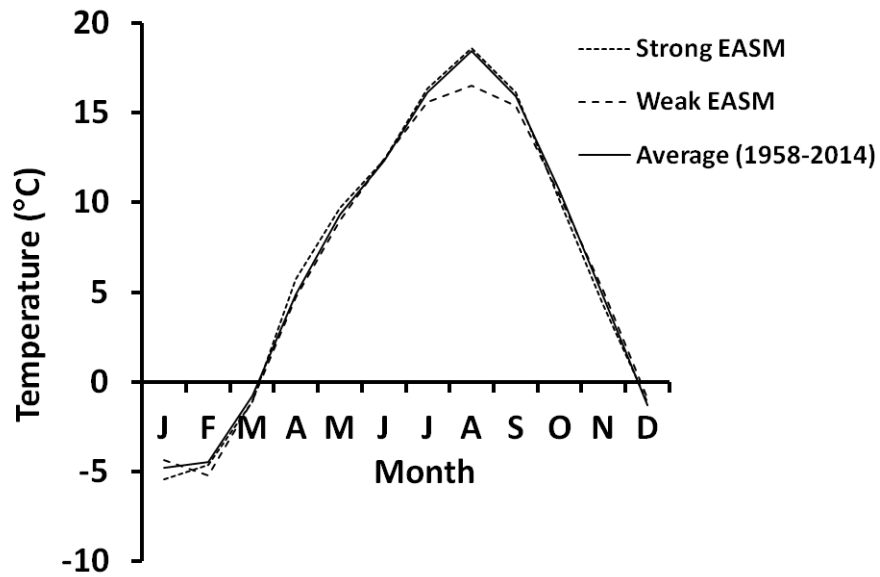


Figure 2-3: Monthly temperature averages during strong EASM (small dashed line) and weak EASM (large dashed line) years compared with average (1958-2014) monthly temperature values (solid line).

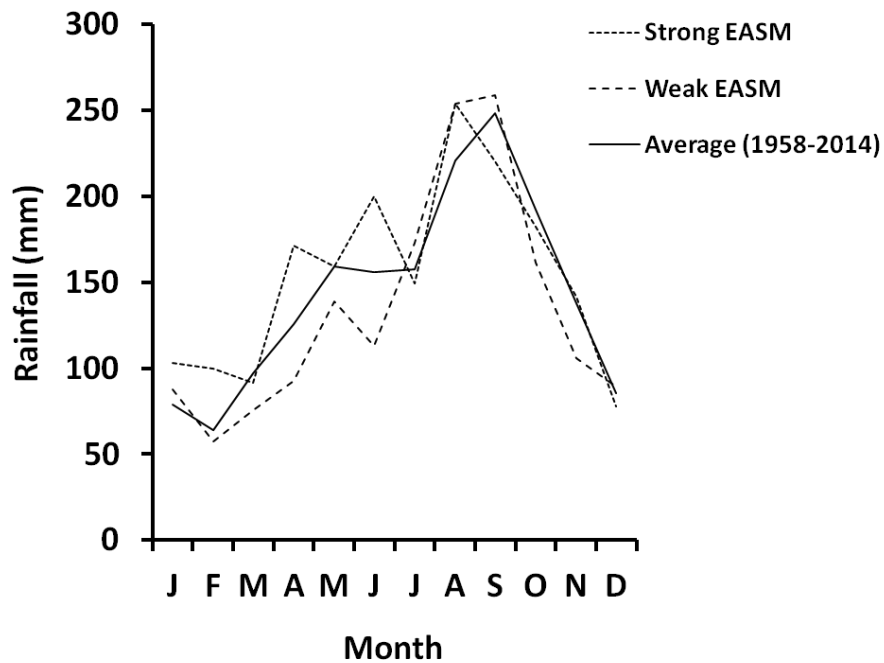


Figure 2-4: Monthly rainfall averages during strong EASM (small dashed line) and weak EASM (large dashed line) years compared with average (1958-2014) monthly rainfall values (solid line).

2.2.1.2 East Asian Winter Monsoon (EAWM)

During winter, solar radiation is considerably weaker than summer and air over land cools faster and becomes denser than the air over the ocean and sinks from higher levels in the atmosphere. This downward movement creates an area of high pressure over Siberia (Siberian High; [SibH]). The overall movement of cold, dry air flow is down-and-out from land to ocean. The cool, dry winter air from the Siberian High pressure system picks up heat and moisture as it flows over the Tsushima Current in the Sea of Japan resulting in heavy snowfall to Hokkaido. IN order to determine the influence of the EAWM on the climate in Hokkaido, a 10-year period of a strong EAWM (1976-1985) and weak EAWM (1988-1997) are used based on the EAWM index by Jhun and Lee (2004b). This index uses data from the National Centres for Environmental Prediction-National Centre for Atmospheric Research and it reflects the 300-hPa meridional wind shear associated with the jet stream. The EAWM index is defined as the difference in the area-averaged zonal wind speed at the 300-hPa level between the two boxed regions ([27.5°-37.5°N, 110°-170°E] and [50°-60°N, 80°-140°E]). During a strong (weak) EAWM, the upper-level jet stream is stronger (weaker), the SibH and Aleutian low is stronger (weaker) and low-level northeasterly winds are increased (decreased). We find that the 10-year period associated with a strong EAWM (1976-1985; Jhun and Lee, 2004b) shows a large decrease in temperature (Figure 2-5) and rainfall (Figure 2-6) throughout the year. For example, the average temperature between 1958 and 2014 was 6.8°C, whereas during strong EAWM years the temperature decreased to an average of 6.3°C and during weak EAWM years the average temperature increased to 7.0°C. The difference in temperature is particularly apparent during winter months (Figure 2-5). The average rainfall amount is 1723mm per year (averaged from 1958-2014), during strong (weak) EAWM years, rainfall decreases (increases) to 1486mm (1837mm).

On the other hand, a 10-year period associated with a weakening of the EAWM (1988-1997; Jhun and Lee, 2004b) shows higher than average winter temperatures and an increase in rainfall. Notably, rainfall increases significantly in August and September during weak EAWM years (Figure 2-6), which is associated with EASM rainfall (Shurin rainfall). Rainfall is also slightly increased in June, which is associated with Baiu monsoonal rainfall. This suggests that a

weakening (strengthening) of the EAWM results in a strengthening (weakening) of the EASM at this site.

In addition to temperature and rainfall, snowfall depth (cm) was also influenced by the strength of the EAWM (Figure 2-7). During strong (weak) EAWM years, annual snowfall depth (cm) increased (decreased) to 326.8cm (287.9cm) compared to average values (318.9cm; 1958-2014). This increase in snowfall depth (cm) is particularly apparent during the month of March, which received on average 103.3cm of snowfall compared to the average amount of 78.1cm. Thus, strong (weak) EAWM years are associated with lower (higher) temperatures, decreased (increased) rainfall and increased (decreased) snowfall, particularly during the month of March.

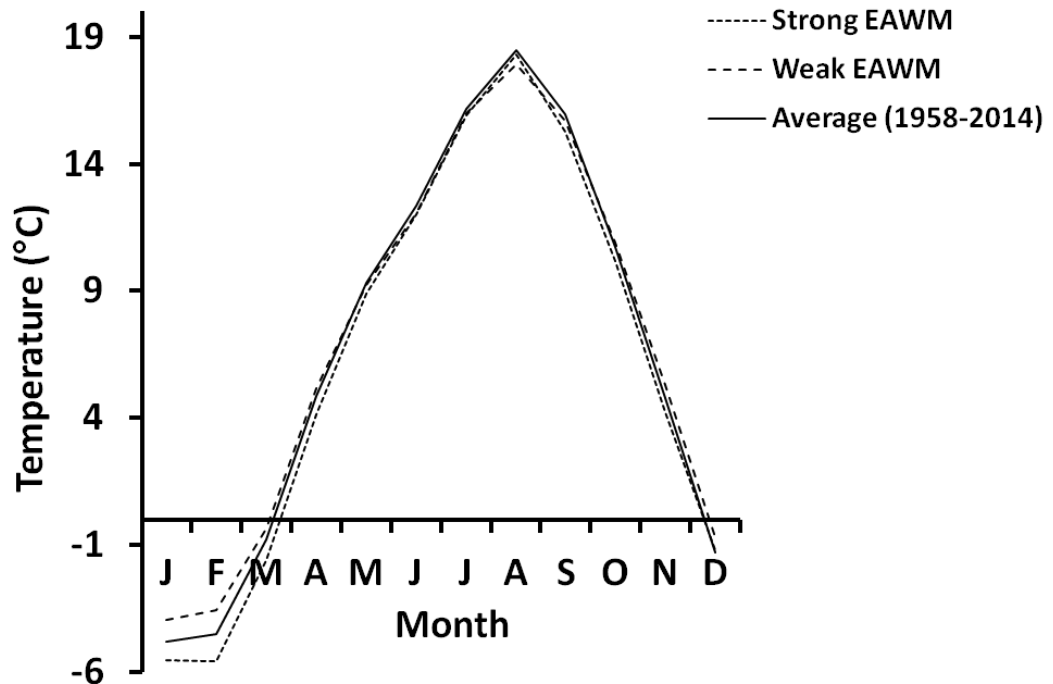


Figure 2-5: Monthly temperature averages during strong EAWM (small dashed line) and weak EAWM (large dashed line) years compared with average (1958-2014) monthly temperature values (solid line).

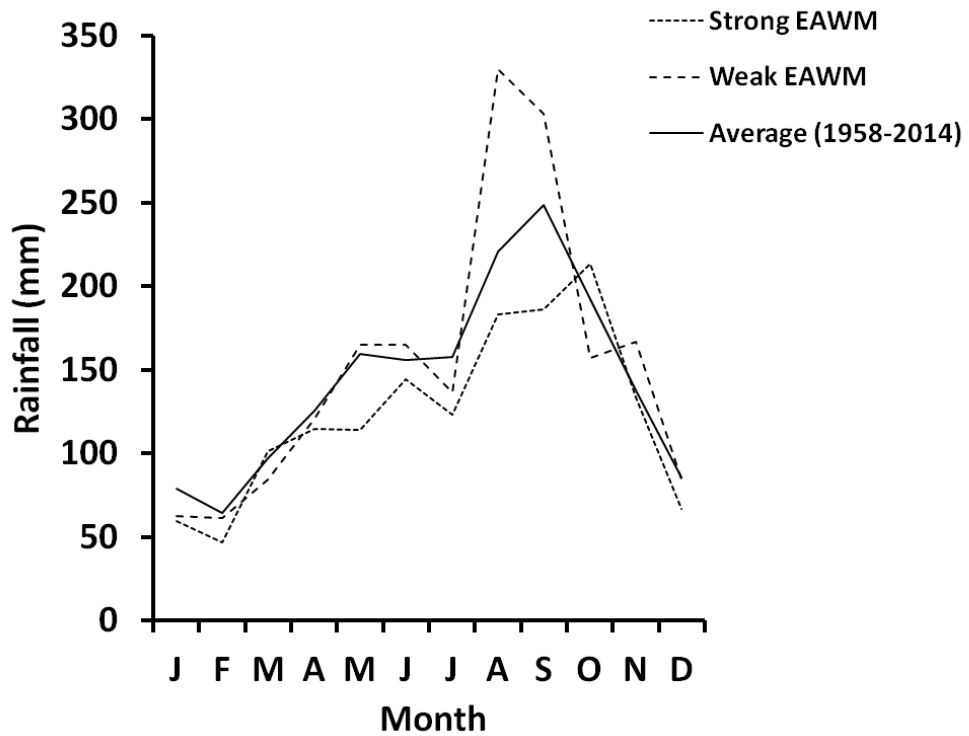


Figure 2-6: Monthly rainfall averages during strong EAWM (small dashed line) and weak EAWM (large dashed line) years compared with average (1958-2014) monthly rainfall values (solid line).

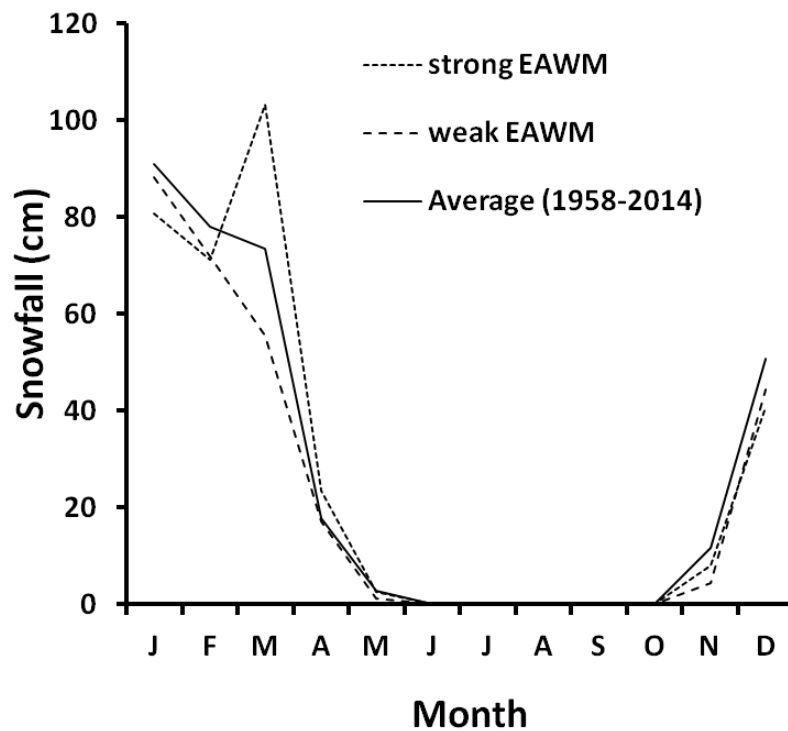


Figure 2-7: Monthly snowfall averages during strong EAWM (small dashed line) and weak EAWM (large dashed line) years compared with average (1958-2014) monthly snowfall values (solid line).

2.2.2 Arctic Oscillation (AO)

A teleconnection known to significantly influence climate in Hokkaido is the AO (Tsuji et al., 2008). The AO refers to the difference in sea level pressure (SLP) averaged between middle and high latitudes in the Northern Hemisphere. It is the dominant mode of atmospheric circulation in the Northern Hemisphere and has significant influence on the Asian climate. In particular, temperature and rainfall patterns in the Northern Hemisphere are strongly influenced by the AO (Thompson and Wallace, 1998, Thompson et al., 2000). During positive AO, warmer surface temperatures, weaker weather variances, and less frequent cold surges are observed over Asia (Mao et al., 2010). The reverse is true for a negative AO phase.

In order to analyse the effect of the phase of the AO on temperature and rainfall in Hokkaido, we used data from NOAA's Centre for weather and climate prediction (2016; Figure 2-8). We identified strong positive (negative) AO years based on values higher (lower) than 0.5 (-0.5). Positive AO years were; 1967, 1989, 1990, 1994 and 2011. Negative AO years were 1958, 1960, 1963, 1965, 1966, 1968, 1969, 1980, 1985, 1987, 1996, 2010. We find that increased temperatures in both winter and summer months during the positive phase of the AO (

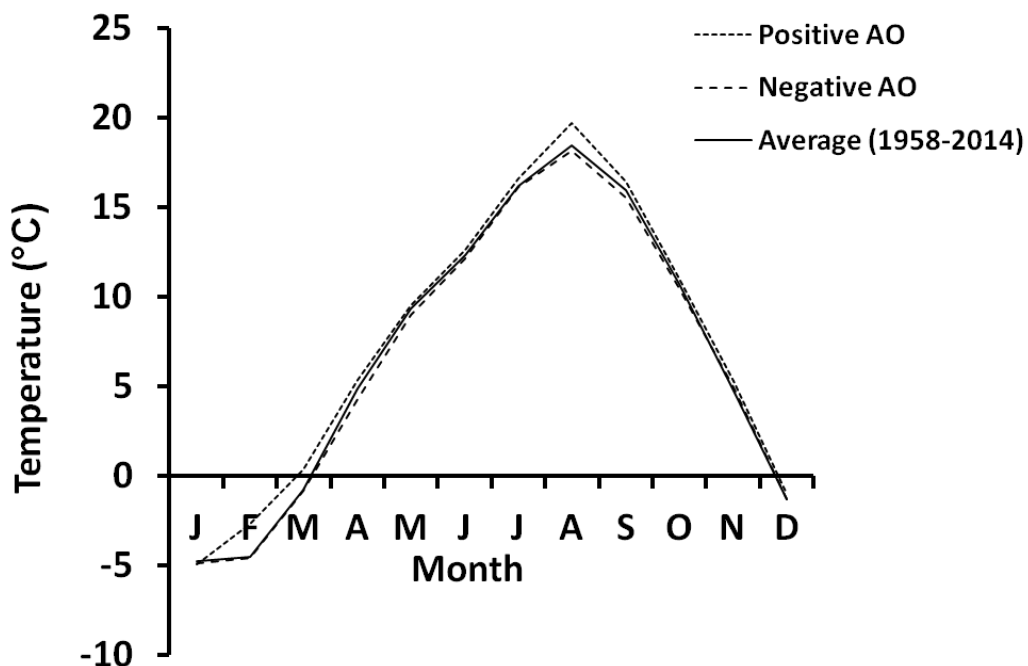


Figure 2-9). Annual temperatures are 0.7°C (0.1°) warmer (cooler) in positive (negative) AO years. Pronounced temperature variations were found in February and August. In August, temperatures were on average 1.2°C (0.4°C) warmer (colder) during the positive (negative) phase of the AO. In February, temperatures were 1.8°C warmer than average. The influence of the AO on rainfall is presented in (Figure 2-10). We find that annual rainfall increases (decreases) during the positive (negative) phase of the AO. For example during positive (negative) AO years, rainfall was 1771mm (1675mm) compared to the average of 1723mm. Rainfall during the positive phase of the AO is greatly increased in September, with 404mm of rainfall during this month compared to the average of 249mm. The influence of the AO on snowfall at this site is presented in Figure 2-11. We find that the negative (positive) phase of the AO results in increased (decreased) snowfall amount (Figure 2-11).

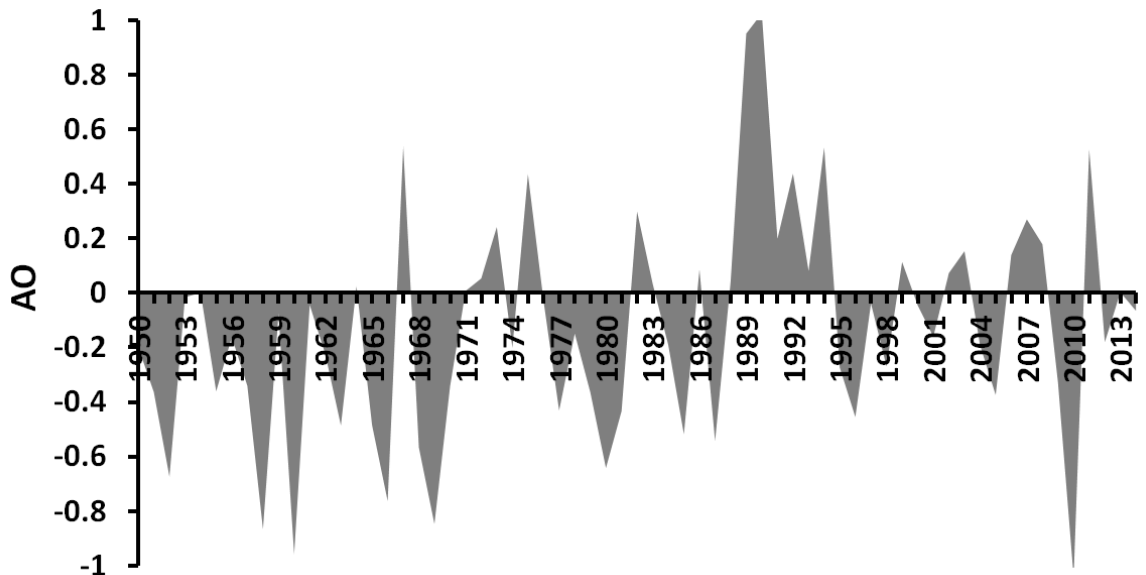


Figure 2-8: Variations in the phase of the AO since 1950 from from NOAA's Centre for weather and climate prediction (2016).

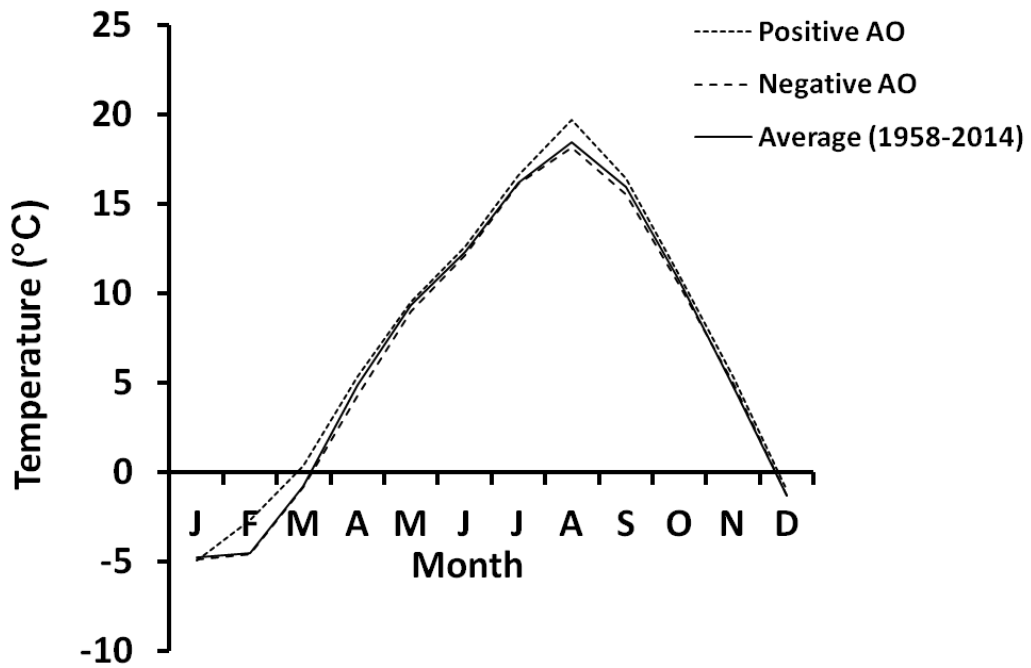


Figure 2-9: Monthly temperature averages during strong positive (small dashed line) and negative (large dashed line) AO years compared with average (1958-2014) monthly temperature values

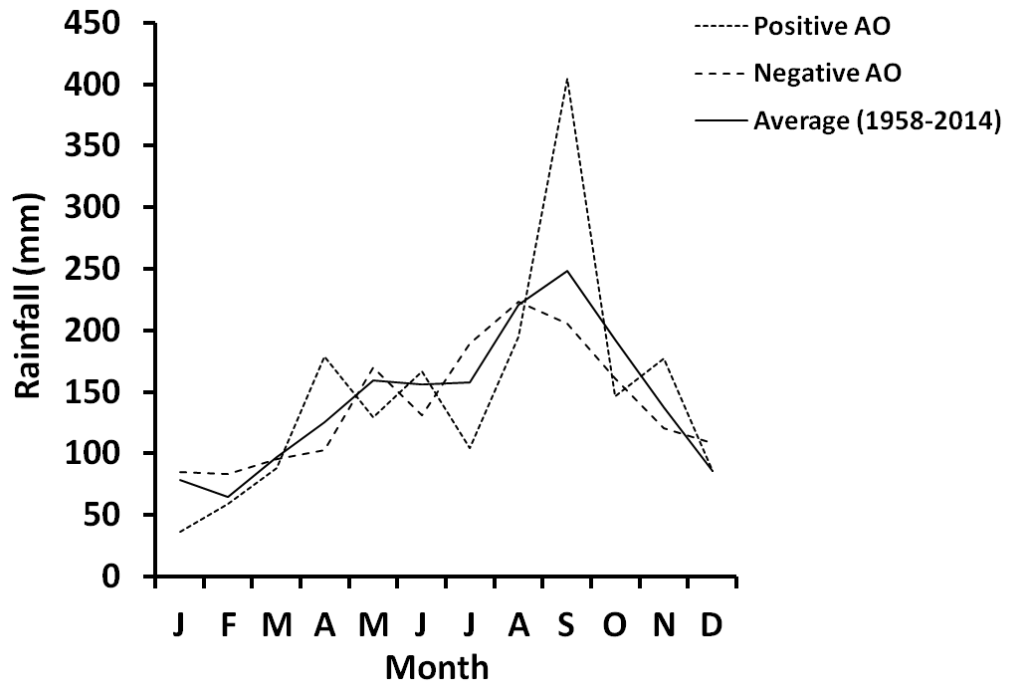


Figure 2-10: Monthly rainfall averages during strong positive (small dashed line) and negative (large dashed line) AO years compared with average (1958-2014) monthly rainfall values.

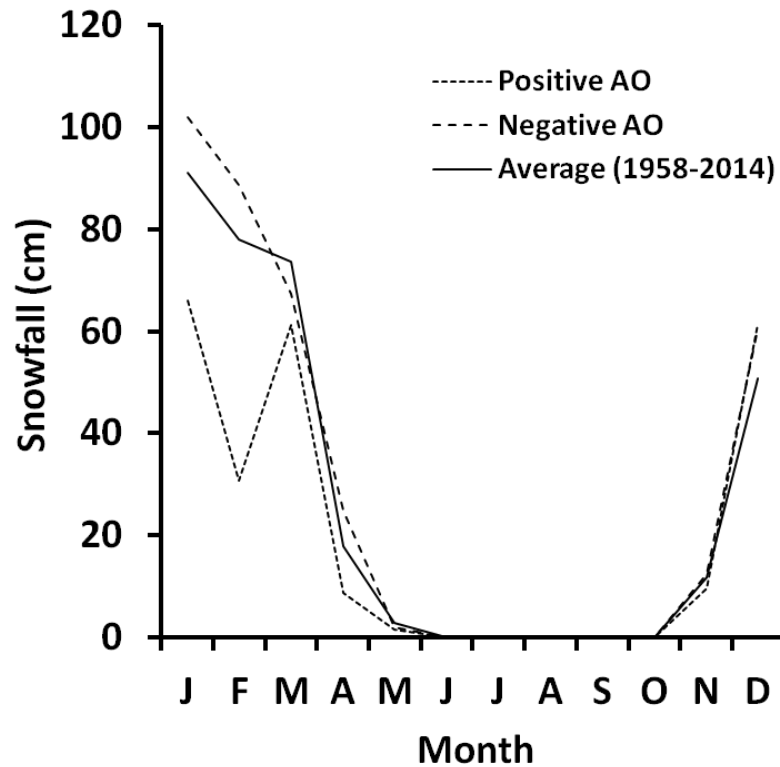


Figure 2-11: Monthly snowfall averages during strong positive (small dashed line) and negative (large dashed line) AO years compared with average (1958-2014) monthly snowfall values. No snowfall occurs in June, July, August and September.

2.2.2.1 AO and the EASM

In section 1.2.1, it was identified that the intensification of the EASM/weakening of the EAWM results in increased rainfall in June (Baiu) and August and September (Shurin). We find that during the positive phase of the AO, rainfall increased in June and September (Figure 2-10), suggesting that the positive phase of the AO has a positive influence on the intensity of the EASM in Hokkaido. Previous studies have also found a connection between EASM intensity and the positive phase of the AO (e.g. Gong and Ho, 2003). The positive phase of the AO influences the intensity of the NPSH as well as the position of the East Asian subtropical jet (EASJ), which in turn influences the EASM. During the positive phase of the AO, the EASJ migrates northwards, resulting in a strong EASM (Lee and Park, 2015). The EASJ is usually located around $\sim 40^{\circ}\text{N}$ during summer (Lake Toyoni is located at 42°N) (Figure 2-2). However, during years with positive AO values, the EASJ is located to $\sim 45^{\circ}\text{N}$ (Gong and Ho, 2003).

2.2.2.2 AO and the EAWM

Strong (weak) EAWM years are associated with lower (higher) winter temperatures, decreased (increased) rainfall and increased (decreased) snowfall. We find that the positive phase of the AO results in increased winter temperatures, increased rainfall and a decrease in snowfall suggesting that the positive phase of the AO weakens the EAWM. Previous studies have suggested that the negative AO has strong influence on intensifying the EAWM. We find that the negative phase of the AO results in a decrease in rainfall and increased snowfall. However, winter temperature was unaffected by the negative phase of the AO. This suggests a potential influence of the negative phase of the AO on the strengthening of the EAWM.

The negative phase of the AO influences the EAWM due to its association with the westerly jet and the SibH. When the AO is in its negative phase there is high pressure in the high latitudes and low pressure in the lower latitudes resulting in a advection of polar air mass to more southerly locations (Hurrell, 1995, Thompson and Wallace, 1998). The westerly jet transports this cold air from the arctic region to mid-latitude East Asia, resulting in colder winters and a stronger EAWM (Jhun and Lee, 2004b). An increase in cold air-mass in Asia increases snow and ice cover extent. Increased snow and ice also increases the albedo, reduces the amount of solar radiation absorbed and lowers air temperatures, creating an enhanced SibH, which refers to the semi-permanent pressure system that accumulates cold, dry air in northeastern Siberia. The AO therefore positively influences the SibH (Gong et al., 2001), which in turn intensifies the EAWM (Ding, 1990, Zhang et al., 1997, Wu et al., 2006a).

2.2.2.3 AO and the Westerlies

The Westerlies are a global wind pattern that transport cold dry air-mass across Eurasia to Japan (Fukusawa, 1999). The air-mass originates from the Atlantic Ocean. The annual cycle of the Westerlies, described by Kuang and Zhang (2005) and Lim and Matsumoto (2008), shows that the Westerlies strongly influence the study site in July during their northward migration and in September during their southward migration. Variations in the Westerlies are mainly related to changes in the North Atlantic Oscillation (NAO) and the AO (Hurrell et al., 2003).

In order to investigate the influence of the Westerlies at our study site, we compared average (1958-2014) temperature and rainfall data from Hiroo weather station to temperature and rainfall data from positive AO years (

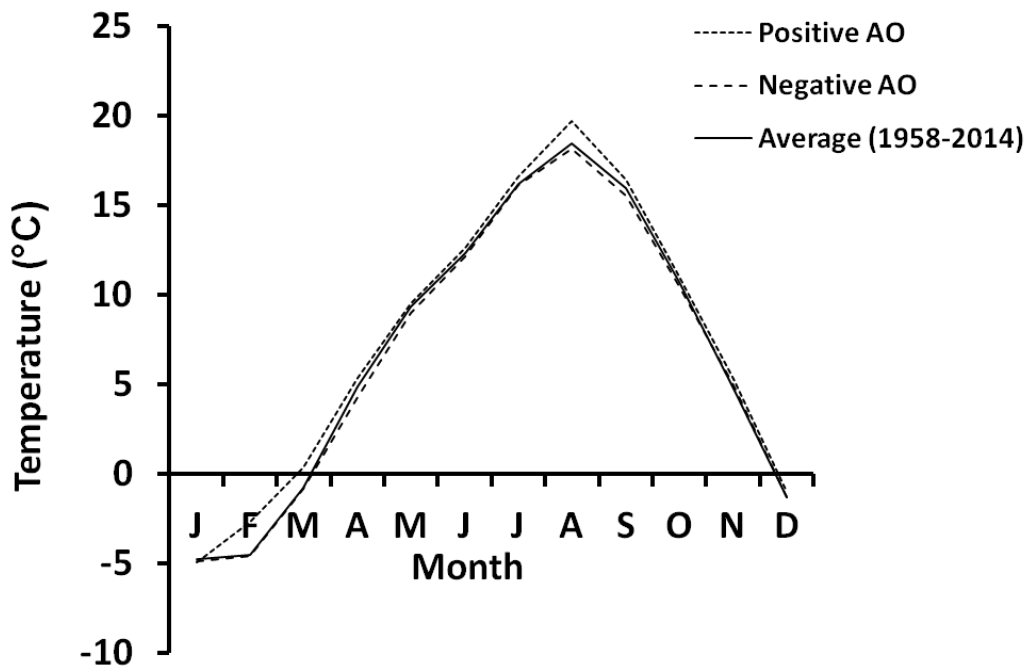


Figure 2-9 and Figure 2-10). Significantly, we found that in positive AO years, rainfall in July, when the Westerlies significantly influence our site, is reduced (Figure 2-10). The NPSH is also enhanced by intensive Westerlies (Mishima et al., 2010) and as a result rainfall during August and September is enhanced when the Westerlies intensify (during positive AO years) (Figure 2-10). The intensification of the Westerlies therefore has a strong influence on the precipitation in Hokkaido, with a reduction in July during the northward migration of the Westerlies and an increase in September during the southward migration of the Westerlies.

2.2.3 Pacific Decadal Oscillation (PDO)

Another teleconnection known to significantly influence Hokkaido is the PDO (Tsuji et al., 2008). The PDO is a long-lived ENSO-like pattern of climate variability in the North Pacific (Mantua and Hare, 2002) (Figure 2-12). The spatial distribution is similar to ENSO except the PDO can persist for several decades in comparison to a single year with ENSO. During a positive (negative) PDO mode, warmer (colder) conditions prevail in the eastern side of the Pacific Ocean (e.g. USA) and colder (warmer) temperatures are experienced in the

western side of the Pacific Ocean (e.g. Asia) (Zhang et al., 1998, Mantua and Hare, 2002).

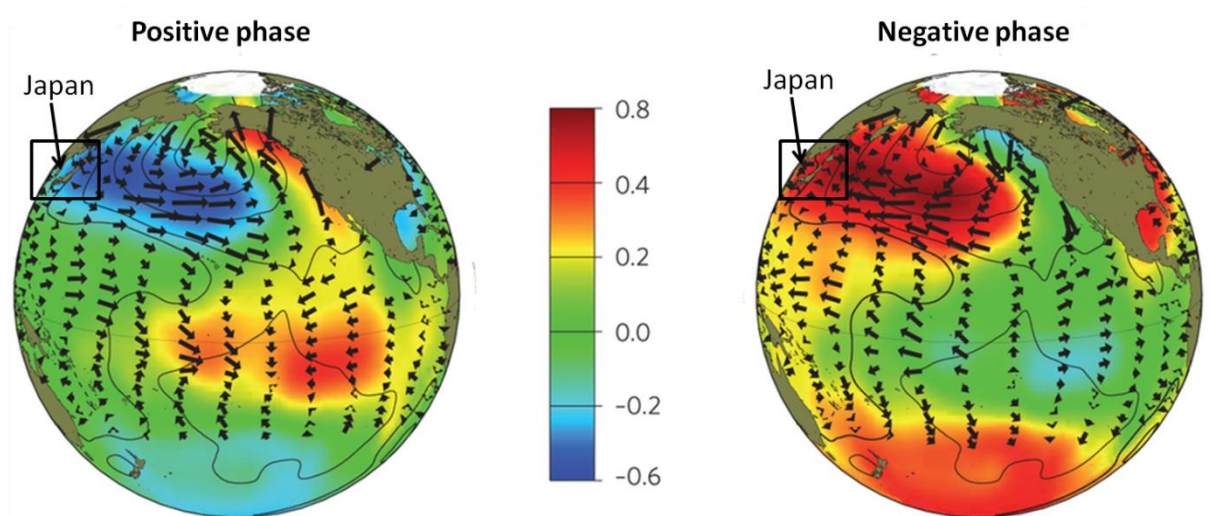


Figure 2-12: sea surface temperature differences during the positive and negative phase of the PDO (Figure adapted from; Goddard, 2014)

The variations in the phase of the PDO since 1990AD have been reported by Mantua et al. (1997) using observed Pacific sea surface temperature (SST) and SLP patterns. Notably, during the time period of weather station data (1958-present), negative PDO regimes prevailed between 1960 and 1976 and positive PDO regimes prevailed between 1977 and 1988. We find that during years with negative (positive) PDO values, temperature is 6.6°C (6.2°C) compared to the average (1958-2014) of 6.8°C. Notably, winter temperatures are lower during the positive phase of the PDO, for example, in February the temperature is -6°C compared to the average -4.5°C (Figure 2-14). Precipitation during the negative (positive) phase of the PDO increases (decreases) to 1743mm (1538mm) compared to the average (1958-2014) of 1723mm (Figure 2-15). The negative phase of the PDO has increased precipitation in June and September (Figure 2-15). The positive phase, on the other hand, has slightly increased precipitation in August (Figure 2-15). During years with negative (positive) PDO values, snowfall is 321.7cm (335.2cm) compared to the average (1958-2014) of 318.9cm. Snowfall increases in February during the negative phase of the PDO, whereas snowfall increased in March during the positive phase of the PDO (Figure 2-16).

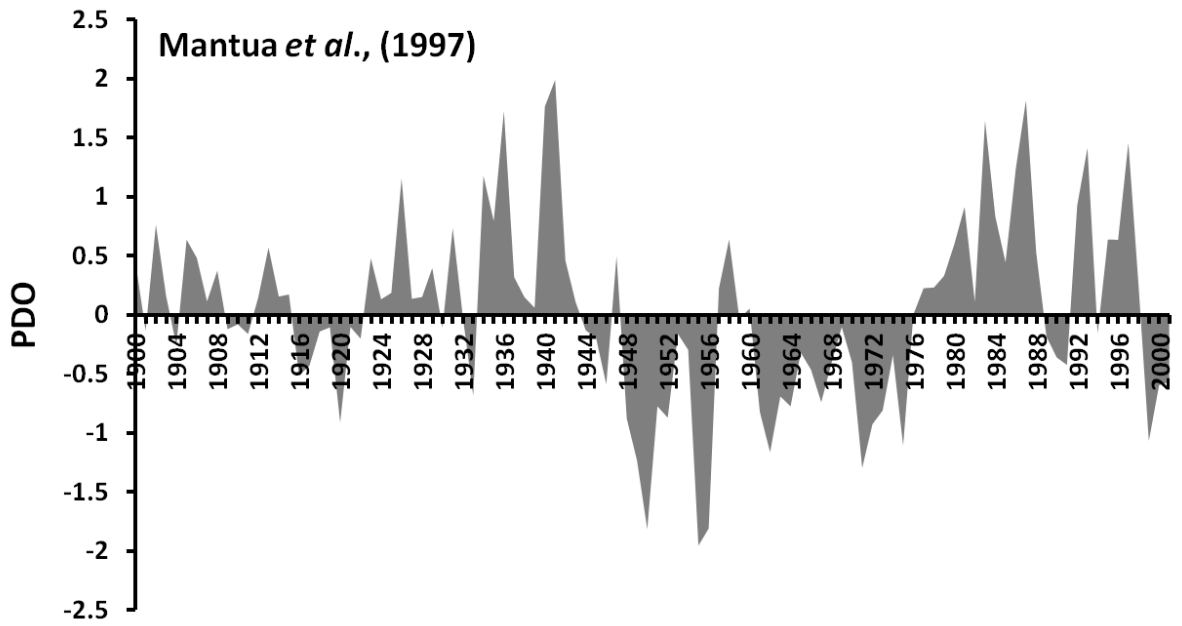


Figure 2-13: Variations in the phase of the PDO since 1990 by Mantua et al.,(1997).

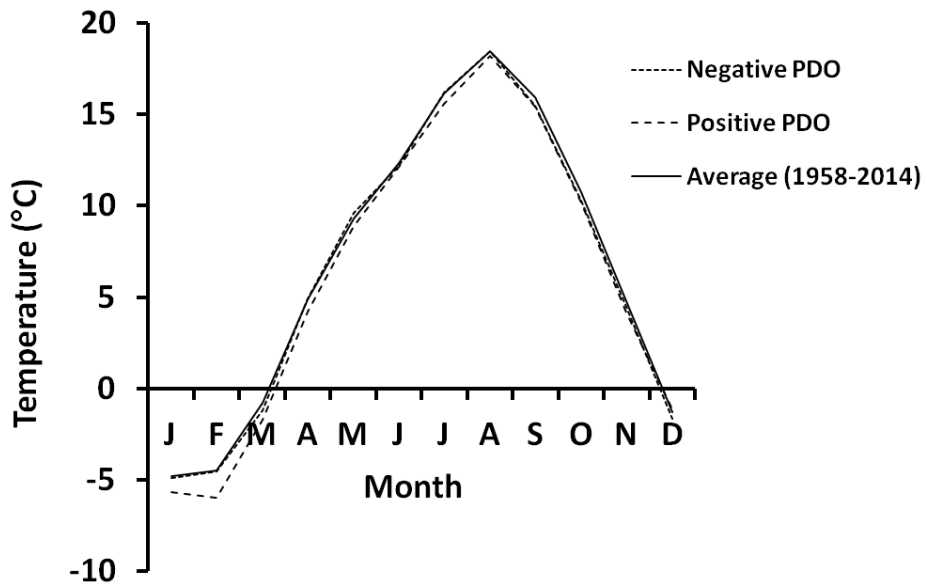


Figure 2-14: Monthly temperature averages during negative (small dashed line) and positive (large dashed line) PDO years compared with average (1958-2014) monthly temperature values (solid line).

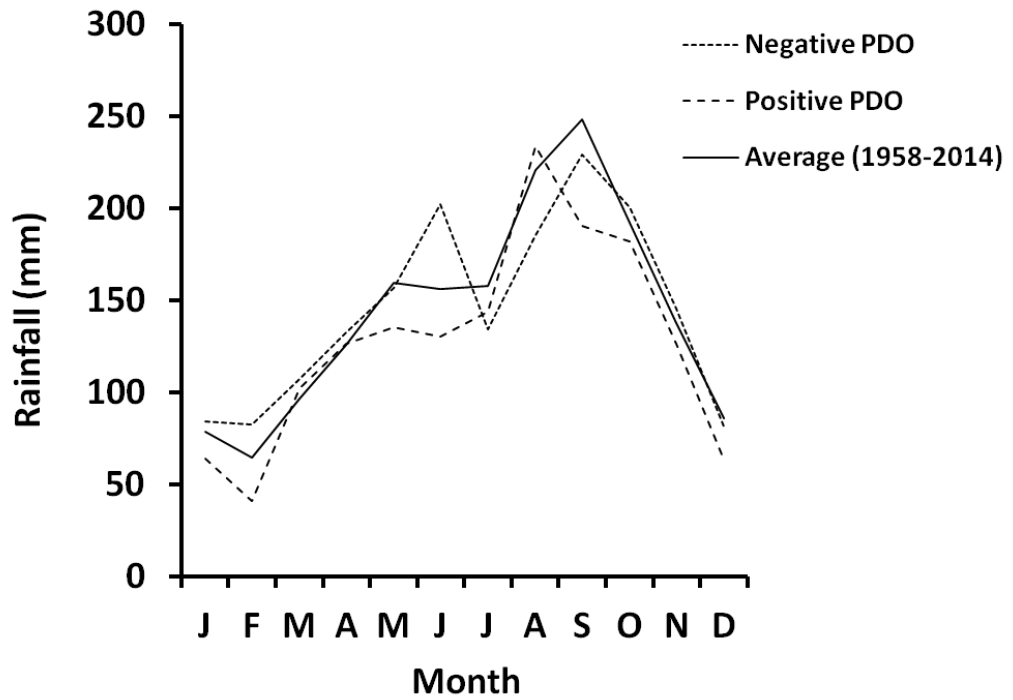


Figure 2-15: Monthly precipitation averages during negative (small dashed line) and positive (large dashed line) PDO years compared with average (1958-2014) monthly precipitation values (solid line).

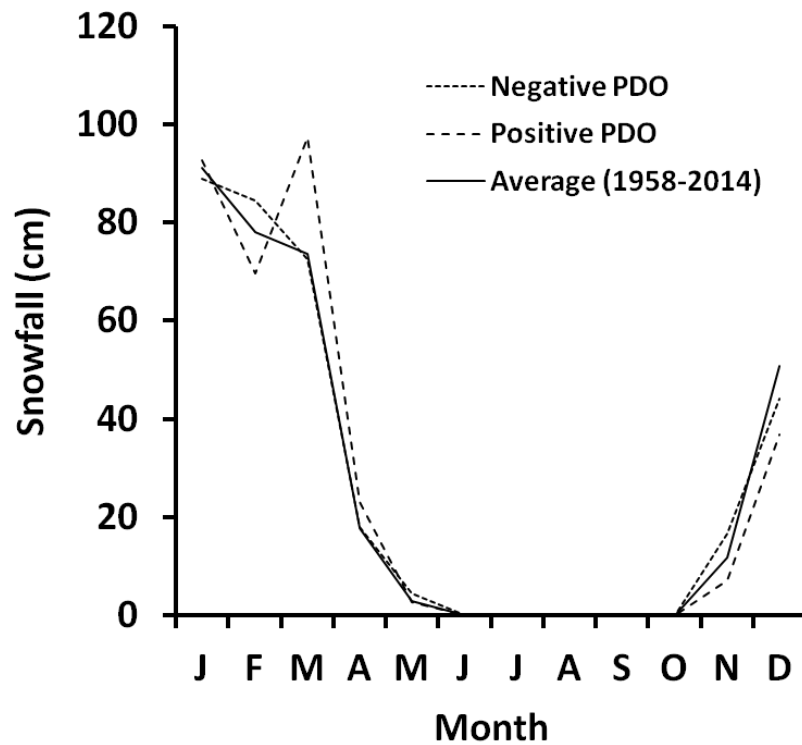


Figure 2-16: Monthly snowfall averages during negative (small dashed line) and positive (large dashed line) PDO years compared with average (1958-2014) monthly snowfall values (solid line).

2.2.3.1 PDO and the EASM

When the EASM is enhanced in this region, we find that EASM-precipitation in June (Baiu rainfall) increases. Although the highest precipitation occurs in September, although this is slightly lower than average (1958-2014) values. This suggests that the negative phase of the PDO has a positive influence on the EASM in this region. However, it is noteworthy that precipitation in August was enhanced during the positive phase of the PDO. This suggests that the positive phase of the PDO may also have an influence on the EASM during the Shurin rainfall (late summer/autumn).

The phase of the PDO has a strong influence on the EASM through its influence on the position of the NPSH. During positive phase of the PDO, the summer monsoon is weak (less rainfall), and the strong NPSH is located southward (Gong and He, 2002). Within Hokkaido, Tsuji et al. (2008) also found that relative humidity, a proxy for the EASM, increased when the PDO was in its negative phase due to the intensification of the NPSH.

2.2.3.2 PDO and the EAWM

When the EAWM is enhanced at our site, we find that temperature (Figure 2-5) and precipitation (Figure 2-6) is lower and there is increased snowfall in March (Figure 2-7) at our site. Based on these findings, the positive phase of the PDO appears to have an influence on the intensity of the EAWM at our site. During the positive phase of the PDO, we find that temperatures are lower in winter, precipitation decreases and snowfall increases in March, suggesting that the positive phase of the PDO has a strong influence on the EAWM in this region.

2.2.4 ENSO

An El Niño (La Niña) event is a phenomenon in which SSTs are higher (lower) than normal across a wide area from the centre of the equatorial Pacific to the region off the coast of Peru for a period of between half a year and 1.5 years. El Niño and La Niña events occur once every few years and have an impact on global atmospheric and weather conditions.

The prominent El Niño and La Niña episodes in the tropical Pacific are defined using 3-month running mean Nino-3.4 SST anomalies and the following two criteria. (a) The maximum (minimum) SST anomaly exceeds one standard deviation (about 1.0°C), and (b) SST anomalies exceeding 0.5°C persist for at least 8 months. According to these criteria, seven major El Niño (1958, 1965, 1972, 1982/83, 1986/87, 1991/92, 1997/98) and five major La Niña (1970/71, 1973/74, 1975/76, 1984/85, and 1988/89) episodes are identified for the period from 1958 to 1998. (after Wang et al., 2000).

At our site, we find although annual averages are slightly lower during La Niña years, summer temperatures are above-average during La Niña years and below-average during El Niño years. For example during La Niña (El Niño July, August and September temperatures were 16.0°C (15.7°C), 18.8°C (17.8°C) and 15.2°C (15.6°C), respectively (Figure 2-17). These findings are also supported by a tree-ring temperature reconstruction in Hokkaido by Davi et al. (2002). The authors found that the temperature reconstruction was significantly and positively correlated with ENSO; with low summer temperatures linked to El Niño and higher summer temperatures linked to La Niña episodes.

Annual precipitation amount between El Niño, La Niña and average years were very similar. Slightly higher annual precipitation values occurred during La Niña years (1727mm) and slightly lower annual precipitation values occurred during El Niño years (1717mm), compared to average values (1723mm). However, it was notable that the months of increased precipitation were different in El Niño and La Niña years. For example, during El Niño years, rainfall increases in July, August and September from average (1958-2014) value of 158mm, 221mm and 249mm to 177mm, 254mm and 324mm, respectively (Figure 2-18). It is notable that increased precipitation in September is also associated with typhoon season in Japan (Lee, 1974, Nogami et al., 1980), suggesting that El Niño conditions influence the strength and/or occurrences of typhoons in this region. Previous studies have also found a connection between the strengthening of typhoons in Japan during El Niño years (Woodruff et al., 2009). Precipitation in January and February also increased during El Niño years. However, precipitation during spring and early summer is lower. We also found that snowfall increased in January and February, and decreased in March during El Niño years (Figure 2-18). During La Niña years, on the other hand, we found that precipitation was

increased in March, June and October and was lower in the remaining months (Figure 2-18). Annual snowfall amount was lower during El Niño years (306.4cm) than average years (318.9cm), however there was notably higher values in January and February (Figure 2-19). Annual snowfall amount was similar between La Niña years (318.5cm) and average years (318.9cm), however higher values were noted in March (Figure 2-19).

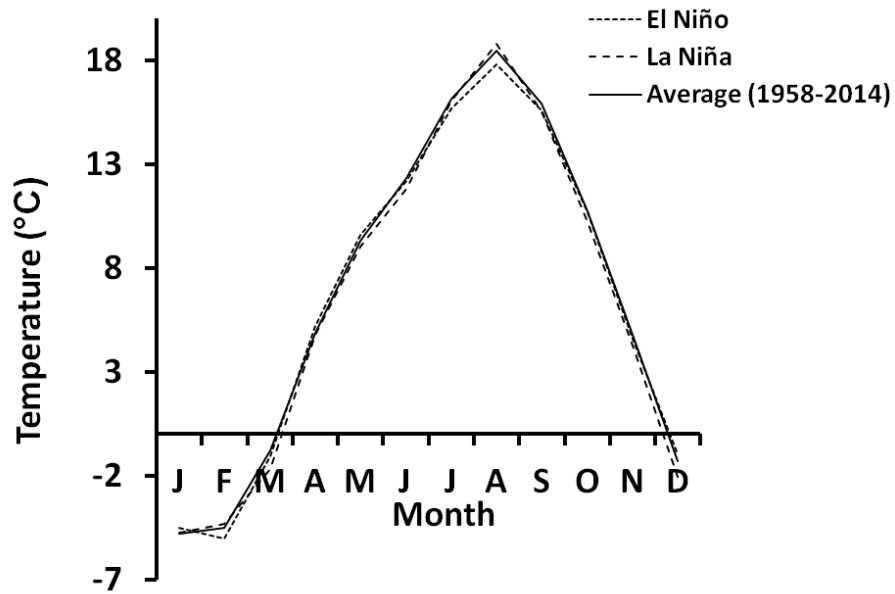


Figure 2-17: Monthly temperature averages during El Niño (small dashed line) and La Niña (large dashed line) years compared with average (1958-2014) monthly temperature values (solid line).

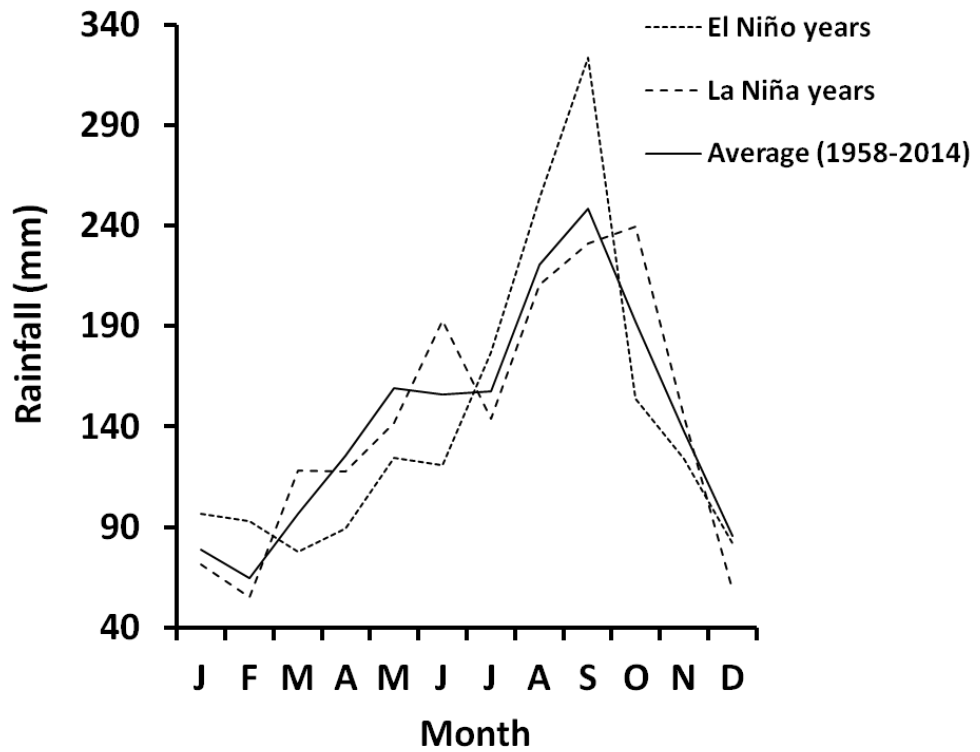


Figure 2-18: Monthly precipitation averages during El Niño (small dashed line) and La Niña (large dashed line) years compared with average (1958-2014) monthly precipitation values (solid line).

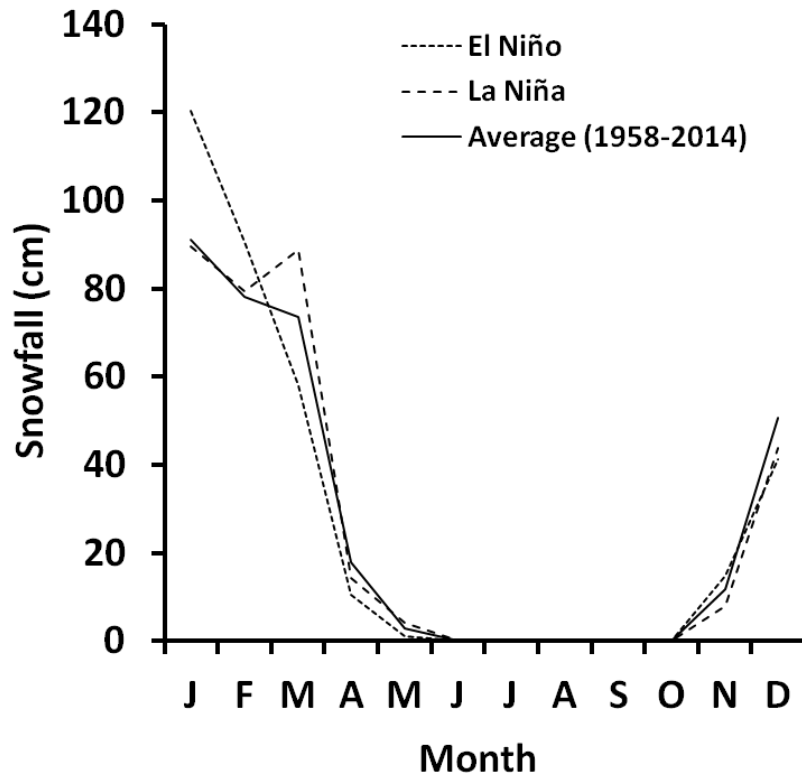


Figure 2-19: Monthly snowfall averages during El Niño (small dashed line) and La Niña (large dashed line) years compared with average (1958-2014) monthly snowfall values (solid line).

2.2.4.1 ENSO and the EASM

El Niño has been identified as a strong influence on the intensity of the EASM (e.g. Zhang et al., 1996, Wang et al., 2003, Hong et al., 2005). However, classifying EASM intensity simply according to strong El Niño years is not meaningful because the influence of El Niño on the intensity of the EASM occurs in the summer after El Niño reaches its mature phase, rather than the actual year when El Niño develops (Wang et al., 2001). A suggested reason for this is due to the westward movement of the western NPSH in the summer following the mature phase of El Niño, which in turn enhances the EASM (Wang et al., 2001). We find that when we separate El Niño developing years (e.g., 1965, 1968, 1972, 1976, 1982, 1986, and 1997; after Wang and Chan, 2002) and the years after the mature phase of El Niño (e.g., 1970, 1983, 1992, 1995, and 1998; after Wang and Chan, 2002) there is a clear difference in the intensity of the EASM (Figure 2-20). In the years following the mature phase of El Niño, we find that precipitation at our site increases in June (Baiu precipitation) and August (Shurin precipitation); which is associated with EASM precipitation. However, in El Niño developing years, we find that precipitation is lower in June and August. Temperature also slightly increased in August and September during the summer following the mature phase of El Niño compared to El Niño developing years. In August and September, temperature was 18°C (17.8°C) and 15.6°C (15.4°C), respectively during the mature phase and developing phase of El Niño. This suggests that during El Niño developing years, El Niño has no influence on the EASM intensity, however, in the summer following the mature phase of El Niño, the EASM intensity increases.

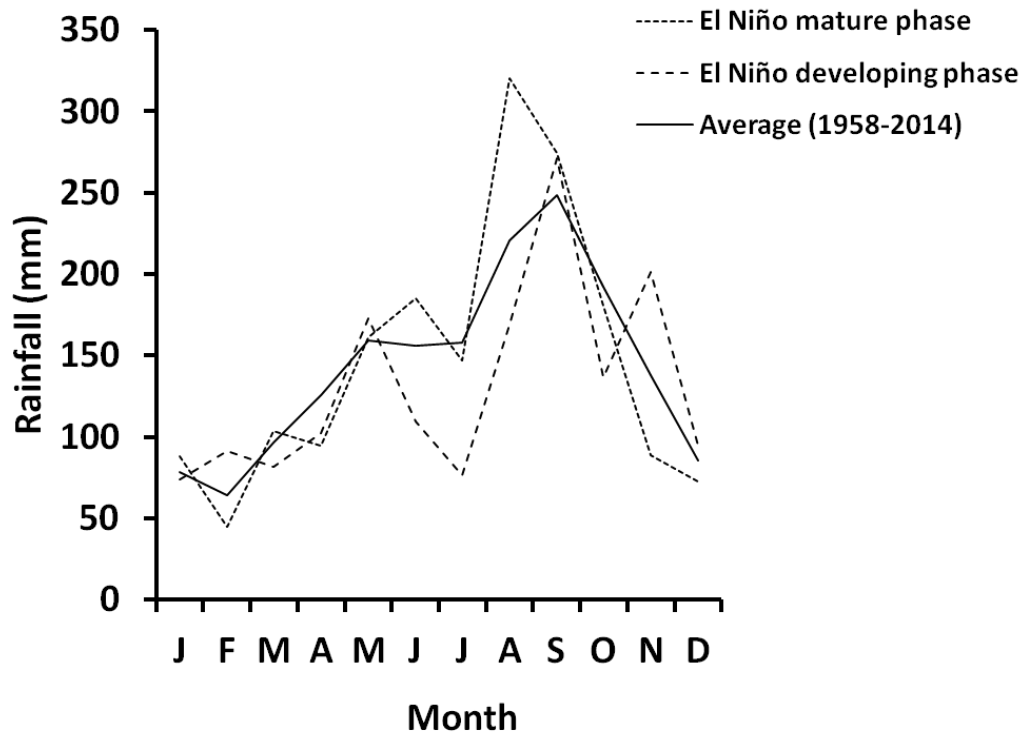


Figure 2-20: Monthly precipitation averages during the summer following El Niño (small dashed line) and El Niño developing (large dashed line) years compared with average (1958-2014) monthly precipitation values (solid line).

2.2.4.2 ENSO and the EAWM

The EAWM is weak during El Niño years and strong during La Niña years (Tomita and Yasunari, 1996, Zhang et al., 1996, Chen et al., 2000, Chen et al., 2013, Chen et al., 2014, Wang and Chen, 2014). We identified that a strong EAWM results in increased snowfall, particularly during the month of March (Figure 2-7). We find that during La Niña years snowfall in March increases, suggesting that the EAWM is stronger during La Niña years. A suggested reason for La Niña positively influencing the EAWM is due to the correlation between ENSO and the inter-annual variation of winter northerlies and cold surges near the South China Sea (Zhang et al., 1997). La Niña conditions result in cooling over the equatorial Eastern Pacific, however the western Pacific is not influenced by this cooling and therefore remains warm during La Niña conditions (Chen et al., 2000) During La Niña events, the occurrence of East Asian cold surges increases and also the strength of the northerlies increases (Zhang et al., 1997), this triggers a decrease in temperature in East Asia. As a result, there is a large land-sea thermal contrast during La Niña conditions which results in a movement from the Asian continent towards Japan.

2.2.5 Summary

Table 2-1: Summary table detailing the average temperature, precipitation and snowfall change during strong/weak EASM/EAWM years, the positive and negative phase of the AO/NAO and the PDO and also during El Niño and La Niña years. Average annual values between 1958 and 2014 provided in bold.

	Temperature change	Error	Precipitation change	Error	Snowfall change	Error
Average (1958-2014)	6.8°C	±0.6°C	1723mm	±303mm	319cm	±88mm
Strong EASM	No change		↑126 mm	±343mm		
Weak EASM	↓0.3°C	±0.7°C	↓115 mm	±100mm		
Strong EAWM	↓0.5°C	±0.6°C	↓237 mm	±277mm	↑8cm	±52cm
Weak EAWM	↑0.2°C	±0.3°C	↑114 mm	±282mm	↓31cm	±55cm
Positive AO/NAO	↑0.7°C	±0.5°C	↑48 mm	±363mm		
Negative AO/NAO	↓0.1°C	±0.6°C	↓48mm	±297mm		
Positive PDO	↓0.6°C	±0.3°C	↓185mm	±268mm		
Negative PDO	↓0.2°C	±0.5°C	↑ 20mm	±270mm		
El Nino	No change		↓6mm	±360mm	↓13cm	±70cm
La Nina	↓0.2°C	±0.5°C	↑ 4mm	±404mm	No change	

Study site and methods

3.1 Location

3.1.1 Lake survey

In the summer of 2008, surface sediment samples were collected from eight lakes in Hokkaido, Japan (Table 1) using an Ekman grab sampler and Kajak corer. Following the detection of alkenones in surface sediments of Lake Toyoni (Table 1), this location was chosen for palaeo-climate investigations.

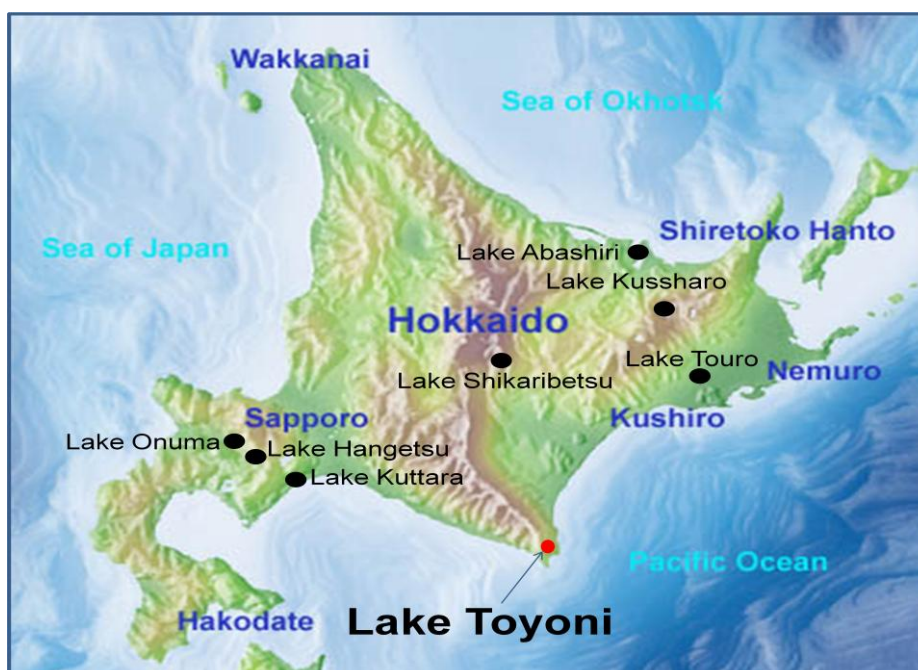


Figure 3-1: Location of lakes surveyed in 2008

Table 3-1: Lakes surveyed in Hokkaido for alkenones in 2008.

Lake Name	Lat long	Elevation (m)	Depth (m)	Temp (°C)	pH	Salinity (g/L)	Alkenones (Detected/not-detected)
Lake Abashiri	N: 43°58'20.9'' E:144°10'36.5''	0	16.1	20.6	8.7	2.8	Not-detected
Lake Hangetsu	N: 42°50.952'' E: 140°45.216''	295	17	18	8.3	0	Not-detected
Lake Kussharo	N: 43°39'10.6'' E:144°19'24.9''	127	42.3	14.5	7.8	0.1	Not-detected
Lake Kuttara	N: 42°29'967'' E: 141°10'945''	297	145	18	7.8	0	Not-detected
Lake Ohnuma	N: 42°53'47.6'' E:140°37'02.3''	847	14	12	7.7	0	Not-detected
Lake Shikaribetsu	N:43°16'19.15'' E:143°06'21.54'	810	98.5	15.3	8.4	0.1	Not-detected
Lake Touro	N: 43°09'02.4'' E:144°33'06.6''	25	4	20	9.4	0	Not-detected
Lake Toyoni	N: 42°05'.443' E: 143°16.226'	256	19	16	7.2	0	Detected

3.1.2 Site description

Lake Toyoni is located on Japan's northern island, Hokkaido (Figure 3-2; 42°05'N; 143°16'E) and is a small (0.3km²), dimictic freshwater (0psu) lake. Lake Toyoni is a closed-basin lake with an average water depth of 12m and a maximum water depth of 19m. The lake is ice-covered from the end of November until early April. The catchment of Lake Toyoni is densely covered in vegetation and has steep slopes surrounding the lake (Figure 3-3). The nearest local habitation is 25km from Lake Toyoni and there is a weather station located in this town (Hiroo).

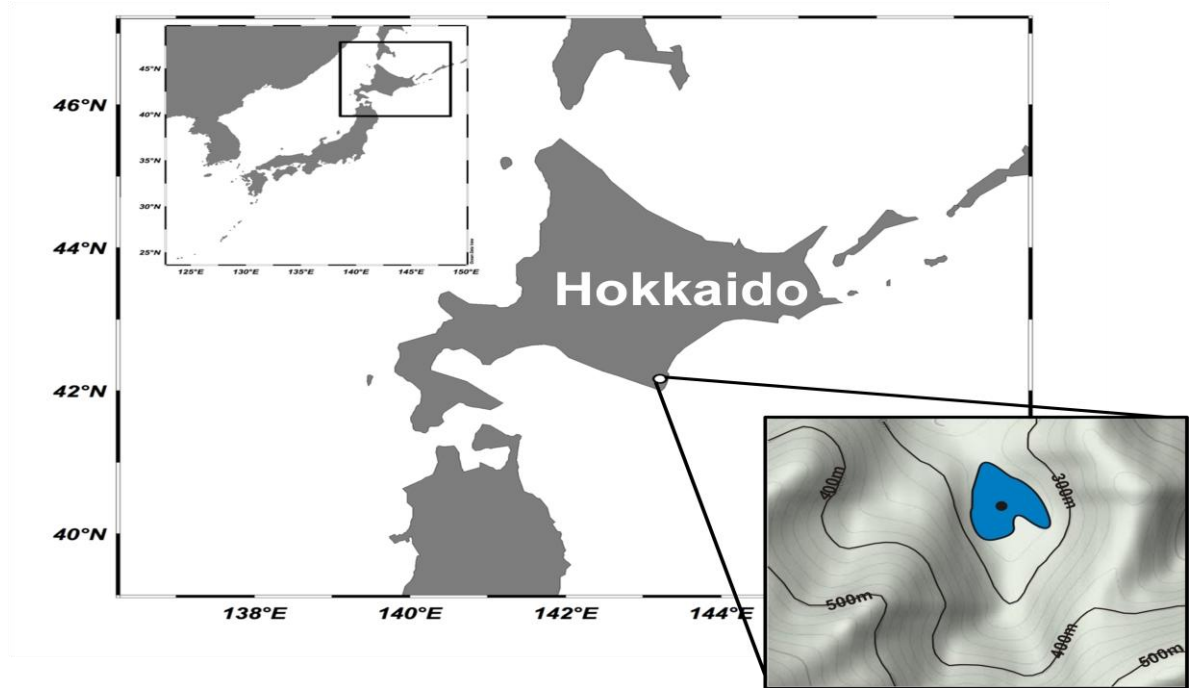


Figure 3-2: Location of Lake Toyoni, Hokkaido, Japan.



Figure 3-3: Pictures of Lake Toyoni and the catchment area.

3.1.3 Water probe data

Water probe data (temperature [°C], pH, dissolved oxygen [mg/L]) was collected from the lake on a monthly basis between September 2010 and October 2011 (during the ice-free season). Monthly temperature is presented in Figure 3-4. The data show that the water column was well mixed in April and November suggesting that the lake overturns in spring and autumn (Figure 3-4). In addition, we find that when we compare surface temperature values to the average temperature during that particular month and year (from Hiroo weather station), the surface water temperatures in Lake Toyoni corresponds to changes in air temperature (Figure 3-5; $R^2=0.97$). Small differences are due to weather station data being a monthly average and water probe data being taken on a single day. In addition, the water probe data was usually taken in the last week of every month and is therefore bias towards end of month temperatures. Monthly dissolved oxygen (mg/L) data is also presented in Figure 3-6. The bottom water of Lake Toyoni becomes hypoxic ($O_2 < 2.0 \text{ mg l}^{-1}$, (Diaz, 2001, Zimmerman and Canuel, 2000) between July and October (Figure 3-6) due to thermal stratification occurring (Figure 3-4) and a lack of mixing within the water column. Monthly pH values are presented in Figure 3-7. The pH data show that Lake Toyoni is a slightly acidic lake.

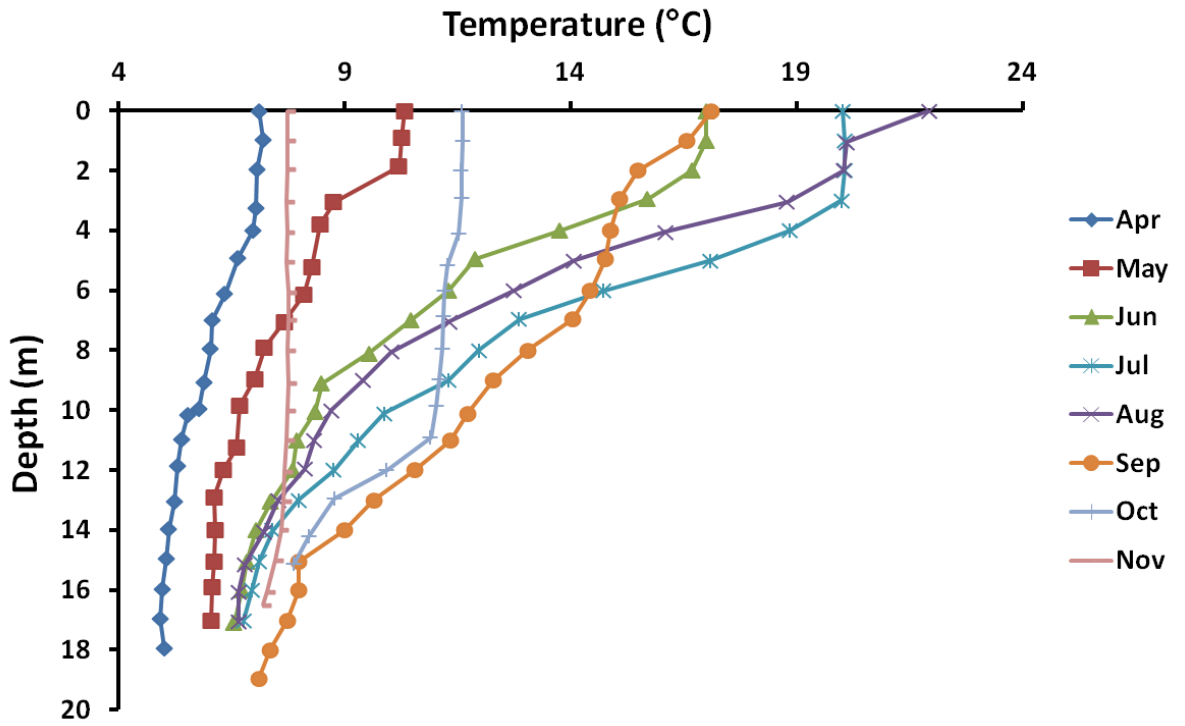


Figure 3-4: Water temperature against depth between April and November.

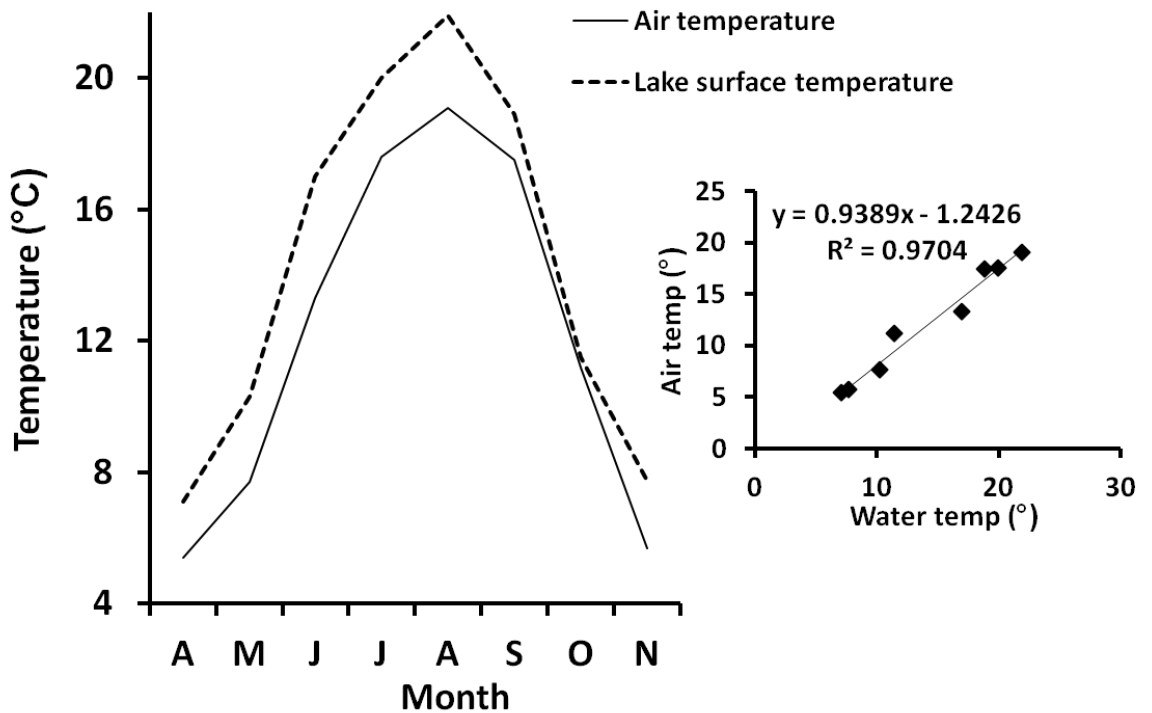


Figure 3-5: A: Comparison between surface water column temperature and air temperature. B: Scatter plot between lake surface temperature and air temperature.

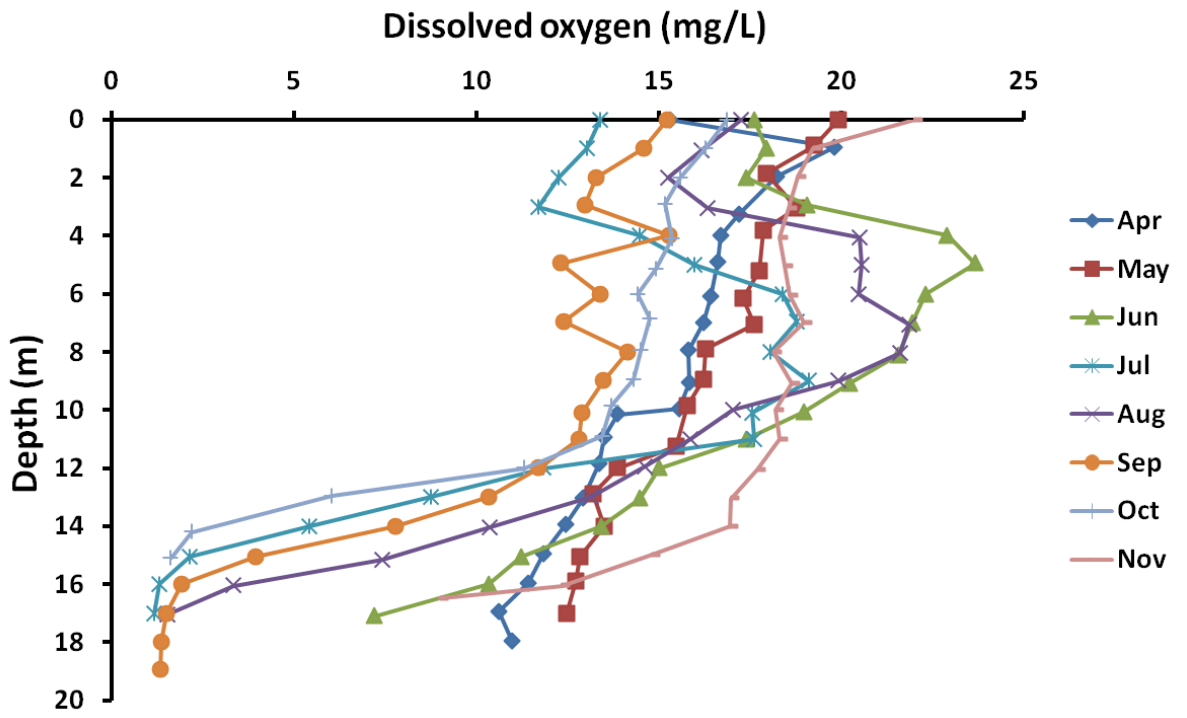


Figure 3-6: Dissolved oxygen against depth between April and November.

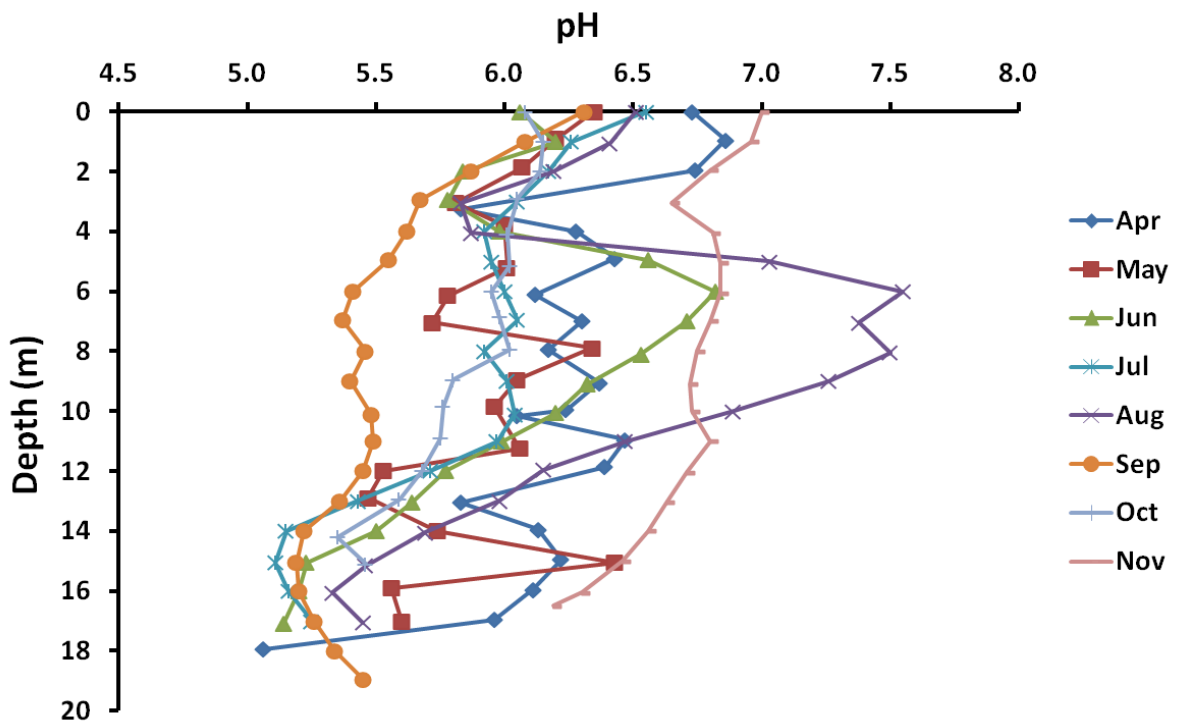


Figure 3-7: pH against depth between April and November

3.1.3.1 Geology

The majority of the catchment surrounding Lake Toyoni consists mainly of Late Cretaceous to Early Oligocene muddy turbidite of accretionary complex. The main rock types consist of alternation of sandstone and mudstone (muddy) (Figure 3-8). West of the catchment is Eocene to Oligocene migmatite plutonic rocks (Hidaka) (Figure 3-8).

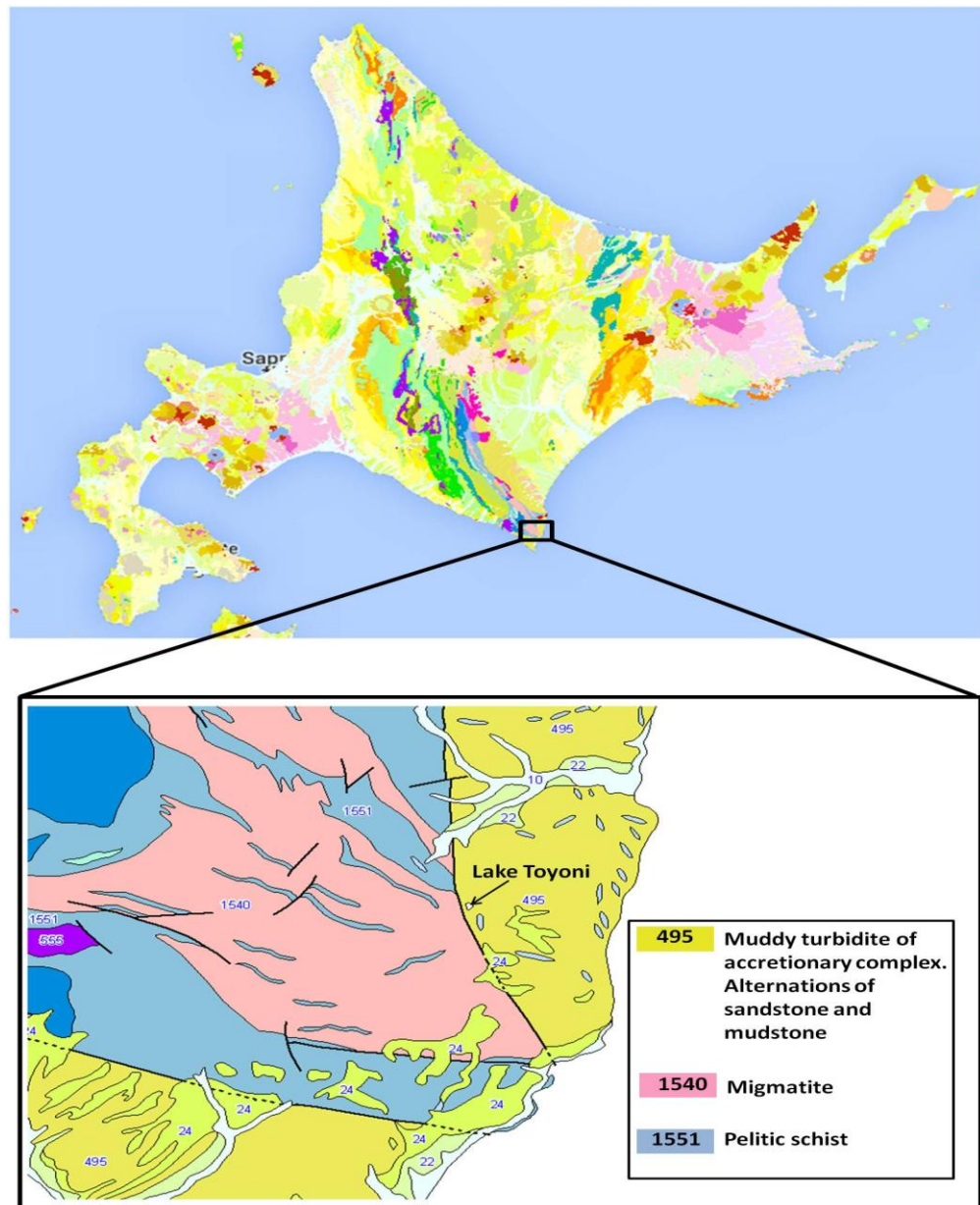


Figure 3-8: Geology of Lake Toyoni

3.2 Core collection

In July 2009, a 250cm long sediment core (TY09) (from 3 overlapping drives) was recovered from a water depth of 19m from Lake Toyoni using a platform deployed Livingstone corer. In September 2012, a 12cm long sediment core (TY11) was recovered from a water depth of 19m from Lake Toyoni using a gravity corer. The core was sub-sampled at Hokkaido University Sapporo (Japan).

3.3 Age model

TY11 was plutonium (Pu) dated (Figure 3-9) and TY09 was radiocarbon dated (Table 3-2). The cores will be discussed separate throughout the text.

3.3.1 TY11

High-resolution (every 0.5cm) Plutonium (Pu) dating on sediment core TY11 was completed in February 2012 at the department of chemistry and biochemistry, Northern Arizona University by Michael E. Ketterer. The sediment intervals were processed in order to chemically isolate Pu fractions in aqueous ammonium oxalate solution suitable for measurements by quadrupole inductively coupled plasma-mass spectrometry (ICP-MS). A Thermo X Series II instrument equipped with a ESI Scientific APEX HF high-efficiency sample introduction system with concentric PFA nebulizer was used. The chemical procedures for isolation of Pu followed Ketterer et al. (2004). Sediment samples were dry-ashed at 600°C for 16 hours to remove organic matter, then mixed with a ^{242}Pu spike (NIST 4334g solution, 0.00468Bq or 32.03 picograms) and 5mL of 16 mol Nitric acid (HNO_3) (Ketterer et al., 2004). Samples were leached at 80°C for 16 hours, then diluted to 10mL, filtered through a cotton wool plug, and then treated with aqueous Ferrous Sulfate (FeSO_4) and Sodium Nitrite (NaNO_2) to convert Pu to Pu(IV) (Ketterer et al., 2004). The Pu was retained on a 30mg TEVA resin column (bulk resin from Eichrom, Lisle, IL, USA); the columns were rinsed a series of 2M Nitric acid (HNO_3) and 8 mol Hydrogen Chloride (HCl) solutions to remove matrix elements, Uranium (U) and Thorium (Th). Pu was eluted with water (H_2O) and 0.05M aqueous ammonium oxalate to produce 1.4mL aqueous fractions that were analysed directly by ICPMS. The results show TY11 exhibits a clear $^{239+240}\text{Pu}$ activity maximum in the 2.0 cm interval (Figure 3-8), which is associated with

atmospheric bomb testing between 1963-1964AD. The ratio results all agree well with the known $^{240}\text{Pu}/^{239}\text{Pu}$ of 0.180 ± 0.014 for Pu of stratospheric fallout origin deposited in the mid-latitude regions of the Northern Hemisphere (Kelley et al., 1999). Therefore an age model is not available for TY11 as we only have one age at 2cm (1963). This core will therefore be discussed against depth, rather than age.

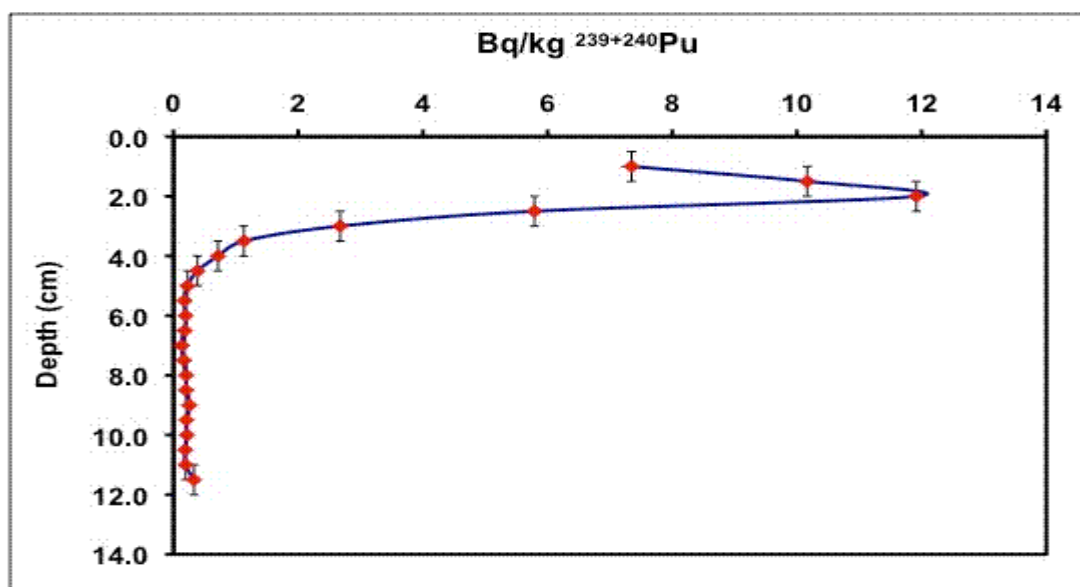


Figure 3-9: Pu dating of TY11. Quadrupole inductively coupled plasma mass spectrometry has been used to rapidly establish the chronology of recent sediments from Lake Toyoni (TY11) via measurements of the activities of ^{239}Pu , ^{240}Pu , and the atom ratio $^{240}\text{Pu}/^{239}\text{Pu}$. $\text{Bq/Kg } ^{239+240}\text{Pu}$ exhibits maximum activity at 2cm horizon which is interpreted as spanning the 1963-1964AD time frame associated with atmospheric testing of nuclear weapons.

3.3.2 TY09

Five range finder ^{14}C dates from TY09 were analysed in 2010 at the National Institute for Environmental Studies (NIES), Japan (Table 2). Subsequently, three additional radiocarbon dates were completed on terrestrial plant material at the National Environmental Research Council (NERC) facility (East Kilbride), which is hosted by Scottish Universities Environmental Research Centre (SUERC). Dates were calculated using CALIB (V6.0). The age model for TY09 was reconstructed using the Heegard model (Heegard, 2005; R version 3.1.2) (Figure 3-10). Two samples were identified as outliers (16cm and 192cm). A suggested reason for the

outliers are that they were small single leaf samples and potentially there was not enough material to get an accurate date. Both samples were also analysed at a different lab, several years after the rest of the samples (except 100cm).

Table 3-2: Age model of core TY09. It is based on six ^{14}C dates of leaf samples and one bulk sediment ^{14}C date

Depth in TY09	Depth + 10cm (lost core)	Material dated	Accession #	14C age	14C age error	Age (AD)
16cm	26cm	Leaves	SUERC-55214	261	38	1689
30cm	40cm	Plant material	TERRA-102510b27	224	42	1814
70cm	80cm	Leaf	TERRA-102510b28	370	47	1637
100cm	110cm	Leaves	SUERC-55217	387	36	1563
191cm	201cm	Plant material	TERRA-102510b33	973	54	1193
192cm	202cm	leaf	SUERC-55219	604	38	1346
211cm	221cm	Leaves	TERRA-102510b34	992	54	1167
231cm	241cm	Bulk sediment	TERRA-102510b34	1175	70	990

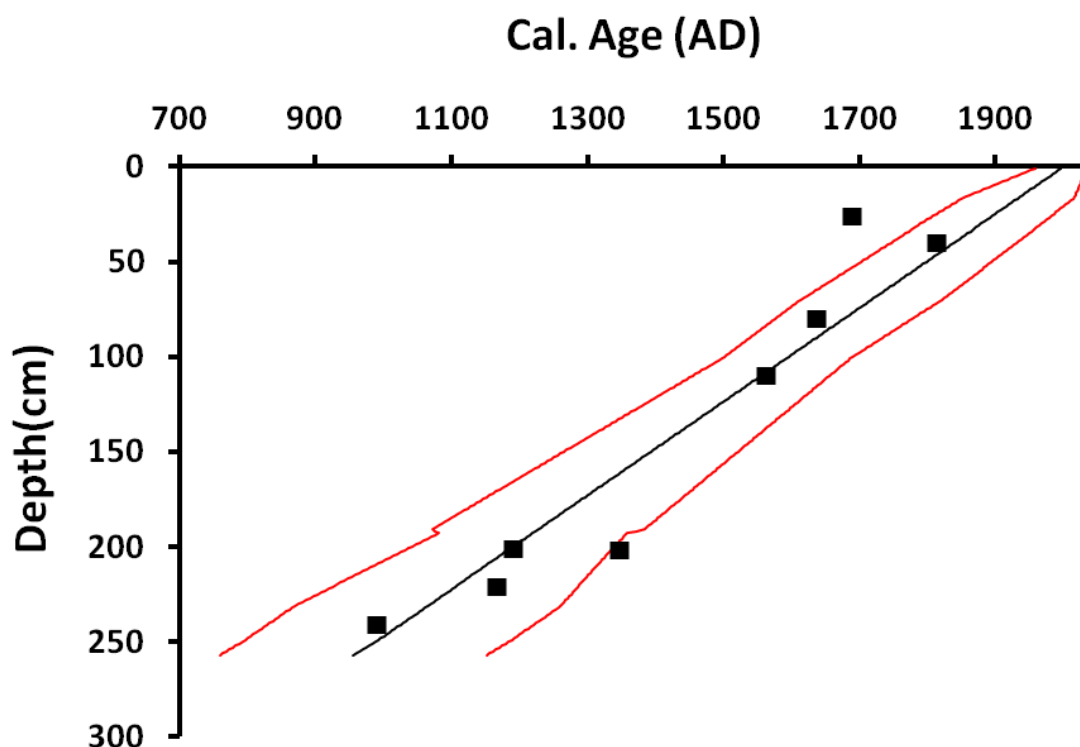


Figure 3-10: Age depth model for TY09

3.3.3 Lithological description

A stratigraphic and sedimentological description of a sediment core is important for palaeo-limnological studies. Information gathered during visual description of the cores helps to understand past environmental changes. The classification of the sediment core TY09 was divided into different units that were defined by identifying colour with a Standard Munsell soil colour chart (Munsell Colour Company, 1994) and/or structural changes along the core. The texture of the sediment was also noted, with particular reference to tephra layers and changes in grain size.

3.3.4 X-ray Fluorescence (XRF) and magnetic susceptibility (MS)

In February, 2012, the archived core (TY09) was scanned for bulk elemental composition, digitally photographed and subjected to X-ray Fluorescence (XRF) at 0.5mm resolution using an Itrax® XRF core scanner equipped with a 3 kW molybdenum target tube that can operate up to 60kV and 50mA at Aberystwyth University in collaboration with Dr. Andrew Henderson. In addition, the archived core was scanned for magnetic susceptibility (MS) using a Geotek Multisensor

Core Logger (MSCL) at 1cm resolution. MS was used in order to match the overlapping sections in sediment core TY09.

The quality of data obtained from XRF can also be affected by gaps and cracks in the sediment sequence. To account for this, sharp drops in elemental peak area integrals were detected from the stratigraphic profiles and mean standard error readings and removed from the measurement sequence before down core variations were graphically presented. To look at longer terms trends in the very highly resolved XRF dataset (0.02cm resolution), running averages have been used to smooth the XRF data to generally average out or mask very high and low values that make the signal noisy. This was achieved using Excel moving average functions. 150 sample running means were conducted to achieve decadal-resolved palaeo-climate record.

3.3.4.1 Normalising data

The XRF data was normalised to Rb (Guyard et al., 2007), a conservative element, unless otherwise stated. By normalising elements to a conservative element, background input is removed (Rothwell and Rack, 2006). Al is commonly used to normalise elemental data; however, corrections using Al could not be made due to low detection of Al.

3.3.5 Particle size analysis (PSA)

Particle size analysis took place in April 2013 at Glasgow University using a Coulter LS 230. 1.5-3.5g of sediment taken at ~4cm resolution was placed into a furnace for 8 hours at 600°C to remove organic carbon. 60ml of Calgon (pre-made using 35g Sodium Hexametaphosphate and 7g Sodium Carbonate to 1 litre of distilled water) was added to the sediment to disperse the sediment. Every sample was run 3 times and an average of the three runs was used. Samples were statistically analysed using GRADISTAT (Blott and Pye, 2001).

3.3.6 Organic C/N ratio

20mg (± 2 mg) of freeze-dried sediment was placed into a 2ml ampoule. Carbonate was removed following the adapted methodologies of Verardo et al. (1990). 0.8ml of sulphurous acid was added to the ampoule, and the vial was gently tapped to remove reaction bubbles from the sediment. The samples were then left overnight to react in a fume cupboard and transferred to a vacuum desiccator and held under vacuum for 2-3 hours to degas. Samples were then frozen and placed in freeze drier for 24 hours. The dry residue was agitated using a vortex and was placed into a 5x9mm tin capsule. These were then sealed by folding prior to loading into the auto-sampler.

Carbon and nitrogen analysis was completed using the methodologies of Roleda et al. (2013) by Dr. Richard Abell at the Scottish Association for Marine Science (SAMS). A Costech International Elemental Combustion System (ECS) 4010 with Helium ($>99.9\%$) as the carrier gas was used for carbon and nitrogen analysis (Roleda et al., 2013). The temperature in left and right combustion furnace was set at 950°C and 630°C , respectively (Roleda et al., 2013). The gas chromatographic separation oven was set to 50°C (Roleda et al., 2013).

Before analysis took place, three empty tin capsules were measured to correct for any carbon and nitrogen within a blank sample. Three standards of acetanilide (BDH Chemicals - 10.36% Nitrogen, 71.09% Carbon) with weights ranging from 0.1 mg to 1.0mg (Roleda et al., 2013) were also measured prior to analysis. In addition a standard was also run every 15 samples to correct for drift within the instrument (Roleda et al., 2013). Each sample was run for 30 minutes on the 'Semi- μ ' setting.

3.3.7 rDNA haptophyte identification

3.3.7.1 Surface sediment collection

A surface sediment sample for rDNA analysis was retrieved in September 2011 using an Ekman grab sampler. The surface sample was kept at 4°C until DNA extraction took place.

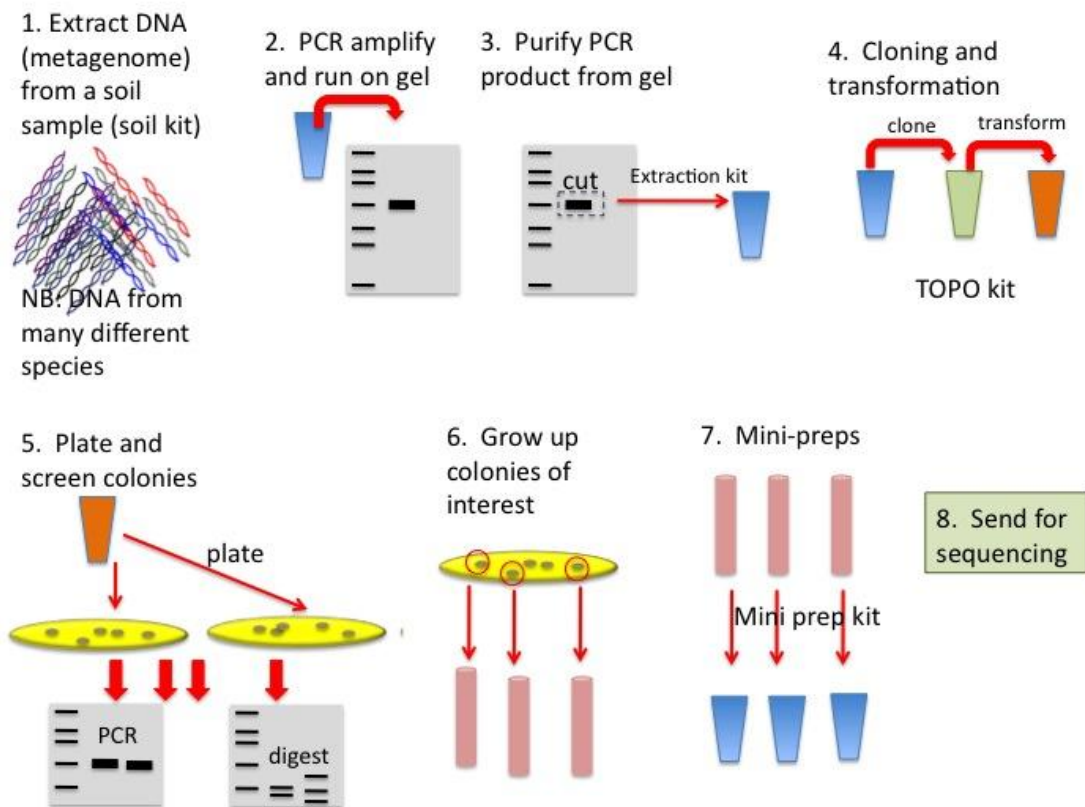


Figure 3-11: DNA sample procedure © Dr Jillian Couto, Science and Engineering, University of Glasgow

3.3.7.2 Extraction

DNA was extracted from 0.5g of wet surface sediment from Lake Toyoni using a FastDNA™ Spin Kit for soils and sediments (MP Biomedical) according to the manufacturing specifications. Total extracted DNA yields were quantified using a QUBIT™ (Invitrogen) fluorescence assay. The quality and fragment length of DNA in the extracts were checked by agarose gel electrophoresis (Figure 3-11).

3.3.7.3 Amplification and sequencing

An 887 base pair (bp) fragment of the gene that encodes haptophyte 18S ribosomal DNA (herein referred to as rDNA) was amplified using a BIOTAQ PCR kit (bioline BIO-2107). Polymerase chain reaction (PCR) was performed using the following thermal cycle conditions: 4 minutes of initial denaturing at 95°C, 35 cycles of denaturing for 30 seconds at 95°C, 40 seconds of primer annealing at 57°C, and 40 seconds of primer extension at 72°C, with a final extension of 10 minutes at 72°C. 18S rDNA amplification was completed using a forward universal eukaryotic primer (EUKA-F; AC CTG GTT GAT CCT GCC AGT) and a re-

designed haptophyte-specific reverse primer (Pym887-Ra; DVAATACGARTRCCCCYRAC) targeting 18S rRNA coding regions (Table 3). Genomic DNA extracted from isolated strains of haptophyte algae (*Emiliana huxleyi*; CCAP 920/8 and *Chrysofila lamellosa*; CCAP 918/1) were used for positive control during PCR amplification.

The PCR amplicon was resolved on a 0.8% gel and cleaned using a Macherey-Nagel NucleoSpin® Extract II kit according to manufacturing guidelines. The amplicon was then cloned using an Invitrogen TOPO TA Cloning® Kit for sequencing. 100 colonies were screened for unique clones using a restriction digest with Hpa II. Colonies that contained unique clones were grown overnight and plasmids were extracted using a Qiagen Mini-Prep Spin Kit, (Qiagen, Germany). Clones were sequenced from both the 5' and 3' directions using standard T7F and T3 primers by Source biosciences (Nottingham, UK).

3.3.7.4 Bioinformatics and phylogenetic reconstructions

The closest relatives to our 18 environmental clone sequences (OTU1-18) were identified using the GenBank database (NCBI) with the Basic Local Alignment Search Tool (BLAST) (Altschul et al., 1997). Bayesian analysis of our samples was performed using MrBayes under the GTR model of substitution considering invariants and a gamma-shaped distribution of the rates of distribution among sites. The number of cycles for the Markov Chain Monte Carlo (MCMC) analysis was set to 1,000,000 generations with trees sampled every 100 generations. The first 10,000 trees were discarded as burn-in for the tree topology and posterior probability. OTU1-18 were analysed to infer OTU species' identities along with full-length 18S rRNA gene sequences from reference taxa after Theroux et al., (2010). In addition, a partial-length phylogenetic tree was constructed using OUT 7 along with partial-length 18S rRNA sequences from *Prymnesiophytes* isolated from Ace Lake, Antarctica (Coolen et al., 2004c), Greenland lakes (D'Andrea et al., 2006) and also lakes in Canada, China and the USA (Theroux et al., 2010). *Cyclonexis annularis*, *Chrysoxys* sp., *Ochromonas danica*, *Odontella sinensis* and *Thraustochytrium multirudimentale* were selected as outgroups for both full-length and partial-length Bayesian analyses (after de Vargas et al., 2007).

3.3.8 Lipid analysis

All samples were freeze dried for 72 hours prior to the sample work-up and all sediment samples were homogenised using a solvent cleaned agate mortar and pestle. All glassware (e.g. test tubes, pipettes etc) used in the following processes were cleaned and then furnace at 450°C for 8 hours prior to use. All samples presented in this thesis followed the general method in Figure 3-12, except the analysis of the vegetation samples in Chapter 8, which were slightly adapted (discussed further in Section 3.3.10). The hydrogen isotopic measurements of the *n*-alkanes in Chapter 8 also required additional sample work-up, which is further discussed in Section 3.3.11.

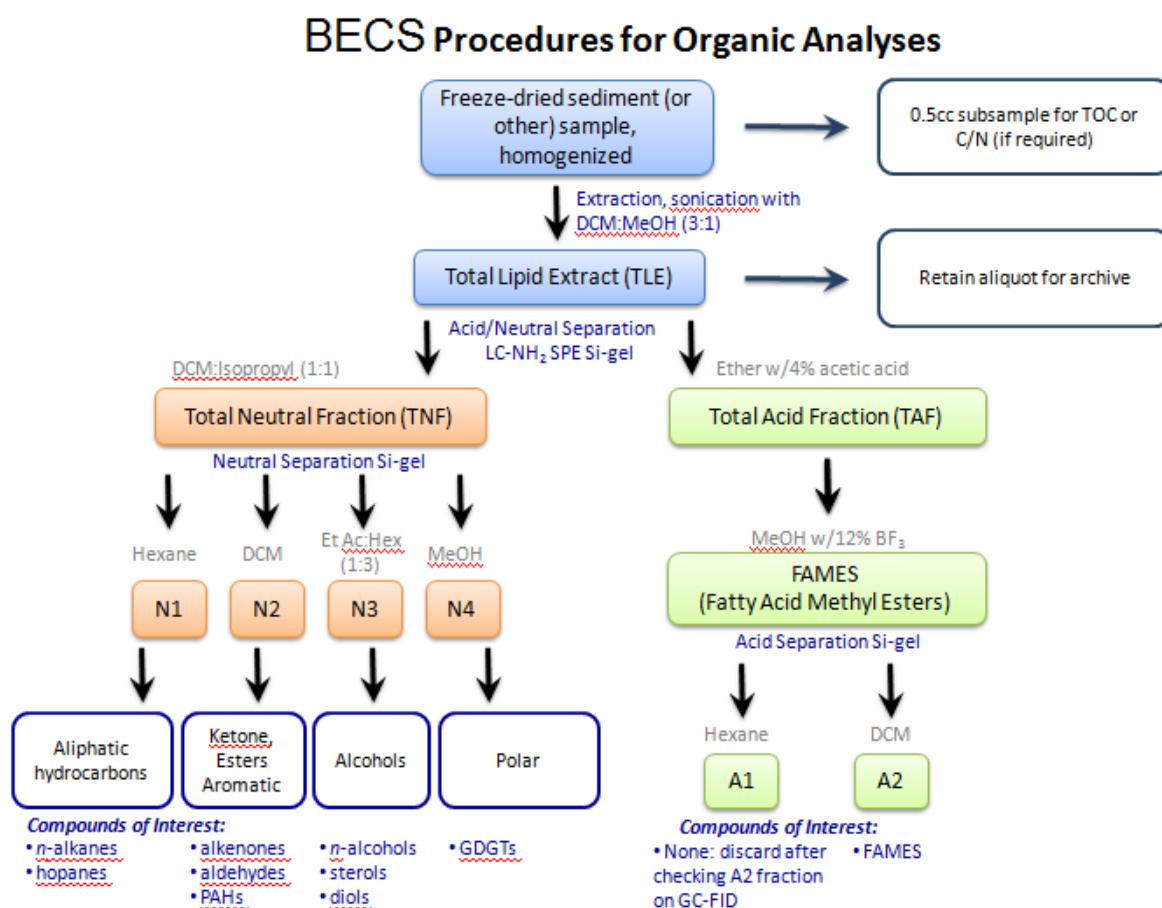


Figure 3-12: BECS sample procedure for organic lipid analysis (figure from Dr. Jaime Toney).

3.3.8.1 Extraction

Sediment samples (ranging from 1-5g) were placed in a pre-weighed 30 ml test tubes. 20 ml of a solvent mixture of dichloromethane:methanol (DCM:MeOH; 3:1) were added into the test tube and each sample was suspended using a vortex mixer. The samples were then ultrasonicated for 20 minutes and were placed on a hotplate and heated at 55 °C for one hour. Following this heat treatment, the samples were placed in a centrifuge at 3300 rounds per minute (rpm) for 3 minutes to separate the sediment from the solvent. The solvent was then transferred into another 30ml test tube using a pipette (9" borosilicate Pasteur). This processes was repeated at least three more times, or until the solvent was completely clear, using 10 ml of DCM:MeOH (3:1) each time. All extracts of the samples were combined and the solvent was evaporated using a rotary evaporator. The total lipid extract (TLE) obtained from each sample was transferred into a pre-weighed 8ml vial, dried down under N₂, and stored.

3.3.8.2 Column chromatography

3.3.8.2.1 Acid and neutral separation

The TLE's were separated into neutral and acid fractions via flash chromatography with LC-NH₂ SPE silica gel eluted with DCM:isopropanol (v 1:1) and 4% acetic acid in ether, respectively (Huang et al., 2002). No more than 10mg of the TLE was used for the column chromatography. Samples containing more than 10mg were split and the remaining TLE was archived. The silica gel columns were made by adding glass wool to a pipette (5 ¾" borosilicate Pasteur), which acted as a stopper to prevent Si-gel beads from passing, but allowing flow of solvent. 1.2g (~4cm) of silica (LC-NH₂ SPE) was then added on top of the glass wool and a small amount (~4mm) of furnaced sand was added on top of the silica gel. The LC-NH₂ SPE column was cleaned with 3 bed-volumes (8 ml) of 1:1 DCM:isopropyl alcohol. The TLE was re-dissolved and transferred to the column using a small amount of 1:1 DCM:ISO (x3). The TLE then seeps into the silica gel. The Total Neutral Fraction (TNF) was eluted with 4ml of 1:1 DCM:ISO and the TNF was collected into an 8ml sample vial. The Total Acid Fraction (TAF) was eluted with 4ml of ether with 4% acetic acid and the TAF was collected into an 8ml sample vial.

3.3.8.2.2 Neutral separation

The neutral fraction was further separated into four fractions. The silica gel columns were made following the same process as the acid and neutral silica columns except the silica used for neutral separation was 230-400 mesh/35-70 micron silica powder. The Silica gel was cleaned by eluting with 4ml of hexane. The TNF was re-dissolved in a small amount of hexane (~200ul, x3), using sonication. The aliphatic hydrocarbons were eluted with 4ml of n-hexane. The alkenones were eluted with 4ml of dichloromethane (DCM). The alcohols were eluted with 4ml of ethyl acetate:hexane (v 1:3) and the polar fraction was eluted using 4ml of methanol (MeOH) (Toney et al., 2010). Each of the four fractions was transferred into a 2.5 ml GC-vials, dried down under N₂, and stored in a fridge.

3.3.9 Gas chromatography and mass spectroscopy

The aliphatic hydrocarbons fraction (N1) and the alkenone fraction (N2) were analysed on a Shimadzu 2010 Gas Chromatograph Flame Ionization Detector (GC-FID) for quantification. A BP-1 GC Column (60m × 0.25mm × 0.25µm) was used with the following temperature program: an initial temperature of 60 °C (hold 2 minute), ramp 30°C/min to 120°C (hold 0 min) then 3 °C/minute to 350°C, GC temperature program (hold 20 minute). All analysed compounds were identified by comparing the retention time (RT) of the compounds in the samples to the RT of standard substances. In addition, a Shimadzu OP2010-Plus Mass Spectrometer (MS) interfaced with a Shimadzu 2010 GC using the same temperature programme as the GC-FID was also used to identify compounds. The carrier gas for the GC-MS was Helium and the ion source temperature was 200 °C and the interface temperature was 300°C. When using the GC-FID and the GC-MS, three standards were analysed before every run, as well as a standard every 10 samples and a standard at the end of every run was analysed. This was performed to check the conditions of the machine were optimal and there was no contamination before and during every run.

3.3.10 Vegetation samples

Vegetation samples were collected from the catchment of Lake Toyoni in July 2012. Leaf samples were freeze dried and soaked in dichloromethane:methanol (3:1) and ultrasonicated for 15 min to extract lipids. This extraction procedure was repeated three times (method adapted from Hou et al., (2008)). All vegetation samples were separated and analysed using the same procedure as the sediment samples (see above).

3.3.11 Compound specific hydrogen isotopes

Hydrogen stable isotopic values (δD) of *n*-alkanes derived from higher plant waxes (δD_{HPW}) were performed on sediment and vegetation samples at the Institute of Low Temperature Science at the Hokkaido University, Japan in collaboration with Dr. Osamu Seki. The δD_{HPW} of the sediment samples were analysed in summer 2014 by Jill McColl as part of a Japanese Society for the Promotion of Science (JSPS) funded trip to Hokkaido. Additional sediment samples as well as all of the vegetation samples were measured by Dr. Osamu Seki.

δD_{HPW} were determined using a GC/thermal conversion system consisting of a HP 6890 gas chromatograph connected to a Finnigan MAT Delta Plus XL mass spectrometer. The chromatographic separation of the *n*-alkanes was accomplished using a HP5-MS column (30m length). The following GC oven temperature program was used: the temperature was ramped up from 50 to 120°C at 30°C min⁻¹, and then from 120°C to 310°C at 5°C min⁻¹, where the temperature was held for 15 minutes. Thermal conversion was performed at 1450°C in a microvolume ceramic tube coated with glassy carbon.

The δD_{HPW} was calculated relative to the isotopic composition of an internal standard (methyl ester of *n*-C₂₀ alkanic acid) with a known hydrogen isotopic value. The isotopic values are expressed as per mil (‰) vs. Standard Mean Ocean Water (SMOW) for the hydrogen isotopic measurements. In order to evaluate the instrument accuracy, an external standard consisting of an *n*-alkane mix (C₁₆-C₃₀) with a known hydrogen isotopic composition was injected daily.

Decadal-resolved terrestrial and biological input into Lake Toyoni.

4.1 Introduction

Lakes, such as Lake Toyoni, are valuable palaeo-climate archives for investigating aquatic productivity variability because they have continuous high sedimentation rates, which allows for high-resolution palaeo-productivity reconstructions. The sedimentation rates in Lake Toyoni are mainly controlled by the amount of terrestrial material entering the lake and also the extent of productivity within the lake. A 2.5m sediment core taken from Lake Toyoni records 1000 years of sedimentation, which is an important time period for investigating both natural- and human-driven environmental change.

4.1.1 Human controls on environmental change during the past 1000 years in Hokkaido, Japan

Hokkaido offers an ideal location for investigating human-induced environmental change, because the population of this island substantially increased from 120,000 in 1872 (Bureau of Statistics, Imperial Cabinet, Japan, 1993) to 2,360,000 in 1920 (Bureau of Statistics, Imperial Cabinet, Japan, 1924). This large increase in population size in Hokkaido occurred after Japan took over the island, following a perceived threat from Russia (Kitayama et al., 2006). At the same time, Japan went from being controlled by feudal government to being controlled by the emperor, known as the Meiji period (Kitayama et al., 2006). As a result of the change in government, Samurais (feudal warriors) lost their

means of living and were recruited to Hokkaido to create settlements (Kitayama et al., 2006). Prior to Japan taking control over Hokkaido, the island was known as Ezo and was inhabited with Ainu indigenous population. Following the initial settlements by the Samurais, Japan encouraged additional Japanese people to Hokkaido through the development of new laws allowing the use of land for development and immigrant support which not only allowed people to move to Hokkaido and use the land for agricultural practises but also provided financial support with travelling expenses, housing, food and farming tools. The new laws made it attractive for people to move to Hokkaido and start a new life there; therefore, the population dramatically increased during a relatively short period of time.

Increased human activities following the settlement of Japanese people in Hokkaido in the 1870's resulted in an increase in agriculture activities, deforestation and also building activities (e.g. roads, housing and dams) (Kitayama et al., 2006), which has been attributed to the main cause of a decline in Japanese wolf (Knight, 1997) and the Blakiston's fish owl (Omote et al., 2015) in recent years. In addition, Matsubayashi et al. (2014) also found that increased human activities in Hokkaido during this time period caused a long-term shift in feeding activities of brown bears due to increased human population in their feeding grounds. Moreover, eutrophication in Omuna Lake, Hokkaido, has also been report in recent years due to increased nutrient input from human activity in the surrounding area (Ochiai et al., 2015, Sun et al., 2015). Hokkaido therefore records environmental changes due to increased human activity in this region. The effect of increased human activities (e.g. agricultural and building activities) will be recorded in an increase in productivity in Lake Toyoni due to an increase in nutrient run-off into the lake Toyoni.

4.1.2 Environmental controls on productivity in Lake Toyoni

In addition to nutrient input, the extent of aquatic primary production in lacustrine systems is controlled by a number of factors, including temperature (Xiao et al., 1997a, Liu et al., 2009b), light availability (Karlsson et al., 2009), the degree of mixing within the lake (Qiu et al., 1993, Meyers, 1997, Zimmerman

and Canuel, 2000, Diaz, 2001, Chu et al., 2002), which in return can provide information on the climatic conditions (Xiao et al., 1997b).

In sub-arctic lakes, such as Lake Toyoni, the extent of productivity is influenced by temperature change through its effect on the duration of the ice-free season (Shiomoto et al., 2012, Wang et al., 2012). The duration of the ice-free season has a significant effect on light and nutrient availability, which are essential requirements for photosynthesis to occur (Wang et al., 2012). In Lake Toyoni, the timing of ice-off is consistent with the timing when the lake overturns and is well-mixed (Chapter 3), which occurs during the spring overturning (April-May) and also during autumn (October-November). The degree of mixing within the lake is responsible for recycling of nutrients within the lake, which increases primary productivity (Qiu et al., 1993, Meyers, 1997, Zimmerman and Canuel, 2000, Diaz, 2001, Chu et al., 2002). During winter, when there is extensive ice-cover on Lake Toyoni, dissolved oxygen becomes depleted at the bottom of the lake by bacteria by respiration (Denys, 2010). Respiration releases nutrients from the sediments to the water column (e.g Nowlin et al., 2005, Burt et al., 2013) and when the lake overturns, the water column becomes mixed resulting in circulation of oxygen and nutrients throughout the water column (Denys, 2010). The duration of the ice-cover on Lake Toyoni therefore influences the extent of aquatic productivity through the duration of time the lake remains well mixed.

The duration of the ice-cover on Lake Toyoni likely occurs between December and March, when the temperatures are below 0°C in Hokkaido (Chapter 2). The duration of ice-cover is ultimately controlled by temperature, which is dependent on the intensity of the EAWM during winter in Hokkaido. When the EAWM winds intensifies, it brings more cold air and temperatures in EAWM domain decrease significantly due to the strong advection by strong EAWM winds (Jhun and Lee, 2004a). As a result of this cold temperature, the ice stays on Lake Toyoni for a longer period of time. On the other hand, when the EAWM weakens the temperature becomes warmer earlier (Chapter 2) and results in ice-off occurring earlier in the lake. The ice-cover will therefore remain on the lake longer when the EAWM intensifies and will remain on the lake for a shorter time when the EAWM weakens. In addition to changes in the ice duration, a weak EAWM also has a profound influence on the precipitation during summer

(Chapter 2). Periods of low productivity therefore reflect an intensification of the EAWM and periods of high productivity therefore reflect a weakening of the EAWM.

In addition to the variability of the EAWM determining the timing of ice-off in Lake Toyoni, previous studies have also suggested a link between teleconnections (e.g. PDO, NAO, ENSO) and the timing of the ice-off in other lakes (Todd and Mackay, 2003, Bonsal et al., 2006, Ghanbari et al., 2009, Mishra et al., 2011, Katsuki et al., 2012). The hydro-climate in Hokkaido is significantly influenced by the PDO (Tsuji et al., 2008). Variations in both temperature and precipitation are expected depending on the phase of the PDO. The positive phase of the PDO is associated with a decrease in sea surface temperatures; whereas in the eastern part of the Pacific Ocean (e.g. US) temperatures increase (Mantua et al., 1997), the opposite is true during the negative phase. A negative correlation exists between relative humidity and the PDO in Hokkaido (Tsuji et al., 2008). When the PDO is in its negative phase, an increase in humid southerly winds blows towards Hokkaido resulting in warmer and wetter conditions (Tsuji et al., 2008). This is demonstrated in the weather station data from Hiroo weather station (25km from Lake Toyoni). The most predominant change from “negative” to “positive” phase occurred in 1976. The negative phase (1960-1975) had average temperatures of 6.6°C and average rainfall was 1771mm compared with the positive PDO phase (1976-1988), which had average temperatures of 6.2°C and average rainfall of 1517mm. (Chapter 2) The time period of the positive PDO is consistent with the timing of a strong EAWM time period, because the EAWM and the positive phase of the PDO are also linked (Ding et al., 2014). The temperature change associated with the change in the phase of the PDO directly influences the timing of ice-off on Lake Toyoni. During the positive phase of the PDO there are colder conditions in Hokkaido and hence the timing of ice-off will be later and productivity is lower as a result. In comparison, when the PDO is in its negative phase, there are warmer conditions in Hokkaido which results in ice-off occurring earlier and productivity being enhanced during this time period. The PDO therefore influences productivity in Lake Toyoni through its influence on ice duration on the lake (controlled by temperature). In addition, the PDO also influences productivity in the lake through increased

precipitation associated with the negative phase resulting in increased run-off and soil erosion transporting nutrients into the lake.

Run-off into lakes is usually controlled by rivers; however, Lake Toyoni has no river input into the lake. The main method of fluvial transport in Lake Toyoni is therefore ephemeral streams that form during times of increased rainfall or during the snowmelt season in spring. The steep slopes surrounding Lake Toyoni promote downward movement of terrestrial material during intense run-off events. In Hokkaido, precipitation during the ice-free season is associated with the EASM (D'Arrigo et al., 2001, Davi et al., 2002, Tsuji et al., 2008, Igarashi et al., 2011), which supplies lakes with nutrients via run-off into the lake and as a result enhances productivity (Xiao et al., 1997a, Chu et al., 2002, Zeng et al., 2014). Palaeo-climate studies in EAM domain have therefore used lake productivity to infer changes in the EASM (e.g. Liu et al., 2009b). The timing of monsoonal precipitation in Hokkaido is associated with August and September when precipitation significantly increases. The increase in nutrients transported into Lake Toyoni during monsoonal precipitation in August and September supports the second bloom in October-November when the water column of Lake Toyoni overturns and becomes well-mixed once again (Chapter 3). Based on meteorological data from a nearby weather station, a 10 year period associated with a weakening of the EAWM (1988-1997; Jhun and Lee, 2004a) show a large increase in precipitation in August and September (Chapter 2), which is associated with EASM precipitation. This suggests that a weakening of the EAWM results in an intensification of the EASM at this site. An increase in precipitation and soil erosion, through an enhanced EASM, results in higher productivity in Lake Toyoni. On the other hand, when the EASM weakens and/or the EAWM intensifies, there is less run-off and soil erosion through a decrease in precipitation and as a result productivity in the lake also decreases. Therefore, the record of productivity over the past 1000 years in Lake Toyoni will provide valuable insights into the variability of the East Asian Monsoon (EAM) over the time scale. Increases in productivity suggest warm and wet environment with an extended duration of the spring mixing time and hence an enhancement of the EASM. A decrease in productivity, on the other hand, suggests that the ice-cover on the lake was extended as a result from an enhanced EAWM. The extended duration of the ice-cover negatively influence productivity in the lake through a

decrease in the duration of mixing in the lake. In addition, rainfall in summer is also reduced during an enhanced EAWM, which limits the supply of nutrients for the secondary bloom in late autumn (October-November).

4.1.3 Climatic significance of the proxy indices in the sedimentary record of Lake Toyoni

4.1.3.1 Magnetic susceptibility as a proxy for tephra layers, anoxic conditions and transportation processes

A multi-proxy approach to elucidate changes in productivity over the past 1000 years has been adopted. Firstly, the magnetic susceptibility (MS) in the down-core record, which records the response of sediments to magnetism. This has been used in a number of palaeo-climate records from marine (e.g. Somayajulu et al., 1978, Larrasoña et al., 2008), lacustrine (e.g. Yancheva et al., 2007, Wang et al., 2008b, Gebhardt et al., 2013) and aeolian sediments (e.g. Chen et al., 1997, An, 2000, Vandenberghe et al., 2004) from locations all over the world.

The MS response within lake sediments will vary between different lakes depending on what climatic processes MS is controlled by, because all lakes are unique (Shouyun et al., 2002). In order to use MS in lakes it is therefore important to understand processes controlling MS within the sedimentary record at that given site (Shouyun et al., 2002). Although MS mainly reflects the supply of allochthonous magnetic minerals from the catchment into the lake (Dearing et al., 1981, Wang et al., 2008b), other sources such as the presence of tephra (Lozano-Garcia et al., 1993, Calanchi et al., 1998, Haberle and Lumley, 1998, Hallett et al., 2001), dust from aeolian processes (Yancheva et al., 2007), biogenic materials (Lowenstam, 1981), dissolution under reduction conditions (Nowaczyk et al., 2002, Yancheva et al., 2007, Gebhardt et al., 2013) and minerals that form within the lake, referred to as authigenic minerals (Shouyun et al., 2002) also influence the MS of the sedimentary record.

In Lake Toyoni, MS likely represents the presence of tephra layers because Hokkaido is tectonically active; therefore, fallout from volcanic eruptions into Lake Toyoni will significantly increase the MS in the down-core record. In addition, MS in the Lake Toyoni record also provides valuable information on

past anoxic events. Magnetic minerals can become dissolved when the oxygen content of the sediments is low (hypoxic; $O_2 < 2.0 \text{ mg l}^{-1}$) (Diaz, 2001, Zimmerman and Canuel, 2000) or absent (anoxic; $O_2 < 0.2 \text{ mg l}^{-1}$) (Zimmerman and Canuel, 2000). Low oxygen content results in dissolution of magnetic minerals and hence a lower MS (Nowaczyk et al., 2002, Yancheva et al., 2007, Gebhardt et al., 2013). In comparison, when there are oxic conditions magnetic minerals are well preserved (Nowaczyk et al., 2002). The bottom water of Lake Toyoni becomes hypoxic ($O_2 < 2.0 \text{ mg l}^{-1}$) between July and October in the modern day environment due to thermal stratification occurring and a lack of mixing within the water column (Chapter 3). MS in Lake Toyoni likely reflects oxygen content of the bottom sediments; with high values representing oxic conditions (increased mixing and reduce thermal stratification) and low values representing anoxic conditions reduced mixing and increased thermal stratification). Anoxic conditions can also prevail following time periods of increased biological activity (e.g. Nowaczyk et al., 2002, Zimmerman and Canuel, 2000, Diaz, 2001, Kemp, 1996). When biological productivity increases, there is an increase in the flux of OM to the lake bottom resulting in degradation, which in turn results in less oxygen content (Nowaczyk et al., 2002, Diaz, 2001).

MS in the Lake Toyoni sedimentary record may also reflect weathering processes within the catchment and the mechanisms associated with the transport of magnetic minerals into the lake, e.g. fluvial and aeolian processes. The influence of aeolian processes on the MS in the Lake Toyoni sedimentary record is further discussed in chapter 5. Fluvial input into Lake Toyoni is controlled by the amount of precipitation, which in Hokkaido is supplied in summer (August and September) by the EASM (568mm of precipitation based on data from 1958-2014) and in winter (November, December, January and February) by the EAWM (366mm of precipitation based on data from 1958-2014); therefore, both monsoon systems result in high precipitation amount in this region. Run-off into lakes is usually controlled by rivers; however, Lake Toyoni has no river input into the lake. The main method of fluvial transport in Lake Toyoni is therefore ephemeral streams that form during times of increased rainfall or during the snowmelt season in spring. The steep slopes surrounding Lake Toyoni promote downward movement of terrestrial material during intense run-off events. Fluvial input into the lake also influences productivity and hence increased

precipitation in the catchment of Lake Toyoni results in an increase in OM from the catchment and also promotes productivity in the lake.

4.1.3.2 Rb/Sr ratio as a chemical weathering proxy

Precipitation, as well as temperature, can influence the amount of chemical weathering (Chen et al., 1999a, Jin et al., 2001, Wu et al., 2006b) and hence the amount of terrestrial input within the lake. An increase in precipitation and chemical weathering results in an increase in terrestrial material transported by fluvial processes into the lake. Lakes therefore act as a trap for weathering material within the catchment making them excellent palaeo-archives to study chemical weathering within the catchment.

Although the Rb/Sr ratio mainly reflects the chemical weathering within the catchment, physical weathering can also influence this ratio. In particular, physical weathering is important to consider on short times scales, e.g. decadal timescales (Xu et al., 2010a). When physical weathering increases within the catchment, more clastic material (e.g. Rb) is transported into the lake, which can dilute the Sr signal (Xu et al., 2010a). Chemical and physical weathering are both influenced by precipitation; however, this is recorded in the Rb/Sr ratio in opposite directions. For example, chemical weathering will be recorded with decrease in Rb/Sr values; whereas, physical weathering would record an increase in Rb/Sr values due to Sr being diluted by other terrestrial material (Xu et al., 2010a). The dilution effect in the Toyoni record is not likely to influence the Rb/Sr ratio in Hokkaido since the record extends throughout the last millennium; whereas, the dilution effect by physical weathering mainly only influences Rb/Sr ratio at decadal time-scales.

To determine the extent of chemical weathering within the catchment, the ratio between Rb and Sr is used (Jin et al., 2001, Jin et al., 2006, Chu et al., 2013, Liu et al., 2014a, Zeng et al., 2014). Warm and wet conditions enhance chemical weathering within the catchment, which preferably releases Sr over Rb (Dasch, 1969, Liu et al., 1999, Chen et al., 1999a) resulting in more Sr being transported into the lake (Jin et al., 2001, Jin et al., 2006). This leads to an increase in the Rb/Sr ratio within catchment and a decrease in the Rb/Sr proxy within lakes since Sr is lost from the catchment and increased in lakes with respect to Rb (Jin

et al., 2001, Jin et al., 2006). In comparison, when conditions are cold or dry or both, Sr is not leached from the catchment rocks and therefore less Sr is transported into the lake, reflected by an increase in the Rb/Sr ratio within lake sediments (Chen et al., 1999a, Jin et al., 2001, Wu et al., 2006b).

4.1.3.3 Inc/Coh ratio as a proxy for OM content of sediments

The Inc/Coh ratio is used to infer information on OM content of the sediments (Guyard et al., 2007, Burnett et al., 2011, Liu et al., 2013b, Liu et al., 2014b). The Inc/Coh ratio is dependent on the loss of energy between two different types of scattering during the scanning of the core. A loss of energy occurs during the scanning process when the atomic number of the target atom is lighter than the X-Ray photon resulting in stronger incoherent scatter (Kylander et al., 2012). No loss of energy during scattering occurs when measuring elements with a larger atomic number (weaker incoherent scattering) (Kylander et al., 2012). OM produces higher incoherent scatter and as a result the Inc/Coh ratio will have a greater value when sediments contain more OM and a lower value when measuring inorganic materials (Guyard et al., 2007).

Sources of OM in lacustrine sediments are primarily controlled by the ecology within the lake as well as the surrounding catchment (Meyers and Ishiwatari, 1993b). Thus, OM in lake sediments can be either provided by primary production in the lake (autochthonous component) or terrestrial plant material (allochthonous component) washed into the lake by run-off via rainfall and/or snow-melt (Meyers, 1997). An increase in precipitation favours soil erosion and an increase in transport of OM into the lake (after Zeng et al., 2014). Algae production is also enhanced due to an increase in nutrients during increased run-off into the lake. As a result, Inc/Coh ratio can provide information on past precipitation history of the lake.

4.1.3.4 C/N ratio as a proxy for the source of OM

Where the Inc/Coh ratio provides information on the extent of OM within the sedimentary record, the C/N ratio provides information on the source of the OM. The C/N ratio is therefore an important proxy to assess the relative contributions of terrestrial and aquatic OM in lake sediments (Meyers, 1997). The C/N ratio of bulk sediments changes with respect to the concentration cellulose

in the plant sources of OM (Meyers and Ishiwatari, 1993a). Nonvascular aquatic plants or algae have low concentrations of cellulose and typically have a C/N ratio between 4 and 10. In comparison, land plants contain high concentrations of cellulose and have C/N ratios ≥ 20 (Meyers, 1994). The C/N ratio found in the bulk sediments of lakes mostly reflects a mix of both aquatic and terrestrial sources of OM (Meyers, 1994).

The C/N ratios in the sedimentary record of Lake Toyoni is strongly influenced by terrestrial OM from the dense vegetation in the catchment of Lake Toyoni. In addition, aquatic productivity in the lake also influences the C/N ratios in Lake Toyoni. During time periods of enhanced aquatic productivity, the C/N ratio in the sedimentary record will decrease and vice versa. As previously discussed, productivity in Lake Toyoni is enhanced when the EASM intensifies and/or the EAWM weakens, resulting in increased nutrients run-off into the Lake. The duration of time available for primary production in Lake Toyoni to occur is dependent on the ice-cover duration. As a result, when the ice-cover duration decreases; productivity increases in the lake. Lower C/N ratios in the down-core record are used to indicate increased aquatic productivity within the lake due to warmer conditions and an enhanced contribution from the EASM. Higher C/N ratios, on the other hand, suggests an increase in terrestrially derived OM. The catchment of Lake Toyoni is densely covered in vegetation and wind and fluvial input transports this material into the lake. High C/N ratios therefore reflect an increase in wind and/or fluvial transport into the lake.

4.1.3.5 *n*-Alkane biomarkers as a proxy for source of OM

In addition to the C/N ratios, *n*-alkanes can also provide valuable information on the contribution of terrestrially- and aquatic-derived OM based on the fact that aquatic algae and terrestrial higher plants produce distinctly different chain lengths. Aquatic algae produce short chain homologues (C_{17} - C_{21} *n*-alkanes) (Giger et al., 1980, Cranwell et al., 1987), whereas terrestrial organisms produce long-chain *n*-alkanes (C_{25} - C_{33} *n*-alkanes). In between are the mid-chain homologues (C_{23} , C_{24} and/or C_{25} *n*-alkanes), which are produced by submerged aquatic macrophytes (Ficken et al., 2000). The difference between short-chain and long chain *n*-alkanes therefore reflects the source organism. When conditions in the lake change (e.g. nutrient levels, mixing extent, ice-cover), the contribution of

short-chain *n*-alkanes will change accordingly. For example, when environmental conditions change and there is a corresponding increase in aquatic productivity, more short-chained *n*-alkanes will be produced and vice versa. The changes in the molecular composition of *n*-alkanes in the down-core sedimentary record therefore provides valuable information on changes in aquatic versus terrestrial productivity over a given time period.

n-Alkanes derived from terrestrial higher plants are transported into Lake Toyoni by fluvial and/or aeolian processes. Due to the dense vegetation in the catchment of Lake Toyon it is assumed that the majority of *n*-alkanes in the Lake Toyoni sedimentary record are sourced from the catchment area and washed into the lake during run-off during the spring melt and summer rainfall and also transported via aeolian processes. *n*-Alkanes derived from aquatic algae (short chained) and submerged plants (mid chains) (Ficken et al., 2000) increase when aquatic productivity increases. The molecular compositions of *n*-alkanes therefore provide information on variations on terrestrial- and aquatic input in the lake.

The molecular compositions of *n*-alkanes provide a number of *n*-alkane based indices; for example, the carbon preference index (CPI index), Average Chain Length (ACL) and the proportion aquatic (Paq). The CPI index gives information of the extent of odd over even carbon number predominance (Bray and Evans, 1961). *n*-Alkanes produced by higher plants have a strong odd over even carbon number predominance (Eglinton and Hamilton, 1967). In contrast, algal *n*-alkanes do not contain the strong odd over even carbon number predominance. Biomarkers from different biological origins have different CPI values; therefore, the *n*-alkane CPI in sediment is an indicator of the sources of biological origin (e.g. Simoneit et al., 1979). High CPI values (>3) results from a strong odd/even predominance which is a characteristics of higher plant wax *n*-alkanes. In contrast, *n*-alkanes from bacteria and algae show a weak odd/even predominance and give low CPI values (~1) (Cranwell et al., 1987). In addition, *n*-alkane distributions in sediments altered by diagenesis or bacteria may lack the strong odd over even preference of primary plant-wax *n*-alkanes (Meyers and Ishiwatari, 1993a); therefore, low CPI values may also indicate increased microbial activity during the time of deposition.

Variations in the CPI values offer insights into the source of *n*-alkanes. Xie et al. (2004) have shown that CPI values from loess/paleosol sequences of western Chinese Loess Plateau demonstrated that low CPI values of paleosol layers represent warmer and wetter climatic conditions; whereas, high CPI values represent colder and drier climatic conditions (Xie et al., 2004). Similarly, this trend was also found in two Japan Sea marine sediment cores which indicated that the variation of CPI values was in consistent with glacial/interglacial cycles, with lower CPI values occurring in warmer and wetter interglacial periods (Ishiwatari et al., 1994, Yamada and Ishiwatari, 1999). The variability of the CPI values in the Japan Sea was attributed to species variations of terrestrial higher plants due to changes in the climate; CPI values were lower in warmer climates (Ishiwatari et al., 1994). In the case of Lake Toyoni, an increase in temperature would promote aquatic productivity in the lake and a decrease in CPI values. Lake Toyoni will also be strongly influenced by the dense vegetation in the catchment area of the lake, and hence high CPI values.

Another *n*-alkane molecular composition proxy is the ACL proxy. Vegetation types are the main influence on chain length of terrigenous leaf lipids. For example, *n*-alkanes derived from grasslands have longer chain lengths than leaf lipids from plants in forests (Cranwell, 1973). In the case of Lake Toyoni, the understory in the modern day environment is bamboo, which will have a significant influence on the ACL values. Changes in the vegetation over time are reflected in the ACL values. In addition to ACL value and vegetation type, a relationship between ACL and plant stresses (e.g. temperature and/or aridity) have been previously suggested (Gagosian and Peltzer, 1986, Kawamura et al., 2003). The humidity in Hokkaido during the growing season (June-September; Seki et al., 2010) is >70%; therefore, aridity will not influence the ACL values at this site. Temperature on the other hand may influence ACL values. Increasing the ACL raises the melting point of protective leaf surface waxes and thus plants growing at higher temperatures may synthesize longer chain *n*-alkanes in order to maintain the protective waxy coating on their leaves (Rommerskirchen et al., 2003). Hence, plants produce longer chain compounds; therefore, higher ACL values, in warmer climates (Poynter et al., 1989).

The *Paq* index was developed to reflect the relative contribution of aquatic macrophytes and emergent aquatic and terrestrial plants based on a survey of African Lakes, which found that the distribution of *n*-alkanes from floating/submerged macrophytes maximise at C₂₃ and C₂₅ (Ficken et al., 2000). Emergent aquatic plants, on the other hand, had *n*-alkane distributions similar to those of the terrestrial vegetation, typically dominated by the long-chain length homologues (>C₂₉). According to Ficken et al. (2000), *Paq* values greater than 0.4 indicate the dominance of submerged and floating macrophytes (Ficken et al., 2000). For the modern plants, this proxy gives average values of 0.09 for terrestrial (range 0.01-0.23), 0.25 for emergent (range 0.07-0.61) and 0.69 for submerged/floating species (range 0.48-0.94). However, mid-chained *n*-alkanes are not exclusively produced by emergent and floating/submerged macrophytes. Mid-chained *n*-alkanes are also produced by higher plants (Eglinton and Hamilton, 1963), which is particularly important with respect to Lake Toyoni, because higher plants from the catchment of Lake Toyoni will have a strong influence on the *n*-alkane distributions in the down-core sedimentary record. Mid-chained *n*-alkanes in Lake Toyoni are unlikely to be exclusively derived from emergent and floating/submerged macrophytes, however, the *Paq* index will provide an approximate measure of variations in the sedimentary contribution from submerged/floating aquatic macrophytes in Lake Toyoni however will not reflect the dominance of floating/submerged macrophytes.

4.1.3.6 Si/Rb as a proxy for diatom productivity

Where the C/N ratios and *n*-alkane proxies provide general information on variations in aquatic versus terrestrial contribution to the sedimentary record, the ratio between Si and Rb is used to reflect the deposition of biogenic silica (BSi) (e.g. Melles et al., 2012, Gebhardt et al., 2013, Liu et al., 2013b), which indicates increased diatom productivity (Johnson et al., 2002), because diatoms form cell walls made of silica (SiO₂) (Peinerud, 2000).

Diatom productivity in lakes is associated with a well mixed water column; in Lake Toyoni this occurs during spring (April-May) and autumn (October-November). The timing of ice-off in Lake Toyoni determines the time period the lake stays well mixed before thermal stratification occurs in June. When ice-off occurs earlier in the year, the timing of a well mixed water column, and hence

productivity, is extended. Similarly, a previous study from a lagoon north of Lake Toyoni found the duration of diatom blooms increased when the ice-cover was reduced during winter (Shiomoto et al., 2012). Typical diatom blooms in this Lagoon are ~1 month; however, this was extended to ~3 months when ice-cover is reduced (Shiomoto et al., 2012). Therefore, a change in diatom productivity in Lake Toyoni provides information on the timing of ice-off conditions in Lake Toyoni. The timing of ice-off in Hokkaido is driven by the intensity of the EAWM and the PDO; therefore, the extent of BSi in Lake Toyoni provides information on the phase of the PDO and the intensity of the EAWM. Higher Si/Rb values represent time period when diatom productivity increased due to a reduced ice-cover on the lake during a weakened EAWM and/or a negative phase of the PDO. Low Si/Rb values represent time period when the ice-cover remained on the lake for longer time periods, during an enhanced EAWM and/or positive phase of the PDO, reducing the time period of diatom productivity and hence the Si/Rb ratio in the sedimentary record.

Table 4-1: Summary table of the different climatic influences (EAM and PDO) on the processes involved in Lake Toyoni.

	Temperature	Run-off	Preservation of magnetite	Ice-free season	productivity
Strong EASM/ weak EAWM	↑	↑	↓	↑	↑
Weak EASM/ strong EAWM	↓	↓	↑	↓	↓
Positive PDO	↓	↓	↑	↓	↓
Negative PDO	↑	↑	↓	↑	↑

4.1.3.7 Aims

It is hypothesised that productivity in Lake Toyoni has varied in response to changes in the EAM intensity and the phase of the PDO over the past 1000 years in Hokkaido. The key aims of this chapter are:

1. To determine how productivity varied over the past 1000 years
2. To determine possible forcing mechanisms (e.g. solar irradiance and the PDO) driving productivity changes, and hence EAM variability, in Northern Japan.

1. Catchment weathering

Increased precipitation increases chemical and physical weathering in the catchment surrounding the lake

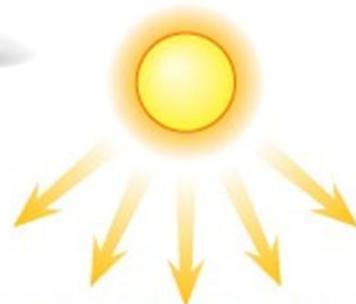


2. Run-off

Nutrients are transported into lake by rainwater and snowmelt



sunlight



3. Productivity

Sunlight and nutrient input promotes productivity

4. Circulation

Lake overturns in spring and autumn



5. Stratification

Lake stratifies during summer

22°C

18°C

15°C

12°C

10°C

8°C

5°C

algae layer

decomposers

nutrient material

6. Anoxic sediments

Bacteria break down organic matter using oxygen. Stratification during summer prevents mixing of the water column .

Figure 4-1: Diagram outlining the key processes influencing Lake Toyoni.

4.2 Results

4.2.1 Core description

The core was split and described using a Munsell colour chart. Seven lithofacies were identified in

Table 4-2. Lithofacies A is characterised by very dark greyish brown (3/2) 2.5Y with faint laminations (5/2 greyish brown 5/2 Y). Lithofacies B is characterised by 3/1 very dark grey 2.5Y. Lithofacies C is characterised by very dark greyish brown (3/2) 2.5Y. Lithofacies D characterised by 5/3 light olive brown 2.5Y with laminations. These sections of the core are relatively small (averaging around 5cm thick). Lithofacies E is characterised by greyish brown (5/2). Lithofacies F is characterised by 4/2 dark greyish brown. Lithofacies G is characterised by 4/3 olive brown 2.5Y and visually has a change in grain size from finer to coarse grains. In addition, two tephra layers were visually identified in the sedimentary record. Tephra 1 at ~1250AD and tephra 2 at ~1630AD were both characterised by 6/4 light yellowish brown 2.5 Y.

4.2.2 MS

MS is lowest in the earliest part of the record (1000-1170AD), followed by a sharp increase around 1174AD (Figure 4-2). Between 1174AD and 1879AD, MS is variable and there is a second spike in MS around 1604AD >1879AD, MS is relatively low. Visible tephra explain maxima in MS at 1187AD and 1604AD (Figure 4-2).

4.2.3 Rb/Sr

The highest values of Rb/Sr are recorded in the earliest section of the record (1000-1200AD). High values are also recorded between 1450-1500AD, 1575-1620AD and 1804-1854AD. Low values are recorded between 1300-1450AD, 1500-1575AD and 1610-1800AD (Figure 4-3).

4.2.4 Inc/Coh

High Inc/Coh ratios between 1000 and 1300AD are recorded in the earliest part of the record. A sharp decrease between 1300-1350AD was followed by low values to 1600AD. After 1600AD, Inc/Coh ratio generally increases to the most recent part of the record (Figure 4-3).

4.2.5 C/N ratios

In the earliest part of the record to 1200AD, C/N values are ~16. C/N ratios then increase to ~21 at 1500AD and remain high till 1600AD. There is a sharp decrease in values to ~18 between 1600 and 1700AD. C/N values then remain relatively constant to ~1900AD (Figure 4-3).

Table 4-2: Lithofacies and visual description of the core.

lithofacies	Description/colour	depth	Cal. Age (AD)
A	Very dark greyish brown (3/2) 2.5Y with faint laminations (greyish brown 5/2 Y)	10-61cm 202-end of core	1960-1746 1183-end of core
B	very dark grey (3/1) 2.5Y	61-85cm	1750-1656
C	Very dark greyish brown (3/2) 2.5Y, coarser grain size noted	85-121cm	1656-1511
D	5/3 light olive brown 2.5Y with laminations	121-126cm 183-189cm 197-202cm	1511-1490 1260-1239 1203-1183
E	greyish brown (5/2)2.5 Y	126-154cm	1490-1377
F	olive brown (4/3) 2.5Y (change in grain size)	154-161cm	1377-1349
G	dark greyish brown (4/2)	161-183cm 189-197cm	1349-1260 1203-1239

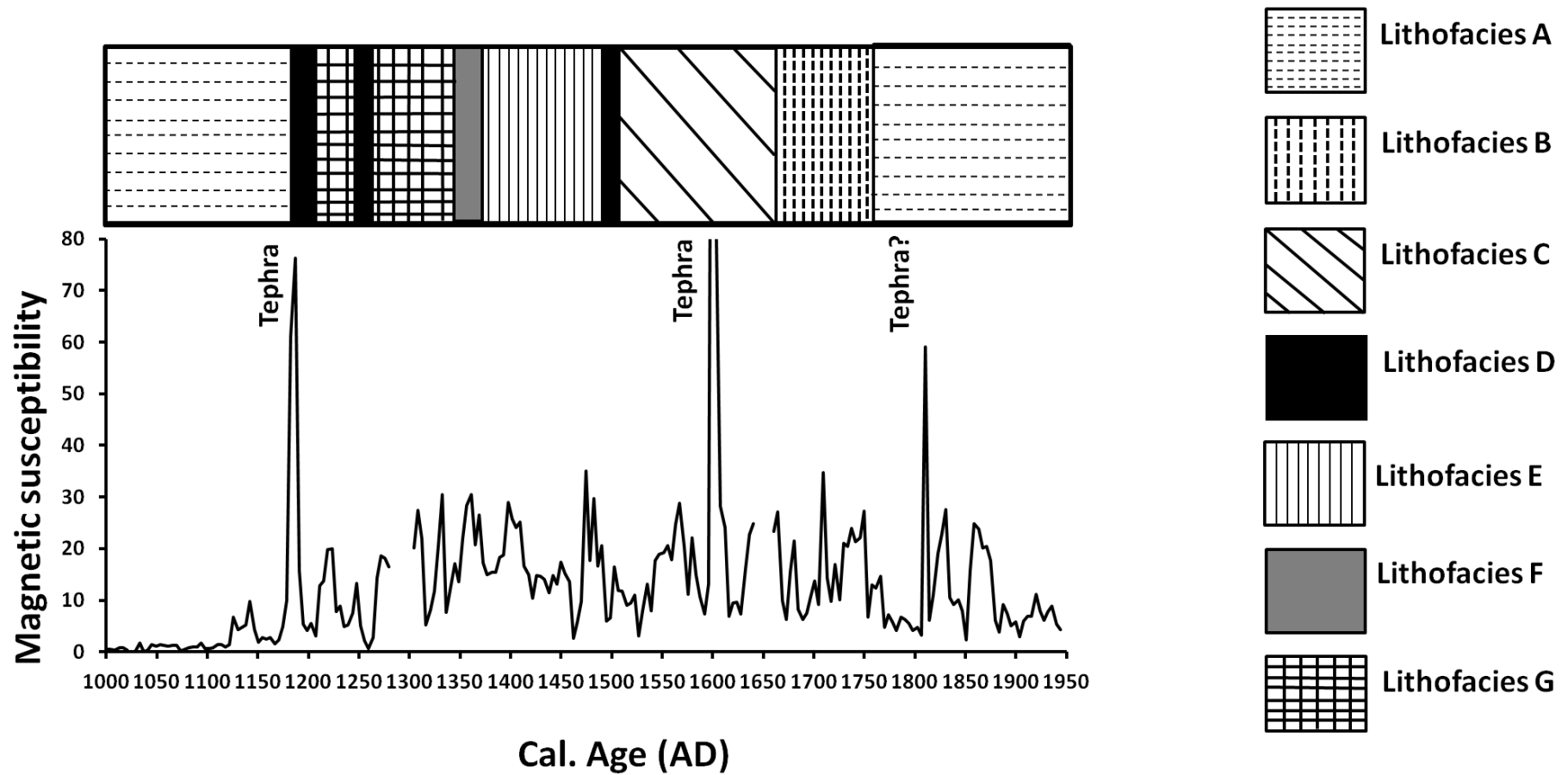


Figure 4-2: Magnetic susceptibility and lithofacies changes in the down-core sedimentary record.

4.2.6 *n*-Alkanes

4.2.7 CPI

The CPI₂₅₋₃₅ values significantly vary between 0.6 and 15.3 over the late Holocene (~1000 years; Figure 4-4). The oldest sample at ~955AD has a CPI₂₅₋₃₅ value of 7.3. The CPI₂₅₋₃₅ values initially rise to 11.4 at ~1053AD followed by a general decrease to 7.7 at ~1308AD. The CPI₂₅₋₃₅ values rise again to 10.7 at ~1413AD, followed by a decrease to 6.8 at ~1490AD. CPI₂₅₋₃₅ values then increase to 12.5 in ~1563AD followed by another decrease to 7.0 at ~1628AD. There is a sharp increase in CPI₂₅₋₃₅ values at ~1897AD to the highest values recorded (15.3).

4.2.8 ACL

The ACL₂₅₋₃₅ values show significant variations over the past 1000 years (ACL₂₅₋₃₅ values ranging from 27.3 to 29.4; Figure 4-4). Between ~955 and ~1110AD, the ACL values range from 29.0 and 28.3. There is a general decrease in ACL₂₅₋₃₅ values between 1110 and 1357AD to 8.3 followed by an increase to 29.2 at 1446AD. ACL₂₅₋₃₅ values were variable with a general decrease to 28.3 in 1782. Following this decrease, ACL₂₅₋₃₅ values steadily increase to 29.2 in ~1952AD.

4.2.9 Paq

The Paq values show significant variations (0.2-0.8) over the period of the late Holocene (~1000 years; Figure 4-4). Between 955 and ~1033AD Paq values decrease to 0.2, followed by an increase to 0.4 at 1098AD. The Paq values then decrease to 0.2 at 1118AD, followed by an increase to 0.4 at 1357AD. Between 1357 and 1563AD, Paq values are variable with a general decrease in values. Paq values increase to 0.5 at 1628, followed by a general decrease to 0.2 at 1897AD.

4.2.10 Si/Rb

In the earliest part of the record (955-1170AD), the Si/Rb ratio is high. Between 1200 and 1610AD, Si/Rb is relatively low and constant. At 1620 AD there is a large increase in Si/Rb to 1660AD, followed low values to the most recent section of the core.

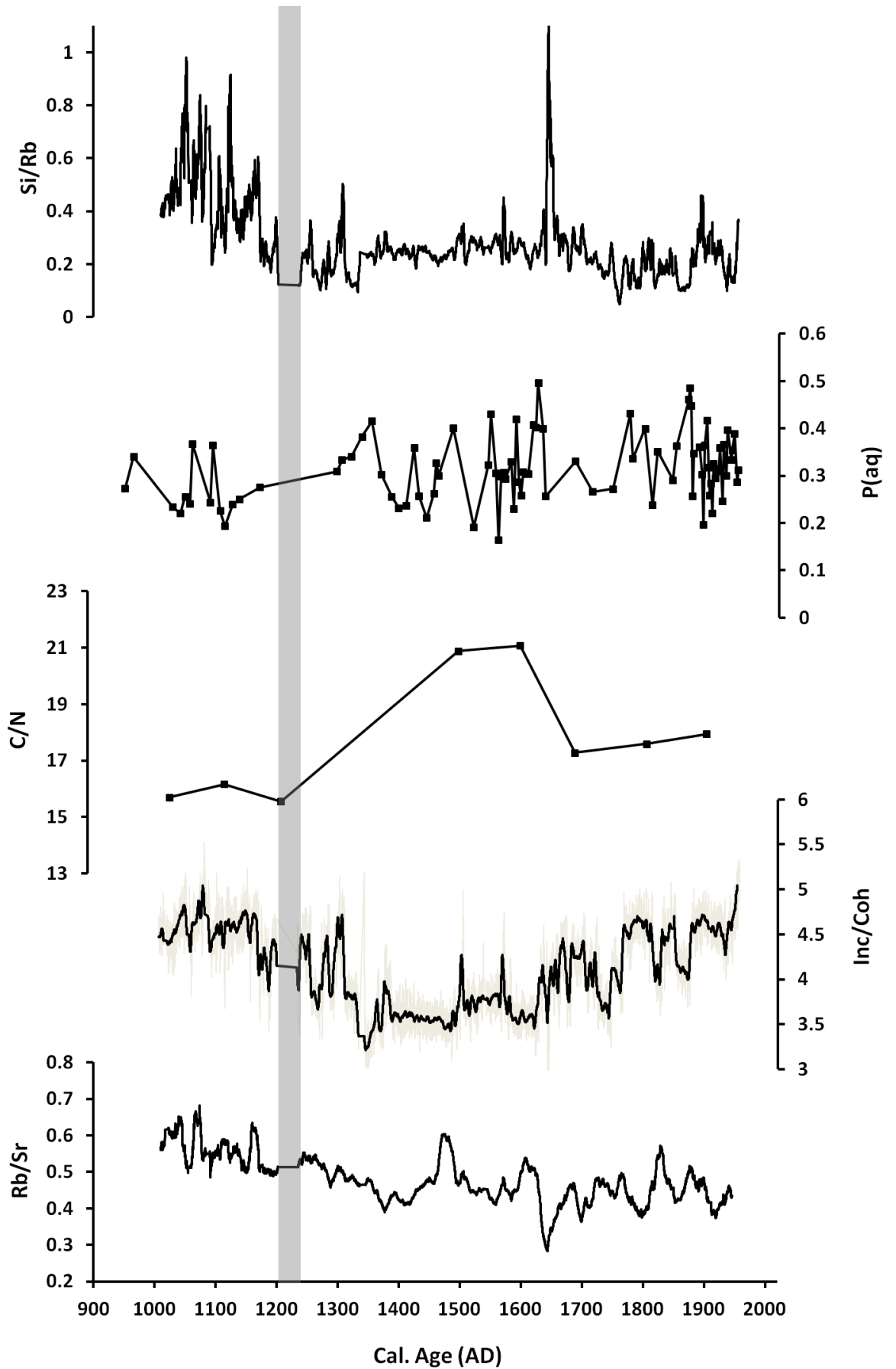


Figure 4-3: Variations in productivity over the past 1000 years in Lake Toyoni. From bottom to top; Rb/Sr ratio, Inc/Coh ratio, C/N ratio, Paq and Si/Rb ratio. Grey bar represent missing XRF data.

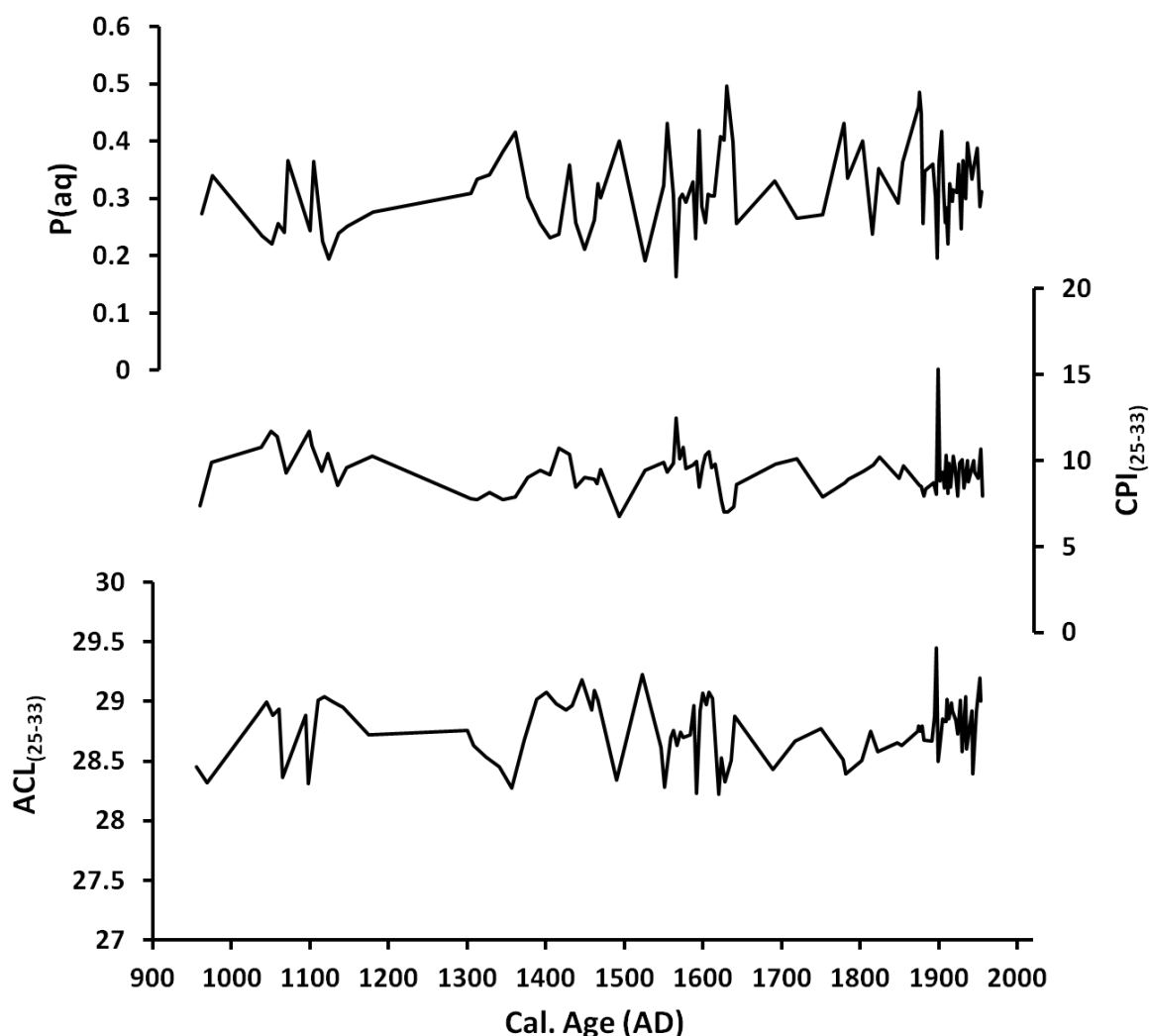


Figure 4-4: Variations in molecular composition of *n*-alkanes over the past 1000 years. From bottom to top; ACL, CPI and Paq proxies. ACL and CPI equations are both derived using the same data (C_{25-33}). The P(aq) equation also uses short chain *n*-alkanes and will be used as a representative for the molecular composition of *n*-alkanes in future discussions. Higher resolution sampling (half cm resolution) at the start of the core therefore higher resolution between 1900 and 2000AD.

4.3 Discussion

4.3.1 Productivity during the MWP (955-1300AD)

At Lake Toyoni, the Inc/Coh ratio indicates the OM content of the sediments. OM input is enhanced from ~1000-1300AD (MWP; Figure 4-3). While this is likely due to organic material being washed into the lake during increased precipitation, we also expect that the amount of precipitation also influenced productivity in the lake. Increased precipitation enhances run off, and hence nutrient input into the lake, which in turn promotes productivity. An increase in productivity during

the MWP is supported by high Si/Rb and low C/N ratios, suggesting that warm and wet conditions during the MWP promoted productivity in the lake.

The lowest MS is recorded in the earliest part of the record (1000-1170AD) (Figure 4-2) suggesting that during this time period there is a reduction in input of magnetic minerals (e.g. from wind and run-off input) into Lake Toyoni. However, high Inc/Coh ratio values suggest an increase in precipitation during this time period, which in turn would transport magnetic minerals into the lake. An alternative explanation is the low MS may represent anoxic conditions within the lake. Closed lakes, such as Lake Toyoni, are particularly prone to anoxic conditions. Low oxygen conditions (<2mg/L) prevail in Lake Toyoni when the water column becomes thermally stratified between June and October. When anoxia occurs, magnetic minerals within the sediments are dissolved or transformed into authigenic iron sulphides resulting in a decrease in MS (Nowaczyk et al., 2002, Ortega et al., 2006, Ao et al., 2010). Anoxic conditions in lakes also occur when the duration of ice-cover on the lake increases (Gebhardt et al., 2013) and also when productivity increases (Diaz, 2001, Nowaczyk et al., 2002). The time period between 1000-1200AD is characterised by low C/N ratios and high Si/Rb suggesting that productivity increased during this time period and may be responsible for anoxic conditions during this time period. Alternatively, the high OM content, as inferred from Inc/Coh ratio, may be responsible for low MS values. Anoxic conditions can preserve organic material that has a lower MS than clastic material. Within this time period, Lithofacies D appears once for a relatively short time period. Lithofacies D is characterised by faint laminations. Faint laminations are formed when the bottom water is anoxic (Kemp, 1996, Kotilainen et al., 2007), providing further evidence for anoxic conditions during this time period. Low MS values during the MWP is a result of high content of OM and/or dissolution processes during this time period as a result of anoxic sediments from increase productivity in the lake.

The anoxic conditions associated with the MWP suggest that thermal stratification during this time period was intense. When there is low oxygen content in the sediments, bacteria respire and nutrients are released into the water column. These nutrients will be available during the spring and autumn overturn of the lake. This combined with an increased in runoff (as inferred from

increase in Inc/Coh ratio values; Figure 4-3) supplying nutrients into the lake and increased temperatures during the MWP promoted an increase in biological production during this time period. An increased biological productivity would increase the amount of OM supplied to the lake floor. The increased flux of OM would in turn facilitate keeping sediments anoxic.

Based on the high productivity (high Si/Rb and low C/N ratios) and increased precipitation (high Inc/Coh ratios), it is suggested that the EASM intensified and/or the EAWM weakened during this time period. The warm conditions during the MWP resulted in stratification of the water column, which led to low oxygen conditions in the sediments, which are beneficial to the preservation of OM in sediments (Bralower & Thierstein, 1984). The duration of the ice-cover on Lake Toyoni during the MWP was significantly reduced resulting in an increase in the mixing time period in the lake during spring. At the same time, precipitation associated with an intense EASM increased during August and September, which transported nutrients into the lake. During the autumn overturn, the combined nutrients from run-off into the lake, along with nutrients released from anoxic bottom waters, resulted in a strong autumn bloom.

In addition to the high productivity of the MWP, high Rb/Sr values are also recorded during the MWP (Figure 4-3). Temperature reconstructions show warming during the MWP in Japan (e.g. Sakaguchi, 1983, Kitagawa and Matsumoto, 1995, Yamada et al., 2010). As previously stated, warm and wet conditions promote chemical weathering. If temperature was controlling the Rb/Sr ratio during this time period, we would expect to see a reduction in Rb/Sr values. Therefore, temperature is not controlling the Rb/Sr proxy, at least during this time period. Another control is precipitation, with increased precipitation leading to increased chemical weathering, and hence lower Rb/Sr values. It was suggested that precipitation increased during this time period based on an increase in Inc/Coh ratios. However, the Rb/Sr ratio is high during this time, which indicates a drier environment with reduced chemical weathering, opposite to findings based on Inc/Coh ratio. Furthermore, the Rb/Sr values are opposite to Jin et al. (2006) (Figure 4-6) showing lower Rb/Sr values during the MWP. It is suggested that the high Rb/Sr values during this time period are not reflecting chemical weathering but in fact other chemical processes within the sediments. In the previous section, it was suggested that

anoxic conditions were present during the MWP based on very low magnetic susceptibility values. Anoxic conditions prevail when increased organic material is transported to the bottom of the lake, which increases respiration of bacteria, resulting in low oxygen levels. The chemical composition of material transported from water column to sediments is changed by diagenetic processes (Billon et al., 2002). Billon et al. (2002) found that Sr can interact with calcium carbonate, which removes Sr from the sediments by precipitation and adsorption with calcite or a combination of both processes. Anoxic conditions decreased the amount of Sr within the sediments resulting in high Rb/Sr values even during a time period when chemical weathering was enhanced.

4.3.1.1 Productivity LIA (1300-1850AD)

The highly productive time period of the MWP was followed by low productivity (low Si/Rb values) and OM (low Inc/Coh values) at the onset of the LIA (Figure 4-3). The reduction in aquatic productivity and increased terrestrially derived OM (as inferred from high C/N ratios) continued between 1300-1610AD (Figure 4-3). The slight increase in Inc/Coh ratio around ~1500AD (Figure 4-3) is explained due to an influx of terrestrially derived OM via increased run off or wind input into the lake. Another explanation for the reduction in BSi could be competition between diatoms and with other species (e.g. cyanobacteria, haptophyte algae). However, the C/N ratios also increased during this time period suggesting an increase in terrestrial material and a reduction in overall productivity in the lake.

Within this reduced productivity time period, Lithofacies D appears ~1511-1490AD (Figure 4-2), which is characterised by faint laminations. Faint laminations are interpreted as anoxic bottom water (Kemp, 1996, Kotilainen et al., 2007), which may be caused by increased ice-cover of the lake and therefore less mixing time and low oxygen levels in the sediments (Gebhardt et al., 2013). An alternative explanation for laminations during this time period is clastic material gathering on top of the ice of the lake during winter resulting in a large input of material into the lake during melting period.

Subsequent to the low Si/Rb ratios between 1300 and 1620AD, there is a sharp increase in Si/Rb ratios ~1620AD (Figure 4-3) suggesting increased productivity.

This increase in Si/Rb ratios is consistent with a significant decrease in C/N ratios (Figure 4-3). This time period is also associated with a tephra layer (Figure 4-2) suggesting increased Si/Rb ratios (Figure 4-3) may also be attributed to the water column becoming enriched with nutrients following the deposition of ash from volcanic fall out (Lotter et al., 1995). As a result, diatom concentrations have been shown to increase after tephra deposition (Telford et al., 2004). Alternatively, since Silica is deposited into the lake as part of the tephra layers, the increased Si/Rb during this time period (Figure 4-3) may not be related to increased productivity but rather reflecting the increased Si from the tephra layer (as inferred from high MS values). We suggest that productivity increased during this time period, because the C/N ratios sharply decrease (Figure 4-3) suggesting an increased influence of algae OM during this time period. If tephra is having an effect on productivity due to increased nutrients in the lake Toyoni record during this time period, it is a short-term event and is not prolonged for long periods of time after the deposition of tephra in Lake Toyoni.

Ash associated with volcanic eruptions influences the MS during this section of the core. In general the LIA is characterised by an increase in MS (Figure 4-2); however, this is highly variable. The presence of two tephra layers within this time period may also be responsible for the increase in MS due to ash remaining within the catchment and being transported into the lake after the timing of the tephra layer via run off processes. The increase in C/N ratios suggests an increased influence from terrestrial input during this time period. The high MS values therefore likely represent an increase in terrestrial input (e.g. increased wind activity and run-off via precipitation and/or snow-melt) into the lake. It is suggested that wind activity increased during this time period, which would have also kept the water column well mixed and the sediments oxic, which is conducive for preserving magnetic minerals (wind processes are further discussed in the following chapter).

The oxic conditions during the LIA will not negatively influence the Rb/Sr ratio during this time period suggesting that the proxy is reliable during the LIA compared to the MWP where it was influenced by anoxic conditions. High Rb/Sr values are recorded in 1445-1500AD, 1575-1620AD and 1800-1840AD (Figure 4-3) suggest a decrease in chemical weathering within the catchment. Between 1445-1500AD there is a reduction in solar irradiance (Figure 4-7). Colder

temperatures, associated with a decrease in solar irradiance, decrease the rate of chemical weathering in the catchment. Therefore, it is suggested that cold conditions during this period of time resulted in a reduction in chemical weathering. In comparison, solar irradiance between 1750-1850AD is higher (Figure 4-7) and therefore a decrease in chemical weathering may be associated with drier conditions, via reduced rainfall or snowfall.

Chemical weathering increased (reduction in Rb/Sr ratio) between 1300-1450AD, 1570-1575AD and 1610-1800AD (Figure 4-3) suggesting that terrestrial material increased during this time period suggesting this time period received more precipitation via rainfall and/or snowfall during this period of time. Jin et al. (2006) found an enhancement of chemical weathering in both record between 1300-1450AD (Figure 4-6). This time period has variable temperature reconstructions with some records showing cooling (Ge et al., 2011) during this time and some records showing warming (Tan et al., 2003) (Figure 4-6). Increased warming during this time period is suggested possibly due to an intensification of the EASM increasing rainfall in this region and promoting increased chemical weathering. The lowest Rb/Sr values are ~1640AD, which is also the timing of tephra 2 and also increased productivity (increased Si/Rb and decreased C/N ratios) in the core (Figure 4-3). Low Rb/Sr values during this time suggest that the drop in the Rb/Sr ratio is associated with tephra deposition rather than increased chemical weathering in the core.

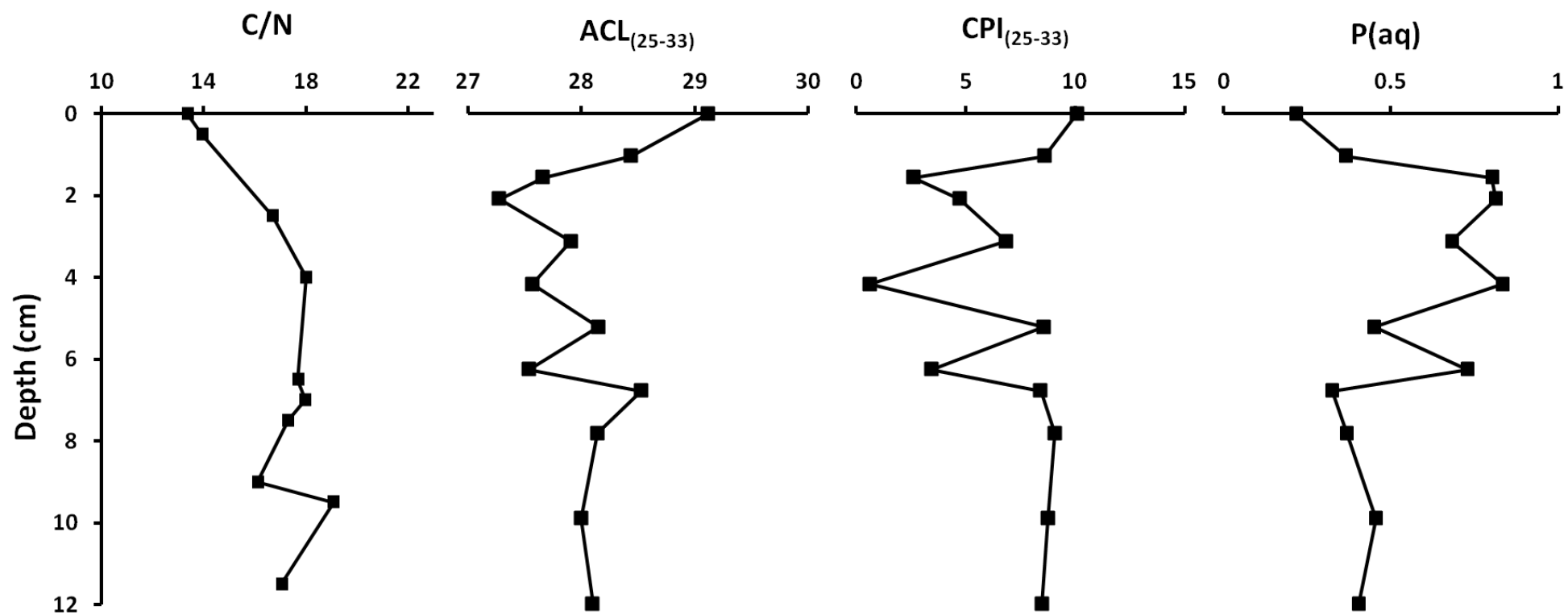


Figure 4-5: Variations in C/N ratios and the molecular composition of *n*-alkanes (ACL, CPI and Paq) in short core TY11.

4.3.1.2 Productivity recorded in short core TY11

The short core (12cm) taken from Lake Toyoni records a dramatic decrease in C/N and Paq values in comparison to the data from TY09 (Figure 4-5). This suggests that the productivity increased significantly during his time period. This time period is also associated with an increase human population in Hokkaido also increased significantly. It is suggested that aquatic productivity increased during this time period in Lake Toyoni is mainly driven by human-induced environmental change rather than natural climate factors. A previous study from a lake in Hokkaido, Lake Onuma (N:42°00'09'', E:140°41'28''), also found an increase in algae productivity over the past ~100 years. The authors' suggested the increase in algae productivity reflects an increased input of inorganic nutrients into the lake. The increased anthropogenic nitrogen inflow, for example from livestock and sewage water, promoted eutrophication of Lake Onuma, which is recorded in higher $\delta^{15}\text{N}$ values. Lake Toyoni is relatively close to Lake Onuma, we therefore suggest that anthropogenic influence has also affected Lake Toyoni in recent years by increasing nutrient content of the lake and promoting productivity. We suggest that the increased nutrients associated with an increase in human activity led to an increase in aquatic production in the lake. In particular the influence of submerged and floating macrophytes, as inferred from higher Paq values and low ACL values (Figure 4-5). This increase in productivity resulted in anoxic sediments and stimulated a large increase in bacterial growth in the sediments, which have C/N ratio values lower than 4 (Lamb et al., 2006). Further evidence for bacterial degradation is the low CPI values (Figure 4-5) during this time period.

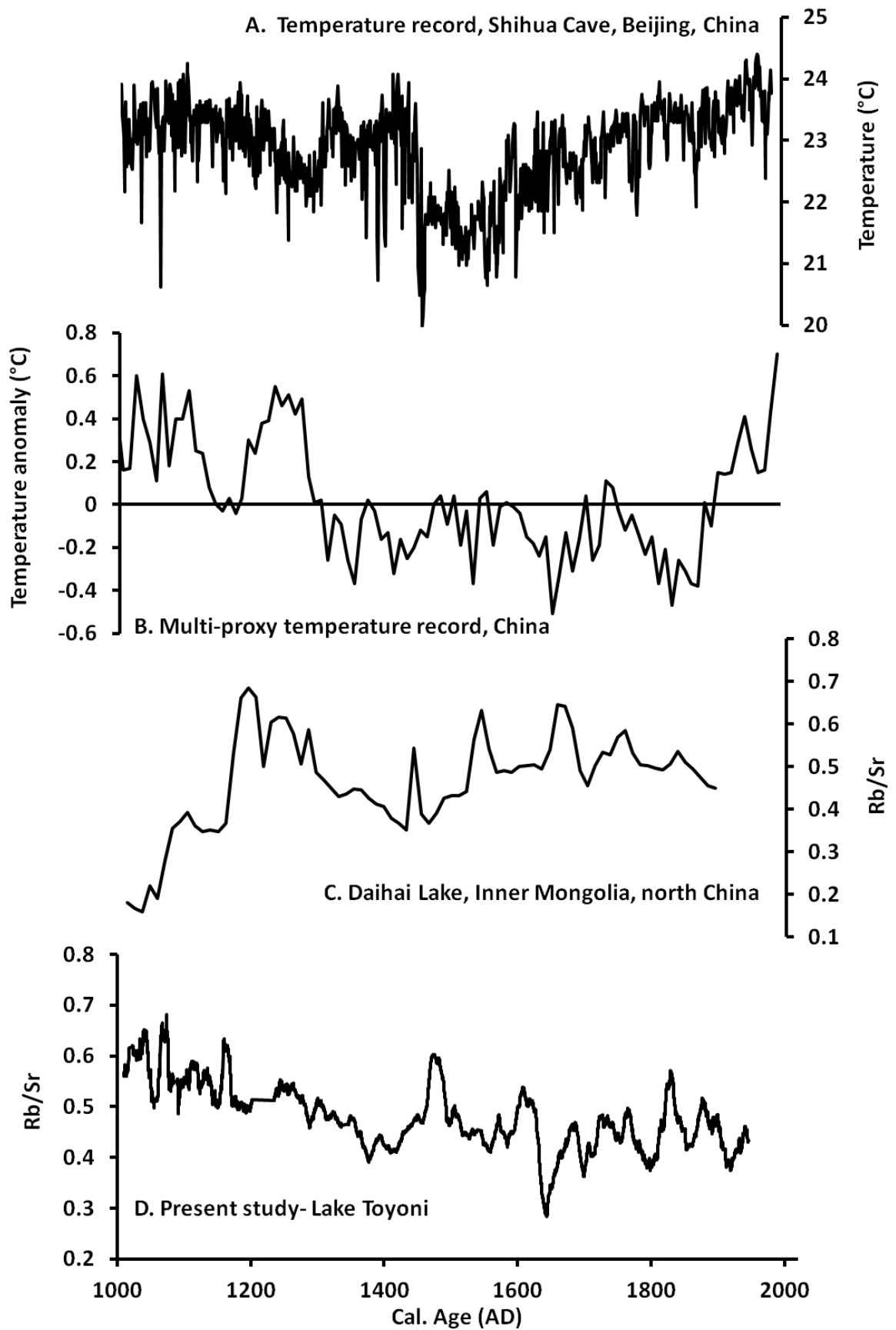


Figure 4-6: Variations in the Rb/Sr ratios and temperature records from Asia. A is a temperature record derived from Shihua Cave, Beijing, China (Tan et al., 2003). B is a temperature reconstruction using proxy temperature data with relatively high confidence levels from five regions across China (Ge et al., 2011). C is the Rb/Sr ratio from Daihai Lake (Jin et al., 2006) and D is the Rb/Sr ratio from Lake Toyoni.

4.3.2 Possible forcing mechanisms

4.3.2.1 Solar irradiance

The results have clearly shown that productivity in Lake Toyoni has varied significantly over the past 1000 years, and in particular responded to changes in the EAWM and EASM intensity. In order to determine the possible forcing mechanisms, the results are discussed in relation to solar irradiance and the phase of the PDO.

The link between increased solar irradiance and a stronger EAM is also well documented (e.g. Dykoski et al., 2005, Wang et al., 2005, Xiao et al., 2006, Liu et al., 2009b, He et al., 2013, Sagawa et al., 2014). The influence of solar activity on the EAM is based on amplified solar radiation causing increased warming the land over middle and high latitudes compared to lower latitudes (Zhou et al., 2011). In addition, land warms at a faster rate than oceans promoting a temperature difference between the land and ocean (Zhou et al., 2011). Moist air is transported from the ocean to the land resulting in warm and wet conditions in Hokkaido, which enhances productivity in Lake Toyoni via increased run-off into the lake. When solar activity decreases, there is less heating of the land resulting in a higher-pressure system developing over Siberia and as a result the EAWM strength increases (Kim et al., 2013).

To establish the relationship between solar activity and the EASM precipitation in Hokkaido, the Inc/Coh record (proxy for monsoonal precipitation) is compared to the reconstructed solar irradiance record of Bard et al. (2000). Bard et al. (2000) derived solar irradiance variations based on the production rates of cosmogenic nuclides (^{14}C and ^{10}Be) from an ice-core record at the South Pole (Bard et al., 2000). When solar irradiance is high, the magnetic fields of solar winds deflect proportions of the charged cosmic particles, resulting in lower production of cosmogenic nuclides. On the other hand, when solar irradiance is low, there is a higher production of cosmogenic nuclides. The record has been geomagnetically corrected based on records proposed by Korte and Constable (2005) and also assuming that the geomagnetic modulation is reduced by a factor of 0.8 at the pole (Bard et al., 2000). The record of solar irradiance from Bard et al. (2000) over the past 1000 years is presented in Figure 4-7. As

expected, the results show a clear relationship between the Inc/Coh values at Lake Toyoni and the solar activity over the past 1000 years (Figure 4-8; higher Inc/Coh values (suggesting enhanced EASM precipitation) generally corresponds to higher solar irradiance; whereas, lower Inc/Coh values (suggesting a reduction in EASM precipitation) correlates to lower solar irradiance. An exception is ~1700AD which shows an increase in precipitation despite a reduction in the EASM (Figure 4-8). This time period is associated with a change from the positive phase of the PDO to a negative phase of the PDO and is further discussed in the following section. The lowest solar irradiance values occur during the LIA and the highest during the MWP. As expected, the Inc/Coh values also follow the same trend, with increased EASM precipitation during the MWP and decreased EASM precipitation during the LIA. The similarity between the Inc/Coh ratio and the solar irradiance record suggests that they vary together over the past 1000 years (Figure 4-8) suggesting that solar activity is a key control on the EASM precipitation in Hokkaido, Japan. Significantly, productivity (as inferred from Si/Rb and C/N ratios) also increased when the EASM precipitation was enhanced suggesting that the EASM positively influences productivity in Lake Toyoni.

4.3.2.2 PDO

In addition to solar irradiance, another climate driver in Hokkaido is the PDO (Tsuji et al., 2008). It was found that, in addition to the strength of the EAM, the PDO exerts the strongest control on precipitation in Hokkaido. For example, there is a 200mm difference in precipitation between the positive and negative phase of the PDO in the instrumental data (Chapter 2). To examine the relationship between the PDO and productivity in Lake Toyoni, the productivity results (Inc/Coh, C/N and Si/Rb ratios) are compared to the PDO index from Macdonald and Case (2005) for the past 1000 years and is presented in Figure 4-7. The PDO Index was reconstructed using tree-ring chronologies from *Pinus flexilis* in California and Alberta (western Canada). The two sites are located at opposite ends of the PDO precipitation dipole and hence the hydrological variability associated with the PDO is opposite signs in the two regions; making these tree-ring records sensitive to the variability of the PDO. The relationship between the phase of the PDO and precipitation, as inferred from the Inc/Coh ratio, is apparent over the past 1000 years. During the negative phase of the PDO there is increased Inc/Coh ratio values, and vice versa.

The PDO record shows that the MWP is characterised by the negative phase and there is a distinct shift to the positive phase during the LIA. The negative phase of the PDO is characterised by warmer and wetter conditions in Hokkaido. The negative phase of the PDO positively influenced the productivity during the MWP through a reduction in ice duration on the lake, which extended the mixing period in the lake and enhanced productivity. In addition, an increase in precipitation resulted in an increase in nutrient input into the lake, which also positively influenced productivity in Lake Toyoni.

Productivity during the positive phase of the PDO was significantly reduced during the LIA (1300-1800AD). A reduction in precipitation and longer ice conditions on the lake resulted in lower productivity. An exception is ~1600AD, where there was enhanced productivity in the lake, as inferred from a reduction in C/N values and increased Si/Rb values. The large spike in Si/Rb values is likely due to the visible tephra layer at this time period; however C/N values remain lower throughout this time period suggesting that productivity continued to be high after the tephra-induced diatom bloom. This time period is associated with a reduction in the EASM intensity (Figure 4-8). Significantly, the phase of the PDO changed from positive to negative during this time period, which increased precipitation and supplied the lake with nutrients required for productivity to occur. This suggests that although the EASM intensity has a key role in controlling productivity in Lake Toyoni on a seasonal basis, the phase of the PDO further modifies productivity in the lake on decadal time scales, which may overshadow the seasonal influence of the EASM on productivity in the lake.

During the LIA, the PDO shifted from positive to negative at the same time that the C/N ratios dramatically decreased (~1600AD; Figure 4-7). This shift in the phase of the PDO may be responsible for the large change in lake productivity during this time period, combined with increased run-off due to the dramatic increase in human population. The increased run-off into Lake Toyoni during this time period, as a result of the negative phase of the PDO or/and human-induced environmental change significantly changed the productivity status of the Lake. Significantly, models indicate a weak shift towards more occurrences of the negative phase of the PDO (IPCC, 2014). In addition, the IPCC report also suggests that the climate will warm by 0.8-2.6°C by 2050 (IPCC, 2014). The combination of the warming and also increased occurrences of the negative

phase of the PDO in Hokkaido will result in enhanced productivity in Lake Toyoni. An enhancement of primary productivity in Lake Toyoni may lead to eutrophication of the lake.

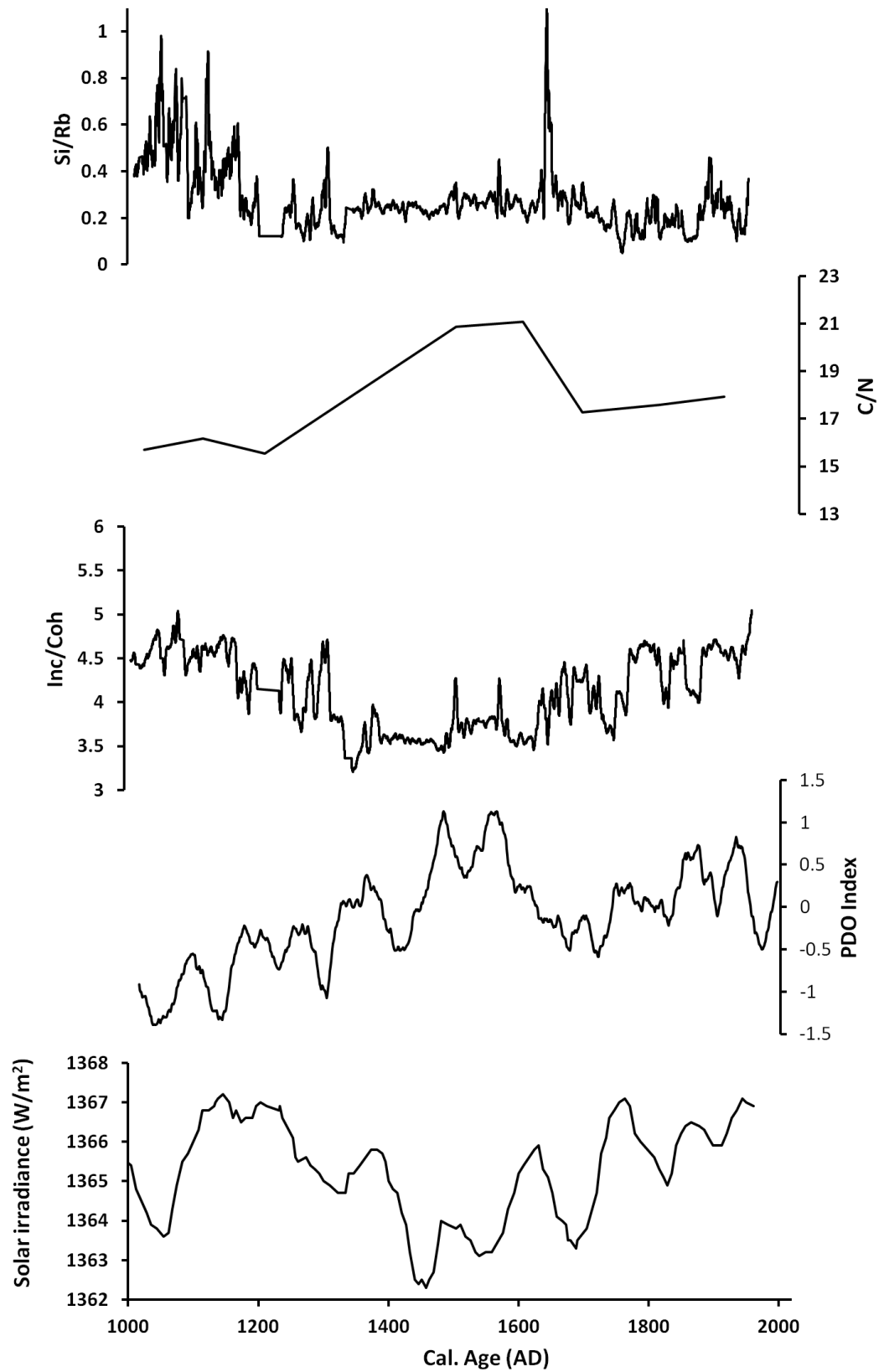


Figure 4-7: Variations in lake productivity compared with solar irradiance (W/m^2) and the PDO index. From top to bottom; Si/Rb, CN and Inc/Coh ratio values (all from present study), PDO Index by Macdonald and case., (2005) and solar irradiance (W/m^2) by Bard et al., (2000).

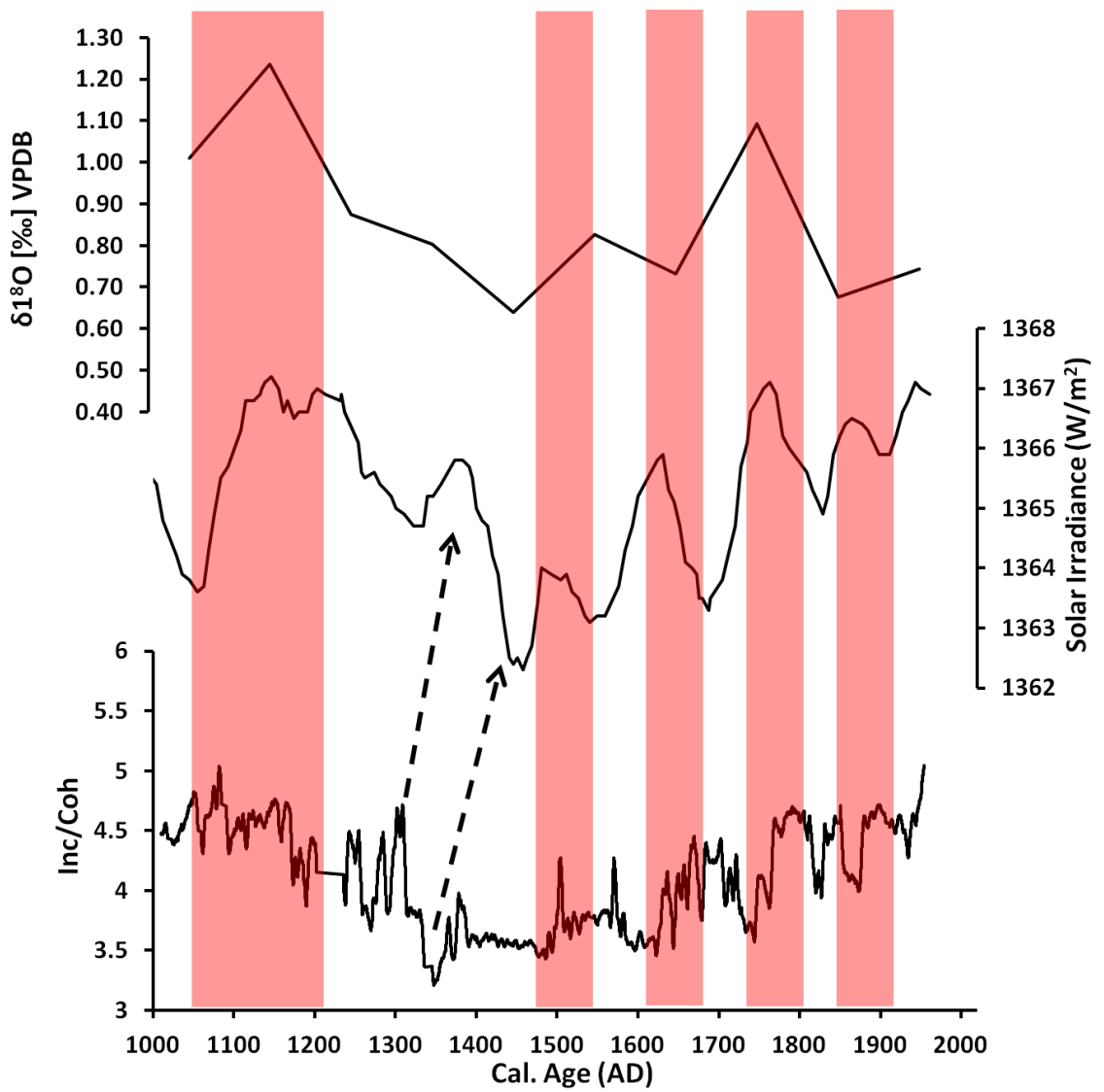


Figure 4-8: Comparison of monsoonal precipitation variations (as inferred from Inc/Coh ratio; bottom graph) over the past 1000 years with solar irradiance (Bard et al., 2000) and EAM record of Hu et al. (2008). The top graph is the original $\delta^{18}\text{O}$ values from the Heshang stalagmite (Hu et al., 2008), the middle graph is solar irradiance (Bard et al., 2000) and bottom graph is Inc/Coh ratio.

4.4 Conclusions

A multi-proxy reconstruction of productivity variability over the past 1000 years from Lake Toyoni includes; MS (proxy for magnetite preservation), Si/Rb (proxy for diatom productivity), Inc/Coh (proxy for OM), and molecular composition of n-alkanes; CPI, ACL and Paq (proxies for source of n-alkanes, temperature and productivity, respectively). Sediment transport into Lake Toyoni is restricted to the ice-free months when temperatures are above 0°C, which usually occurs between ~March-December. During spring, ice-off occurs in Lake Toyoni and precipitation and melt-water from ice on top of the lake and snow in the catchment enters the lake. Thermal stratification occurs between June-September and the bottom waters of the lake become hypoxic during this time period. Oxidic bottom water conditions, when thermal stratification weakens, results in good preservation of magnetite and degradation of OM. Whereas anoxic bottom water conditions, when thermal stratification in Lake Toyoni is more intense, results in magnetite dissolution and well-preserved OM content of the sediments.

Seasonally, the climate of Hokkaido is strongly influenced by the EAM (the EASM during summer and the EAWM during winter). On decadal time-scales, the climate of Hokkaido is further modified by the phase of the PDO. The negative phase of the PDO is associated with warmer and wetter conditions in Hokkaido; whereas, the positive phase is associated with colder and drier conditions. Lake Toyoni is therefore influenced by the EAM and the PDO, resulting in a key location to assess the relationship between the EAM and PDO on lake productivity. The phase of the PDO, along with the intensity of the EASM, significantly influences productivity in Lake Toyoni over the past 1000 years.

During the MWP (~955-1300AD), the climate conditions in Hokkaido were warm and wet (due to an increased EASM and negative phase of the PDO) resulting in an increased duration of the mixing time period during spring due to ice-off occurring earlier in the year. In addition, the increased precipitation associated with the negative phase of the PDO and the EASM resulted in increased run-off into the lake, which sustained the autumn bloom when the water column in Lake Toyoni becomes mixed. Thermal stratification during the MWP was intense and also productivity was high leading to anoxic bottom waters and hence low MS.

Based on the high productivity and increased precipitation during the MPW, it is suggested that the EASM intensified and/or the EAWM weakened during this time period.

The highly productive MWP was followed by a period of low productivity during the early LIA (1300-1600AD). Conditions during this time period were colder resulting in an increase in the ice duration and a reduction in the thermal stratification of the water column. Nutrient input from run-off was reduced during this time period resulting in a decrease in productivity. A combination of a reduction of productivity and reduction in thermal stratification resulted in oxic bottom waters, leading to good preservation of magnetite and degradation of OM. Based on the low productivity and decreased precipitation during the LIA, it is suggested that the EAWM intensified and/or the EASM weakened during this time period. Productivity was enhanced during the late LIA (~1600-1800AD) due to a significant shift in the phase of the PDO from positive to negative. The phase change resulted in increased run-off into the lake following increased precipitation associated with the negative phase of the PDO.

Following the LIA, the population of Hokkaido abruptly increased (~1870AD). The increase in population resulted in an increase in agriculture activities, road and house development and increased pollution. We find that the conditions of the lake changed significantly in the short core (TY09), possibly reflecting human-induced environmental change. We suggest that the increased nutrients associated with an increase in human activity led to an increase in aquatic production in the lake (e.g. submerged and floating macrophytes and also algae). An increase in productivity resulted in anoxic sediments and stimulated a large increase in bacterial growth in the sediments.

5

Assessing the contribution of dust from global (the Westerlies) and regional (the EAWM) wind patterns

5.1 Introduction

Asian dust plays an important role in palaeo-climate studies because it can be used as a proxy of changes in global and regional wind systems (Uematsu et al., 1983, Porter and Zhisheng, 1995, Xiao et al., 1995, Xiao et al., 1999, Xiao et al., 1997b, Yamada et al., 2010) as well as continent environmental (temperature and aridity) conditions (Rea et al., 1998, Mischke et al., 2009, Wang et al., 2013b). In Japan, previous studies have found the amount of dust transported to Japan was consistently higher during cold periods, for example, the last glacial maximum (LGM) (Yoshinaga, 1996, Ono and Naruse, 1997). Dust is accumulated in terrestrial settings (e.g. lakes and peat bogs) and marine settings allowing variability in past aeolian input to be analysed.

Aeolian activities are common in the arid and semi-arid environment of Central Asia, which is usually regarded as a major dust source in the world (Prospero et al., 2002). Japan is located down-wind of these dust source regions and therefore offers a key location for investigating past variability in aeolian activity. Moreover, terrestrial settings within Hokkaido are key places for the investigation of variability in dust into in the past because most of the dust is

expected to occur between 25-55°N (Tsunogai et al., 1988), reaching 40m/s, occurring between 30°N and 40°N (Duce et al., 1980). Lake Toyoni is situated at 42°N and is therefore a key location for studying variability in dust input over the past millennium. Lake Toyoni is also expected to record a strong aeolian input because there are no rivers or permanent streams into the lake therefore this lake is natural trap for aeolian input. Thus, the dust record from Lake Toyoni is important for understanding in global and regional wind circulation patterns and changes of the regional environmental (temperature and aridity) variability in the dust source regions.

5.1.1 Global and regional wind circulation patterns

The main wind patterns transporting dust to Hokkaido are the East Asian Winter Monsoon (EAWM) (Porter and Zhisheng, 1995, Xiao et al., 1995, Xiao et al., 1997b) and the Westerlies (Uematsu et al., 1983). Dust transported to Japan via the Westerlies and the EAWM originates from different sources (Ferrat et al., 2011) and can be distinguished by the grain size of the dust.

5.1.1.1 Westerlies

The Westerlies are a global wind pattern which transport fine-grained dust (1-10 μ m) (Mikami et al., 2006) to Hokkaido from the Taklimakan desert (

Figure 5-1) (Lim and Matsumoto, 2006), which is entrained to an elevation of 5000m (Lim and Matsumoto, 2006, Mikami et al., 2006). The Westerlies intensify during spring (Tsunogai et al., 1988, Uematsu et al., 1983) bringing an increase in dust input during this time and weaken during summer, reducing the amount of dust is transported to Japan (Uematsu et al., 1983). This means that increases in fine-grained particles (1-10 μ m) at Lake Toyoni should indicate increased input from the Westerlies in Hokkaido.

5.1.1.2 The EAWM

In contrast, the EAWM is a regional wind pattern and transports coarse-grained dust (Xiao et al., 1997a, Yamada et al., 2010, An et al., 2011) from the Gobi Desert in southern Mongolia and the adjoining Gobi and sand deserts in China (

Figure 5-1) (Lim and Matsumoto, 2006, Liu et al., 2014c) and can only be entrained to an elevation of <3000m (Lim and Matsumoto, 2006, Mikami et al.,

2006). Coarse-grained dust particles as a proxy for the EAWM has been defined as 50-200 μm by Yamada et al. (2010), based on lacustrine sediments from northern Japan and also >63 μm by An et al. (2011), based on lacustrine sediments from arid Central Asia. We interpret coarse-grained sediment input by the EAWM as 50-200 μm based on the close proximity between Lake Toyoni and Lakes Ni-no-Megata and San-no-Megata, northeastern Japan (Yamada et al., 2010). As a result, increases in coarse-grained particles (50-200 μm) at Lake Toyoni should indicate an enhancement of the EAWM in Hokkaido. There are two main indices of the EAWM; firstly, is the temperature in East Asia (Gong et al., 2001). Secondly, the intensity of the Siberian High (SibH) (Ding, 1990, Zhang et al., 1997, Wu et al., 2006a, Gong et al., 2001) which is defined as the average sea level pressure (SLP) (Gong et al., 2001). The SibH is strongly influenced by the negative phase of the Arctic Oscillation (AO) (Wu and Wang, 2002, Gong et al., 2001, Chen et al., 2013). When the SibH intensifies and/or temperatures decrease, the EAWM is more intense, resulting in an increase of coarse-grained dust into Lake Toyoni.

Environmental conditions at the dust source region

Environmental conditions (e.g. aridity and/or temperature) can be a potential cause of an increase in dust storm frequency (Yang et al., 2007). Dust storm frequency increases when the environment is arid due to its influence on soil moisture content and vegetation cover. When precipitation increases, vegetation cover also increases, which in turn reduces storm frequency. In contrast, when aridity increases, soil moisture and vegetation is reduced. As a result, dust particles are more prone to movement and dust storms increase. In addition to aridity, temperature also influences the occurrence of dust storms at the source region. Qian et al. (2002b) found that when temperatures decrease, the Siberian High intensifies and is located further south. These conditions results in cold surges and an increase in dust storm frequency. The occurrence of dust storms at the source regions also influence other regions, such as Hokkaido, as dust can be transported long distances. Therefore an increase in dust storms within the source regions will also be reflected in the Lake Toyoni sedimentary record.

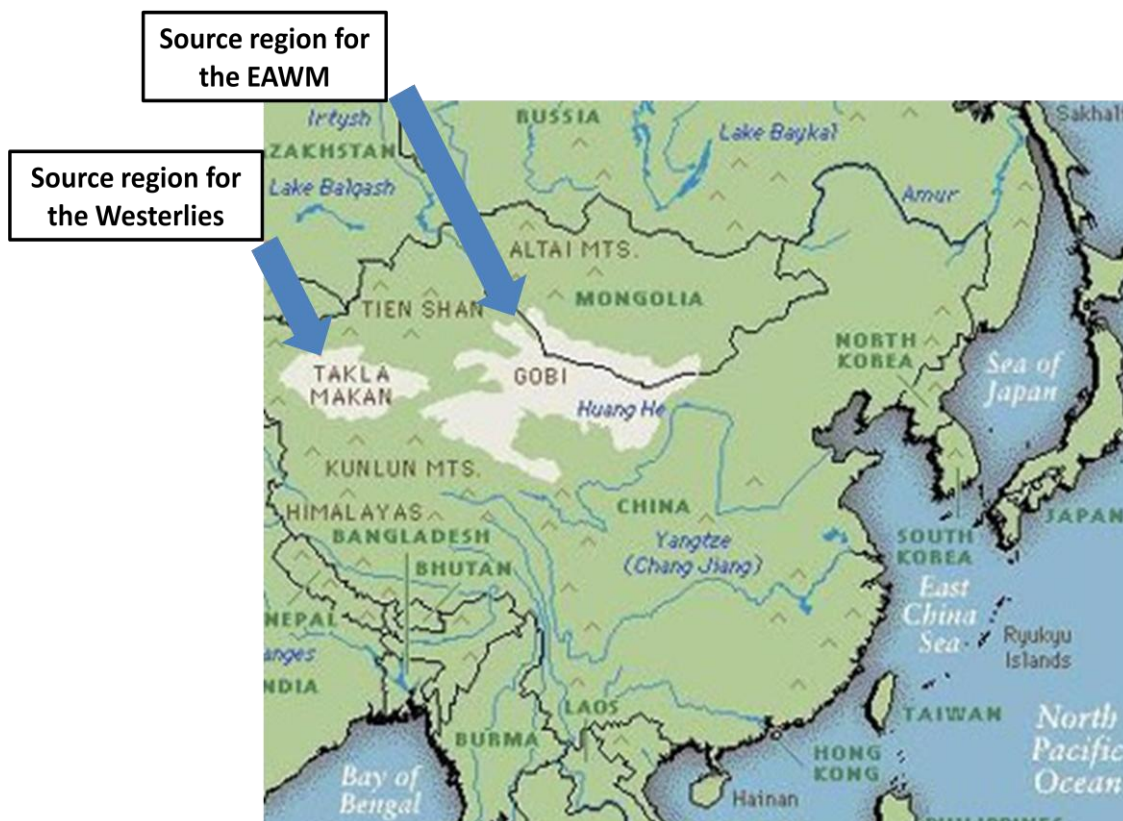


Figure 5-1: Map of the locations of the Taklamakan Desert in northwestern China (source region of the Westerlies) and also the Gobi Desert in northern and northwestern China as well as southern Mongolia (source region of the EAWM).

5.1.2 Proxies for dust input into Lake Toyoni

In order to assess dust input into Lake Toyoni, we investigated the Titanium (Ti) content within the lake (Yancheva et al., 2007). Significantly, using Ti as a proxy aeolian input, Yancheva et al. (2007) reconstructed the EAWM intensity over the past 16,000 from lacustrine sediments in South China. Ti is particularly useful for determining the variability of aeolian input because it is not influenced by redox conditions (Yancheva et al., 2007). Subsequently, Zhou et al. (2007) responded to the validation of Ti being used as an aeolian proxy and suggested that Ti in Lake Huguang Maar sediment reflected hydrological variability within the catchment. Therefore in order to use Ti as a proxy for aeolian input, we must first be sure that Ti is not solely coming from the catchment of the lake. In the present study, we correct for the catchment effect by normalising Ti to Rb to highlight the proportion of Ti transported by aeolian input.

In addition, magnetic susceptibility can also provide information on aeolian input into lakes (e.g. Yancheva et al., 2007). Yancheva et al. (2007) suggested that wind processes can influence the MS in two ways; firstly, an increase in magnetite minerals, which are two times denser than other common minerals (e.g. aluminosilicates) (Yancheva et al., 2007) transported by the EAWM can increase the MS response within sediments (Yancheva et al., 2007). Secondly, stronger winds can promote mixing within the water column preventing stratification of the water column and as a result preventing less oxygen conditions within the bottom water (Yancheva et al., 2007, Nowaczyk et al., 2002). Low oxygen content can result in dissolution of magnetic minerals and hence a lower MS (Nowaczyk et al., 2002, Yancheva et al., 2007, Gebhardt et al., 2013). In comparison, when there are oxic conditions magnetic minerals are well preserved (Nowaczyk et al., 2002).

To sum up, the distribution of the flux (Ti/Rb ratio and magnetic susceptibility), the grain size of aeolian dust in palaeo-climate archives (e.g. lake sediments) reflect the environmental conditions (aridity and temperature) of the source region as well as the strength and pattern of the wind system (Zhou et al., 2007, Leinen et al., 1986). The deposition of dust into Lake Toyoni over the past 1000 years is discussed in relation to the MWP, LIA and the CWP. The aims of this chapter are to:

1. Distinguish time periods of intensification of the EAWM and the Westerlies
2. Determine if the environmental conditions at the source region influences dust deposition in Lake Toyoni
3. Determine the key teleconnections influencing the Westerlies and the EAWM

5.2 Results

5.2.1 PSA

Percent (%) coarse-grained sediments (50-200 μ m) and % fine-grained sediment (1-10 μ m) are presented in Figure 5-2. Fine-grained sediments are the dominant grain size within the sedimentary record. Coarse-grained sediments (%) varies between 1.5-61.5% in the down-core record and fine-grained sediments (%) varies between 38.5-98.5%. The coarse-grained sediment content was generally low between 1000AD and 1200AD. High values are recorded between 1215-1460AD, with the highest values recorded at 1458AD. Values then decrease to 17.2% in 1543AD and then sharply increase again between 1556-1632AD. Values then decrease again to 14.8% in 1681 and remain low until 1745AD; a slight increase in coarse-grained sediments is recorded within this time period between 1700 and 1715AD. There is a sharp increase to 52.1% in 1794AD, followed by a sharp decrease to 9.9% in 1822 where values remain low to 1887AD, which is the most modern data point. All increases in coarse-grained sediments (%) are associated with a decrease in fine-grained sediments(%).

5.2.2 Ti/Rb

The earliest part of the record has high Ti/Rb values (1000-1170AD), followed by a period of low values between 1170-1320AD. Ti/Rb values then increase briefly between 1350 and 1715AD, decrease between 1715 and 1800AD, followed by increased values between 1800-1950AD (Figure 5-2)

5.2.3 Magnetic susceptibility (MS)

MS has been previously discussed in section 4.2.2.

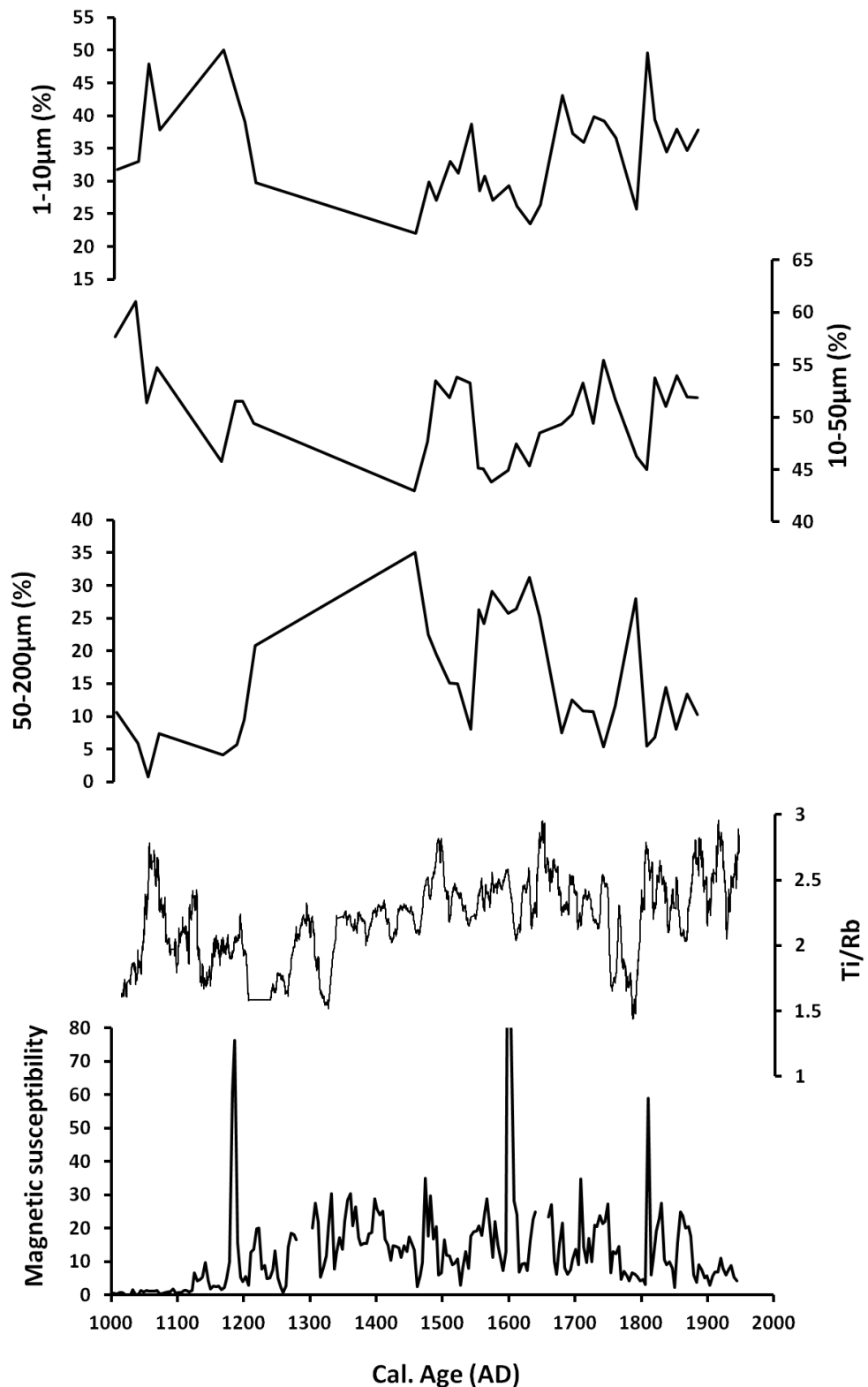


Figure 5-2: Proxies for aeolian input and transport mechanisms into Lake Toyoni. The top graph is percent fine-grained sediments (1-10µm), which is a proxy for the Westerlies. Below is the percent coarse-grained sediments (50-200µm), which is a proxy for the EAWM. Below is the Ti/Rb ratio and the bottom graph is magnetic susceptibility, which are proxies for general aeolian input into Lake Toyoni over the past 1000 years.

5.3 Discussion

5.3.1 Grain-size and dust input (Ti/Rb ratio) as a proxy for global and regional wind systems

Dust is transported to Hokkaido via global and regional wind systems; the Westerlies and the EAWM, respectively. The Westerlies transport fine-grained aeolian material into Lake Toyoni. Time periods associated with increased fine-grained sediments and also an increase in Ti/Rb proxy are 1000-1120AD, 1490-1600AD, 1680-1730AD and 1810-1957AD, which suggests an enhancement of input by the Westerlies during these time periods (Figure 5-2). The EAWM transports coarse-grained aeolian material into Lake Toyoni. Time periods associated with increased coarse-grained sediments and also an increase in Ti/Rb proxy occur 1340-1460AD and 1555-1630AD, which suggests an enhancement of input by the EAWM during these time periods (Figure 5-2). Dust input into Lake Toyoni is discussed in relation to the MWP, the LIA and the current warm period (CWP). Potential drivers of the EAWM and/or Westerlies are also investigated.

5.3.2 MWP (~1000-1300AD)

The lowest values of coarser-grained sediments, magnetic susceptibility and Ti/Rb ratios were recorded in the earliest part of the record (1000-1300AD), suggesting a weak EAWM. This time period is associated with an enhancement in the East Asian Summer Monsoon (EASM) (e.g. Hu et al., 2008; Lee and Park, 2015), which results in increased precipitation in Hokkaido. It is suggested that the fine-grained sediments deposited during the MWP are a result of increased catchment erosion under an enhanced EASM being transported into the lake via ephemeral streams that form during times of increased rainfall.

Within the context of a strong EASM during the MWP, an exception is 1050-1120AD, which shows a marked increase in the Ti/Rb ratio. Particle size data shows an increase in fine-grained sediments in this section of the core, which is interpreted as transport via Westerlies. Previous studies have reported a brief dry event around the same time period (~1100AD) in other Asian records (Wang et al., 2007; Liu et al., 2013). This has been attributed to a weakening of the

EASM for a short time period within the MWP (Liu et al., 2013a). We find that during the weakening of the EASM, the Westerlies intensified, which may be responsible for the cold and dry conditions reported in previous studies.

This time period (1050-1120AD) is also associated with a slight increase in the SibH intensity (blue shading; Figure 5-3). The reconstruction of the SibH is based on non sea-salt potassium content in a Greenland ice core. Potassium within the ice-core is interpreted as dust input from central Asia (Meeker and Mayewski, 2002). An intensified SibH positively influences dust transport by both the Westerlies and the EAWM to Hokkaido. The SibH intensifies when temperatures decrease resulting in an increase in cold surges in the dust source regions, which increases dust storm activity. The cold temperatures associated with a strong SibH increases dust storm frequency in the source regions. When dust storm frequency increases at the dust sources regions, particles are picked up and transported towards Japan by both the Westerlies and the EAWM. In addition, an intensified SibH also enhances the EAWM, which also increases dust transport towards Japan. When temperatures are cold, the SibH is located further south and becomes more intense leading to an enhanced EAWM.

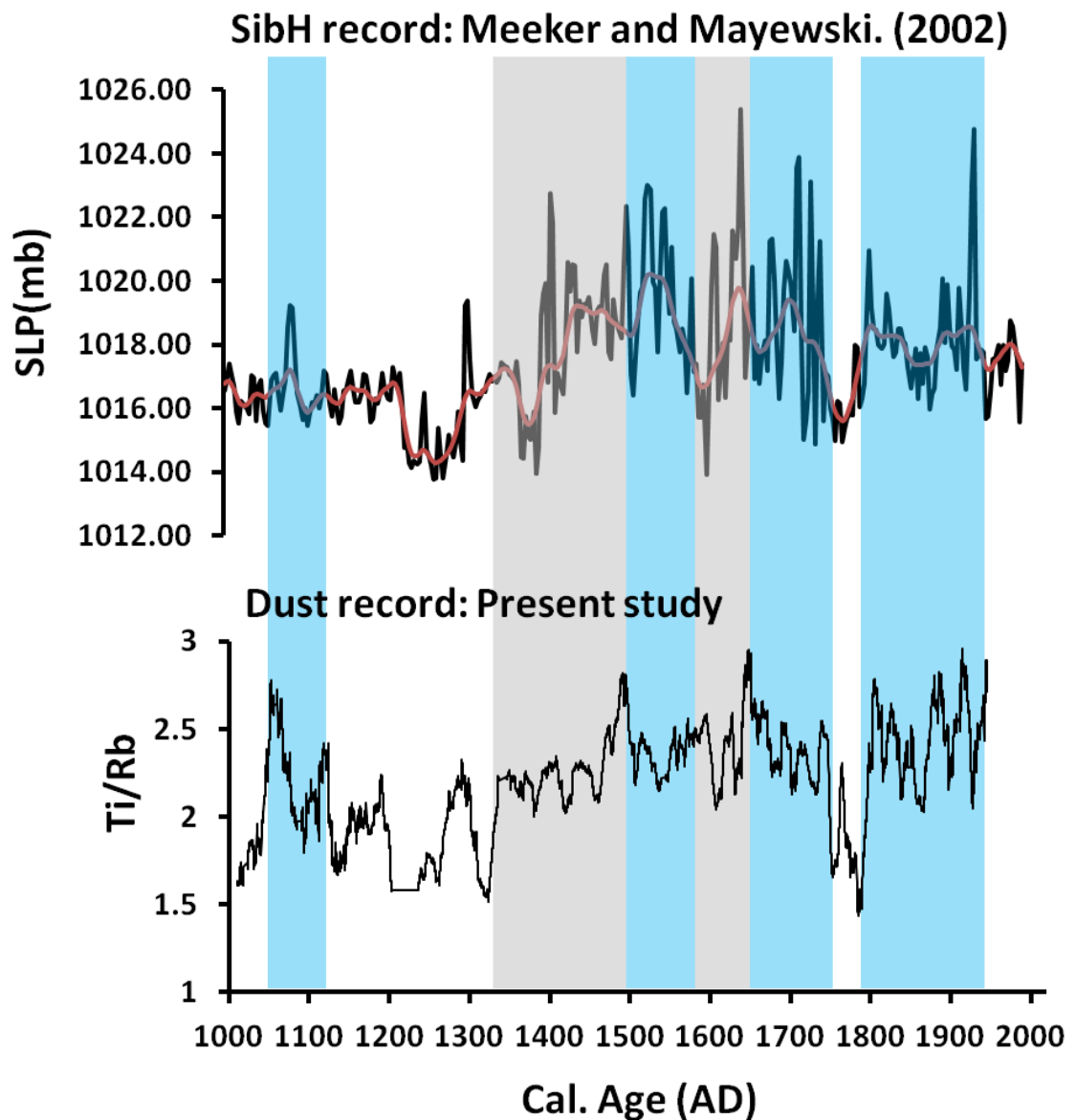


Figure 5-3: Variations in the aeolian input into Lake Toyoni and the SibH intensity. The top graph is a reconstruction of the SibH intensity by Meeker and Mayewski, (2002) based on non sea-salt potassium content in a Greenland ice core (values are in sea level pressures). The bottom graph is the Ti/Rb ratio, which is a proxy for dust input into Lake Toyoni. Grey shading indicates time periods of the intensification of the EAWM and blue shading indicates timing of the intensification of the Westerlies.

5.3.3 LIA (~1300-1800AD)

In addition to the SibH intensifying briefly during the MWP (1050-1120AD), the SibH was notably stronger within the LIA. Yoshino (1978) suggested that the SibH and the polar front shifted southward during the LIA, which significantly strengthened the EAWM. The polar front is the boundary of the northern edge of the EASM, where the warm tropical air meets the cold polar air mass. When the

polar front is located further south, the influence of the warm air mass from the south is reduced and colder temperatures are experienced in Hokkaido and East Asia.

A reconstruction of the SibH is presented in Figure 5-3. The SibH reconstruction shows that the SibH was strongest between 1400-1700AD (Figure 5-3). This time period is associated with an increase in dust in the Lake Toyoni record (as inferred from an increase in the Ti/Rb ratio and magnetic susceptibility; Figure 5-2), suggesting that the intensity of the SibH has an important influence on dust input to Hokkaido. The increase in dust input into Lake Toyoni during the LIA suggests an intensification of the EAWM and/or Westerlies. The intensification of the EAWM during the LIA has also been suggested in other work (e.g. Qiao et al., 2011, Liu et al., 2009b). Using grain-size data, we can determine the main transport mechanisms of the dust input into Lake Toyoni. We find that the EAWM (as inferred from coarse-grained sediments) intensified between 1340-1460AD and 1555-1630AD and the Westerlies intensified between 1490-1600AD and 1680-1730AD.

5.3.3.1 EAWM intensification during the LIA

We find that the EAWM intensified in 1340-1460AD and 1555-1630AD based on an increased coarse-grained material and increased dust input, as inferred from Ti/Rb proxy (Figure 5-2). In addition to increased wind activity, the EAWM is also associated with a decrease in temperature. We compared our record with a winter temperature (October-April) record from central region of eastern China over the past 2000 years (Figure 5-4; Ge et al., 2003). The temperature record was reconstructed using phenological cold/warm events recorded in Chinese historical documents (Ge et al., 2003). This region is sensitive to the EAWM and therefore the winter temperatures recorded likely reflect the EAWM. We find that the temperatures in 1340-1460AD and 1555-1630AD were lower than normal providing further evidence for an intensification of the EAWM during these time periods. In the brief time period between these EAWM intensification events, Ge et al. (2003) reported slightly warmer temperatures. The warm winter temperatures and a decrease in coarse-grained sediments suggest a weakening in the EAWM. The highest Ti/Rb ratio values during the LIA are associated with an increase in coarse-grained sediments suggesting that the EAWM is responsible

for the highest levels of dust input into Lake Toyoni. An intensification of the EAWM during the LIA has been reported in other palaeo-climate records. For example, dust input using quartz isolate from bulk sediments into a marine core in the East China Sea also found that the EAWM intensified during the LIA (Qiao et al., 2011). Previous studies have also suggested an inverse relationship between the EAWM and the EASM (e.g. Yamada et al., 2010).

To further evaluate the relationship between the EAWM (Ti/Rb and coarse-grained sediments [%]) and the EASM, we compared our findings with a stalagmite $\Delta\delta^{18}\text{O}$ record by Hu et al. (2008) (Figure 5-5). The $\Delta\delta^{18}\text{O}$ stalagmite record records regional precipitation, and hence the intensity of the EASM. This particular record was chosen to compare with the Toyoni record because the authors chose to use the difference between two stalagmite records (Hershang and Dongge caves) in a close range from each other. By choosing to do this, any site-specific effects on the $\Delta\delta^{18}\text{O}$ record are removed whereas the regional signal is preserved (Hu et al., 2008). As a result, the Hu et al. (2008) EASM record offers a reliable reconstruction to compare with findings on the East Asian Monsoon (EAM) system from the Lake Toyoni sedimentary record. We find that during time period when the EASM weakened, there is an intensification of the EAWM (highlighted with grey bars in Figure 5-5). In particular, the time periods of EAWM intensity correspond to a weakening of the EASM occur in 1340-1460AD and 1555-1630AD (Hu et al., 2008; Zhou et al., 2011). Our results therefore show that time periods associated with a weakening in the EASM are associated with an intensified EAWM, providing evidence for an inverse relationship between the EASM and EAWM, at least during these time periods.

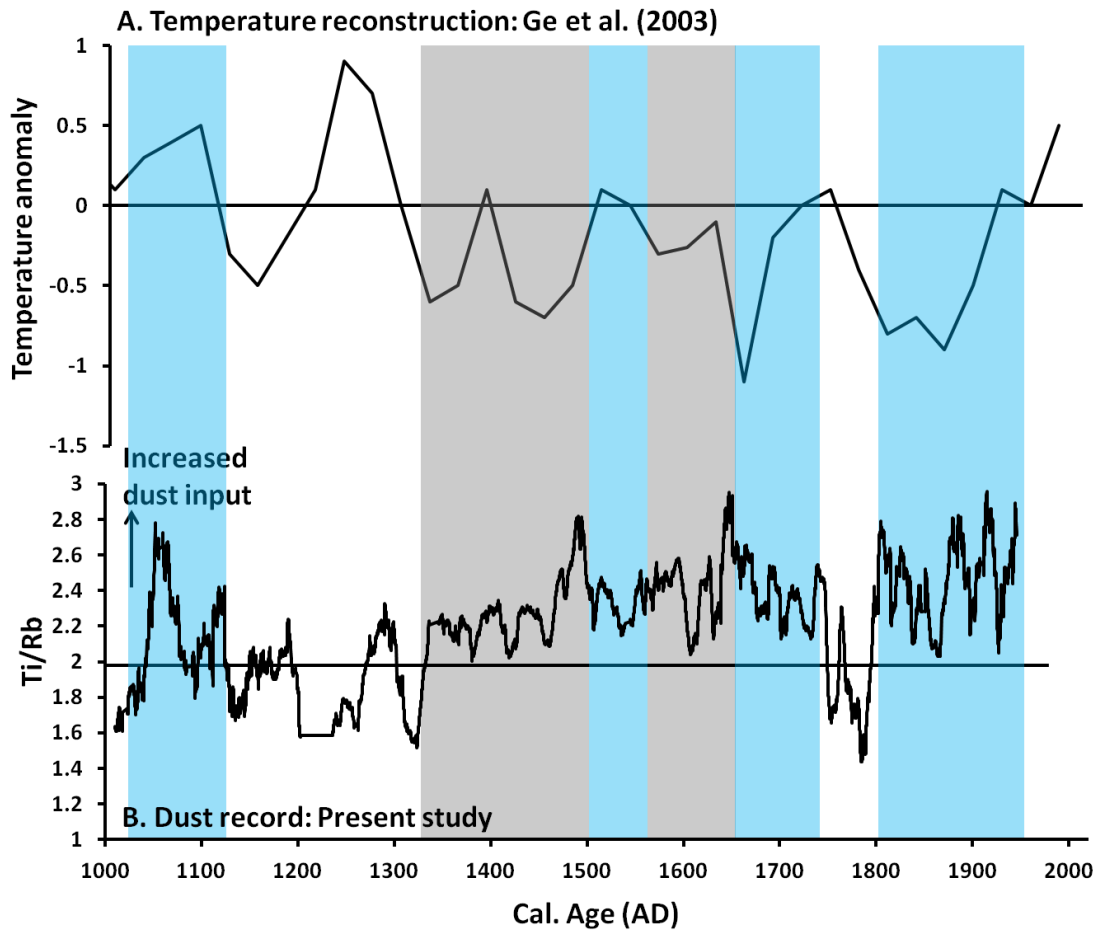


Figure 5-4: Relationship between winter temperatures and dust input into Lake Toyoni. The top graph is a winter (October-April) temperature reconstruction by Ge et al (2003) based on historical documents in central region of eastern China. The bottom graph is Ti/Rb ratio, a proxy for aeolian input into Lake Toyoni. Grey bars represent time periods where there is low temperature and increased aeolian input (higher Ti/Rb values).

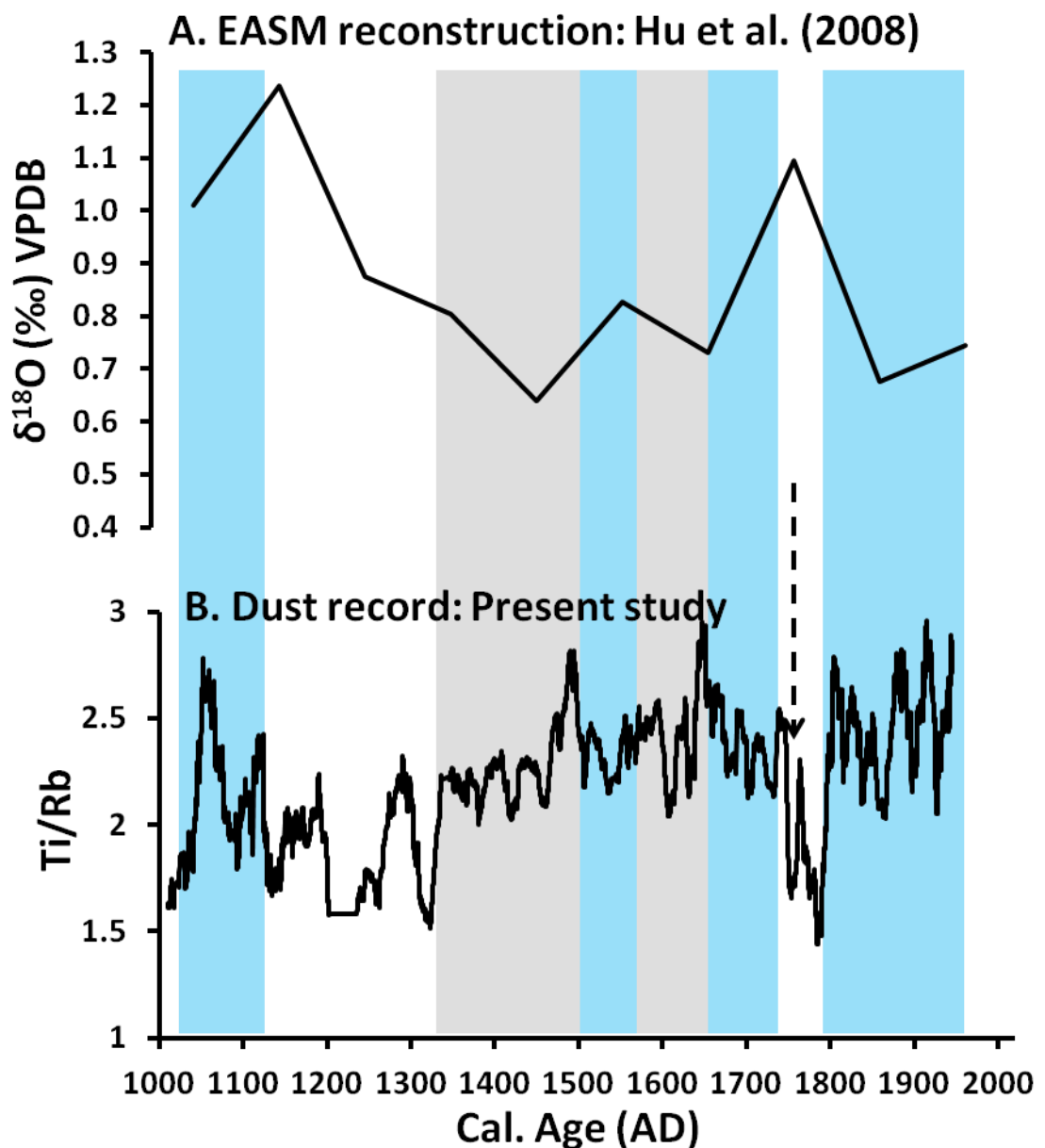


Figure 5-5: Variations in the Westerlies, the EAWM and the EASM over the past ~1000 years. Blue bars indicate time periods of the Westerlies intensification and grey bars indicates time periods of intensification of the EAWM. A: $\Delta\delta^{18}\text{O}$ (‰VDB) from Hu et al. (2008); a proxy for the EASM and B: dust record (present study).

5.3.3.2 Westerlies intensification during the LIA

Following an intensification of the EAWM in 1340-1460AD, the Westerlies were enhanced briefly between 1490-1600AD and 1680-1730AD, as inferred from an increase in fine-grained sediments (Figure 5-2). Interestingly, this time periods are associated with a stronger SibH providing further evidence for a relationship between the SibH and the intensity of the Westerlies.

Laminations can be formed in the sedimentary record when dust input is high. For example, (Yamada et al., 2010) interpreted laminations in the sedimentary records of Lakes Ni-no-Megata and San-no-Megata in northeastern Japan to be a result of dust accumulating on top of ice and being deposited as a distinct layer in the sedimentary record after ice-melt. This would also be a suitable mechanism at Lake Toyoni, which freezes annually. We find a change in lithofacies between 1490-1511AD, which is associated with faint laminations (lithofacies D; Chapter 4). These faint laminations may have been caused by a thick layer of dust accumulating on top of the ice on Lake Toyoni as a result of intensified Westerlies, which was then deposited rapidly during the ice-melt season. We suggest that this time period (1490-1511AD) was cooler than the rest of the 50-year Westerlies intensification period (1490-1600AD). The colder weather resulted in a longer time period of ice cover on Lake Toyoni and hence increased the timing for dust accumulation on top of the ice.

5.3.3.3 EAWM weakening during the LIA

Although most of the LIA is associated with an increase in the intensity of the EAWM, the EAWM appeared to weaken at the end of the LIA (1740-1800AD). During the time period, the Ti/Rb ratio dramatically decreased and the magnetic susceptibility also decreased, which is interpreted as a reduction in dust deposition. The timing of the EAWM weakening is consistent with the timing of warm winter temperatures in China (Figure 5-4) and also a significant decrease in the intensity of the SibH (Figure 5-3). The weakening of the EAWM is not surprising because the EAWM intensifies when there is cold temperatures and when the SibH is more intense.

This time period is also consistent with the timing of the intensification of the EASM (Figure 5-5; Hu et al., 2008). This provides further evidence for an inverse relationship between the EASM and the EAWM; when the EASM intensifies, the EAWM weakens. The grain size in this section of the sedimentary record shows an increase in coarse-grained sediments. This may be due to ash from a possible tephra layer, as inferred from a large spike in magnetic susceptibility (Figure 5-2). On the other hand, the increase in coarse-grained sediments may be related to an increase in run-off from increased rainfall associated with the EASM.

5.3.4 >1800AD

The period between 1800AD and 1957AD is characterised by high dust input (Ti/Rb ratios), a decrease in magnetic susceptibility and fine-grained sediments (Figure 5-2). Based on increased dust input and fine-grained sediments, we suggest an enhancement of the Westerlies. Similarly to the intensification of the Westerlies between 1500-1500AD, the NOA is also in its positive phase between 1800-1957AD. The North Atlantic Oscillation (NAO) index is being used as a proxy for the AO in this study. The link between the positive phase of the NAO and the Westerlies provides further evidence for the positive phase of the AO resulting in an intensification of the Westerlies (after Hurrell et al., 2015).

Dust input into Lake Toyoni as a proxy for environmental changes in dust source regions

Environmental conditions (e.g. aridity and/or temperature) can be a potential cause of an increase in dust storm frequency (Yang et al., 2007), which can result in increased dust input into Lake Toyoni. Therefore dust input may reflect environmental conditions at the source regions.

5.3.4.1 Climate in the Taklimakan Desert (Westerlies source region)

Previous studies have suggested that increased dust deposition reflects increased aridity in the dust source regions (Rea et al., 1998, Wang et al., 2013b) with increased aridity favouring an increase in dust flux. In order to compare our dust record (as inferred from Ti/Rb ratio) to the environmental conditions in the Taklimakan Desert (the source region for dust transported via the Westerlies), we use net accumulation and $\delta^{18}\text{O}$ from Guliya ice-cap (Thompson et al., 1995, Yao et al., 1995), which is located on the southern border of the Taklimakan Desert (35°17N, 80°29E) (Figure 5-6). Since the publication of the net accumulation and $\delta^{18}\text{O}$, these records have been used for precipitation and temperature, respectively. The precipitation record is based on the net accumulation record from Guliya ice-gap (Thompson et al., 1995), which has been shown to be correlated ($r^2=0.55$ $p<0.01$) with standardised precipitation variations in the Xinjiang region (Yang et al., 2004). The temperature record is based on $\delta^{18}\text{O}$ record from Guliya ice-core (Yang et al., 2004, Thompson et al., 2003).

The records show that the MWP was generally warm and dry, whereas the LIA was cold and wet (Figure 5-6). A warm and dry MWP and cold and wet LIA is also consistent with 34 hydro-climate records from Arid Central Asia (ACA) (Chen et al., 2015b). Our record suggested that the Westerlies intensified during the MWP between 1000-11200AD, briefly within the LIA between 1490-1600AD and 1680-1730AD and also between 1810-1957AD. Although the MWP was characterised by generally warm and dry conditions, temperature (Yang et al., 2004) and rainfall (Thompson et al., 1995) decreased between ~1070-1170AD (Figure 5-6). Temperature and aridity between 1000-1120AD in the Taklimakan Desert region was therefore cold and dry based on reconstructions of Yang et al. (2004) and Thompson et al. (1995). Climate conditions between 1490-1600AD on the other hand were cold and wet (Figure 5-6). This time period is associated with the wettest conditions over the past 1000 years, based on the reconstruction of Thompson et al. (1995). Temperature and aridity between 1680-1730AD was cold and drier. Temperature and aridity between 1810-1957AD was slightly colder and drier. This suggests that a decrease in temperature, and to a lesser degree, increased aridity in the Taklimakan Desert region has an important influence on dust input into Lake Toyoni via the Westerlies.

5.3.4.2 Climate in the Gobi Desert (EAWM source region)

In order to compare our dust record (as inferred from Ti/Rb ratio) to the environmental conditions in the Gobi Desert (the source region for dust transported via the EAWM), we use $\delta^{18}\text{O}$ from Dunde ice-cap (Thompson et al., 1989), which is located to the south of the Gobi Desert (38°06'N, 96°24'E). The $\delta^{18}\text{O}$ from Dunde ice-cap is controlled by temperature therefore provides a record of temperature over the past 1000 years (Thompson et al., 2003). In addition, we use a precipitation record using ring-width chronologies from Delingha (Qinghai Basin) by Shao et al (2005) (Figure 5-7). This record is justified given its location close to the Gobi Desert and also because annual precipitation accounts for 63% of the variance in the calibration period (1955-2002) making this a good quality precipitation reconstruction to compare our findings with.

Our records suggest that the EAWM intensified in 1340-1460AD, 1555-1630AD. We also suggest that the EAWM weakened ~1750AD. The climate between 1340 and 1460AD in the Gobi Desert was cold and wet and the climate between 1555 and

1630AD was also cold and wet (Figure 5-7). This suggests that cold temperatures at the source region control dust input to Hokkaido via the EAWM. Interestingly, the climate in the Gobi Desert region between 1740-1800AD (EAWM weakening) was warm and wet (Figure 5-7). This suggests that temperature at the source region does have an influence on the supply of dust to Hokkaido via the EAWM.

Based on the comparison of our dust record and climate at the dust source regions (Talkaman and Gobi Deserts), we find that overall temperature has a larger influence on dust input into Lake Toyoni compared with aridity. Temperature at the source regions is strongly influenced by the SibH, which was previously identified as a controlling factor of dust input into Lake Toyoni. The SibH not only influences the strength of the Westerlies and the EAWM, but also influences the temperatures at the dust source regions, which in turn influences dust input into Lake Toyoni.

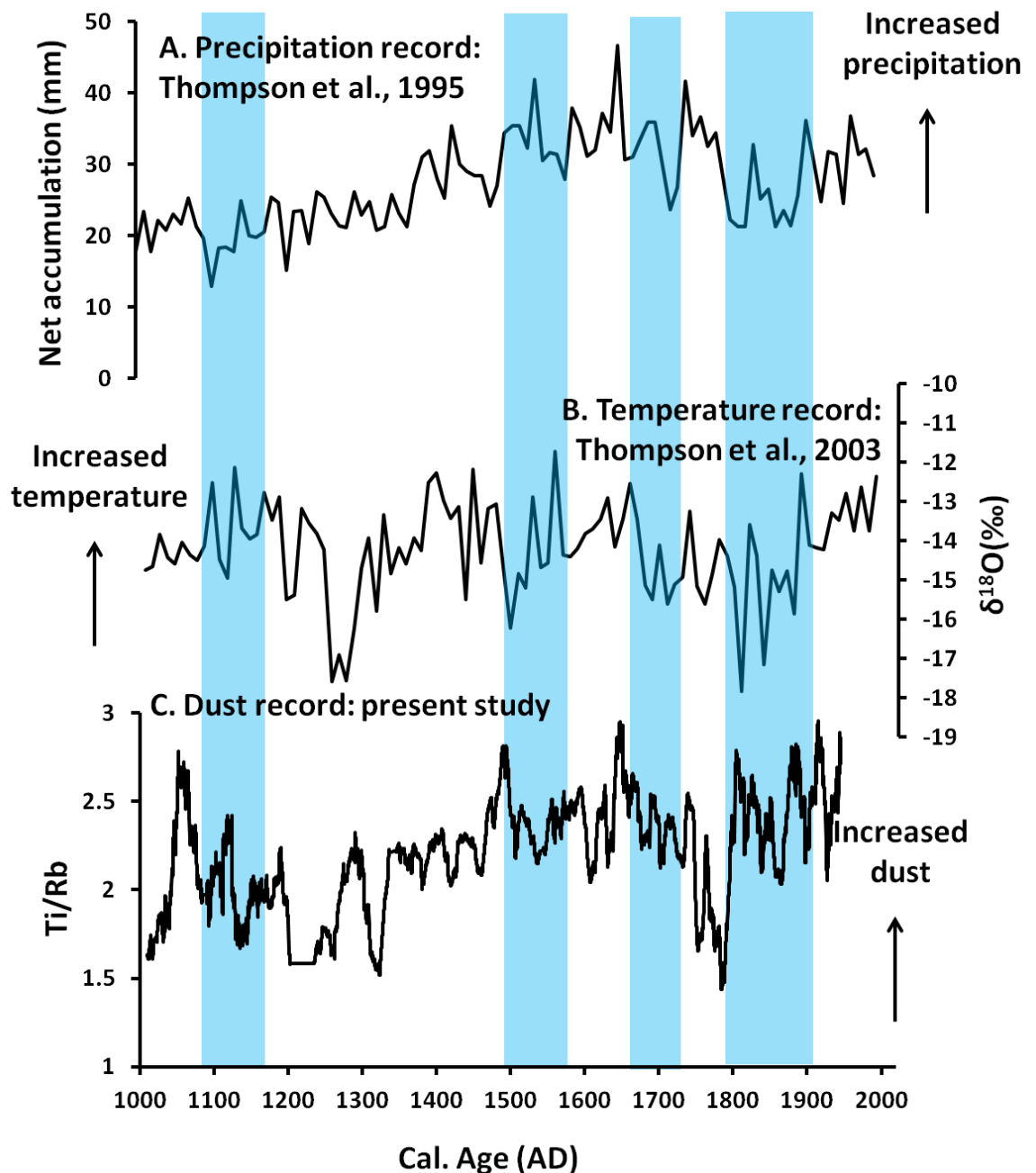


Figure 5-6: comparison of dust input into Lake Toyoni via the Westerlies and environmental conditions in the Taklimakan Desert (the source region for dust transported via the Westerlies). Bottom graph; Ti/Rb ratio (present study), middle graph; temperature record is based on $\delta^{18}\text{O}$ record from Guliya ice-core (Yang et al., 2004, Thompson et al., 2003). Top graph; a precipitation record is based on the net accumulation record from Guliya ice-gap (Thompson et al., 1995). Blue shading highlights time periods identified as an intensification of the Westerlies (increase in fine-grained sediments and Ti/Rb ratio values).

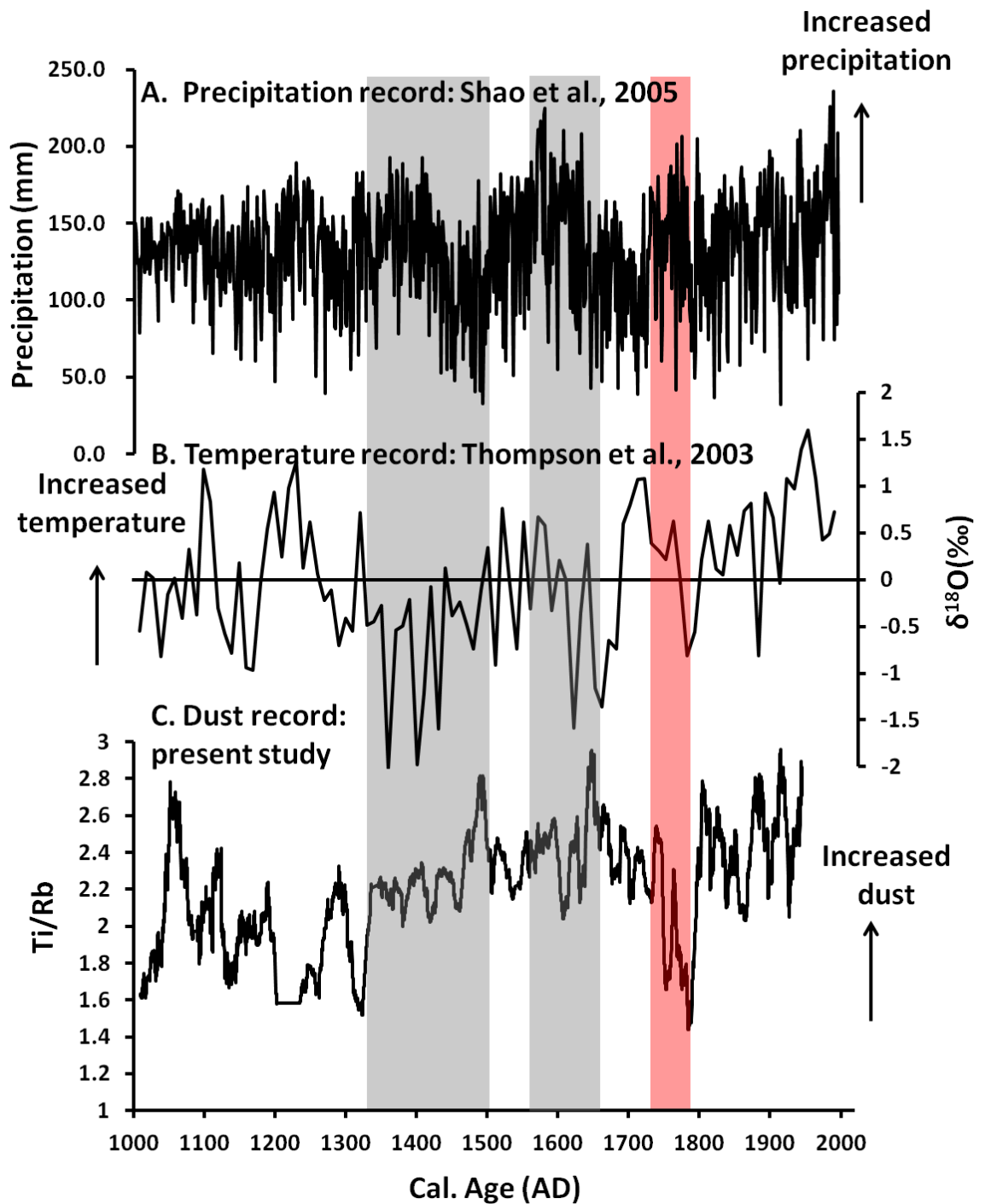


Figure 5-7: comparison of dust input into Lake Toyoni via the EAWM and environmental conditions in the Gobi Desert (the source region for dust transported via the EAWM). Bottom graph; Ti/Rb (present study), middle graph $\delta^{18}\text{O}$ isotope record from Dunde ice-core and top graph is a precipitation record using ring-width chronologies from Delingha (Shao et al., 2005). Grey shading highlights time periods identified as an intensification of the EAWM (increase in coarse-grained sediments and Ti/Rb ratio values) and red shading highlights time period identified as a weakening in the EAWM (low Ti/Rb ratio values).

5.3.5 Potential climate drivers

In order to evaluate the influence of teleconnections on the Westerlies and the EAWM, the down-core dust record from Lake Toyoni is compared with:

1. A record of El Niño Southern Oscillation (ENSO) variability (Yan et al., 2011a) over the past 2000 years, which is based on precipitation records from Indo-Pacific and Galapagos (Figure 5.8). The Indonesian rainfall was derived from a salinity reconstruction based on planktonic-foraminifera $\delta^{18}\text{O}$ and the magnesium/calcium (Mg/Ca) ratio (Oppo et al., 2009). The precipitation variability in the Galapagos is derived from a lake level reconstruction which is based on the grain size data from the Lago El Junco sediment core (Conroy et al., 2008). The Southern Oscillation Index (SOI) is positively correlated with precipitation over the Indo-Pacific warm pool, and negatively correlated with precipitation over the eastern and mid-tropical Pacific and as a result, ENSO can be reconstruction by the difference between these precipitation records (Yan et al., 2011a).
2. The Pacific Decadal index (PDO) index from Macdonald and Case (2005) over the past 1000 years (Figure 5.8). As previously discussed in Chapter 4, the PDO Index was reconstructed using tree-ring chronologies from *Pinus flexilis* in California and Alberta (western Canada). The two sites are located at opposite end of the PDO precipitation dipole and hence the hydrological variability associated with the PDO is opposite signs in the two regions; making these tree-ring records sensitive to the variability of the PDO.
3. A record of the AO over the past 1000 years is not available, however, the AO index is closely related to the NAO index (Thompson and Wallace, 1998) and therefore the NAO index by Trouet et al. (2009) will represent the AO in this study (after Lee and Park, 2015) (Figure 5.8). The NAO index was reconstructed using a combination of high-resolution proxy records and model simulations.

5.3.5.1 ENSO

The ENSO record over the past millennium (Yan et al., 2012) is shown in Figure 5.8. We find that the intensification of the EAWM occurs during La Niña conditions. Notably, the first intensification of the EAWM occurred during a change from predominantly El Niño to La Niña conditions. The Westerlies, on the other hand, intensified during both El Niño and La Niña conditions.

5.3.5.2 PDO

The PDO record over the past millennium (MacDonald and Case, 2005) is shown in Figure 5-8. The reconstructed PDO index shows a negative PDO phase during the MWP, and a shift to a positive phase during the LIA (Figure 5-8). Comparison of the PDO record with our results shows that the EAWM intensified twice within the LIA (as inferred from increases in the Ti/Rb ratio and coarse-grained sediments). The timing of the intensification of the EAWM occurred when the PDO was in its positive phase (highlighted with grey shading Figure 5-8) suggesting a negative PDO strengthens the EAWM. Lee and Park. (2015) suggested a relationship between the EASM and the PDO in a recent study. They found that the EASM intensified and weakened when the PDO was in its negative and positive modes, respectively. Therefore, when the PDO is in its positive mode, the EASM weakens (Lee and Park. 2015) and we find evidence for the intensification of the EAWM. It is suggested that the PDO may play an important role in the inverse relationship between the EASM and the EAWM; where by one intensifies and the other weakens.

5.3.5.3 NAO/AO

The relationship between the AO and the Westerlies has been previously suggested by Hurrell et al. (2015). In order to investigate the relationship between the Westerlies and the AO in Hokkaido, we compared our results to a record of the NAO by Trouet et al. (2009), which is closely related to the AO (Thompson and Wallace, 1998) (Figure 5-8). Our relationships show a clear relationship between the intensification of the Westerlies and the positive phase of the NAO/AO (previously discussed throughout). The Westerlies intensified between 1000-1120AD during the MWP, between 1490-1600AD and 1680-1730AD during the LIA and between 1810-1957AD during the CWP, which are all

associated with the positive phase of the NAO/AO. Previous studies have suggested that the positive phase of the NAO/AO enhances the Westerlies (Hurrell et al., 2015). During time periods where the AO is in its negative phase, there is higher pressure in the Arctic and weaker Westerlies (Hurrell et al., 2015). The opposite occurs when the AO is in its positive phase and hence the Westerlies intensify.

The positive phase of the NAO persists for the entire MWP (Figure 5-8). However the LIA has frequent shifts to the negative phase of the NAO. These phases occur between 1441-1464AD, 1557-1569AD, 1598-1624AD, 1665-1690AD, 1713-1731AD and 1750-1795AD). Our results show that during the two time periods of EAWM intensification during the LIA (e.g. 1340-1460AD and 1555-1630AD) is associated with the negative phase of the NAO. The negative phase of the AO strongly influences the SibH (Wu and Wang, 2002, Gong et al., 2001, Chen et al., 2013), which in turn also influences the EAWM (Ding, 1990, Zhang et al., 1997, Wu et al., 2006a, Gong et al., 2001). The AO therefore influences the strength of the EAWM through the intensity of the SibH. Overall, this suggests that there is a relationship between the positive phase of the NAO/AO and the intensification of the Westerlies and a relationship between the negative phase of the NAO/AO and the intensification of the EAWM.

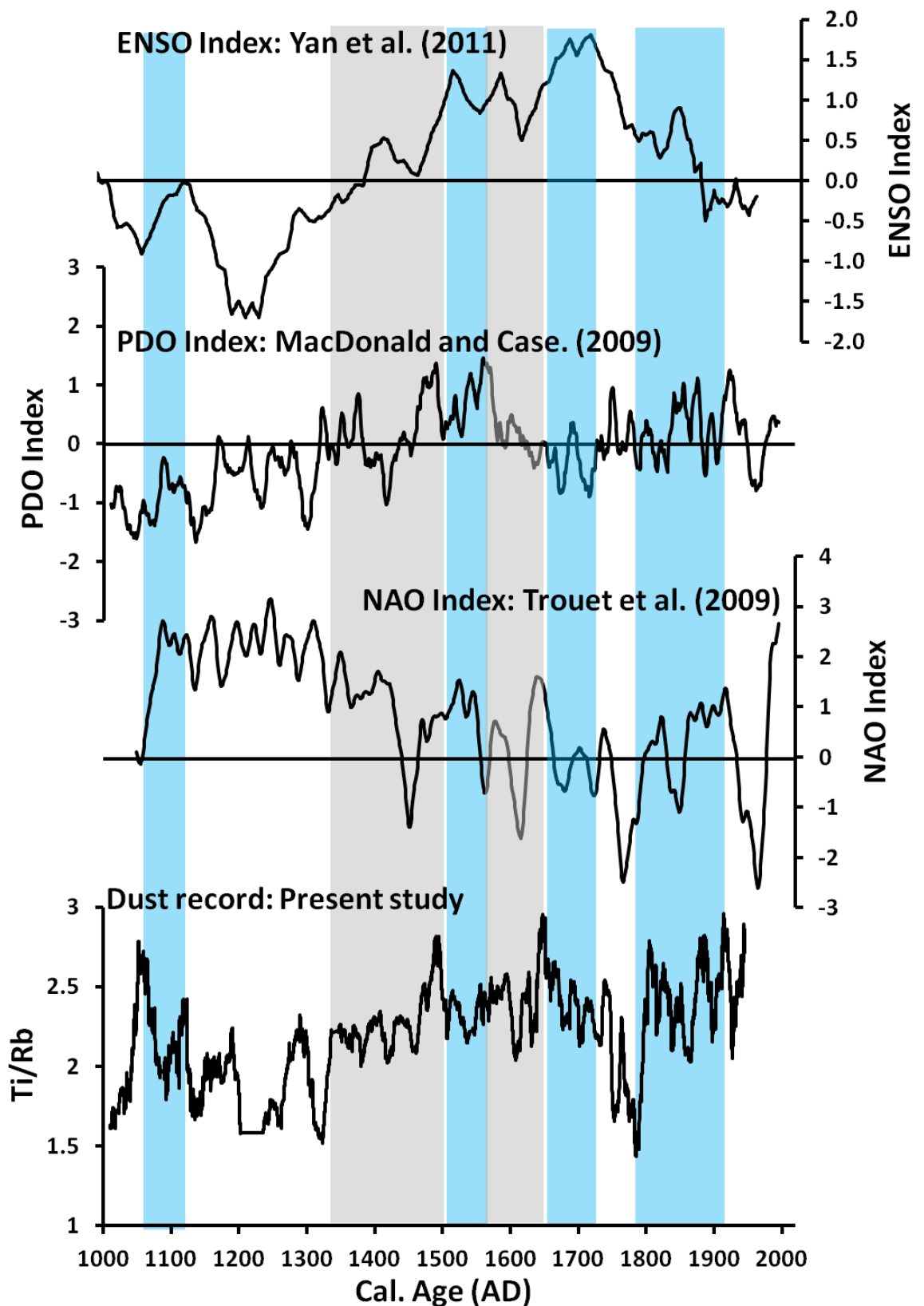


Figure 5-8: Variations in the aeolian record compared with the PDO index by Macdonald and Case (2009) (top graph; please note that the axis has been inverted) and the NAO index by Trouet et al. (2009) (Middle graph). The bottom graph shows down-core variations in the Ti/Rb values. Grey bars highlights the time periods interpreted as a strong EAWM. Blue bars highlights time periods interpreted as strong Westerly input.

5.4 Conclusions

The variations of the Westerlies and the EAWM during late Holocene (past 1000 years) is recorded in grain-size, magnetic susceptibility and Ti/Rb ratios in the Lake Toyoni sedimentary record. The transport mechanisms by the Westerlies and the EAWM are separated by grain-size. The Westerlies transport fine-grained sediments whereas the EAWM transports coarser-grained sediments. The results show a general weakening of the EAWM during the MWP and an intensification of the EAWM during the LIA. In particular, the EAWM increased in intensity between 1340-1460AD and 1555-1630AD. The intensity of the EAWM was controlled by temperature in the source regions as well as the strength of the SibH. When the SibH was strong and temperatures were colder, the EAWM intensified, bringing more coarse-grained sediments to Lake Toyoni. There is a relationship between the negative phase of the NAO/AO and the intensity of the EAWM. When the NAO/AO is in its negative phase, the SibH intensifies and hence a stronger EAWM prevails. On the other hand, the EAWM weakened and the EASM intensified between 1430-1800AD, which was also associated with a decrease in the intensity of the SibH. The results show a clear anti-phase relationship between the EAWM and the EASM. The Westerlies, on the other hand, increased between 1000-1120AD during the MWP, between 1490-1600AD and 1680-1730AD during the LIA and between 1810-1957AD during the CWP, which are all associated with the positive phase of the NAO/AO. To sum up, dust input into Lake Toyoni is controlled by the EAWM and the Westerlies as well as temperature at the dust source regions. All three mechanisms are influenced by the SibH therefore the dust record from Lake Toyoni (as inferred by the Ti/Rb ratio) is strongly reflecting the intensity of the SibH over the past 1000 years.

6

18S rDNA analysis of the alkenone-producer(s) in Lake Toyoni, Japan

6.1 Introduction

Long chain alkenones are a class of C₃₅-C₄₀ unsaturated ketones that have been extensively used as a proxy for quantitative sea surface temperature (SST) based on the degree of unsaturation in the ketone molecule (e.g. Brassell et al., 1986, Prahl and Wakeham, 1987, Herbert et al., 2003). Since Cranwell (1985) first reported the occurrence of alkenones in lakes, this successful SST proxy has started to be applied to lacustrine settings, with a number of calibration studies and down-core lake surface water temperature reconstructions (Wang and Zheng, 1997, Zink et al., 2001, Chu et al., 2005, D'Andrea and Huang, 2005, Liu et al., 2006b, Sun et al., 2007, Pearson et al., 2008, Toney et al., 2010, Toney et al., 2011). Alkenones are produced exclusively by certain species of haptophyte algae (Volkman et al., 1980, Marlowe et al., 1984, Volkman et al., 1995, Coolen et al., 2004c, D'Andrea et al., 2006, Theroux et al., 2010) and one of the remaining challenges for applying the alkenone unsaturation index as a temperature proxy in lake systems is determining the precursor organism.

The producer of alkenones in the marine environment is dominated by calcifying haptophytes *Emiliana huxleyi* and *Gephyrocapsa oceanica* in the open ocean (de Leeuw et al., 1980, Volkman et al., 1995) and by non-calcifying species

Isochrysis galbana and *Chrysothila lamellosa* in the coastal marine setting (Marlowe et al., 1984). However, in lacustrine environments, the diversity of haptophytes producing alkenones varies according to their ecology and environment. As a result it is not possible to make general assumptions about the likely alkenone producer(s) in lakes. Previous studies have identified alkenone producers that are similar species to the coastal haptophyte species *Isochrysis galbana* (Coolen et al., 2004a) and *Chrysothila lamellosa* (Sun et al., 2007). In addition, several novel alkenone producers, which have not been fully classified taxonomically, have also been discovered (D'Andrea et al., 2006, Theroux et al., 2010). As haptophyte algal species have the potential to produce different temperature calibrations, individual alkenone-containing lakes require unique calibration datasets dependent on species of haptophyte algae present (Chu et al., 2005, D'Andrea et al., 2006). Identifying the alkenone precursor organism prior to down-core temperature reconstructions is therefore essential for selecting the most appropriate temperature calibration and validating the interpretation of alkenones in the lacustrine system.

Identifying a lacustrine alkenone producer through microscopy is challenging due to their relatively small size and seasonal production (Zink et al., 2001). Instead, researchers using lacustrine alkenones have shifted approaches to using environmental genomics to identify precursor organisms (e.g., D'Andrea et al., 2006, Randlett et al., 2014). The ultimate species-specific biomarkers are genes that code for small subunit ribosomal RNA (rRNA) (18S in Eukaryotes, 16S in Prokaryotes). The 18S molecular marker is present in all eukaryotes (Olsen et al., 1986, Woese, 1987) and therefore provides species level taxonomic resolution (Sogin et al., 1986, Edvardsen et al., 2000). Analysis of such genes in the sedimentary record provides information on past microbial diversity and ecology (Coolen et al., 2004a). The use of DNA as a biomarker is unfortunately hindered by the unstable nature of DNA in many geological archives (D'Andrea et al., 2006). Conveniently, when remnants of DNA are preserved within sedimentary archives they can be used in conjunction with alkenone biomarkers to provide valuable information when the precursor organism(s) are unknown.

The aims of this chapter are:

1. Identify the alkenone producer(s) in Lake Toyoni using 18S rDNA analysis
2. Examine alkenone distribution variability between Lake Toyoni and other known haptophyte algae species.

6.2 Results

6.2.1 18S rDNA Haptophyte Identification

Eighteen operational taxonomic units (OTUs) were identified based on restriction digest and sequence analyses. Based on BLAST analysis, 17 out of the 18 OTUs do not belong to any known haptophyte species previously catalogued in GenBank. OTU 7 was identified as 96% similar to a haptophyte found in Lake BrayaSø (Greenland) (Table 6-1).

6.2.2 Full-length 18S rRNA gene-based phylogeny

A phylogeny was constructed using the sequence for each OTU along with previously published full-length haptophyte 18S rRNA genes (Figure 6-1). OTU7 falls within the Isochrysidales (posterior probability value of 1.0) and shares a distinct clade with a haptophyte amplified from water column filters from Lake BrayaSø (Greenland) (posterior probability of 0.98) (D'Andrea et al., 2006). The Greenland haptophyte sequence is a full-length sequence (~1800bp) compared to OTU7, which is a partial length sequence (887bp). OTU7 also branched basal to a lineage of coastal/lacustrine haptophytes (posterior probability of 0.90) and shares a common ancestry with marine haptophyte species *E. huxeyli* and *G. oceanica* (posterior probability of 1).

According to the full-length 18S rDNA gene-based phylogenies (~1800bp) (Figure 6-1), the remaining PCR-amplified sequences do not occupy the haptophyte phylotype and were more closely related to other groups of algae in the Bayesian inference (posterior probability of 0.90). This means that only one haptophyte species is found in Lake Toyoni and other algal taxa fall outside the haptophyte group.

6.2.3 Partial length 18S rDNA gene-based phylogeny

A partial-length phylogeny was constructed using a representative OTU7 sequence along with previously published, partial-length haptophyte 18S rDNA genes. According to partial-length (~500bp) (Figure 6-2) 18S rDNA gene-based phylogenies (Figure 6-2), the Isochrysidales clustered into three distinct groups (all with posterior probabilities of 1). OTU7 grouped within Group 1 along with previously published sequences from the Greenland lakes (D'Andrea et al., 2006), Chinese Lakes (Tso Ur and Keluke Hu), American Lakes (Skoal Lake and Medicine Lake) and a Canadian Lake (Upper Murray Lake) (Theroux et al., 2010). Group 2 comprises of the coastal alkenone producers; *C. lamellosa*, *I. galbana*, *I. litoralis* and *P. paradoxa* and the alkenone producers from Ace Lake, Antarctica Coolen et al. (2004a) and Chinese Lakes (Tso Ur and Lake Keluke Hu), American Lakes (Skoal Lake, Medicine Lake, Pyramid Lake and Lake George) (Theroux et al., 2010). Group 3 comprises of the marine haptophyte species *E. huxleyi* and *G. oceanica* and unidentified marine coccoid haptophyte (U40924).

6.2.4 Alkenone Distribution at Lake Toyoni

C₃₇-C₃₉ long-chain alkenones were discovered in surface sediments of freshwater Lake Toyoni, Japan and were absent from all other lake sites surveyed. C₃₇ alkenone concentrations in surface sediments of Lake Toyoni are 18µg C₃₇ g⁻¹ of dry sediment. Generally, alkenones of the same carbon number are dominated by the more unsaturated forms (i.e., tetraenoic > trienoic > dienoic), except C₃₉ alkenone where C_{39:3} dominates over C_{39:4} (Figure 6-3) and the C₄₀ alkenone is not present. C_{37:4} is the dominant C₃₇ alkenone in the surface sediments accounting for 55% of the C₃₇ alkenone production compared with 43% C_{37:3} and 2% C_{37:2} (Figure 6-3).

Table 6-1: Closest BLAST hits to OTUs

OTU	Closest Blast hit	Max identity (%)	%query
OTU1	<i>Chlamydomonas</i> sp. SAG 75.94 18S ribosomal RNA gene, partial sequence	99%	97%
OTU2	Uncultured <i>alveolate</i> clone PAA8SP2005 18S ribosomal RNA gene, partial sequence	95%	99%
OTU3	<i>Chlorophyta</i> sp. I-155 clone A1 18S ribosomal RNA gene, partial sequence	98%	99%
OTU4	Uncultured <i>alveolate</i> clone PAA8SP2005 18S ribosomal RNA gene, partial sequence	95%	99%
OTU5	Uncultured <i>Woloszynskia</i> clone ESS220206.046 18S ribosomal RNA gene, partial sequence	96%	99%
OTU6	Uncultured <i>alveolate</i> clone PAA8SP2005 18S ribosomal RNA gene, partial sequence	95%	99%
OTU7	Uncultured haptophyte clone BrayaSo_water_18S 18S ribosomal RNA gene, partial sequence	96%	99%
OTU8	<i>Dinobryon sertularia</i> small subunit ribosomal RNA gene, partial sequence	99%	99%
OTU9	Uncultured <i>alveolate</i> clone PAA8SP2005 18S ribosomal RNA gene, partial sequence	96%	99%
OTU10	Uncultured <i>Woloszynskia</i> clone ESS220206.046 18S ribosomal RNA gene, partial sequence	96%	99%
OTU11	Uncultured <i>Woloszynskia</i> clone ESS220206.046 18S ribosomal RNA gene, partial sequence	98%	99%
OTU12	Uncultured <i>alveolate</i> clone PAA8SP2005 18S ribosomal RNA gene, partial sequence	95%	99%
OTU13	Uncultured <i>alveolate</i> clone PAA8SP2005 18S ribosomal RNA gene, partial sequence	95%	99%
OTU14	Uncultured eukaryote clone Ch8A2mF4 18S ribosomal RNA gene, partial sequence	97%	95%
OTU15	Uncultured <i>Baniszveld</i> eukaryote clone P2-3m3 18S ribosomal RNA gene, partial sequence	98%	99%
OTU16	Uncultured eukaryote clone KRL01E15 18S ribosomal RNA gene, partial sequence	99%	99%
OTU17	Uncultured <i>alveolate</i> clone PAA8SP2005 18S ribosomal RNA gene, partial sequence	95%	99%
OTU18	<i>Chlorophyta</i> sp. I-155 clone A1 18S ribosomal RNA gene, partial sequence	99%	99%

Table 6-2: The range of primers used to target haptophyte rDNA. rDNA amplification was completed using a forward eukaryotic oligonucleotide primer (EUKA-F; AC CTG GTT GAT CCT GCC AGT) and a re-designed haptophyte reverse primer (DEG Prym887-R; DVAATACGARTRCCCCYRAC; where D = A/G/T; V = A/C/G; R = A/G; Y = C/T)

Primer name	5'-3'	Tm	Reference
Euk A	AC CTG GTT GAT CCT GCC AGT	57	(Medlin <i>et al.</i> , 1988)
Euk B	C TTC TGC AGG TTC ACC TAC	53	(Medlin <i>et al.</i> , 1988)
Prym429F	GCG CGT AAA TTG CCC GAA	65	(Coolen <i>et al.</i> , 2004a)
Prym887R	GGA ATA CGA GTG CCC CTG AC	62	(Simon <i>et al.</i> , 2000)
887DegR	DVA ATA CGA RTR CCC CYR AC	62	This work

Table 6-3: Number of base pairs targeted and successful/unsuccessful PCR with different primer combinations. Successful haptophyte amplification was only found using Prym429(F) + Prym887(R) and EukA(F) + 887DEG(R).

Primer combination	Number of base pairs (bp)	Successful/unsuccessful PCR
EukA(F) + EukB(R)	1792bp	Unsuccessful
Prym429(F) + Prym887(R)	461bp	Successful
Prym429(F) + EukB(R)	1372bp	Unsuccessful
EukA(F) + Prym887(R)	887bp	Unsuccessful
EukA(F) + 887DEG(R)	887bp	Successful

Table 6-4: Alkenone trends among haptophyte algae. (A) Marine haptophytes, (B) Coastal haptophytes, (c) Lacustrine haptophytes. Adapted from Theroux et al.(2010).

Haptophyte species	Dominant alkenone	C ₃₇ /C ₃₈	C ₃₈ MeK	C ₄₀	Phylogenetic group
Marine					
<i>Emiliana huxleyi</i>	C _{37:3}	1-2	Present	Absent	Group III
<i>Gephyrocapsa oceanica</i>	C _{37:3}	< 1	Present	Absent	Group III
Coastal					
<i>Chrysotila lamellosa</i>		> 2	Absent	Present	Group II
<i>Isochrysis galbana</i>		> 3	Absent	Present	Group II
Lacustrine					
<i>Chrysotila lamellosa</i> ^a	C _{37:3}	> 2	Absent	Present	Group II
Ace Lake, Antarctica ^b	C _{37:4} & C _{37:3}	> 2	Absent	Present	Group II
Lake George, USA ^c	C _{37:4}	2	Present	Trace	Group II
Lake BrayaSø Greenland ^d	C _{37:4}	1.3	Present	Absent	Group I
Upper Murray Lake ^e					Group I
Skoal Lake ^c					Group I
Medicine Lake ^c	C _{37:4}				Group I
Tso Ur ^f		<2	Present	Absent	Group I
Lake Toyoni ^g	C _{37:4}	1.9	Present	Absent	Group I

^a (Sun et al., 2007);^b (Coolen et al., 2004b);^c (Toney et al., 2010);^d (D'Andrea and Huang, 2005);^e Besonen et al. (2008);^f <http://www.homepages.ucl.ac.uk/~ucfasdt/Tibet/index.htm>;^g (present study)

6.3 Discussion

6.3.1 Haptophyte DNA amplification and diversity in Lake Toyoni

The production of alkenones is limited to haptophytes within the order Isochrysidales. The successful PCR amplification of haptophyte rDNA confirms the presence of haptophyte algae in Lake Toyoni. Haptophyte rDNA was targeted during PCR-amplification using a range of primers (summarised in Table 6-2). Amplification was successful using haptophyte-specific primers (Prym 429(F) & Prym887(R)) and also a combination of a eukaryotic-specific primer (EukA(F); ACG CTG GTT GAT CCT GCC AGT) and a re-designed haptophyte reverse primer (Prym887(Ra); DVAATACGARTRCCCCYRAC) targeting 18S rRNA coding regions (Table 6-3).

Haptophyte-specific primers show significant diversity in lacustrine environments (Coolen et al., 2004a, D'Andrea et al., 2006, Theroux et al., 2010) and although these primers target the most variable region of the haptophyte 18S rDNA gene (Theroux et al., 2010), they produce relatively short sequences (461bp). Using short sequences limits the ability to match the haptophyte DNA to other haptophyte sequences within GENBANK. In order to target a larger region of the haptophyte 18S rDNA gene, additional amplification using a combination of a eukaryotic forward primer and a redesigned haptophyte reverse was important to target a larger sequence of haptophyte rDNA (887bp compared to 461bp using haptophyte-specific primers), which results in a longer sequence to compare with other haptophyte sequences.

In this study the haptophyte reverse primer was re-designed (Prym887(Ra)) and combined with the EukA(F) primer. The new combination of EukA(F) primer and re-designed haptophyte primer offers an alternative method that allows for longer sequence amplification. Conversely, since the degenerate bases increase variability, this combination of primers can result in amplification of other eukaryotic species other than just haptophyte algae. Indeed, this present study found using this combination of primers, 18 OTUs are identified in Lake Toyoni surface sediments and only one OTU sequence occupied the haptophyte phylotype. The remaining PCR-amplified sequences were more closely related to

other groups of algae in the neighbour joining analysis (posterior probability of 0.90).

Ideally the best primers for haptophyte amplification would be general primers for the domain Eukarya (EukA(F) and EukB(R)) (1792bp using Eukaryotic-specific primers compared to 461bp using haptophyte-specific primers) since the size of the sequence obtained increases the posterior probability. For example, Theroux et al. (2010) found that posterior probability increased from 0.66 to 0.92 when using eukaryotic-specific primers compared to using the haptophyte-specific primers during PCR-amplification. Amplification of the Lake Toyoni surface sediment was however, unsuccessful using generic eukaryote-specific primers. Previous studies have also reported problems using eukaryotic-specific primers to target haptophyte rDNA in the marine (Bittner et al., 2012) and lacustrine environments (Coolen et al., 2004a). Only low concentrations of haptophyte DNA were found in sediments from Ace Lake, Antarctica with eukaryotic-specific primers (Coolen et al., 2004a). In comparison, by using haptophyte-specific primers, haptophyte sequences were detected in sediments where alkenone concentrations were low (Coolen et al., 2004a). As a result, four additional haptophyte sequences, which were missed using the eukaryotic-specific primers, were identified (Coolen et al., 2004a). Empirical obstacles, such as low haptophyte abundance, primer mismatches and a high guanine (G) and cytosine (C) content (up to 57%; (Liu et al., 2009a). GC content can result in unsuccessful amplification means there sometimes unsuccessful amplification using eukaryotic-specific primers (Liu et al., 2009a, Stoeck et al., 2010).

6.3.2 Haptophyte identification

Based on the phylogeny of the alkenone producer in Lake Toyoni it is a newly discovered member of the algal class Haptophyta. This species is 96% similar to an amplified haptophyte sequence from Lake BrayaSø (Greenland) (D'Andrea et al., 2006; Table 6-1). In addition, the alkenone distributions at both these lake sites are very similar including high %C_{37:4} and the presence of C₃₈Me alkenones (Figure 6-3).

The full 18S rDNA sequence (Figure 6-1) from Lake Toyoni and Braya Sø diverged before the lacustrine and coastal *I. galbana* and *C. lamellosa* species. The

alkenone signature of the Lake Toyoni haptophyte shares some features with the well characterised marine alkenone signature, i.e., the presence of C₃₈ MeK, absence of C₄₀, low C₃₇/C₃₈. However, the key exception is the high concentrations of the C_{37:4} homologue compared to the low, and in some cases absent C_{37:4} homologue, in most marine environments. This alkenone signature is very similar to the signature from Lake BrayaSø, Greenland (D'Andrea and Huang, 2005; Figure 6-3). Theroux et al. (2010) attribute the high tetra-unsaturated alkenones in Lake BrayaSø sediments to very cold temperature waters and/or low salinity.

The partial-length 18S rRNA sequence phylogeny shows the Lake Toyoni grouped within Group 1 of the Isochrysidales (Figure 6-2) along with previously published sequences from Greenland lakes (BrayaSø, HundeSø and LimnaeSø), Chinese Lakes (Tso Ur and Keluke Hu), American Lakes (Skoal Lake and Medicine Lake) and a Canadian Lake (Upper Murray lake) (Theroux et al., 2010). Haptophyte species are therefore able to be transported great distances (for example via wind) and may potentially encyst to survive transport (Theroux et al., 2010).

Since Lake Toyoni shares a phylogenetic group with haptophytes found in other Asian Lakes (e.g. down-core sediment sample from 20cm at Tso Ur and Keluke Hu), a similar haptophyte could be responsible for alkenone production in many other Asian Lakes. The surface sediment in Tso Ur however grouped within Group II of the Isochrysidales (Figure 6-2). The Lake Toyoni alkenone signatures are similar to Tso Ur signatures (i.e. C₃₇/C₃₈ values of < 2, the presence of C₃₈ MeK), with the exception that Tso Ur contains C₄₀ compounds (Table 6-4).

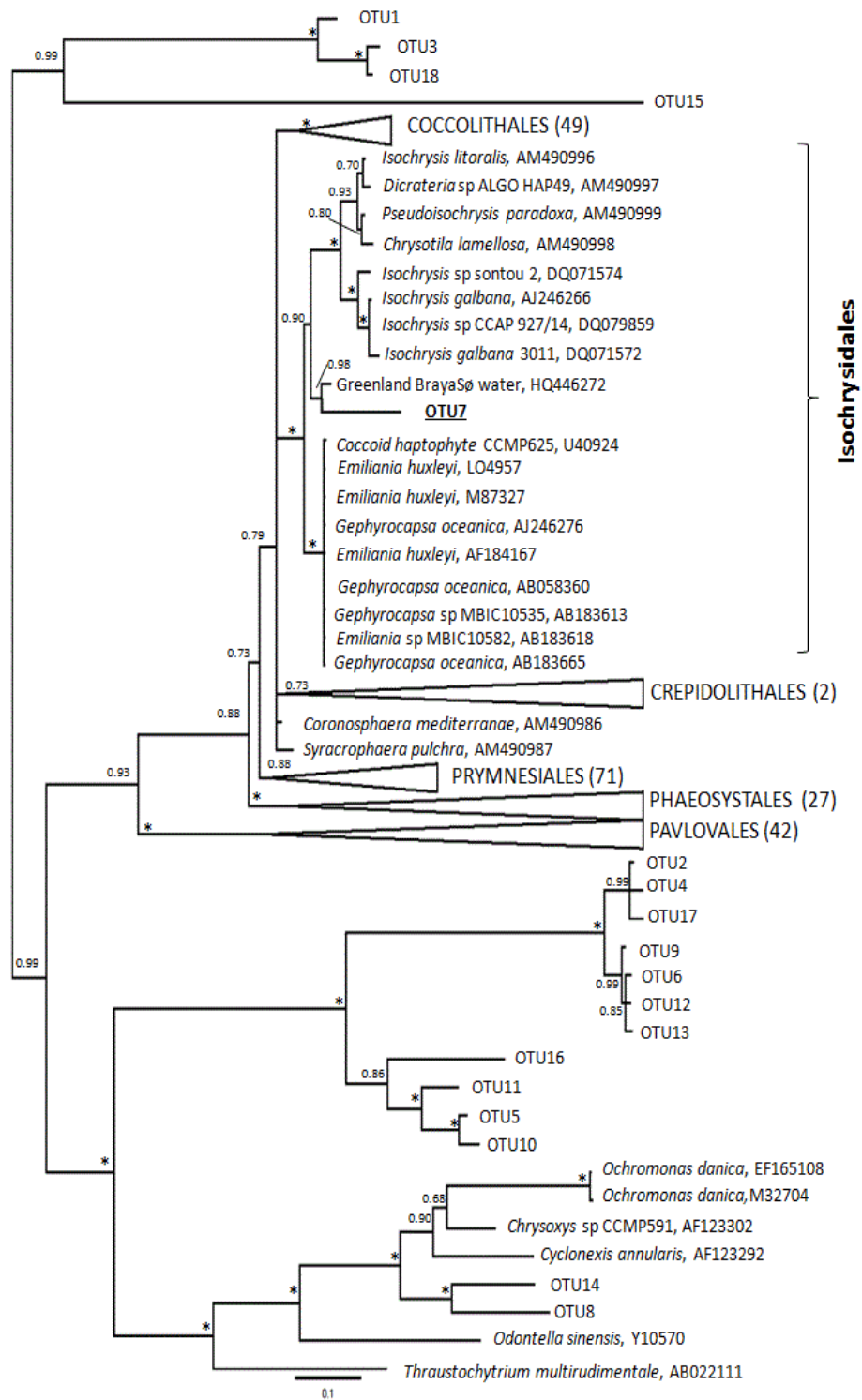


Figure 6-1: A consensus Bayesian phylogenetic tree depicting 18S rRNA gene-inferred relationships among haptophyte algae using only full length sequences. An asterisk (*) indicates posterior probability values of 1.00; all other values as shown. Order classification after de Vargas et al. (2007), with number of sequences per order as indicated. The evolutionary distance for the number of changes per site is represented by the scale bar. GenBank accession numbers follow species and sequence names.

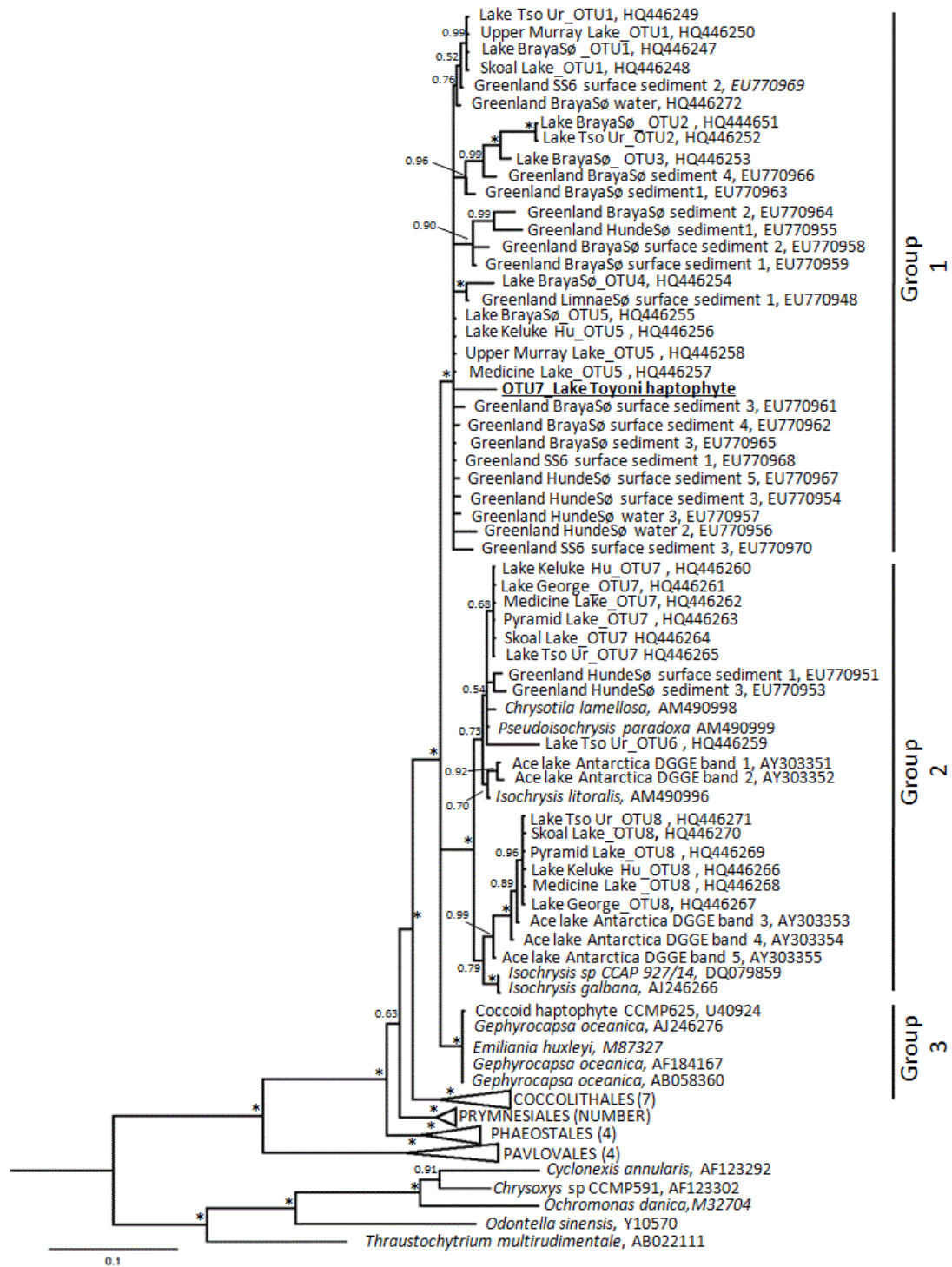


Figure 6-2: A consensus Bayesian phylogenetic tree depicting 18S rRNA gene-inferred relationships among haptophyte algae using partial length sequences. An asterisk (*) indicates posterior probability values of 1.00; all other values as shown. The evolutionary distance for the number of changes per site is represented by the scale bar. GenBank accession numbers follow species names and sequence names.

6.3.3 Alkenone occurrence

The presence of alkenones (and by inference, the presence of prymnesiophyte algae) in the surface sediments in Lake Toyoni, Japan extends the known geographic range of alkenones in lacustrine settings. We suggest elevated salinity is not a strict requirement for the occurrence of alkenones in Japanese lakes and therefore another factor is responsible for the presence of lacustrine alkenone producers (e.g. surrounding geology and/or lake chemistry). Although alkenones have been previously reported from freshwater lakes (e.g. Zink et al., 2001, Zhao et al., 2013) they are more frequently reported from lakes with elevated salinity (Li et al., 1996, Thiel et al., 1997, Chu et al., 2005, D'Andrea and Huang, 2005, Sun et al., 2007, Liu et al., 2008, Pearson et al., 2008). The relationship between lacustrine alkenone occurrence and salinity needs to be further explored. Although salinity is not a strict requirement for alkenone occurrence in lake systems, we suggest salinity may influence the species of algae present at an individual lake site. Hence, the alkenone producer present in Lake Toyoni may also be present in other low salinity/freshwater lacustrine systems (although no alkenones were detected in the other seven lakes surveyed in Hokkaido in this study).

6.3.4 Alkenone distribution

The presence of the tetra-unsaturated alkenones in Lake Toyoni sediments appears to be a characteristic feature of many lacustrine alkenone distributions (Cranwell, 1985, Thiel et al., 1997, Wang and Zheng, 1997, Schouten et al., 2001, Zink et al., 2001, Chu et al., 2005, D'Andrea and Huang, 2005, Sun et al., 2007, Toney et al., 2010). A key exception where the tetra-unsaturated homologues are not detected is in the lakes of the Nebraska Sand Hills (Toney et al., 2010). The dominant homologue in Lake Toyoni is C_{37:4}, which appears to be a common feature from all lakes with Group 1 of Isochrysidales present (Figure 6-2) (e.g. Medicine Lake; Toney et al., 2010) and Greenland lakes (D'Andrea et al., 2006). In comparison, most open waters in the marine environment alkenone distributions are generally characterised by abundant di- and tri-unsaturated compounds and the C_{37:4} homologues are present in only minor abundances or are absent completely (Castañeda and Schouten, 2011). Exceptions are in low salinity marine environments where the relative

abundance of $C_{37:4}$ ($\%C_{37:4}$) is generally higher compared with high salinity environments e.g. coastal/brackish basins (Bendle et al., 2009); the Baltic Sea (Schulz et al., 2000b) and in the open ocean in sub-polar and polar water-masses (Rosell-Melé, 1998, Rosell-Melé et al., 2002, Sicre et al., 2002, Harada et al., 2003, Bendle et al., 2005, Harada et al., 2012). The highest ever reported $\%C_{37:4}$ in the marine realm, ($>77\%$) was extracted from POC samples collected between sea-ice floes (Bendle et al., 2005).

There is some evidence for increased $C_{37:4}$ with decreasing salinity in the lacustrine environments in Asia (Liu et al., 2006b, Chu et al., 2005, Liu et al., 2008). Toney et al. (2010) however found no relationship based on findings in 13 North American lakes. Further studies by Toney et al. (2011) also found no relationship ($r^2 = 0.00061$) based on findings from 13 lakes in Canada. Theroux et al. (2010) also does not support the relationship based on 15 lakes from various geographical regions. Toney et al. (2011) suggested the reason for these differences is either $C_{37:4}$ is related to salinity in only some lakes, or that differences in percent $C_{37:4}$ and salinity may be related to other factors such as SO_4/CO_3 ratios.

Although lacustrine LCAs are often characterised by the dominance of tetra-unsaturated alkenones and higher C_{37}/C_{38} ratios, the presence of C_{38} MeK has been previously attributed to marine haptophyte presence (Schulz et al., 2000a). While many differences between marine alkenone producers and the Lake Toyoni alkenone producer exist (e.g., phylogenetic placement, dominance of $C_{37:4}$, differences in the C_{37}/C_{38} ratio), the main similarity is the presence of the C_{38} MeK (Table 6-4). This was also found in Lake George, USA (Toney et al., 2012) and Greenland lake sediments, as well (D'Andrea et al., 2006). Theroux et al. (2010) also found the presence of the C_{38} MeK in multiple lakes with Group II Isochrysidales (Figure 6-3) (e.g. Great Salt Lake and Pyramid Lake), which are more closely related to lacustrine *Isochrysis* and *Chrysofila* species than marine species. There appears to be no relationship between the grouping of Isochrysidales and the presence of the C_{38} MeK homologue.

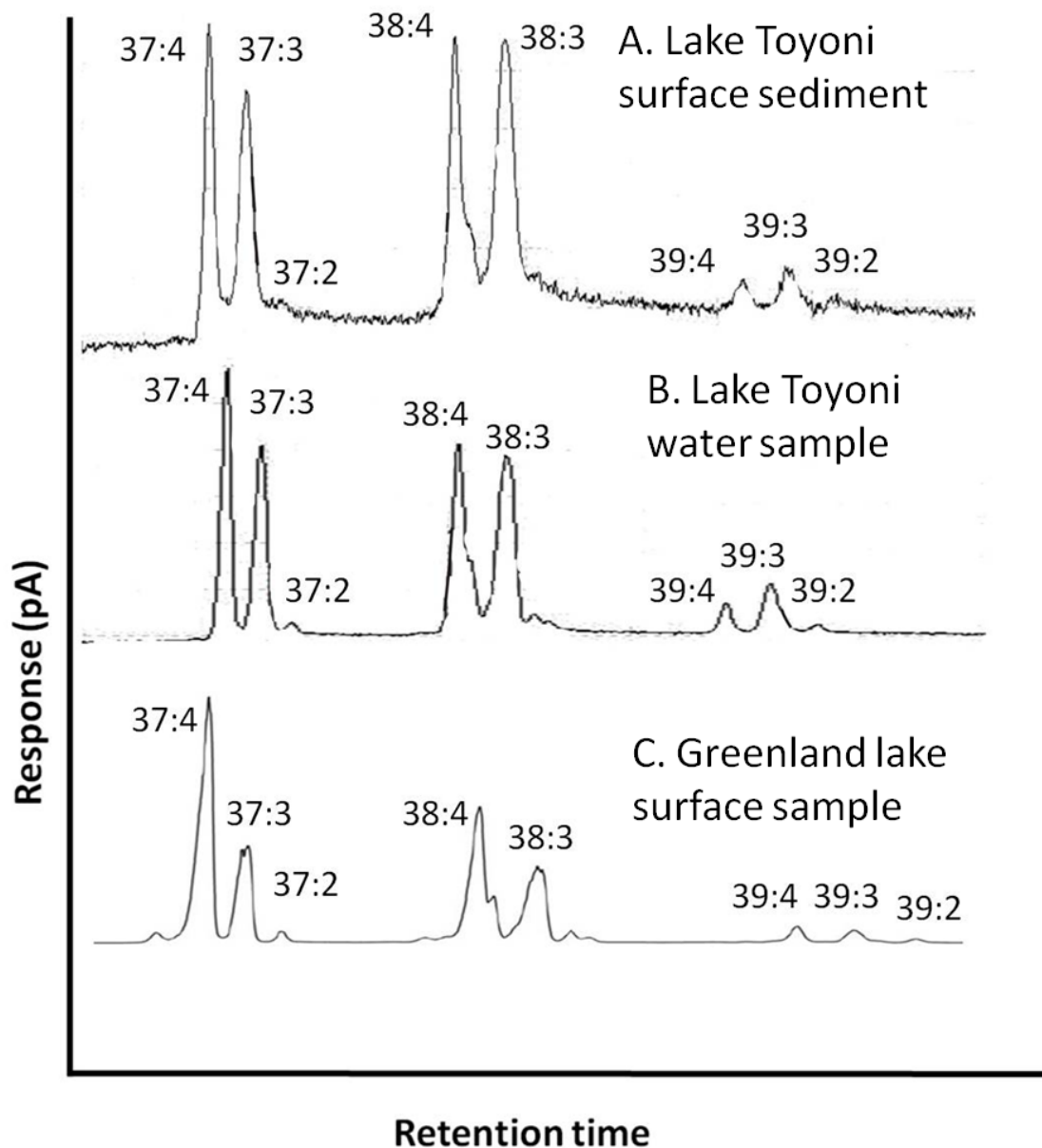


Figure 6-3: Comparison of molecular composition of lacustrine alkenones from Lake Toyoni and Greenland lakes. (A) The molecular composition of alkenones from Lake Toyoni surface sediment and (B) Lake Toyoni water column and (C) Greenland Lake alkenone producer (D'Andrea et al, 2006) all showing the dominance of the tetra-unsaturated alkenones.

6.3.5 Paleotemperature implications

The presence of one haptophyte (OTU7) and the similarity between the alkenone homologue from the water and the surface sediment suggests the alkenones discovered in the surface sample are being produced by a single haptophyte species in the water column. The presence of a single haptophyte phylotype, conservative to the *Isochrysidales*, in Lake Toyoni is promising for the use of this site as a paleotemperature archive. Multiple alkenone producers contributing to the alkenone sedimentary record could influence the reliability, or at least complicate the interpretation, of the alkenone derived palaeotemperature proxy (Theroux et al., 2010) because different haptophytes can have different temperature relationships to unsaturation. Alkenone-based temperature reconstructions from Lake Toyoni would therefore only require a single temperature calibration for the single alkenone producer present. Currently, there is no standard calibration available that is applicable for different alkenone producers at different lake sites. As a result, site-specific or a species-specific calibration for lacustrine environments must be developed to significantly improve the use of the lacustrine alkenone proxy.

An example of a site-specific temperature calibration in lacustrine systems is >>> The temperature calibration ($T = 14.3 [U_{37}^K] + 32.3$; $R^2 = 0.97$; $n = 26$) for lakes in Kangerlussuaq, West Greenland was developed based on U_{37}^K of filtered alkenones and *in situ* temperature (D'Andrea et al., 2011). However, the *in situ* calibration from BrayaSø only provides a calibration for temperatures between -3.5 and 6.5°C during the production time between mid-June and mid-July. Therefore a combination of the *in situ* data from BrayaSø was combined with published data from German/Austrian lakes from Zink et al. (2001) to expand the temperature range of the calibration. The Zink et al. (2001) calibration provides averaged summer surface water temperature reconstructions. The resulting temperature calibration is; $T = 40.8 [U_{37}^K] + 31.8$ ($R^2=0.96$; $n=34$; Figure 6-4), with a mean standard error estimation of 1.3°C . The justification for expanding the temperature calibration using samples from German/Austrian lakes is that the alkenone producer in the West Greenland and German/Austrian lakes are similar based on the dominance of tetra-unsaturation and presence of C_{38} MeK (D'Andrea & Huang, 2005). A key assumption, therefore, is that the alkenone-producer in the lakes in Europe (Zink et al., 2001) and the lakes in

Greenland (D'Andrea et al., 2011) are the same or at least have the same relationship with temperature. This hypothesis, however, has not been tested using genetic fingerprinting therefore the identity of the alkenone-producers in lakes in Europe used in the Zink et al (2001) study is currently unknown. If the alkenone-producers in the lakes in Europe are not the same as the alkenone producers from Greenland lakes, this would result in a large error in the combined temperature calibration because different alkenone-producers have different relationships to temperature.

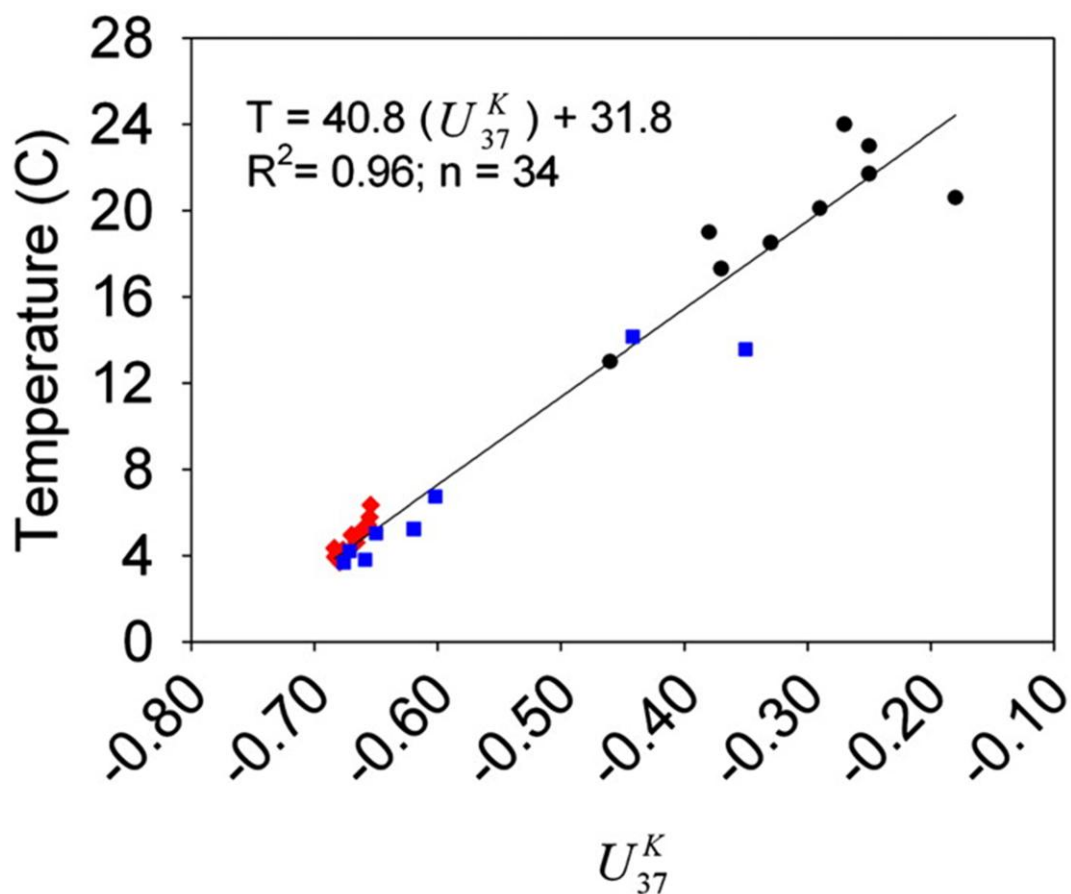


Figure 6-4: Temperature calibration developed for Greenland lake using a combination of in-situ water filter samples from Braya Sø collected during summer 2007 (red diamonds) and 2009 (blue squares) and a previously published calibration from Europe (black circles) by Zink et al (2001).

A site-specific calibration is currently not developed for Lake Toyoni therefore we suggest that a suitable calibration for this lake is the temperature calibration from Greenland lakes by D'Andrea et al. (2011). Justification for choosing to use this calibration is based on the phylogenetic analysis showing that the

haptophyte in Lake Toyoni is 96% (posterior probability of 0.98) similar to the haptophyte in water filter samples from BrayaSø, Greenland (D'Andrea et al., 2006). In addition there is a strong similarity of alkenone distributions in Lake Toyoni and the haptophyte in water filter samples from Lake BrayaSø, Greenland (Figure 6-3). The combination of the 18S rDNA analysis and the alkenone distributions between the lake Toyoni haptophyte and the Greenland lakes haptophytes provides a basis for applying this calibration to a down-core sedimentary record in Lake Toyoni. The similarity of alkenone distributions and 18S rDNA in Lake Toyoni and the haptophyte in water filter samples from Lake BrayaSø, Greenland, (D'Andrea et al., 2006) provides a basis for applying this calibration to a down-core sedimentary record in Lake Toyoni. Applying the Greenland lake calibration to Lake Toyoni surface sediment unsaturation indices (U_{37}^K value=-0.49) gives a reconstructed temperature estimate of 11.8°C.

Alkenones record the temperature during the time period that they are produced which means the alkenone-based temperature reconstruction may have a seasonal bias. To determine a potential seasonal bias at Lake Toyoni, seasonal filter samples were collected on a monthly basis, excluding months where there was ice-cover on the lake. Unfortunately, alkenones were not detected in the filter samples, possibly due to low concentrations of alkenones in the 1L of water collected. As a result, the timing of alkenone production in Lake Toyoni is currently unknown.

Another method for determining the link between the timing of alkenone production and temperature is to use the core-top temperature estimate and compare it with LST's from Lake Toyoni. The core-top temperature estimation based on the application of the calibrate developed by D'Andrea et al. (2011) to the Lake Toyoni surface sediment U_{37}^K values produces a water temperature estimate of 11.8°C. The comparison shows that the core-top alkenone temperature is within the range of observed lake temperature during the ice-free months (April-November (14°C) and also late summer (11.6 in October 2011)). We suggest that alkenones are being produced through-out the ice-free time period (~March-November; please note no data available for March LST, although this temperature would likely lower the average ice-free months temperature closer to the core-top value). It is likely that alkenone production

ceases to occur when the lake is covered by ice due to the reduction in light required for photosynthesis. It is therefore suggested, based on the comparison with the core-top U_{37}^K temperature that alkenone production in Lake Toyoni likely records an average temperature of the ice-free months in Lake Toyoni rather than a mean annual temperature, which would take into account winter temperatures.

6.4 Conclusions

This study reports the first occurrence of alkenones (and by inference, the presence of Prymnesiophyte algae) in Japanese Lakes. A phylogenetic analysis of the Lake Toyoni haptophyte rDNA sequences suggests a single haptophyte alga of the class Prymnesiophyceae produce alkenones in Lake Toyoni. This species represent a new taxon of haptophyte algae that occupies a phylogenetic clade with the BrayaSø Greenland lake haptophyte, which is distinct from the well-studied marine alkenone producers *Emiliana huxleyi*, *Gephyrocapsa oceanica* and coastal alkenone producers *Isochrysis galbana* and *Chrysotila lamellosa*. The presence of a single alkenone producer in Lake Toyoni, which is closely related to alkenone producers in Greenland lakes supports the application of alkenone-based temperature reconstructions using the Greenland lake temperature calibration (D'Andrea et al., 2011).

In conclusion, rDNA analysis has been used in conjunction with lipid biomarkers to identify the alkenone producer in Lake Toyoni. In order for alkenones to become a useful continental temperature proxy, additional lake surveys examining alkenone presence, abundance, and distribution need to be determined. Much still remains unknown about the lacustrine alkenone producers, however further genetic studies will provide insights into understanding the ecology of lacustrine haptophytes which is essential for interpretation of its associated molecular signature.

Alkenone-based temperature reconstruction from Lake Toyoni.

7.1 Introduction

Lake Toyoni is located in southern Hokkaido, whose climate is dominated by the variability of the East Asian Monsoon (EAM); the East Asian Summer Monsoon (EASM) and the East Asian Winter Monsoon (EAWM). The EAM influences a region which is densely populated therefore changes in the variability of the EAM also has an extensive influence on society through its influence on severe flooding and agriculture (e.g. Tao et al., 2004, Huang et al., 2007). The EAM is connected to the global climate system as it influences, and is influenced by El Niño southern oscillation (ENSO) (e.g. Zhang et al., 1996, Wang et al., 2003, Hong et al., 2005) and changes in the North Atlantic (e.g. Liu et al., 2013c). The combination of the scientific and societal importance of the EAM is a key reason for investigating how the monsoon has behaved in the past, and the driving forces behind this variability, is required for a better understanding of future climate variability.

The EAM is driven by the seasonal reversal of the monsoon winds, which in turn is driven by the thermal contrast between the Asian continent and the Pacific Ocean. During summer, the variability of the EAM is associated with the development of the North Pacific Subtropical High (NPSH). The southerly winds along the western edge of the NPSH transports heat and moisture to Japan in summer resulting in warm and wet conditions. Whereas in winter, the variability of the EAM is associated with the development of the Siberian High (SibH)

resulting in cold air mass being transported to Japan in winter. Intensification/weakening of the EAWM and the EASM result in changes in temperature in summer in Hokkaido, Japan. For example, when the EASM intensifies (weakens), the temperature in summer is higher (lower) than average (1958-2014; instrumental data from Hiroo weather station; Chapter 2). It was also noted that the lowest summer temperatures occur when the EAWM is strengthened (Chapter 2), suggesting that a strong EAWM results in a weak EASM. Due to the temperature change in response to intensity of the EAM (EASM and the EAWM), we anticipate that a temperature reconstruction from Hokkaido will reflect the intensity of the EAM.

The most reliable records of temperature variability are from instrumental records, however these records rarely span more than the last ~150 years. In the case of Hokkaido, the first instrument-based meteorological observations began with the establishment of a meteorological station in Hakodate in 1872. Prior to 1872, we must rely on temperature reconstructions from this region using proxies. Proxies of climate can either be from historical documents (historical proxies) or from natural recorders of climate (natural proxies). Here we will investigate, develop and apply the alkenone paleothermometer to evaluate temperature change from Hokkaido, Japan over the last 1000 years.

One of the most well-established quantitative temperature proxies in the marine realm is alkenone paleothermometry. Alkenones not only provide quantitative temperature reconstructions, but their occurrence is widespread and abundant in marine sediments (e.g. Brassell et al., 1986, Rosell-Melé et al., 1994, Bendle and Rosell-Melé, 2004) and they have been detected in sediments up to 160 million years old (Brassell and Dumitrescu, 2004). The successful application of alkenones as a quantitative sea surface temperature (SST) proxy has therefore captured the interest of palaeo-limnologists. Since then, alkenones have been detected in many lacustrine sediments from around the world including; England (Cranwell, 1985) China (Li et al., 1996, Wang and Zheng, 1997, Sheng et al., 1999, Sun et al., 2004, Chu et al., 2005, Liu et al., 2006b, Sun et al., 2007, Liu et al., 2008, Chu et al., 2011, He et al., 2013, Zhao et al., 2013), Turkey (Thiel et al., 1997, Randlett et al., 2014), Antarctica (Volkman et al., 1998, Coolen et al., 2004c), Norway (Innes et al., 1998), Austria, Germany, Russia (Zink et al., 2001), USA (Zink et al., 2001, Toney et al., 2010), Mongolia (Sun et al., 2004),

Greenland (D'Andrea and Huang, 2005, D'Andrea et al., 2011, von Gunten et al., 2012), South America (Theissen et al., 2005), Spain (Pearson et al., 2008), Canada (Toney et al., 2011) and Svalbard (D'Andrea et al., 2012), South Africa (Schmidt et al., 2014). Recent progress also shows alkenones can be used to successfully reconstruct water temperature in lacustrine systems (Liu et al., 2006b, Chu et al., 2011, D'Andrea et al., 2011, D'Andrea et al., 2012, von Gunten et al., 2012, He et al., 2013, Zhao et al., 2013). The development of alkenone-based temperature records from lacustrine sediments have provided key insights into human migration patterns in Greenland (D'Andrea et al., 2011) and the link between temperature and solar irradiance (He et al., 2013).

In Asia, considerable effort has been applied to developing the alkenone proxy in Chinese lakes. For example, Chu et al. (2005) investigated 50 lakes in China and detected alkenones in 45 of them. A relationship was derived between the $U_{37}^{K'}$ index and mean annual air temperatures: $U_{37}^{K'} = 0.025T + 0.153$. Significantly, the slope is very similar to the $U_{37}^{K'}$ -temperature relationship from culture experiments of lake species *Chrysothila lamellosa* under controlled growth temperatures ($U_{37}^{K'} = 0.026T - 0.261$; Sun et al., 2007). Until now, alkenones have not been reported from lakes in Japan therefore Lake Toyoni represents the first Japanese lake from which alkenone-based temperature reconstructions are developed.

Prior to the application of alkenones as a temperature proxy in Lake Toyoni, the precursor organism must be identified (e.g. D'Andrea et al., 2011). Chapter 6 reported on the phylogenetic analysis of the Lake Toyoni haptophyte rDNA sequences. The results found a single haptophyte alga of the class Prymnesiophyceae produces alkenones in Lake Toyoni. This species represents a new taxon of haptophyte algae that occupies a phylogenetic clade with the BrayaSø Greenland lake haptophyte, which is distinct from the well-studied marine alkenone producers *Emiliana huxleyi*, *Gephyrocapsa oceanica* and coastal alkenone producers *Isochrysis galbana* and *Chrysothila lamellosa*. The presence of a single alkenone producer in Lake Toyoni, which is closely related to alkenone producers in Greenland lakes, supports the application of alkenone-based temperature reconstructions using the Greenland lake temperature calibration: $T = 40.8 [U_{37}^K] + 31.8$ (D'Andrea et al., 2011).

Lake water surface temperature (LST) in Lake Toyoni corresponds to changes in air temperature (Chapter 3), which is strongly influenced by the EAM (e.g. D'Arrigo et al., 2001, Davi et al., 2002, Igarashi et al., 2011). Significantly, Lake Toyoni (42°N) is situated at the boundary of the northern edge of the East Asian Summer Monsoon (EASM) (34-44°N; Xu et al., 2010b) making it sensitive to the variability of the EASM (Schöne et al., 2004). The boundary of the northern edge of the EASM is the location where the warm tropical air meets the cold polar air mass, termed the polar front. When the NPSH intensifies, the polar front is located farther north than usual (37°N) and as a result there is an increased influence from tropical maritime air mass from the Pacific Ocean. When the polar front is located farther south, there is a reduction in the influence of the Pacific Ocean and an increased influence from the sub-polar maritime air mass to Hokkaido. For example, in 1978, the NPSH was located farther north than usual. Instrumental data from a nearby meteorological site (Hiroo; 25km from Lake Toyoni) recorded temperatures during June, July and August were 2.3, 2.8 and 1.9°C warmer. When the polar front is located farther south, there is a reduction in the influence of the EASM and an increased influence from the sub-polar air mass and hence lower air temperatures in Hokkaido. As a result, it is hypothesised that Hokkaido is a key location for investigating variability in past temperatures to infer information on the EAM.

7.1.1 Objectives of research

The prime objective of this study is to investigate lake water temperature, and hence air temperature variability, over the past 1000 years in Hokkaido, Japan. The following questions will be considered;

1. Is the Lake Toyoni alkenone-based temperature record driven by the variability of the EAM (EASM and the EAWM)?
2. Does the alkenone-based temperature record provide evidence for globally recognised events (e.g. the MWP, LIA and the CWP) and if so, are the timings of these events synchronous with records with East Asia?
3. Is there a relationship between temperature and famine frequency in Japan?

7.2 Results

The U_{37}^K values are calculated using the following equation:

$$U_{37}^K = \frac{(C_{37:2} - C_{37:4})}{\sum(C_{37:2}:C_{37:3}:C_{37:4})}$$

Equation 7.1: U_{37}^K calibration equation (Brassell et al., 1986).

Based on the similarity between the alkenone producers in Greenland Lakes and Lake Toyoni (Chapter 6), the raw U_{37}^K data is then converted to temperature using the following temperature calibration: $T = 40.8 [U_{37}^K] + 31.8$ (D'Andrea et al., 2011). The down-core alkenone-based temperature reconstruction is presented in (Figure 7-1). We found that the average temperature in the down-core record was 12.5°C. In Lake Toyoni, the temperature between 1000 and 1240AD was generally warm with two periods of cooling (~1198AD and ~1187AD). Average temperatures for this time periods is 13.2°C, however temperatures fluctuated between 10.7-16.6°C (Figure 7-1). Following this warm period, temperatures dropped, and the period from 1330AD to 1450AD was marked by cold temperatures with a mean value of 9.7°C; in particular, the lowest temperature (8.1°C) occurred at 1427AD (Figure 7-1). Between 1300AD and 1800AD, the average temperature was 11.7°C, 0.6°C cooler than the average temperature. Following the notable cool period between 1330-1450D, the average temperature between 1450-1800AD was 12.7, which is slightly warmer than average temperatures and 0.4°C cooler than the MWP. There are two notable peaks in temperature between 1474 and 1482AD (with temperatures reaching 15°C) and also between 1584 and 1640AD (with temperatures reaching 16°C; Figure 7-1). The temperatures then rose to a maximum of 18.3°C between 1843-1887AD and decreased to 10.4 °C in 1956AD.

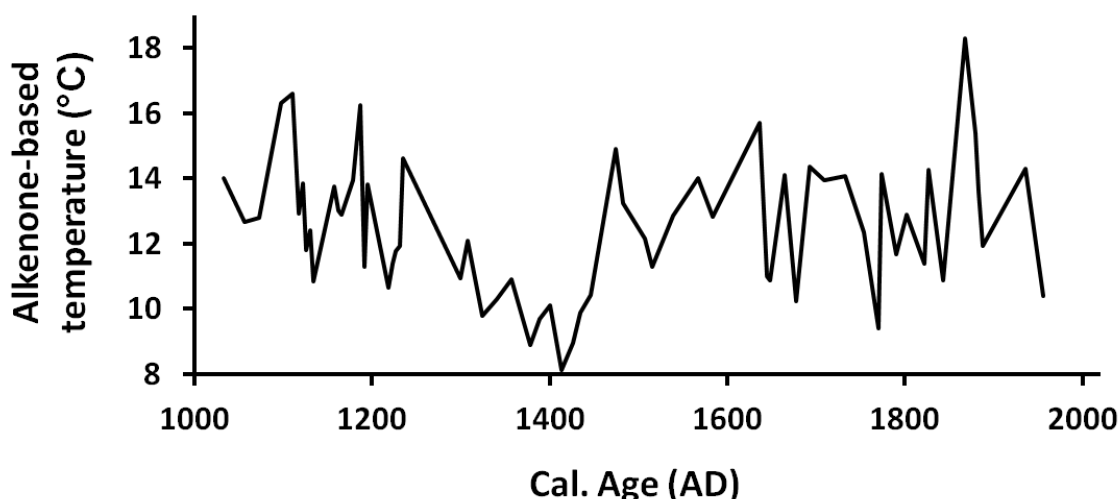


Figure 7-1: Alkenone-based temperature reconstruction reflecting averaged temperature values from the ice-free seasons (spring and summer) over the past 1000 years from Lake Toyoni

7.3 Discussion

7.3.1 Application of the D'Andrea et al (2011) temperature calibration in Lake Toyoni

The justification for using the D'Andrea et al (2011) temperature calibration in Lake Toyoni has been previously discussed in Chapter 6 (section 6.3.5). As previously discussed, the largest assumption is that the alkenone-producers in all the lakes used in the combined calibration are the same species. This has not been tested using genetic fingerprinting therefore has the potential to introduce errors in the temperature calibration. Another key assumption is that the alkenone-producers are all reflecting the a similar time period. For example, alkenones were found to be produced for a very narrow time period between mid-June and mid-July in Greenland lakes (D'Andrea et al., 2011). Zink et al (2001) suggested that alkenones in the lakes studied in Europe reflected an averaged summer temperature, therefore a larger temperature range than the Greenland lakes. The timing of the alkenone production in Lake Toyoni is yet to be determined. As previously discussed in Chapter 6, we suggest that the alkenone-based reconstruction from Lake Toyoni is reflecting a averaged temperature of the ice-free time period (e.g. spring and summer). The temperatures during this time period range from 4.9°C to 18.5°C, which is in line with the temperatures reconstructed using the D'Andrea et al (2011) temperature calibration. Key assumption of using the D'Andrea et al (2011)

calibration is that seasonal differences between the production in the different lakes does not produce a large error using the combined calibration.

The mean standard error on the D'Andrea et al (2011) calibration is 1.3°C . This is an important consideration because a large majority of the temperature changes in the alkenone-based temperature reconstruction from Lake Toyoni may be explained by the error associated with the calibration. The temperature range over the past 1000 years is $8.1^{\circ}\text{C} - 18.3^{\circ}\text{C}$, implying that lake water temperature in Lake Toyoni has varied as much as 7.6°C over the past 1000 years. Key time periods where the calibration reconstructs temperatures greater than the error range are; 1090-1110AD, ~1187AD, ~1639AD and ~1867AD (Figure 7-2) and key time periods where the calibration reconstructs temperatures less than the error range are 1378-1426AD and ~1770AD (Figure 7-2). These key time periods therefore provide more reliable reconstructed temperatures compared to all other time periods, which have temperature changes within the mean standard error.

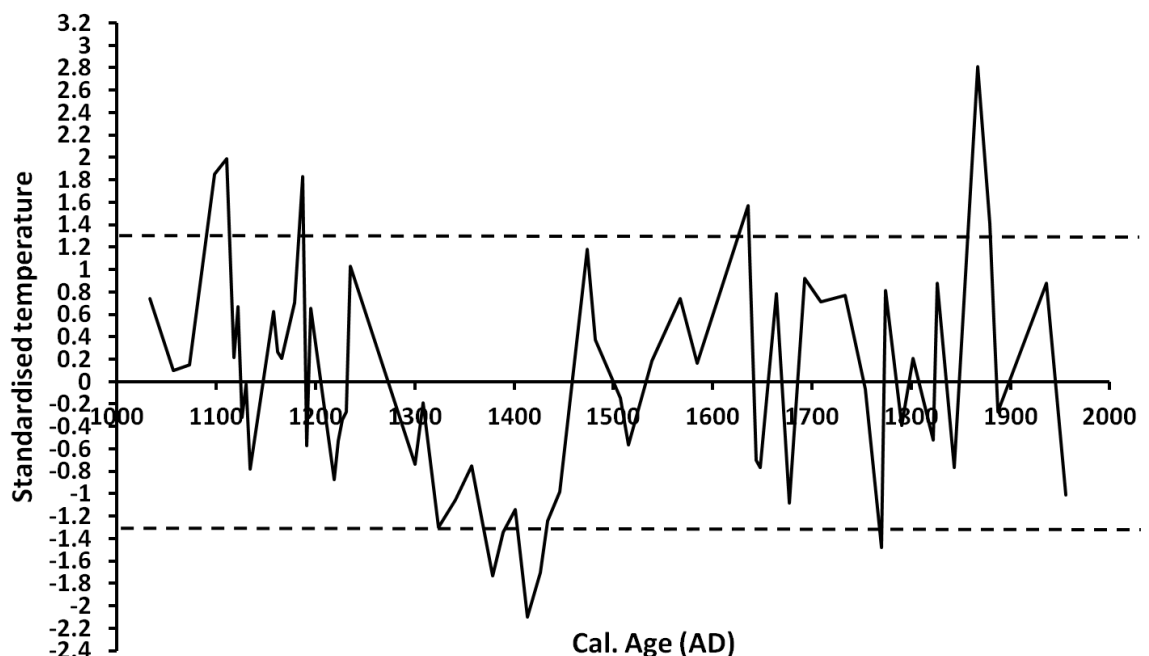


Figure 7-2: Standardised alkenone-based temperatures over the past 1000 years. Values above and below 1.3°C are out with the mean standard calibration error.

7.3.2 Alkenone-based temperature reconstructions: comparison with EAM records

Question 1: Is the Lake Toyoni alkenone-based temperature record driven by the variability of the EAM (EASM and the EAWM)?

The alkenone-based temperature record from Lake Toyoni provides information on changes in temperature over the past 1000 years. It is hypothesised that because Lake Toyoni is situated within the northern limit of the EASM, and the air temperature is influenced by the variability of the EASM in the modern day (Chapter 2), therefore this location is particularly sensitive to the intensification of the EASM and hence will also record a strong EAM climate signal. In order to test this hypothesis, the alkenone-based temperature record from Lake Toyoni is compared with records of the EASM. However, considerable variability in the intensity of the EAM over the past 1000 years has been noted. As a result, the records of the EAM over the past 1000 years do not always match up and hence more reconstructions of the EAM from locations all over East Asia are required to determine the variability of the EAM over the past 1000 years. The chosen records and the justification are as follows:

1. The centennial-scale variations in the EASM over the past 1700 years were investigated using the $\delta^{18}\text{O}$ of shells from the ostracode *Bicorncythere bisanensis* from Lake Nakaumi, Japan, which reflects the bottom salinity changes (Yamada et al., 2016). The bottom water salinity in Lake Nakaumi was negatively correlated with monthly precipitation between April and August 2006-2011 and hence, the bottom salinity of Lake Nakaumi is associated with precipitation during summer, which is controlled by the EASM. Lower salinity values (low $\delta^{18}\text{O}$ values) therefore suggest an increase in precipitation and hence a strong EASM and vice versa. Yamada et al. (2016) also detrended time-series variations by subtracting the 50 yr moving mean from the 500 yr moving mean. By doing this, any changes due to environmental conditions were removed and the 50-500 years periodicity in the EASM was retained. The data was also standardised using the standard deviation of the anomaly (Figure 7-3). The periods in which the standard deviation exceeded 0.5 or was <-0.5 were defined as statistically significant. This study is a key EASM

reconstruction to compare with the alkenone-based temperature records from Lake Toyoni because it is a centennial-scale EASM record from Japan.

2. EAM record from Lakes Ni-no-Megata (39°57'N, 139°43'E) and San-no-Megata (39°56'N, 139°42'E) on the Oga Peninsula of northeastern Japan over the past 2000 years by Yamada et al. (2010). Lake San-no-Megata was used to provide information on the EASM because Lake Ni-No-Megata is influenced by human activity. The *sulphur content* of Lake San-no-Megata was used to gain information on the EASM because it is a proxy for anoxic-oxic bottom water conditions. When the EASM intensifies (weakens), precipitation increases (decreases) and hence lake levels increase (decrease). Yamada et al. (2010) suggested that when lake levels increase (decrease), there is less (more) vertical mixing and anoxic (oxic) bottom waters; which have high (low) sulphur content in Lake San-no-Megata. Lake Ni-no-Megata was used to infer information on the EAWM by the coarse-grained input into the lake. When the lake freezes, dust material transported via the EAWM is deposited on the top of the lake. When conditions in winter are colder, and hence a strong EAWM, the ice stays on the lake for longer and hence more dust material is accumulated. When the ice melts, the coarse-grained material is released into the lake. Lake Ni-no-Megata is more likely to freeze than Lake San-no-Megata therefore Lake Ni-no-Megata is more sensitive to temperature changes in winter. This study is a key EASM reconstruction to compare with the alkenone-based temperature records from Lake Toyoni because both records are located in northern Japan and are sensitive to the variability of the intensification of the EASM.
3. A reconstruction of Holocene rainfall from southwest China, which is strongly influenced by the EAM by Hu et al. (2008) (Figure 7-3a and b). There are two records associated with this reconstruction; the first record is the original $\delta^{18}\text{O}$ values from the Heshang stalagmite (30°27'N, 110°25'E) and the second record is the corrected $\delta^{18}\text{O}$ record. The $\delta^{18}\text{O}$ of stalagmites in this region reflect precipitation amount, with higher (lower) $\delta^{18}\text{O}$ values suggesting increased (decreased) precipitation, which in turn provides information on the EASM. The $\delta^{18}\text{O}$ of stalagmites provide

robust EASM records because of their very precise age controls (e.g. Cheng et al., 2009, Wang et al., 2005). The original stalagmite $\Delta\delta^{18}\text{O}$ record by Hu et al. (2008) may be subjected to site-specific bias. The corrected record is the difference between the original Heshang stalagmite and another stalagmite from a nearby cave (Dongge cave) by Wang et al. (2005). The difference between the two records offers a unique opportunity to remove any site-specific effects on the $\Delta\delta^{18}\text{O}$ record, whereas the regional signal is preserved (Hu et al., 2008). As a result, the $\Delta\delta^{18}\text{O}$ record by Hu et al. (2008) offers a EASM reconstruction, representing south east China, to compare with findings on the EASM system from the Lake Toyoni sedimentary record.

4. Sea surface temperatures (SST's) as inferred from alkenone-based temperature reconstructions and salinity reconstructions as inferred from planktonic foraminiferal oxygen isotope ratio analyses by Lee and Park. (2015)(Figure 7-4). These proxies are robust and well known and provide reliable reconstructions of EASM variability. The alkenone proxy works in the same way in marine sediments as it does in lake sediments (present study). The oxygen isotopic values of planktonic foraminiferal calcite are controlled by temperature of calcification and the local oxygen isotopic composition of sea water, which is a function of salinity. The combination of temperature and salinity reconstructions provides a record of EASM variability because stronger EASM result in warmer and wetter conditions and hence increased SST and freshening of the water column due to increased run-off. This study was chosen to compare with the alkenone-based temperature reconstruction from Lake Toyoni because the reconstruction provides a continuous reconstruction of EASM variability over the past 1300 years, which is a similar time scale as the alkenone-based temperature reconstruction from Lake Toyoni (the past 1000 years) and both records are decadal-resolved and therefore have a similar to the age resolution of Lake Toyoni.
5. A March-temperature reconstruction from Kyoto, Japan (Aono and Kazui, 2008; Figure 7-4). This temperature reconstruction is based on records of the timing of cherry blossoms in newspapers, personal diaries, poetry since 800AD (Aono and Kazui, 2008). The authors found that the timing of

the cherry blossom is linked to the temperature in March. The authors compared the cherry blossom-inferred temperature record with summer- and winter-temperature reconstructions and found that the cherry blossom-inferred temperature reconstruction records winter temperatures (Aono and Kazui, 2008). We have used this record as a EAWM reconstruction because temperatures in winter are controlled mainly by the EAWM in this region. This record provides a unique opportunity to investigate if the variability of the EAWM (as inferred from cherry blossom temperature record) influences temperatures during the ice-free months in Lake Toyoni (as inferred from the alkenone-based temperature reconstruction) in Japan over the past 1000 years.

In summary, we have chosen two studies from Japan, three studies from East Asia and one study from the Sea of Japan, which all cover the past 1000 years to compare with the alkenone-based temperature reconstruction. The combination of these studies provides good spatial coverage of the variability of the EASM and also covers a range of archives including stalagmites, lake and marine sediments. We also chose an EAWM reconstruction from Japan to compare with the alkenone-based temperature reconstruction from Lake Toyoni to determine if the EAWM influences the temperatures during the ice-free months in Lake Toyoni.

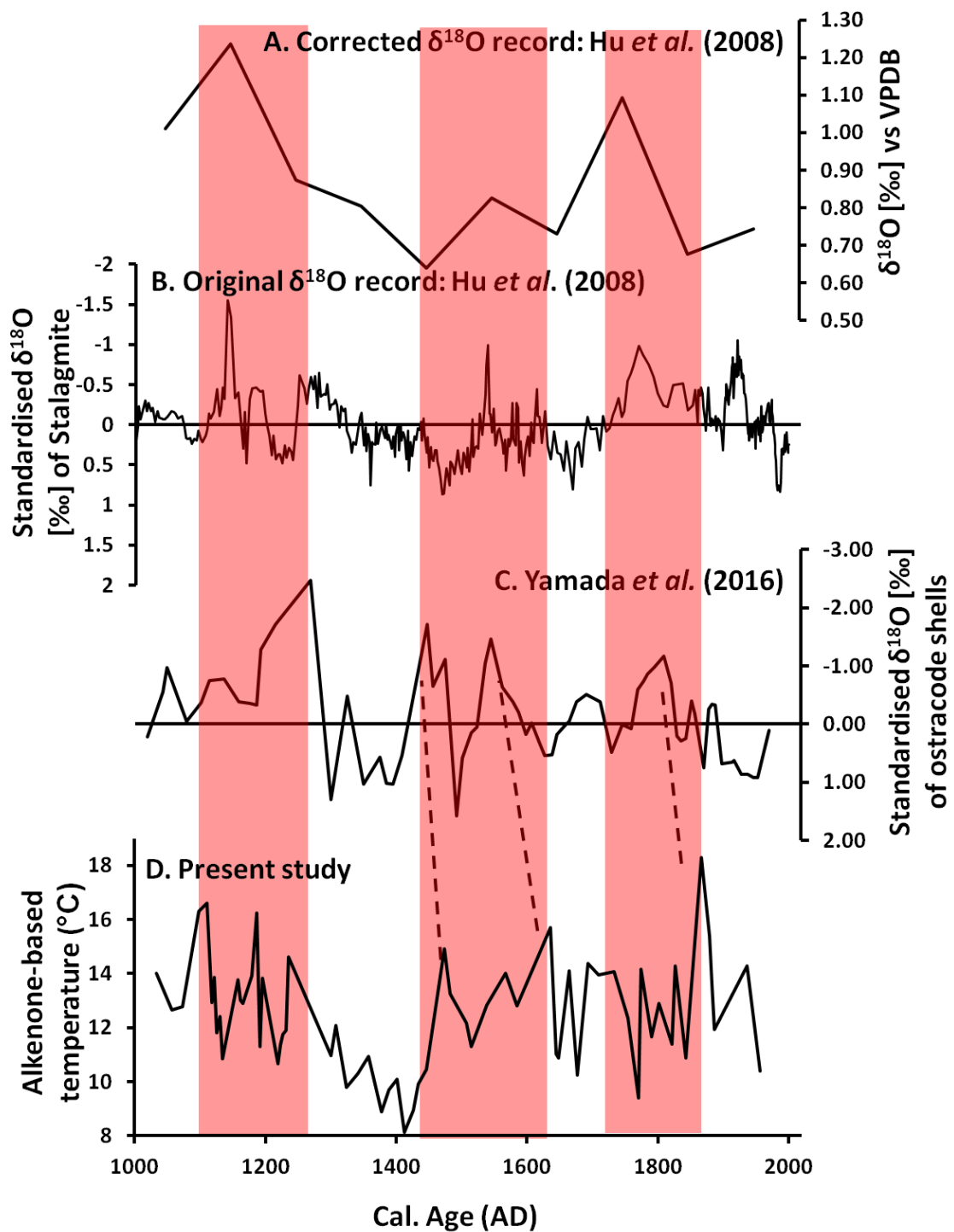


Figure 7-3: Comparison of the alkenone-based temperature record with EASM records. A: Corrected $\delta^{18}\text{O}$ values from the Heshang stalagmite, B: original $\delta^{18}\text{O}$ values from the Heshang stalagmite, C: $\delta^{18}\text{O}$ of shells from the ostracode *Bicornucythere bisanensis* from Lake Nakaumi, Japan, D: alkenone-based temperature reconstruction (present study).

7.3.2.1 Comparison with EASM records

The alkenone-based temperature record from Lake Toyoni is compared to the EASM record of Yamada et al. (2016), Yamada et al (2010), Lee and Park (2015)

and Hu et al (2008) to determine the link between the EASM variability and temperature recorded at Lake Toyoni.

Yamada et al (2016) identified six time periods of EASM intensification and six time periods of EASM weakening over the past 1000 years based on the $\delta^{18}\text{O}$ of shells from the ostracode *Bicornucythere bisanensis* from Lake Nakaumi, Japan. The EASM intensified (values less than -0.5) in 1192-1268AD, 1447-1174AD, 1545AD and 1769-1809AD and weakened (values more than 0.5) in 1299AD, 1350-1395AD, 1492AD, 1627AD, 1898-1953AD. When comparing these findings with the alkenone-based temperature record from Lake Toyoni, we find that the alkenone-based temperature record also records the same warming and cooling trends, however there is a lag between the two sites. For example, we find evidence for a strong EASM between 1166-1235AD (with a slight decrease ~1134AD, time lag 26 years), 1470AD (time lag of 23 years) and 1644AD (time lag 17 years). We also found weak EASM in 1324-1450AD (26 year time lag), 1515AD (23 year time lag) and 1644AD (17 year time lag). Reasons for the time lag are (1) age model errors and (2) the data from Yamada et al (2016) has been detrended to focus on the 50-500 year variations in the EASM using moving means. There is an age error on all radiocarbon dates from leaf samples ranging from ± 36 -54 years and a ± 70 year age error on the radiocarbon measurement from the bulk sediment sample at the base of the core. All time lags therefore fall into the range (± 36 -54 years) of the age model errors providing evidence that age model errors may be responsible for differences between the records. Overall the strong similarities between the EASM record by Yamada et al. (2016) and the alkenone-based temperature record provides strong evidence that the alkenone-based temperature record from Lake Toyoni is recording an EASM signal.

Another EAM record from Japan shows that the EASM was strong between 1000-1200AD and weak between 1200-1500AD and 1700-1820AD (Yamada et al., 2010). This EASM record is based on Sulphur content from Lake San-No-Megata, northern Japan (39°N). Given that this site is closer in location to Lake Toyoni rather than Lake Nakaumi (35°N), we therefore might expect the timing of the changes in the intensity of the EASM to be synchronous. The alkenone-based temperature record also shows warming between 1000-12000, which supports findings of a strong EASM during this time period. Although we find evidence for a weak EASM between 1200-1500AD, the timings are slightly different between the

records. For example, we find that the EASM weakened between 1300-1457AD. We do not find strong evidence for a weakened EASM between 1700-1820AD, however cold temperatures are recorded between 1733-1774AD. The EASM record by Yamada et al (2016) found that the EASM weakened between 1729-1769AD and was strengthened between 1769-1809AD. The alkenone-based temperature record from Lake Toyoni shows low temperatures between 1733 and 1774AD. However, between 1769 and 1809AD the temperature fluctuated around the average temperature, providing no evidence for a strong or weak EASM during this time period. The key difference between these records is therefore the weakening of the EASM 1700-1820AD.

The alkenone-based temperature record is also compared with EASM records outside of Japan (southwest China; Hu et al., 2008). There are three stalagmite records from south china, which all provide valuable information on the centennial-scale variability of the EASM; Hershong Cave: (Hu et al., 2008), Dongge Cave: (Dykoski et al., 2005, Wang et al., 2005) and Lianhua Cave: (Cosford et al., 2008). Cosford et al. (2008) compared these records and found that although there was a general agreement between the patterns and timings of the variability of the $\delta^{18}\text{O}$ records, there are also large differences within the region and significantly also differences between different stalagmites from the same cave. Cosford et al. (2008) suggested the reasons for the differences were due to local environmental factors at the individual sites (e.g. water residence times) and also environmental factors between different stalagmites (e.g. growth rates). We chose the $\delta^{18}\text{O}$ record by Hu et al. (2008) because they attempted to remove local environmental factors by subtracting the original Heshong stalagmite and another stalagmite from a nearby cave (Dongge cave) by Wang et al. (2005). The corrected record therefore should represent the variability of the EASM, without the influence of site-specific bias. We present the original $\Delta\delta^{18}\text{O}$ record and also the corrected $\Delta\delta^{18}\text{O}$ record in Figure 7-3. We find that overall there are strong similarities (Figure 7-3) between the two records. Similarities include strong EASM conditions between 1050 and 1300AD. In addition, the EASM also increased in both records between 1450-1600AD. Both records also show weak EASM conditions between 1300-1450AD, ~1650AD and 1900AD-present. A significant difference between the EASM reconstruction by Hu et al. (2008) and the alkenone-based temperature reconstruction from Lake

Toyoni is the strong EASM recorded at ~1750AD in the Hu et al. (2008) record. Although we find a slight increase in temperatures (Figure 7-3), we do not find evidence for a strong EASM during this time period. A suggested reason for differences between the records is that the $\delta^{18}\text{O}$ values from the Heshang stalagmite is also potentially influenced by precipitation from the Indian monsoon (Yang et al., 2014) and hence may not only record a EASM signal. However, the EASM reconstruction by Yamada et al. (2016) also shows a strong EASM during this time period. In addition, the strong similarities between the alkenone-based reconstruction and the $\delta^{18}\text{O}$ values from the Heshang stalagmite for the majority of the record provides evidence that the $\delta^{18}\text{O}$ values from the Heshang stalagmite is responding to EASM, rather than the Indian monsoon. This therefore suggests that a strong EASM occurred during this time period, however, the alkenone-based temperature reconstruction in Lake Toyoni does not record this strong EASM time period. A suggested reason for this is that another climate driver is controlling the climate in Hokkaido during this time period (e.g. NOA; further discussed in following section 7.4.1).

The alkenone-based temperature reconstruction is also compared with another record outside of Japan by Lee and Park. (2015; Figure 7-4). The EASM record by Lee and Park. (2015) shows a strong EASM during the MWP (950-1250AD), a weakening between 1250-1400AD, followed by stronger EASM intensity between 1400-1950AD, with increases in temperature in the late 1400's, ~1550AD and the early 1600's. There are notable similarities between the alkenone-based temperature record from Lake Toyoni and the EASM reconstruction by Lee and Park. (2015; Figure 7-4). This is expected as both sites are strongly influenced by the intensity of the EASM. The temperatures between 100 and 1250AD were high in both records, followed by a decrease in temperatures to lowest values between 130-140AD. Lee and Park. (2015) found that the temperatures post 1400AD increased with three notably warming periods within the LIA, including; late 1400's, ~1550AD and the early 1600's, which is consistent with the timing of the warm periods identified in the Lake Toyoni sedimentary record. Both records also show warming ~1850AD. The strong similarities between these reconstructions are attributed to the two sites being influenced by the EASM and hence there is evidence to support the hypothesis that the alkenone-based temperature record from Lake Toyoni records EASM variability. Although the

trends are similar, we find that the temperature changes at Lake Toyoni are of higher magnitude than temperature changes recorded in the Sea of Japan. Lake surface temperatures are mediated by local factors such as lake surface area and depth (Schmid et al., 2014) and ice-cover (Austin and Colman, 2007). A potential reason for alkenone-based temperatures from Lake Toyoni recording a larger variability than the alkenone-based temperatures from the Sea of Japan is that increased temperatures reduces the ice-cover on the lake and summer stratification occurs earlier than usual, resulting in surface water warming at a faster rate than air for a longer period of time (Austin and Colman, 2007).

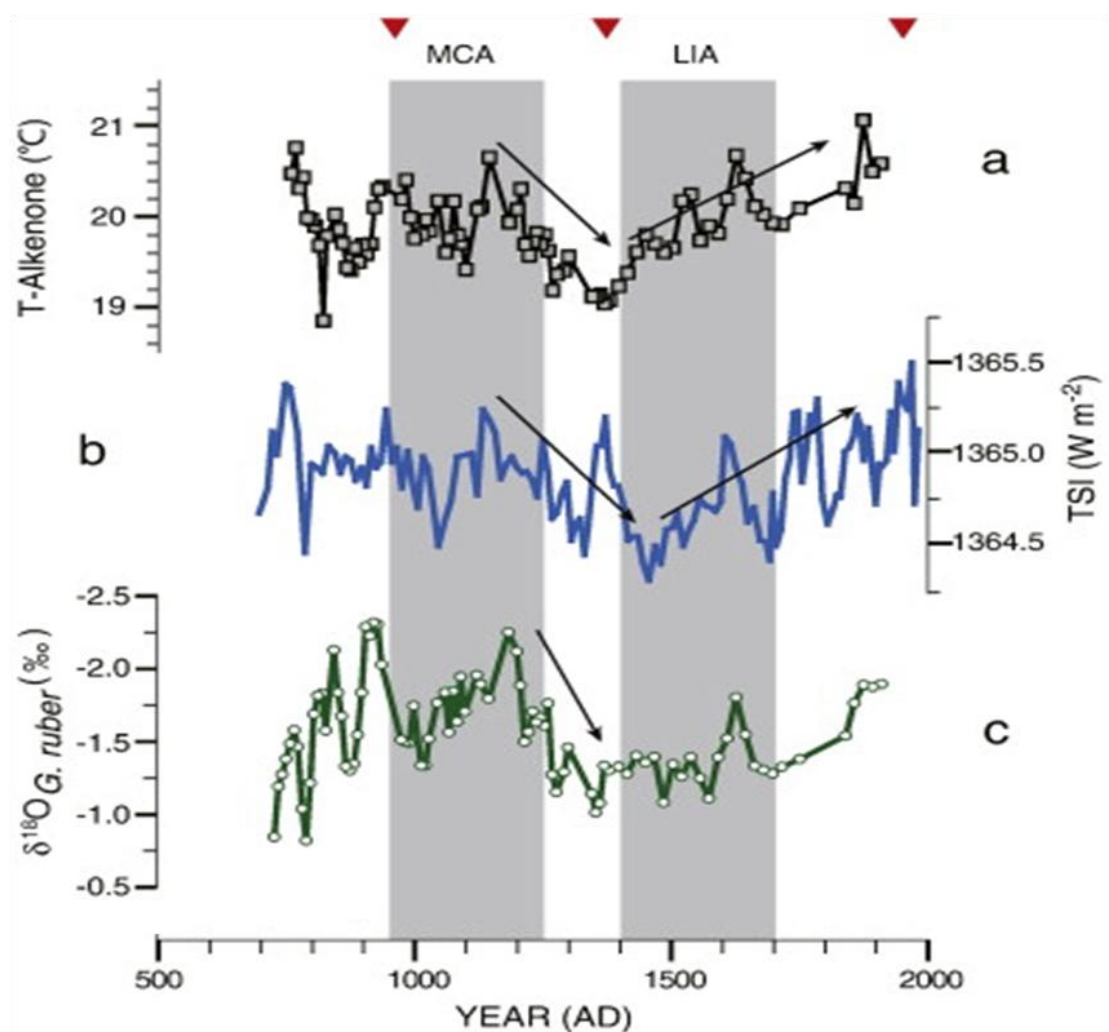


Figure 7-4: SST and salinity records from the Japan Sea compared with solar irradiance over the past 1300 years (Lee and Park., 2015). A: alkenone based SST, B: total solar irradiance (Delaygue and Bard, 2011), C: planktonic foraminiferal oxygen isotope ratio analyses (all data from Lee and Park., 2015).

7.3.2.2 Comparison with the EAWM

The alkenone-based temperature reconstruction is also compared with a winter temperature reconstruction by Aono and Kazui. (2008; Figure 7-5). The authors found that temperatures between 1200-1300AD, 1350-1500AD and 1550 and 1670AD were warm as well as significant warming over the past 200 years (Figure 7-5). They also recorded five cold periods; 1170-1210AD, 1300-1350AD, 1500-1550AD, 1670-1710AD and 1825-1830AD. We also find that both records show warming in 1200-1300AD, 1450-1500AD and 1550-1650AD and cooling in 1150-1200AD, 1300-1350AD and 1500-1550AD. This suggests that in some parts of the record, there is a strong similarity between winter temperatures (cherry blossom-inferred temperatures) and the climate in the ice-free season (April-November) (alkenone-inferred temperatures). Similarities between the winter temperature reconstruction (Aono and Kazui, 2008) and the alkenone-based temperature reconstruction (present study) suggests that the intensity of the EAWM (as inferred from cherry-blossom temperature record) has a strong influence on temperature during the ice-free season (April-November (as inferred by alkenone-based temperature reconstruction at Lake Toyoni). Using instrumental data from a nearby weather station, we also found that the intensification (weakening) of the EAWM results in cooler (warmer) summer temperatures. This suggests that a weakening (strengthening) of the EAWM results in a strengthening (weakening) of the EASM; and hence a potential inverse relationship may exist between the two sub-systems. However, there are differences between the two records, which suggest that the relationship between the EASM and the EAWM may not be as simple as an inverse relationship. Alternatively, differences in the alkenone- and cherry blossom-inferred temperature records also may be due to the 7° latitudinal difference between Hokkaido and Kyoto.

We find a key difference in the temperature records between 1350-1540AD. The Lake Toyoni record shows significant cooling whereas the March temperatures record warmer temperatures (Figure 7-5). A reason for this may be due to the southern location of the EAWM being located farther north and not influencing this site to the same degree as Lake Toyoni. In addition, March temperatures decreased between 1670-1710AD in the cherry blossom temperature reconstruction, whereas alkenone-based temperatures increased to ~14°C

(almost 2°C higher than average) during this time. The alkenone-based temperature record from Lake Toyoni also shows significant warming ~1865AD whereas the temperature reconstruction for March shows cooling during this time period. A suggested reason why the intensity of the EAWM is not influencing ice-free temperatures at Lake Toyoni during these time periods is that another dominant climate driver (e.g. PDO) has a stronger influence during these time periods. The positive phase of the PDO results in colder than average winter conditions and can also intensify the EASM (chapter 2). Significantly, the PDO was in its positive phase during these time periods (1680-1695AD and 1832-844AD) based on a PDO reconstruction by Macdonald and Case (2009), providing evidence to support this suggestion. Significantly, the cherry blossom- inferred temperature records also shows a clear warming over the past 100 years, whereas the alkenone-inferred temperature reconstruction shows cooling during this time period. This suggests that there is a weakening of both the EAWM and the EASM during this time period.

We also compared the alkenone-based temperature record with an EAWM record from northern Japan (Yamada et al., 2010). The authors' found that the EAWM was strong between 1300-1500AD, 1600-1700AD and 1720-1820AD. We find evidence for an increase in the EAWM between 1300-1500AD and between 1600-1700AD, however we find no evidence for the EAWM intensification between 1720-1820AD. Aono and Kazui. (2008) also show that the temperature during this time period was warmer rather than colder, which suggests that the EAWM was not strong during this time period.

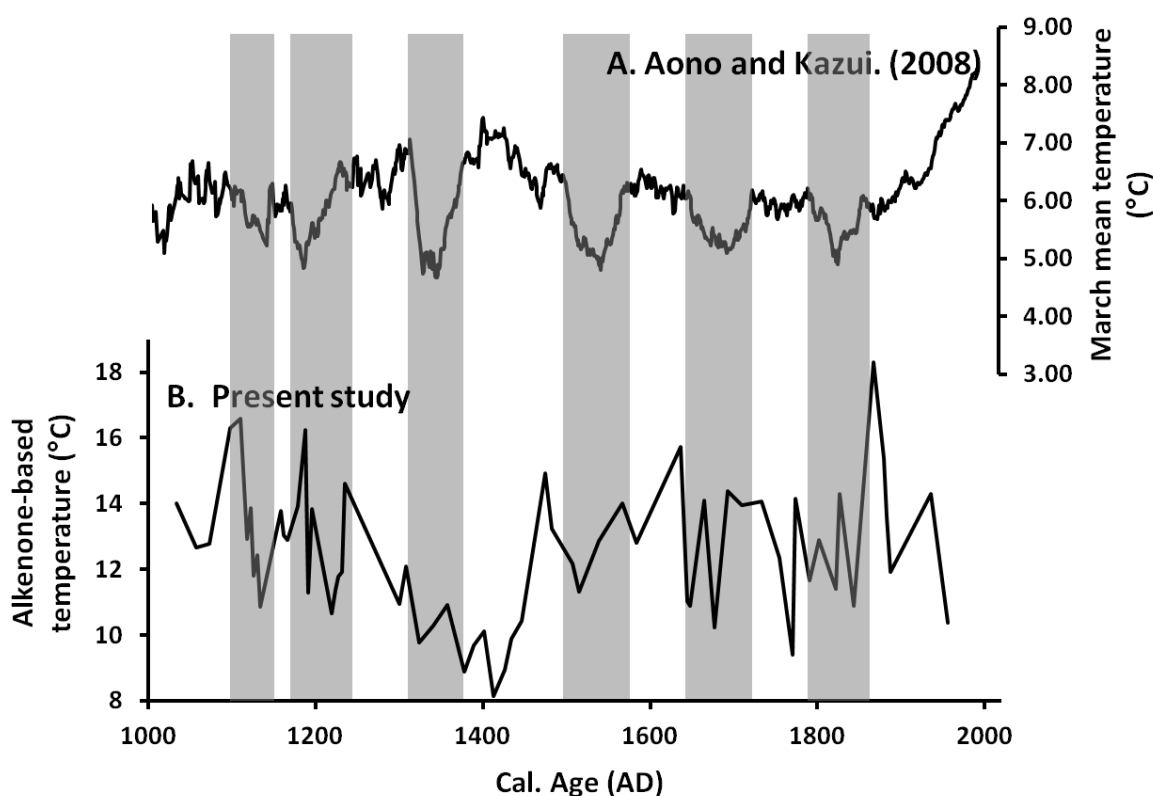


Figure 7-5: Comparison of the alkenone-based temperature records with winter temperature reconstruction from Japan. A. temperature reconstruction from the month of March in Kyoto, Japan, based on the flowering time of cherry blossoms. The bottom graph is the alkenone-based temperature reconstruction from Lake Toyoni.

7.3.2.3 Summary

To sum up, the intensity of the EAM is recorded in the instrumental data from Hiroo weather station, 25km from Lake Toyoni and therefore we hypothesised that the intensity of the EAM would also control temperature variability over the past 1000 years. We find strong similarities between EASM records from Japan and the Sea of the Japan with the alkenone-based temperature reconstruction confirming that this site records EASM variability over the past 1000 years. We also suggest a possible inverse relationship between the intensity of the EAWM on the EASM based on a comparison between a winter temperature record by Anon and Kazui. (2008) and the alkenone-based temperature record from Lake Toyoni.

However, there are some key differences between the alkenone-based temperature reconstruction and the EASM records of Hu et al. (2008) and Yamada et al. (2016). Significantly, between ~1750AD strong EASM conditions are

recorded in both EASM records (Figure 7-3). However, the alkenone-based temperature reconstruction only records a slight warming during this time period. This suggests that another climate driver is controlling the climate in Hokkaido during this time period.

7.3.3 Alkenone-based temperature reconstructions: comparison with NAO/AO reconstruction

Although air temperature in Hokkaido is mainly controlled by the EAM, the NAO/AO also has a strong influence on air temperature based on instrumental data between 1958 and 2014 (Chapter 2). When the NAO is in its positive (negative) phase, temperatures are higher (lower) in Hokkaido (Chapter 2). In addition, there is also a connection between the EAM and the NAO/AO. The positive phase of the NAO/AO results in a strong EASM and the negative phase of the NAO/AO results in a strong EAWM (e.g. Gong and Ho, 2003, Gong et al., 2001). In order to determine if the NAO/AO is controlling air temperature over the past 1000 years in Hokkaido, we compare the alkenone-based temperature record with a NAO reconstruction by Trouet et al. (2009; Figure 7-6). As previously discussed in Chapter 5, the NAO index was developed using a combination of high-resolution proxy records and model simulations. It was found that overall the positive (negative) phase of the NAO coincided with warmer (colder) temperatures. Negative NAO periods occurred between ~1450AD, 1550-1600, 1750-1800AD, ~1850AD and 1920-1960AD. All of these negative NAO time periods were associated with cooling except 1850AD. Therefore a suggested reason for the alkenone-based temperature reconstructed only showing slightly warmer temperatures during this time period is due to the influence of the negative NAO. Positive NAO periods occurred between 1050-1400AD, 1450-1550AD and 1850-1950AD. Overall these periods were also associated with warming except between 1300-1400AD, which shows cooling. The cooling between 1300-1400AD is consistent with EASM records, which show a decrease in the intensity of the EASM. This time period is therefore being strongly influenced by the intensity of EASM, rather than the phase of the NAO. Overall the results suggest that alkenone-based temperature reconstructions from Lake Toyoni are recording a strong EAM signal, however, this is further modulated by the phase of the NAO. When the NAO is in a strong negative phase, air temperatures in Hokkaido are lower.

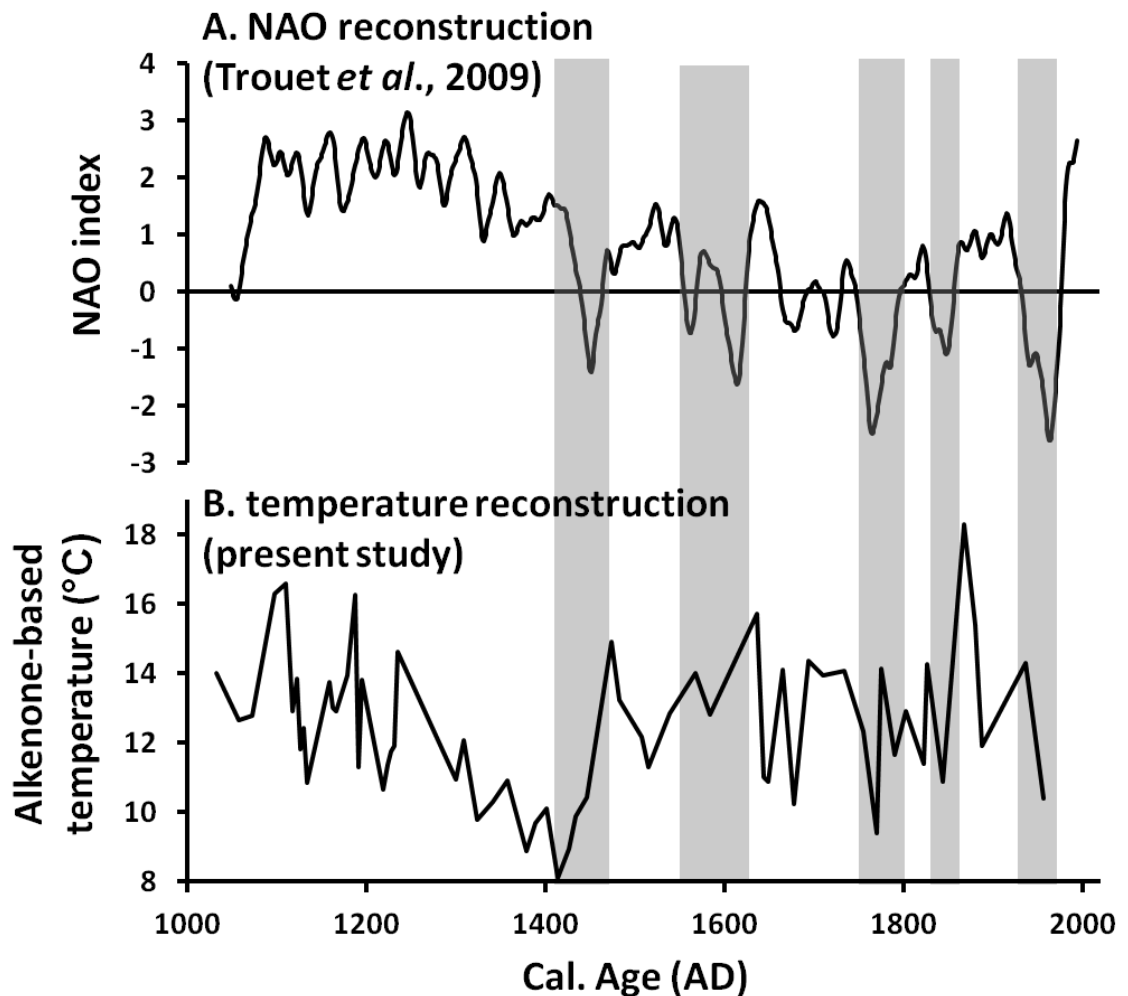


Figure 7-6: Alkenone-based temperature record compared to the NAO Index (Trouet *et al.*, 2009). Grey shading indicates negative NAO time periods.

Alkenone-based temperature reconstructions: comparison with Asian temperature records

Question 2: *Does the alkenone-based temperature record provide evidence for globally recognised events (e.g. the MWP, LIA and the CWP) and if so, are the timings of these events synchronous with records within Asia?*

In order to address question 2, the alkenone-based temperature record from Lake Toyoni is compared with records from Asia. A description of the chosen records and how the proxy provides information on temperature are as follows:

1. A regional temperature series by Shi *et al.* (2015), which provides a record of Asian (eastern and south central) temperature variability during

summer (June-July-August) to compare with the alkenone-based temperature reconstruction (Figure 7-7). The temperature series is based on 418 temperature proxy records and modelling from across Asia.

2. A regional decadal-resolved temperature series from China by Ge et al. (2013), which provides a record of East Asia temperature variability to compare with the alkenone-based temperature record from Lake Toyoni. The temperature reconstruction was developed over the past 2000 years in China using statistical software (specifically principal component regression and partial least squares regression) using 28 records from the whole country and a range of climate proxies (Figure 7-7) This record is an example of an East Asian temperature record which responds to northern hemisphere climate variability (Ge et al., 2013), which is mainly driven by changes in solar activity and volcanic forcing (Crowley, 2000).
3. A local temperature reconstruction based on pollen assemblages (Sakaguchi, 1983) from Japan. Sakaguchi. (1983) investigated percentage of *Pinus* in a peat record spanning the past 8000 years from Oxheghara moor, 150km north of Tokyo (Figure 7-8). *Pinus* pollen increases when conditions are colder therefore higher *Pinus* pollen suggest cooler conditions (Figure 7-8).
4. A temperature record based on total organic carbon (TOC) and total organic nitrogen (TON) over the past 1300 years from Lake Nakatsuna, central Japan by Adikari and Kumon. (2001). TOC and TON are related to summer temperature in Lake Nakatsuna because these parameters increases (decreases) when productivity increases (decreases) under a warm (cold) climate (Figure 7-8).
5. A local temperature reconstruction using the stable carbon isotope ratio ($\delta^{13}\text{C}$) tree-rings of Japanese cedars from Yakushima Island, southern Japan, over the past 2000 years by Kitagawa and Matsumoto. (1995). The $\delta^{13}\text{C}$ tree-rings of Japanese cedars is controlled by the difference between the intercellular $\delta^{13}\text{C}$ and the $\delta^{13}\text{C}$ of the air which is affected by the concentration of atmospheric CO_2 , and hence temperature. This record is a key record to compare with the alkenone-based temperature record

from Lake Toyoni as it a record which is strongly influenced by global climate drivers (e.g. solar variations) rather than local factors (e.g. the EAM).

The records chosen therefore represent Asia (Shi et al., 2015), East Asia (Ge et al., 2013), central Japan (Sakaguchi, 1983, Adhikari and Kumon, 2001) and southern Japan (Kitagawa and Matsumoto, 1995), which provides a good spatial representation to compare with the alkenone-based temperature record from Lake Toyoni. Given the large latitudinal range, the local climate in Japan varies from temperate in the north and tropical in the south. As a result, we might expect that palaeo-climate records from different regions in Japan over a given time period would show clear differences, reflecting local-scale differences. On the other hand, the climate of Japan is ultimately controlled by the EAM, therefore similarities in the records would show a strong regional climate signal (e.g. the EAM).

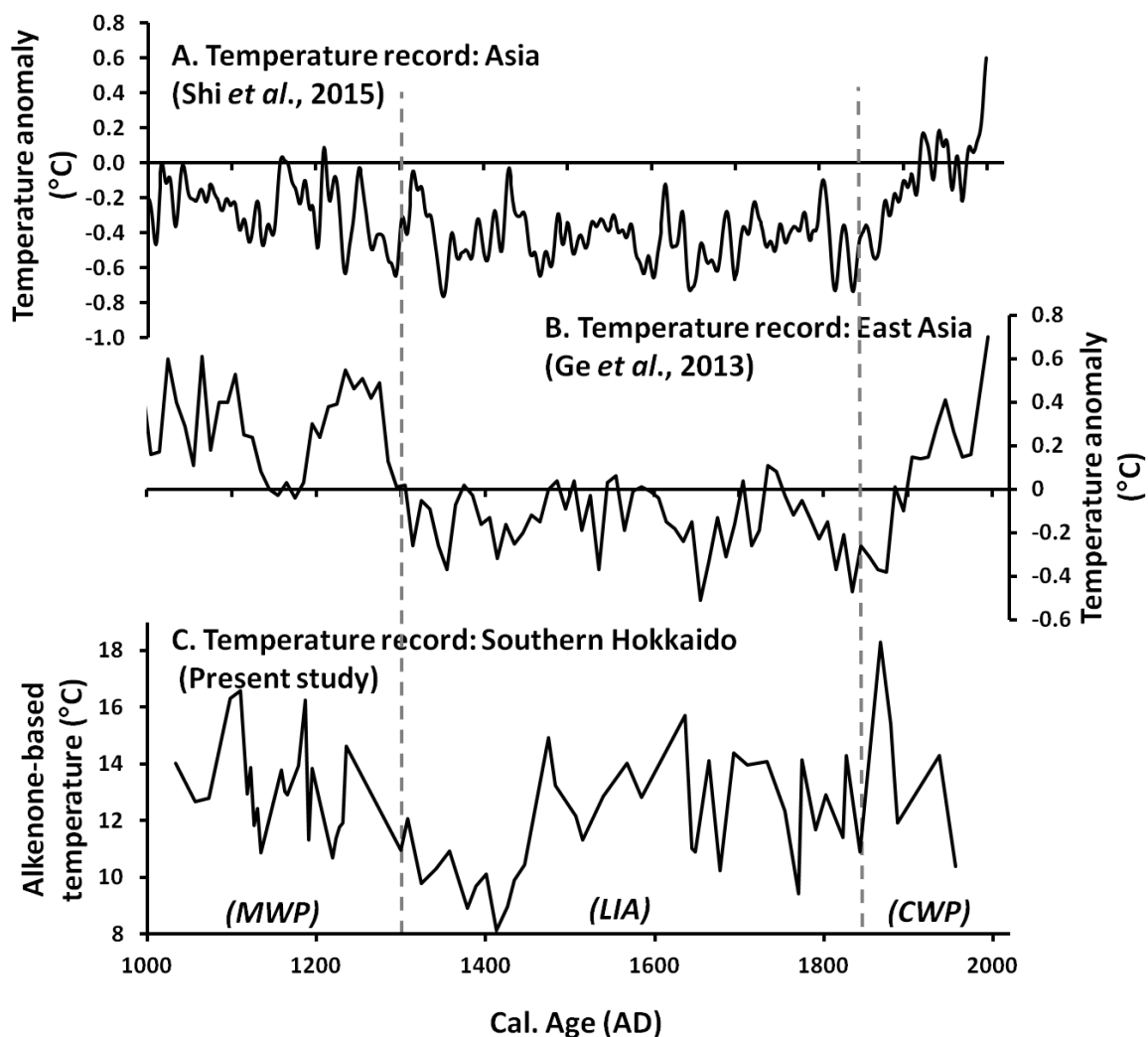


Figure 7-7: Comparison of the alkenone-based temperature variations over the past 1000 years with Asian temperature records. A: a combination of temperature reconstructions in Asia by Shi *et al.* (2015). B: a combination of temperature reconstructions in China using statistical software by Ge *et al.* (2013). C: the alkenone-based temperature variations over the past 1000 years (present study).

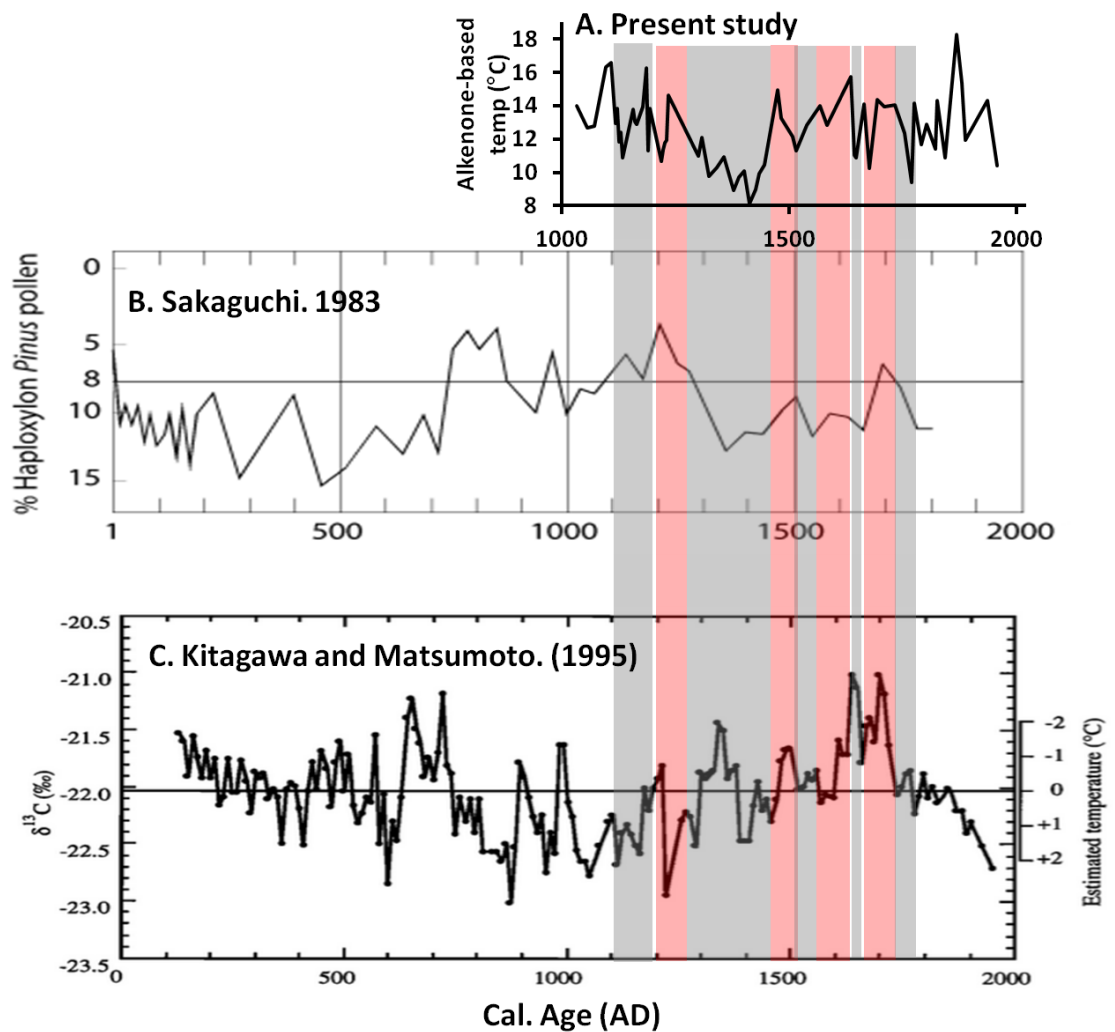


Figure 7-8: Comparison of the alkenone-based temperature record with palaeo-climate records from Japan: A. Alkenone-based temperature record from Lake Toyoni (Present study). B. Pollen record Sakaguchi. (1983). The percentage (%) of *Pinus* in a peat record spanning the past 2000 years from Oxheghara moor, 150km north of Tokyo. Higher *Pinus* pollen (%) is interpreted as lower temperatures and vice versa. C. $\delta^{13}\text{C}$ record of a Japanese cedar tree from Yakushima Island, southern Japan, over the past 2000 years (Kitagawa and Matsumoto, 1995). The average value of pre-1850 year (-22.05 ‰) is indicated by horizontal line. The temperature in the right scale is estimated using the relationship between $\delta^{13}\text{C}$ and temperature (please note the axis is reversed; temperature decrease going up and temperature increase going down).

The alkenone-based temperature reconstruction is compared with temperature records from Asia (Shi et al., 2015) and more specifically from East Asia (Ge et al., 2013). The temperature record from Asia takes into account records from eastern Asia as well as central and southern China. The record shows that during the past millennium, there were three warm periods; the 11th, 12th, and 20th centuries. The late 20th century was the warmest period. Following the warm conditions in the 11th and 12th centuries, temperatures in Asia decreased between 1300-1400AD, and low temperatures were recorded during the 17th century (Figure 7-7). Similar to the Asian temperature reconstruction, we find

warm temperatures between 1000-1200AD, however, there are also strong differences. For example, the Asian temperature reconstruction shows cold temperatures between 1800-1900AD whereas the alkenone-based temperature reconstruction shows significant warming during this time period (Figure 7-7). Moreover, the Asian temperature record shows that the warmest temperatures are between 1900-200AD, however, the warmest temperatures in the alkenone-based temperature record ~1867AD. Suggested reasons for the differences in these records are (1) the temperature at Lake Toyoni is recording an EAM signal whereas the climate within Asia is also influenced by other factors such as the South East Asian Monsoon (2) the temperature reconstruction of Shi et al. (2015) is based on summer (June-July-August) temperatures whereas Lake Toyoni is recording the entire ice-free season which takes into account temperatures from March-November.

The alkenone-based temperature record is also compared to a temperature record from East Asia (Ge et al., 2013). Individual climatic regions of China are driven by different factors, for example, the Northeast is driven by the westerlies, the Northeast, Central East and Southeast are influenced by the Asian monsoon and the Tibetan Plateau is driven by a mixture of the Westerlies and the Asian Monsoon. Therefore, there are local differences in all the records used in this study. However, the reconstruction by Ge et al. (2013) shows that the temperature variations in China are overall in phase with northern hemisphere climate variability. Two key warm periods were identified; 951-1320AD and >1921AD. Within the warming between 951-1320AD, there was two particularly warm events; 981-1100AD and 1201-1270AD. Between 1100-1200AD there was cooling in East Asia. However, Ge et al. (2013) found large inconsistencies between temperature records during the warm periods recorded between 981-1100AD and 1201-1270AD. The authors' suggested more reconstructions from this time period were required from East Asia to determine if the warming during these time periods is comparable to the temperatures of the 20th century. We find evidence for a cold period between 1110-1180AD and warming between 1200-1266AD, with a brief cold period in 1251AD. Based on the alkenone-based temperature reconstruction from Lake Toyoni, we find that the temperatures between 1200-1266AD were 0.4° warmer than average temperatures. Although the Lake Toyoni records a warm period between 1050

and 1300AD, the warming between 1900-2000AD is not recorded in the alkenone-based temperature record from Lake Toyoni. The temperatures between 1900-2000AD were actually lower than average rather than higher than average. The temperature record by Ge et al. (2013) shows that temperatures between 1321-1920AD were lower than average, with three particular cold periods. These cold time periods identified in the Ge et al. (2013) temperature record by Hao et al. (2016) were 1390-1460, 1600-1700 and 1800-1900AD, with the coldest periods being between 1631 and 1690AD and 1811 and 1870AD (Ge et al., 2013). The alkenone-based temperature record also records a cold time period between 1390-1460 and cooling between 1600-1700AD, however the length of the cold period is shorter in the Lake Toyoni record (1635-1690AD) and is not as pronounced as the temperature reconstruction by Ge et al. (2013). The final cold period between 1800-1900AD shows strong differences between the two records. This time period is associated with the warmest temperatures in the Lake Toyoni record, whereas this time period is associated with cooling in China. The cold period between 1635 and 1690AD is characteristic of northern hemisphere cooling events because this time period is the timing of the coldest time periods recorded in the northern hemisphere. As a result, we find that although there are some similarities between the alkenone based temperature record from Lake Toyoni and the regional temperature record from China (Ge et al., 2013) suggesting a northern hemisphere control on the temperature record, our site is more controlled by the strengthening and weakening of the EASM.

In addition to temperature records from Asia (Shi et al., 2015, Ge et al., 2013), we also compare the alkenone-based temperature reconstruction to climate records from Japan. Due to its wide latitudinal range, the local climate in Japan varies from temperate in the north and tropical in the south. As a result, we might expect that palaeo-climate records from different regions in Japan over a given time period would show clear differences, reflecting local-scale differences. On the other hand, the climate of Japan is ultimately controlled by the EAM, therefore similarities in the records would show a strong regional climate signal (e.g. the EAM).

A number of climate records exist from Japan over the Late Holocene to compare with the alkenone-based temperature reconstruction record from Lake Toyoni. A key climate reconstruction to compare our record to is based on

pollen assemblages (e.g. Sakaguchi, 1993). Strong similarities between the alkenone-based temperature reconstruction and the *Pinus* pollen reconstruction occur with a brief cold event between 1100-1200AD and the warm conditions ~1200AD within the MWP. Both records also show significant cooling between 1300-1400AD. During the LIA, both records show warming to 1500AD, followed by cooling ~1550 and warming again to 1600AD. Warming was also found in both records around 1700's. In the *Pinus* pollen reconstruction, the warming in the 1700's was the most pronounced within the LIA whereas in the alkenone record from Lake Toyoni, the most pronounced warming occurred in the early 1600's.

Another temperature record from central Japan is compared with the alkenone-based temperature record. The record is based on TOC and TON content of a lake sediment core, which provides information on past productivity, and hence temperature, over the past 1300 years (Adhikari and Kumon, 2001). Adhikari and Kumon (2001) found three noticeable cold events between 1300 and 1950AD; including 1300-1470AD, 1700-1760AD and 1850-1950AD. These cold events are similar to the timings of the cold events recorded at Lake Toyoni (e.g. 1300-1450AD, 1717-1754 and 1850-1900AD). The time periods of these cooling events are also similar to the time periods of EASM weakening recorded by Yamada et al. (2010) and Yamada et al. (2016) (Figure 7-3). This suggested that this site is recording an EASM signal, similarly to Lake Toyoni, and hence a reason for the strong similarities between the two records.

The alkenone-based temperature record is also compared with a temperature record from Southern Japan based on the $\delta^{13}\text{C}$ tree-ring records (Kitagawa and Matsumoto, 1995), which varies with atmospheric CO_2 and hence temperature. Spectral analysis of the $\delta^{13}\text{C}$ time series provided information on the periodicities present in the record. The significant temperature periodicities were 187, 89, 70, 55 and 44 years. The 187-year cycle closely corresponds to the well-known Suess cycle of solar activity, and that the 89-year cycle compares well with the Gleissberg solar cycle, therefore they concluded that their findings support for a sun-climate relationship. The $\delta^{13}\text{C}$ tree-ring record and the alkenone-based temperature reconstruction both show a general warm MWP, with a cooling event ~1150-1200AD. This cooling event is slightly earlier in the Lake Toyoni record. Both records also show cooling at the start of the LIA ~1300AD. Although this cooling event lasts longer in the Lake Toyoni in northern

Japan record compared to the $\delta^{13}\text{C}$ record from southern Japan. For example ~1400AD shows warming in the $\delta^{13}\text{C}$ record whereas the Lake Toyoni record is still cool during this time period. Between 1450 and 1500AD, the Lake Toyoni record shows warming whereas the $\delta^{13}\text{C}$ of Japanese cedars records cooling during this time period. Significantly, a large cooling event is recorded between 1600-1750AD in the $\delta^{13}\text{C}$ record, with a brief warm event in the middle. Although the alkenone-based temperature reconstruction also shows cooling at the start of the 1600's and the middle 1700's and warming in the middle, the cooling in the Lake Toyoni record is not on the same magnitude as the $\delta^{13}\text{C}$ record. Between 1750AD and present, the $\delta^{13}\text{C}$ record shows distinct warming. The alkenone-based temperature reconstruction shows warming between 1750 and 1850AD, which is then following by cooling. A suggested reason for the key differences between the alkenone-based temperature record from Lake Toyoni and the temperature record by Kitagawa and Matsumoto. (1995) is that the $\delta^{13}\text{C}$ tree-rings of Japanese cedars from Yakushima Island, southern Japan are recording a strong northern hemisphere temperature signal which is strongly influenced by solar activity and volcanic activity (Crowley, 2000). Whereas the Lake Toyoni temperature record is mainly being driven by changes in the EAM system, which is driven by changes in land-sea thermal contrast and the intensity of the SibH (EAWM intensity) and the NWPH (EASM intensity).

7.3.3.1 Medieval warm period 1050-1300AD

The alkenone-based temperature reconstruction shows that the MWP was generally a warm time period in Lake Toyoni, however, there is substantial variability in lake temperatures during this time period.

7.3.3.1.1 Timing of the MWP in Hokkaido, Japan

The MWP has not been fully captured in our record because it should go back to ~900AD, therefore we can determine the timing of the end of the MWP however not the start of it. The end dates of the MWP are highly variable depending upon the geographic region. As a global estimate, the timing of the end of the MWP is ~1250AD (e.g. Mann et al., 2009). Based on the temperature records from Lake Toyoni, we suggest that locally the end of the MWP was ~1300AD, because post 1300AD temperatures are generally lower than average (highlighted in grey; Figure 7-8). This finding is similar to tree-ring records in southern Japan over the

past 2000 years (Kitagawa and Matsumoto., 1995), which also found that the MWP occurred between 750-1300AD and also to pollen record of Sakaguchi. (1984), which also found the end of the MWP was at 1300AD. However, Adhikari and Kumon. (2001) used sedimentary characteristics in Lake Nakatsuna, Japan to reconstruct climate variability over the past 1300 years and identified the timing of the end of the MWP to be 100 years shorter (1200AD). Yamada et al. (2010) also identified the end of the MWP to be 1200AD based on EAM record from Lakes Ni-no-Megata (39° 57'N, 139° 43'E) and San-no-Megata (39° 56'N, 139° 42'E) on the Oga Peninsula of northeastern Japan. In a more regional context, several studies have suggested that the MWP ended ~1250AD based on a EAM record from the Sea of Japan (Lee and Park, 2015) (Figure 7-4), whereas a statistical study taking into account several palaeo-climate reconstructions from China found that the MWP ended ~1320AD (Ge et al., 2013) (Figure 7-7). The timing of the end of the MWP (1300AD) in the Lake Toyoni alkenone-based temperature record therefore falls within the time periods suggested by other studies in Japan and East Asia.

7.3.3.1.2 Magnitude of warming

Despite the cool events within the MWP, the alkenone-based temperature reconstructions from Lake Toyoni suggest that overall the MWP was 0.7°C warmer than the average temperature, although in extreme time periods (e.g. 1098-1110, 1158-1195 and ~1235AD) temperatures reached ~4°C warmer than average. The average temperature rise during the MWP is slightly lower than other studies in Japan. For example, Kitagawa and Matsumoto (1995) investigated the $\delta^{13}\text{C}$ of Japanese cedars from Yakushima Island, southern Japan and found that the MWP was on average 1°C warmer than average. Differences between the magnitude in temperature difference in the MWP between the Lake Toyoni record in northern Japan and the $\delta^{13}\text{C}$ tree-ring record in southern Japan may be due to (1) the difference in geography between the two records and/or (2) the alkenone-based temperatures are averages of several years whereas the tree-ring record is annually resolved.

Within the MWP, there is generally a 100-year warm event, which is referred to as the MWP optimum. Previous studies have suggested that the MWP optimum occurred between 1000-1100AD for Lake Sugan and 1100-1200AD for Lake Gahai and alkenone-based temperatures were higher by ~4.0°C and ~1.9°C (He et al.,

2013). The difference in the magnitude of temperature change between Lake Sugan and Lake Gahai is suggested to be a result of water volume changes in small lakes (as a result of hydrological variability) potentially affecting lake water temperatures. Our alkenone-based temperature record does not record a 100-year warm event during the MWP.

7.3.3.1.3 EAM variability during the MWP

The alkenone-based temperature record shows that temperature was increased during the time between 100-1300AD (the MWP), with the highest temperatures occurring between 1098 and 1110AD. This suggests that the EASM intensified during this time period. When the EASM is strong, the NPSH is located further north and warm and wet conditions occur in summer in Hokkaido. Previous studies have also found that the MWP was characterised by a strong EASM. For example, Hu et al. (2008) also found that the EASM was strong between 1000-1300AD. Lee and Park. (2015) found that the EASM was strong until 1250AD, with the strongest EASM occurring between 1100 and 1200AD in both records. Within this warm period, there are also several cooling events, suggesting that the EASM weakened and/or the EAWM strengthened during the MWP. Other records in Japan have identified cooling within the MWP (Yamada et al., 2010, Zhang et al., 2008, Liu et al., 2011). Therefore although the MWP is characterised by an overall strengthening of the EASM, there is variability during this time period.

7.3.3.2 Little Ice Age 1300-1850AD

The alkenone-based temperature reconstruction shows that the LIA was generally a cooler time period in Lake Toyoni, however, there is substantial variability in lake temperatures during this time period rather than a long period of sustained cold conditions.

7.3.3.2.1 Timing of the LIA in Hokkaido, Japan

The LIA is globally recognised between 1400-1700AD (Mann et al., 2009). The alkenone-based temperature record from Lake Toyoni suggests the LIA occurred between 1300 and 1805AD because 1300AD is the time period of significantly reduced temperatures and 1850AD is the time period when the temperatures significantly increased (Figure 7-1). In Japan, Sakaguchi. (1983) suggested the onset of the LIA was 100 earlier than the global average (1300AD). Since the

publication of the pollen record from Sakaguchi. (1983), other authors' have also provided evidence for the onset of the LIA to occur before the global average of ~1400AD. For example, Adhikari and Kumon. (2001) suggested that although the onset of the Little Ice Age in central Japan (36°N) was 1200AD, the first major cooling event occurred between 1300-1470AD. The authors found that within the LIA (defined in their study as 1200-1950AD), there were three major cold phases which broke up the LIA event; 1300-1470AD, 1700-1760AD and 1850-1950AD. Also within central Japan, a study by Yamada et al. (2010) suggested that the start of the LIA occurred between 1200-present. However, other studies have found that the LIA occurred later than the global average. For example, Kitagawa and Matsumoto. (1995) suggested the LIA occurred between 1580 and 1700AD in southern Japan (30°N).

Within the regional records of East Asia, the timing of the LIA is variable (Figure 7-7). For example Ge et al. (2013) suggested that the LIA occurred between 1321-1920AD, based on a variety of proxy records from China (Figure 7-7). Most recently, Lee and Park. (2015) suggest that the LIA was shorter and occurred between 1400-1700AD. They also found a cooling event between 1250-1400AD, however they did not interpret this as the onset of the LIA (Lee and Park. 2015). Although we find evidence for cooling at 1230AD in our alkenone-based temperature record, we suggest that the onset of the LIA occurs at 1300AD; when there is a substantial and extended time period of cooling.

7.3.3.2.2 Magnitude of cooling

Within the LIA (1300-1850AD), there is considerable variability including warming of up to 3.2°C warmer than average (Figure 7-1). Despite these warm events within the LIA, the alkenone-based temperature reconstructions from Lake Toyoni suggest that overall the LIA (1300-1820AD) was 0.6°C cooler than the average temperature of the past 1000 years, although in extreme cool time periods (e.g. ~1400AD) temperatures reached ~8°C (4°C lower than the average). Previous studies have suggested that the annual air temperature during the LIA in Japan was 2°C cooler than average (Kitagawa and Matsumoto, 1995).

The cold period between 1300-1450AD has been noted in palaeo-archives in Japan (Adhikari and Kumon, 2001, Aono and Kazui, 2008) and also East Asia (Ge et al., 2013), although the exact time period of cooling is variable in all records. For example, Aono and Kazui (2008) suggested that this was a short period of cooling (1330-1350AD) based on the flowering times of cherry blossoms in Kyoto, Japan. On the other hand, Adhikari and Kumon (2001) suggested that the cooling associated with this time period lasted between 1300 and 1470AD, which is very similar to the cooling in the Lake Toyoni record. This reduction in temperature at the onset of the LIA (~1300AD) occurred fairly rapidly. The average water temperature during the MWP was 13.1 °C and the water temperatures dropped to ~8.1 °C by 1427AD, the rate of change equates to ~0.3 °C per year. This rate of cooling is rapid for the relatively short time scale (~160 years).

7.3.3.2.3 EAM variability during the LIA

The onset of the LIA is characterised by the lowest temperatures (1300-1450AD) based on alkenone-based reconstruction from Lake Toyoni. Hu et al. (2008) found that the EASM was weakened till ~1550AD, whereas Lee and Park. (2015) found that the weakest time period of the EASM over the past 1000 years was 50 years earlier; between 1250-1400AD. Although we find evidence for cooling starting at 1250AD, temperatures were not below average (over the past 1000 years) until 1300AD (Figure 7-1). While we do not find that the start and end times of the weak EASM event exactly match up in all records, we do find consistency between the cooling in all records ~1300-1400AD, providing evidence that the alkenone-based temperature record from Lake Toyoni records a weakened EASM during this time period.

A potential reason for the large cooling event at the onset of the LIA may be attributed to monsoon failure during this time period. Lee and Park. (2015) have previously suggested that this time period was the coldest time period over the past 1000 years from an alkenone record in the Japan Sea. The authors' suggested that the reason for the low temperatures during this time was a result of monsoon failure. Their record also shows higher salinity during this time period based on the $\delta^{18}\text{O}$ of planktonic foraminifera. The conditions during the monsoon failure were cold and dry in this region (Lee and Park, 2015). Hu et al. (2008) also found that the EASM was the weakest (lowest $\delta^{18}\text{O}$ values) over the

past 1000 years during this time period (~1450AD) (Figure 7-3). Hokkaido is located on the northern boundary of the EASM resulting in this location being very sensitive to changes in the EASM. This time period is where we the most substantial cold period in the record, providing further evidence for EASM failure in Hokkaido during this time period.

The remainder of the LIA (1470-1850AD) is generally characterised by warmer temperatures with notable increases between 1450-1470AD and 1580-1640AD and cold temperatures were recorded between 1500-1600AD. The time period between 1680-1820AD is slightly warmer than average, however there is considerable variability within this time period. The EASM records from Lee and Park. (2015) and Hu et al., (2008) are significantly different between in this section of the record. For example, Lee and Park. (2015) show that temperatures are steadily increasing between 1470-1800AD. The alkenone-based temperature record from the Sea of Japan also shows notable increases in temperature, and hence strengthening of the EASM, ~1500AD and ~1600AD which is similar timings to the increase in temperature based on alkenone reconstructions from Lake Toyoni (Figure 7-4). Whereas Hu et al., (2008) finds that the EASM is weak between 1470 and 1700AD and strong between 1700-1800AD (Figure 7-3). The differences between the EASM reconstructions during this time period demonstrates the need to further clarify the EASM variability in this region over the late Holocene. Adhikari and Kumon, (2001) also found considerable temperature variability with a notably cold period between 1700-1760AD and slightly warmer periods <1700AD and >1760AD. Out with Japan, Lee and Park. (2015) found three warm events within the LIA late 1400's, ~1550AD and the ~1600's, consistent with the timing of the warm periods identified in the Lake Toyoni sedimentary record.

There are also differences in the magnitude of the cool events within the LIA. For example, the Lake Toyoni record shows that the coldest event was ~1400AD and the cold conditions associated with the late LIA were not as cold as the onset of the LIA. Sakaguchi. (1983) also found the most pronounced cooling of the LIA occurred at the onset ~1400AD. However, this is the opposite in the temperature record by Kitagawa and Matsumoto (1995), which shows a smaller cold event at the onset of the LIA compared to a much larger cooling event in the within the LIA (e.g. ~ 1600AD; Figure 7-8). Outside Japan, Ge et al. (2013)

found that the coolest period of the LIA is ~1650AD (Figure 7-7). The reason for this is that the Kitagawa and Matsumoto. (1995) and the Ge et al. (2013) are responding to northern hemisphere climate drivers (solar and volcanic activity) whereas the alkenone-based temperature reconstruction from Lake Toyoni and the Sakaguchi. (1983) record is responding to variability of the EAM.

7.3.3.3 >1850AD

The past ~200 years has been characterised by warming in Asian records (Figure 7-7). However, we find that there was warming in the 1800's to a maximum of 18.3°C between 1850-1880AD. The warm temperatures ~1860AD is shown in the temperature record from the EASM records of Hu et al. (2008; Figure 7-3) and Lee and Park. (2015; Figure 7-4), however, the warm event is not recorded in regional records from Asia (Shi et al., 2016) or China (Ge et al., 2013; Figure 7-7), which instead show cooling during this time period. Significantly, the presence of this warm period in EASM records and not in regional records from Asia and East Asia provides further evidence that the alkenone-based temperature record at Lake Toyoni is recording EASM variability.

Following this warm period, the alkenone-based temperature reconstruction shows cooling in the early 1900's in the Lake Toyoni alkenone record (Figure 7-1), and hence a weakening in the EASM or a strengthening of the EAWM. The cold temperatures associated with this time period are the opposite of the regional records from Asia in Figure 7-7, which all show warming during this time period; consistent with global temperature increase. A suggested reason why the alkenone-based temperature record does not show warming in this time period is due to a weakened EASM and/or strengthened EAWM over the past 100 years. A weakened EASM over the past ~100 years has been documented in other records from EASM records by Hu et al. (2008) and Yamada et al. (2016) (Figure 7-3). Other studies have suggested that over the past period ~50 years the EASM has weakened (Xu et al., 2006, Ding et al., 2008, Hu et al., 2008, Zhu et al., 2012). The alkenone-based temperature record from Lake Toyoni suggests that the EASM weakened before ~50 years ago and instead has been weakened over the past 1000 years.

7.3.4 Famines in Japan over the past 1000 years

Question 3: Is there a relationship between temperature and famine frequency in Japan?

Detailed records of famine frequencies in Japan exist (Figure 7-9), which allow us to test the link between temperature and famine frequency. We compare our alkenone-based temperature reconstruction with a famine reconstruction since the 1300's (Saito, 2010; Figure 7-9). The famine record is based on a famine point system, for example, 1 point was assigned to a famine which occurred regionally across 5 or more provinces and half a point (0.5) was assigned to famine which occurred in one region. The results show a clear relationship between temperature and famine frequency (Figure 7-9), with a decrease in temperature resulting in an increase in famine frequency. The famine frequency increased from 10 famine points in 1300AD to 15 famine points in 1400AD (Figure 7-9). The corresponding temperature change was from 10.9°C to 9.4°C. The famine frequency decreased to 11.5 famine points in 1450AD and the temperatures increased to 12.9°C. The famine frequency increase to 17 famine points in 1500-1550AD and the average temperature during this time decreased to 12.1°C (Figure 7-9). Between 1550-1600AD, the famine points decreased to 7, corresponding to an increase in temperature to 13.4°C. Famine points increased slightly to 7.5 between 1600-1650AD corresponding to a decrease in temperature to 12.5°C (Figure 7-9). Famine points decreases slightly between 1650-1700AD and the average temperature during this time period increases to 13.3°C (Figure 7-9). Another decrease in famine points to 3 occurred between 1700-1750AD corresponded with a slight temperature rise. Between 1750-1800AD, famine frequency increased to 7.5 and temperatures decreased to 11.9°C (Figure 7-9). Between 1800-1850, famine frequency decreased to 5 and temperatures increased to 14.3°C (Figure 7-9). Between 1850-1900AD, famine frequency was 0.5 and temperatures remained high at 13.6°C (Figure 7-9).

The alkenone-based temperature reconstruction shows a reduction in temperatures at the start of the 1400's and also between 1500-1550AD. This is consistent with an increase in famine points (Figure 7-9). This suggests a link between cold temperatures and the occurrence of famines in Japan. The

temperature in summer is particularly important for the rice crop, which is the staple diet of Japanese people, because rice requires warm and wet conditions in late summer for a successful yield. The strong relationship between famine frequency and alkenone-based temperatures provides further evidence that alkenones are recording summer temperature in Lake Toyoni.

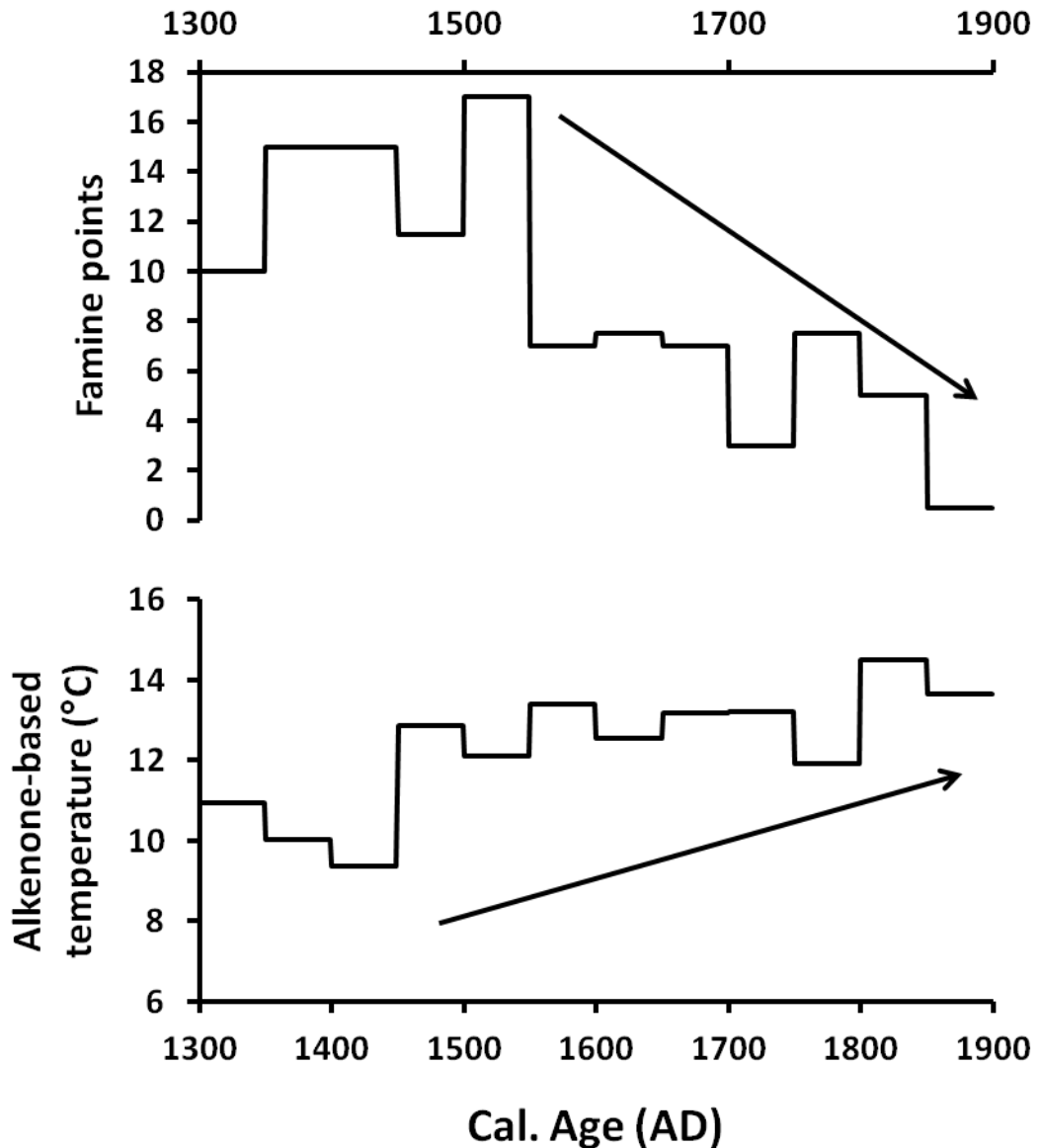


Figure 7-9: Relationship between temperature and famine points in Japan. The top graph is the famine point plot from Saito (2010) per half century. The bottom graph is the average alkenone-based temperature per half century.

7.4 Conclusions

This study contributes to a better understanding of temperature variability in Northern Japan over the past 1000 years. LST was reconstructed using alkenones preserved in the sediments of Lake Toyoni, which corresponds to air temperatures at this site. Air temperature in Hokkaido is currently controlled by the variability EAM therefore alkenone-based temperature reconstructions from Lake Toyoni provide valuable EAM reconstructions in this region. Air temperature in Hokkaido is also related to the phase of the NAO/AO. Therefore, in addition to recording the variability of the EAM, the alkenone-based temperature record from Lake Toyoni is also influenced by the phase of the NAO/AO.

The temperature in Japan shows a large variability over the past 1000 years, such as the Medieval Warm Period (1000-1300AD) and the Little Ice Age (1300-1850AD). We found that the MWP was generally warm and the EASM was intense during this time period. The alkenone-based temperature record shows a distinct cooling event at the onset of the LIA, which has been attributed to monsoon failure. As a result of the monsoon failure during this time period, the conditions were very cold and dry during summer in Hokkaido. The later part of the LIA (1450-1850AD) was characterised by warmer temperatures compared to the onset of the LIA. The past 200 years is characterised by warming in the ~1860AD followed by a decrease in temperature. It is suggested that the EASM has weakening uring this time period in Hokkaido, Japan.

In addition, we find evidence for strong relationship between the frequency of famines and temperature in Japan. During time periods with cold summers, the frequency of famines in Japan increases. This demonstrates that natural forcing mechanisms, without modern human activities, can also lead to strong climate variability and also strongly influence society through agriculture loss.

Hydrogen isotopic composition of higher plant waxes in the catchment and down-core sedimentary records of Lake Toyoni

8.1 Introduction

Long-chain (C_{25} - C_{35}) *n*-alkanes with a strong odd-over-even carbon number preference are produced by vascular plants (Eglinton and Hamilton, 1967). They are a component of the leaf epicuticular waxes, which protect the leaf surfaces (Eglinton and Hamilton, 1967). Leaf wax compounds are mainly transported into lacustrine sediments from the surrounding catchment area by wind (Hou et al., 2007). In addition, wind can transport *n*-alkanes over vast distances (Yamamoto et al., 2011). Although the influence of long-range transport of *n*-alkanes in Lake Toyoni is possible, the catchment surrounding Lake Toyoni has the steep slopes and thick vegetation suggesting that *n*-alkanes are primarily derived from the higher plants within the catchment rather than from long-rang transport. *n*-Alkanes within lacustrine sedimentary records are of interest as palaeo-climate proxies, because they are generally abundant and well-preserved (Meyers, 1997), and their hydrogen isotopic signal is not easily exchanged, because all the hydrogens are covalently bonded to carbons (Sessions et al., 2004, Pedentchouk et al., 2006).

8.1.1 Leaf wax *n*-alkane δD as a recorder of δD of precipitation

The δD_{HPW} from lake sediments are a powerful tool for investigating hydrological change. The main hydrogen source of for plants is environmental water, for example, rainwater, groundwater, and snow-melt, which are all derived from precipitation. Investigations of the δD_{HPW} values with local precipitation and/or catchment water δD values suggest that δD_{PRECIP} is the primary control on δD_{HPW} (Sauer et al., 2001, Sessions, 2006, Hou et al., 2008), therefore; the δD_{HPW} can be used to reconstruct changes in δD_{PRECIP} over a given period of time (e.g. Schefuss et al., 2005, Pagani et al., 2006). In general, the δD_{PRECIP} reflects hydrological and climate processes including temperature, precipitation amount, altitude, latitude, and moisture source (Dansgaard, 1964). Knowledge of the controls of the δD_{PRECIP} at the study site is important for interpreting the δD_{HPW} from palaeo-climate archives.

Although knowledge of the origin of the precipitation and factors controlling the δD_{PRECIP} in Japan is essential to interpret the δD_{HPW} , the coverage of data available with respect to isotopes in precipitation in Japan is sparse. Araguàs-Araguàs et al. (1998) used data from the Global Network of Isotopes in Precipitation (GNIP) program and found that the δD_{PRECIP} from locations above 30°N in Asia are mainly influenced by temperature. In order to visually show the difference in the “amount effect” and the “temperature effect” in Japan, we produced a schematic showing a north-south transect of the monthly average temperature and δD_{PRECIP} using temperature data from meteorological sites and the corresponding δD_{PRECIP} from the “The Online Isotopes in Precipitation Calculator” (OIPC)

[http://wateriso.utah.edu/waterisotopes/pages/data_access/oipc.html],

respectively; in order to explore the spatial and temporal variability of the hydrogen isotopes in precipitation in Japan (Figure 8-1). The OIPC model equation is based on a function of latitude and altitude (which is based on findings from real data). The key assumption that the OIPC makes is that the oxygen lapse rate is similar at all geographic locations. The OIPC estimates the δD_{PRECIP} at a given site by combining an empirical model for isotopic trends related to latitude and altitude based on real isotope data from stations in GNIP. The OIPC data showed that the δD_{PRECIP} in Hokkaido is mainly influenced by temperature (hereby referred to as the “temperature effect”). Temperature

influences the δD_{PRECIP} due to favoured removal of deuterium from air-mass during condensation when it cools, resulting in lower δD values remaining in the air-mass (Dansgaard, 1964). This also results in a latitudinal trend of decreasing δD values with increasing latitude (Dansgaard, 1964). In addition to temperature, the δD_{PRECIP} also reflects the source of the precipitation. In winter, precipitation is cold and originates from the Asian continent as part of the East Asian Winter Monsoon (EAWM) system (Figure 8-2); whereas, in summer precipitation is warm and originates from the Pacific Ocean as part of the East Asian Summer Monsoon (EASM) system (Figure 8-2). The combined influence of temperature and the source of the precipitation are ultimately controlled by the East Asian Monsoon (EAM) system. As a result the δD_{HPW} from the sedimentary record of Lake Toyoni is an indicator for regional atmospheric circulation changes, mainly the intensity of the EAM system.

8.1.2 Environmental controls on the δD values of terrestrial leaf waxes in Hokkaido, Japan

Although δD_{HPW} initially records the δD_{PRECIP} , the δD_{HPW} can be further modified by evapotranspiration, which is influenced by environmental conditions and plant physiological and morphological characteristics of the plants (Chikaraishi et al., 2004, Liu et al., 2006a, Smith and Freeman, 2006, Hou et al., 2007, Pedentchouk et al., 2008, Feakins and Sessions, 2010, Duan and Xu, 2012, Sachse et al., 2012). Therefore, plants using the same precipitation water exhibit different δD_{HPW} values. The difference between the δD_{PRECIP} and δD_{HPW} range between -30‰ to -200‰ (Sachse et al., 2012).

The first explanation for this offset is that in addition to the δD_{HPW} being primarily controlled by δD_{PRECIP} , the δD_{HPW} is also affected by deuterium enrichment in water via evapotranspiration (soil evaporation and leaf transpiration); which is ultimately controlled by climatic factors such as relative humidity (RH) and temperature (e.g. Sachse et al., 2012). The effect of RH on the δD_{HPW} dominates in dry regions and is not a significant control in humid environments, such as Hokkaido. Significantly, Sachse et al. (2012) suggests that the role of RH on δD_{HPW} only becomes significant below 70%. In Hokkaido the main growing season occurs between June and September (Seki et al., 2010), which is when the transpiration effect is most important for influencing isotopic

fractionation in leaf waxes. RH ranges between 73% and 89% during the growing season; therefore, the RH is always above the threshold value (70%) and is not likely to have a large effect on the δD_{HPW} values. The δD_{HPW} from Lake Toyoni sedimentary record is therefore not recording changes in RH.

Another possible explanation for the offset between the δD_{HPW} and δD_{PRECIP} is variations amongst different plant types due to physiological and morphological characteristics of the plants (Chikaraishi et al., 2004, Hou et al., 2007, Pedentchouk et al., 2008, Duan and Xu, 2012, Sachse et al., 2012). For example, deep-rooted plants are not as influenced by soil evaporation (Feakins and Sessions, 2010), compared to shallow-rooted grasses (Smith and Freeman, 2006). In addition, photosynthetic pathways (C3 versus C4; Chikaraishi et al., 2004), taxonomic (e.g. angiosperm versus gymnosperm; Chikaraishi and Naraoka, 2003, Liu et al., 2006a), and growth forms (e.g. monocotyledons versus dicotyledons; Liu et al., 2016) all contribute towards to the offset between the δD_{HPW} and δD_{PRECIP} . For example, the average δD_{HPW} for C3 angiosperms is $-152 \pm 26\text{‰}$, C3 gymnosperms is $149 \pm 16\text{‰}$ and C4 plants is $171 \pm 12\text{‰}$ (Chikaraishi and Naraoka, 2003), whereas, monocotyledonous species values averaging -140‰ and dicotyledonous species averaging -107‰ (Liu et al., 2016). The differences in δD_{HPW} values between different plant types may contribute to changes in the down-core record if the vegetation surrounding the lake changes. Therefore, before applying the δD_{HPW} as a proxy for δD_{PRECIP} , an understanding of the hydrogen isotopic composition of the *n*-alkanes in different plant types growing in the catchment area, and hence contributing to the sedimentary record, is important.

8.1.3 Aims

Although the plants in the catchment are ultimately recording the δD_{PRECIP} , understanding the environmental controls on the δD_{PRECIP} in the modern environment in Hokkaido is essential in order for the δD_{HPW} from the Lake Toyoni sedimentary record to provide accurate interpretations of δD_{PRECIP} over the last 1000 years in this region. The overall aims of the chapter are:

1. To determine the environmental controls of δD_{PRECIP} in the modern environment in Hokkaido, Japan to aid in the interpretation of the δD_{HPW} from the sedimentary record of Lake Toyoni.
2. Reconstruct hydrological variability over the past 1000 years in Hokkaido, Japan.

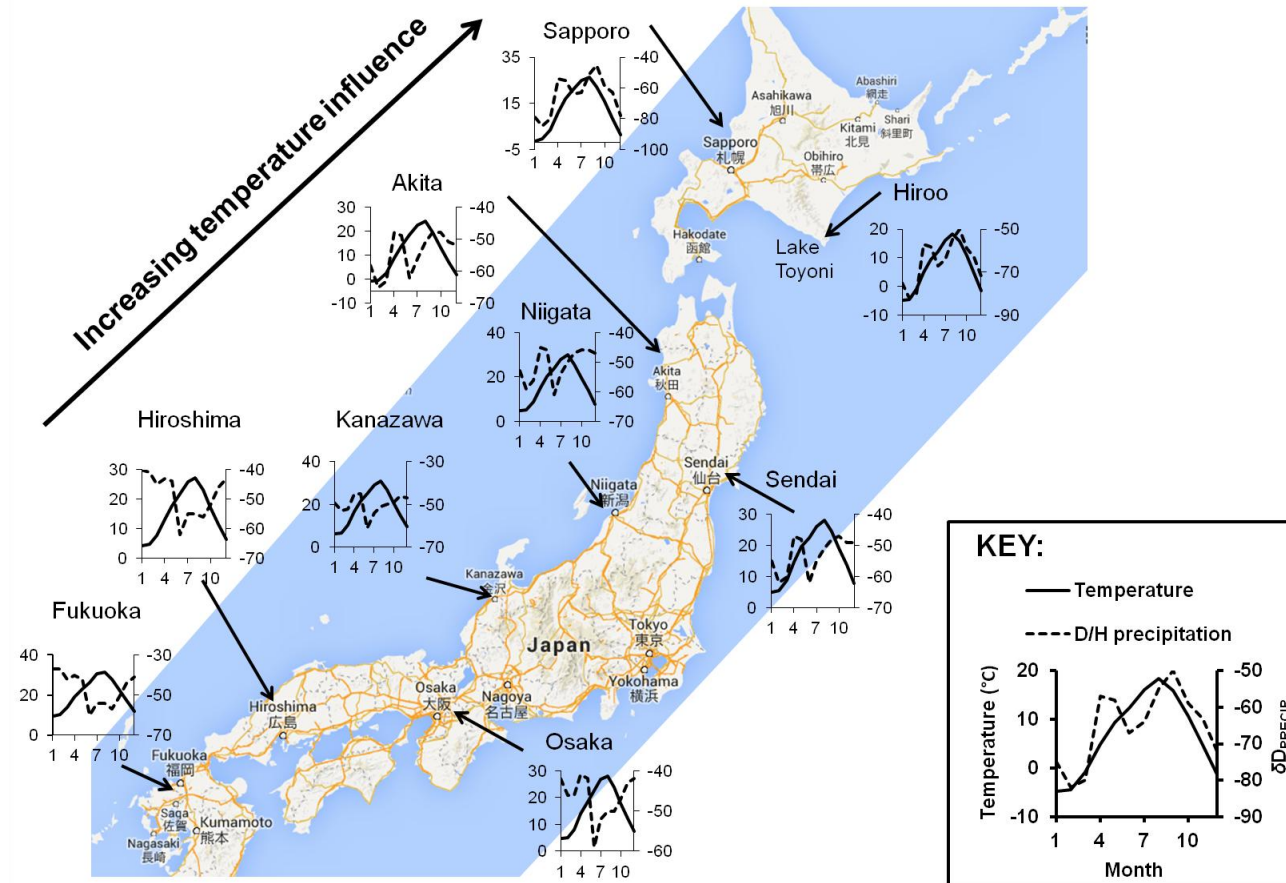


Figure 8-1: North-South transect of the monthly average temperature and δD_{PRECIP} developed using temperature data from meteorological site and the corresponding δD_{PRECIP} from the OIPC. X axis is month (1=Jan, 2=Feb, 3=Mar...).

8.2 Background

8.2.1 Source of precipitation in Hokkaido, Japan

Japan's northern island, Hokkaido, is strongly influenced by both polar and tropical air-masses (Figure 8-2). During winter, the air-masses influencing Hokkaido are controlled by a high-pressure system that develops over Siberia (Siberian High [SibH]) resulting in cold dry air-masses being transported towards the Pacific Ocean. This air-mass picks up moisture from the Sea of Japan resulting in heavy snowfall conditions. During summer, the wind systems reverse and Hokkaido comes under the influence of the sub-tropical air-mass originating from the Pacific High (NPSH), which is formed in the northwest sub-tropical Pacific. In August, the NPSH moves northward exposing Hokkaido to the influence of the monsoonal winds of the Pacific Ocean. Prior to the movement of the NPSH, the polar air-mass influences Northern Japan. The polar air-mass is enhanced by the influence of a high-pressure system that develops over the Okhotsk Sea (referred to as the Okhotsk High [OH]), which results in cool summers in Hokkaido.

The moisture source of precipitation in Hokkaido is therefore strongly influenced by the EAM (e.g. D'Arrigo et al., 2001, Davi et al., 2002, Tsuji et al., 2008, Igarashi et al., 2011). In addition, Lake Toyoni (42°N) is situated at the boundary of the northern edge of the EASM (34-44°N; Xu et al., 2010b) making it sensitive to the enhancement of the EASM (Schone et al., 2004). The boundary of the northern edge of the EASM is the location where the warm tropical air meets the cold polar air-mass, termed the polar front. When the NPSH intensifies the polar front is located further north than usual and as a result there is an increased influence from tropical maritime air-mass from the Pacific Ocean. When the polar front is located further south, there is a reduction in the influence of the Pacific Ocean and an increased influence from the sub-polar maritime air-mass to Hokkaido.

The difference in precipitation sources between EASM and EAWM is reflected in the deuterium-excess values of precipitation, which is negatively correlated to RH and temperature at the source region of the precipitation (Merlivat and

Jouzel, 1979, Froehlich et al., 2001). The deuterium excess is defined as $d = \delta D - 8 \times \delta^{18}O$ (Dansgaard, 1964) and can therefore be used to track changes in the source of moisture in precipitation (Masson-Delmotte et al., 2005). The seasonal trend in monthly deuterium excess values is illustrated for Lake Toyoni using δD and $\delta^{18}O$ data from the OIPC. At Lake Toyoni, deuterium excess values ranged from 0.8 to 16 (Figure 8-3). During winter, deuterium excess values are high (average of 8.9 between December and March) due to the incorporation of moisture from the Sea of Japan by the EAWM. During summer, deuterium excess values are low (average of 5.1 between June and September) due to the moist air-mass originating from the OH in early summer and the moisture generated under high humidity from the Pacific Ocean, which is brought to Japan by the EASM.

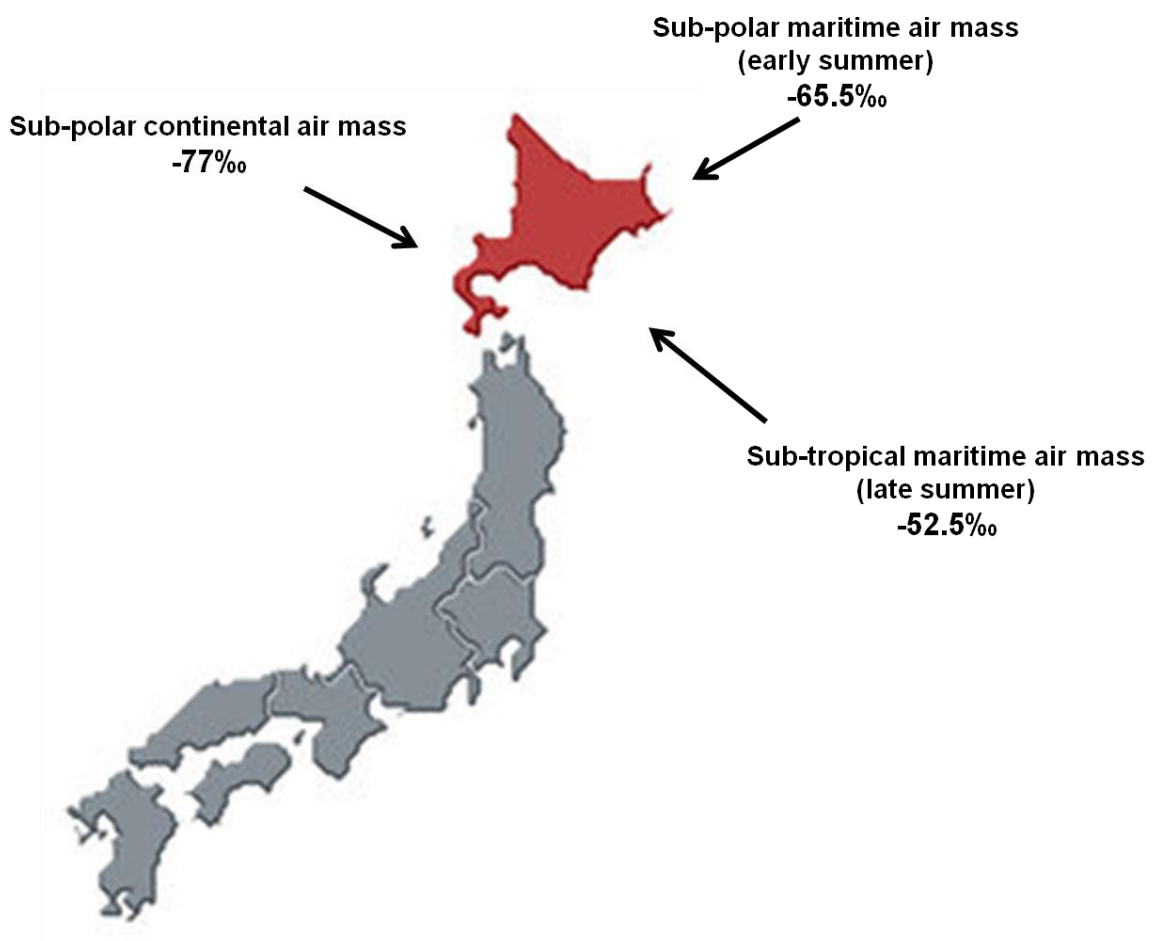


Figure 8-2: Map of Japan and the air-masses influencing Hokkaido. The averaged δD_{PRECIP} value is also provided for the different air-masses. There is an average of 24.5‰ difference between the δD_{PRECIP} from the EAWM and the EASM.

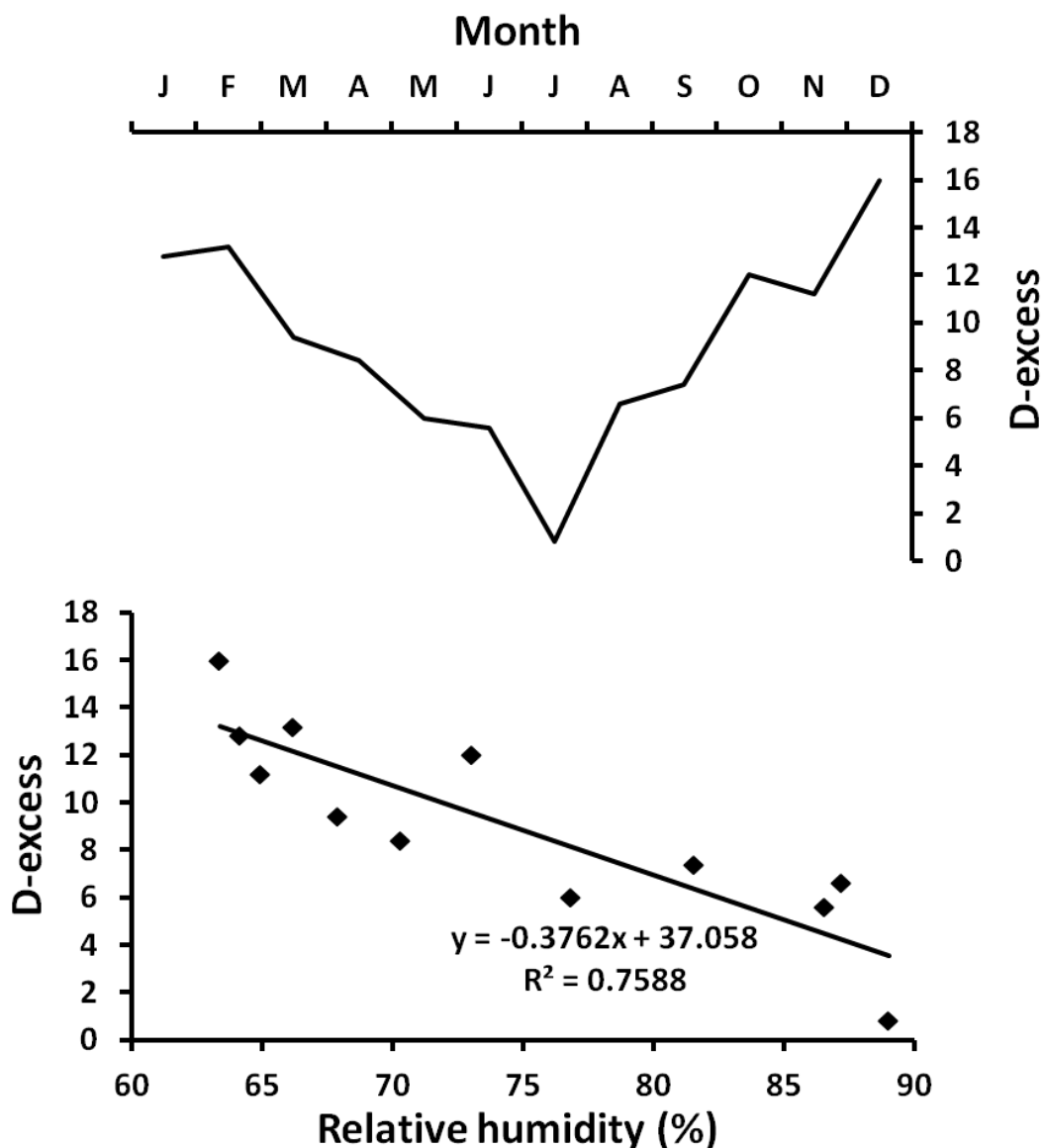


Figure 8-3: The monthly deuterium excess values (top graph) and the correlation between deuterium excess and RH (%) from Lake Toyoni, Southern Hokkaido. The deuterium excess values were taken from the OCIP website and represent values from Lake Toyoni. Relative humidity values were taken from Hiroo weather station (25km from Lake Toyoni). The correlation is $R^2 = 0.76$ suggesting a strong correlation between deuterium excess and RH (%).

8.2.2 Temporal and spatial pattern of modern-day precipitation δD in Hokkaido, Japan

In addition to the change in the moisture source between summer and winter, the EAM system also controls the temperature and the precipitation amount in Japan, which is ultimately reflected in the δD_{PRECIP} . The EASM brings warm and

wet conditions to Japan; whereas, the EAWM brings cold and heavy snowfall conditions to Japan.

The δD_{PRECIP} in Japan is mainly influenced by the temperature effect or the amount effect or a mixture of the temperature and the amount effect (Araguàs-Araguàs et al., 1998). The temperature effect and the amount effect influence the δD_{PRECIP} in opposite directions. For example, if temperature is the controlling factor of the δD_{PRECIP} , an increase (decrease) in temperature will correspond to an increase (decrease) in δD values. Alternatively, if the amount effect is the controlling factor of the δD_{PRECIP} , an increase (decrease) in precipitation will correspond to a decrease (increase) in δD values.

The dominant control (temperature versus precipitation amount) on the δD_{PRECIP} is dependent on the latitude of the study site in Japan. The islands of Japan cover a large latitudinal gradient (30-45°N), and as a result the controls of the δD_{PRECIP} in Hokkaido (northern Japan) are not the same for the other regions in Japan (Figure 8-1). For example, the seasonal variation in precipitation is controlled by temperature effect at higher latitudes of Japan; whereas, lower latitudes are controlled by the amount effect (Araguàs-Araguàs et al., 1998). Locations in between (e.g. central Japan) are controlled by a mixture of the temperature effect and the amount effect (Figure 8-1). Dansgaard (1964) suggested that the temperature effect controls winter δD_{PRECIP} values; whereas, the amount effect controls summer δD_{PRECIP} values in Tokyo (35°N).

To evaluate the temperature control on the δD_{PRECIP} , we present the seasonal trend in monthly temperature and δD_{PRECIP} for the study site (Lake Toyoni) using weather station data from a nearby metrological site 25km from Lake Toyoni and δD_{PRECIP} data from IPOC. A positive correlation between monthly temperature and δD_{PRECIP} exists ($R^2=0.65$; Figure 8-5) showing that temperature is the dominant control on the δD_{PRECIP} in this location. If the amount effect influenced the δD_{PRECIP} in Hokkaido, we would see a reduction in δD_{PRECIP} values when rainfall increased. However, in Hokkaido the opposite trend is present, which demonstrates that the amount effect will not complicate the δD_{PRECIP} signal in this location.

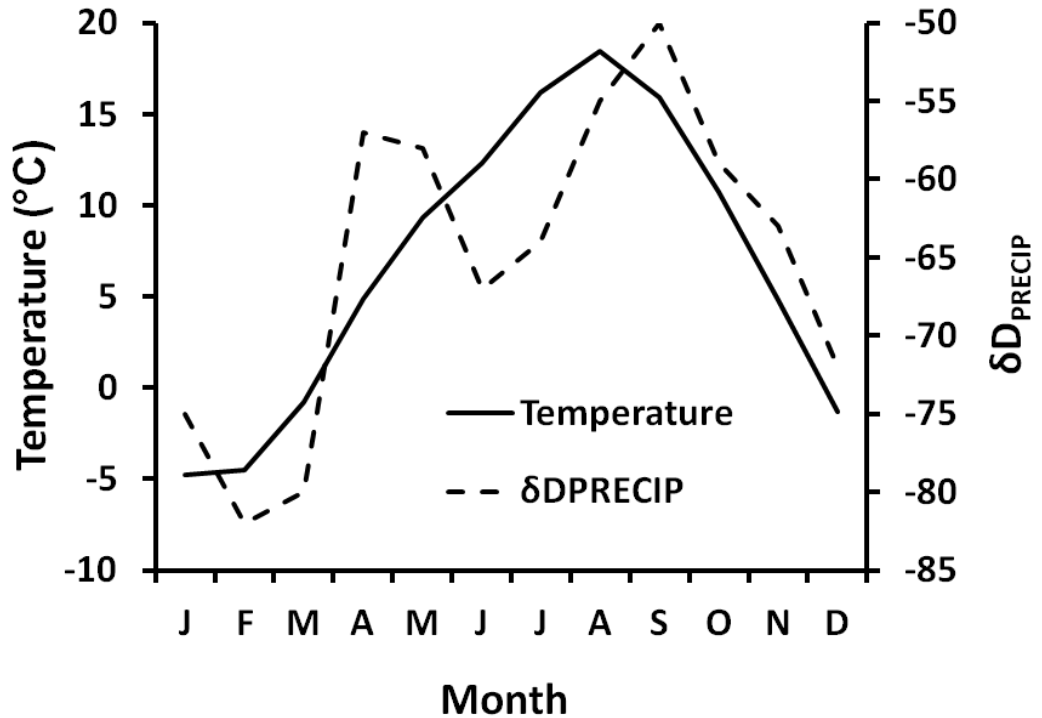


Figure 8-4: Monthly air temperature data from Hiroo weather station (averaged 1958-2014) and δD_{PRECIP} from OCIP. Lower δD_{PRECIP} values are recorded during winter and higher δD_{PRECIP} values are recorded during summer. The highest δD_{PRECIP} values occur when the NPSH moves North in August and exposes Hokkaido to the influence of the EASM.

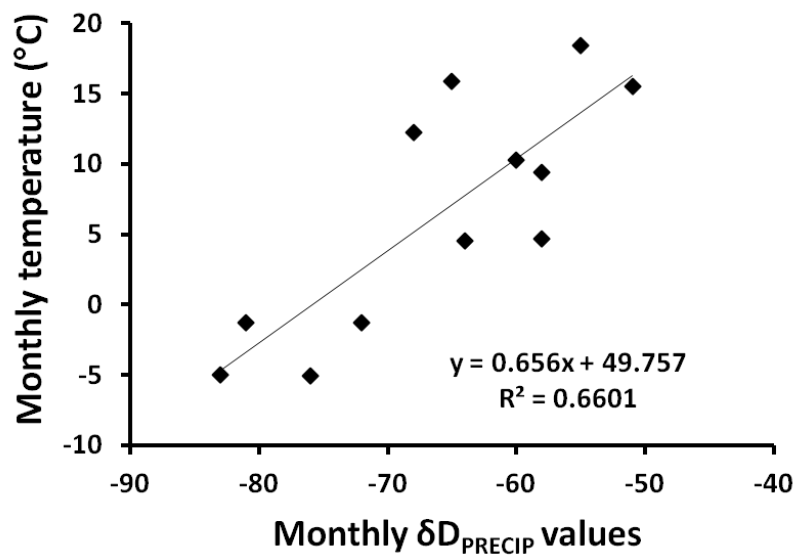


Figure 8-5: Scatter plot of monthly air temperature data from Hiroo weather station (averaged 1958-2014) and δD_{PRECIP} from OCIP.

For temperature to be the only control, we would expect to see the hottest month (August) to have the highest δD_{PRECIP} values and the coldest month (January) to have the lowest. However, the results show that the highest δD_{PRECIP} values are in September and the lowest δD_{PRECIP} values are in February suggesting there is a one-month lag between temperature and the δD_{PRECIP} . The other control on the δD_{PRECIP} is the origin of the precipitation, which is ultimately linked to latitude and temperature during formation.

Precipitation during winter in Hokkaido originates from higher latitudes and is associated with the EAWM and records lower δD values due to condensation associated with lower temperatures. Precipitation in Hokkaido during summer has two main sources: (1) the sub-arctic air-mass, which results in cold summers in Hokkaido and has lower δD values; and (2) the Pacific Ocean air-mass that exposes Hokkaido to the influence of the EASM winds when the NPSH moves north during late summer. Air-masses originating from the Pacific have higher δD values due to evaporation under higher temperatures (summarised in Figure 8-4). These different moisture sources are strongly influenced by the EAM system. This means that the δD_{HPW} , which records the signal of the δD_{PRECIP} , can be used to infer information on the variability of the EAM over the past 1000 years in Hokkaido.

8.2.3 Interpretation of the δD_{HPW}

The application of δD_{HPW} as a proxy for the variability in the EAM is based on the assumption that the plants in the Lake Toyoni catchment are using precipitation from winter as well as summer. Although the growing season in Hokkaido is restricted to a short summer (June to September) (Seki et al., 2010), the plants around Lake Toyoni likely use winter precipitation in the form of snowmelt. Winter precipitation contributes to the signal recorded in the plant leaf waxes when the soils retain water from the spring snowmelt. Given the high RH in Hokkaido and shading from the densely vegetated catchment, the soils in the catchment do not dry out and therefore retain their winter precipitation signal. Therefore, although plants may be slightly bias towards summer precipitation,

water from winter precipitation is also utilised by plants in the catchment of Lake Toyoni, and hence record an EAM signal.

The EAM is driven by temperature differences between the Asian continent and the surrounding Oceans (the Pacific Ocean and the Indian Ocean). The EASM and the EAWM are significantly different from each other based on two key characteristics; the wind direction (from the South in summer and the North in winter) and the prevailing climate (warm and wet associated with the EASM and cold and drier/heavy snowfall associated with the EAWM). As a result, in this study, we can infer the change of the wind direction and temperature based on the differences in the δD_{HPW} . For example, when the wind direction is northerly during winter, the δD_{PRECIP} is low, thus δD_{HPW} will also be low. On the other hand, the δD_{PRECIP} during summer is high and has a southerly wind direction. There are three different air-masses that influence Hokkaido (summarised in Figure 8-2).

8.2.3.1 Sub-tropical maritime air-mass (high δD values)

A stronger influence from southerly winds enhances moisture transport from the Pacific Ocean and advances the northern limit of the EASM to Northern Japan resulting in increased exposure to the EASM in Hokkaido. In the modern day, wind input from the Pacific Ocean occurs in August when the high-pressure system advances northward and exposes Hokkaido to the influence of the Pacific Ocean air-mass. When the EASM intensifies, the NPSH-pressure system is located further north for a longer period of time resulting in an increased influence from the Pacific Ocean. This is documented in the modern day weather station data, which shows an increase in precipitation in August and September (Shurin precipitation) when the EASM intensifies (Chapter 2). The EASM is intensified in the year following an El Niño episode (Wang et al., 2001), the negative phase of the PDO (Tsuji et al., 2008) and the positive phase of the North Atlantic Oscillation (NAO)/Arctic Oscillation (AO)(Gong and Ho, 2003). These findings are also supported by modern day data from Hokkaido (Chapter 2). High δD_{HPW} values therefore reflect an intensification of the EASM, which results in warmer and wetter conditions in Hokkaido.

8.2.3.2 Sub-polar maritime air-mass (low δD values)

Sub-tropical air-mass therefore influences Hokkaido in August and September, whereas during early summer Hokkaido is influenced by sub-polar air-mass. The influence of sub-polar air-mass is increased when the OH develops over the Okhotsk Sea in early summer.

The occurrence and frequency of the OH is intermittent throughout the summer (Nakamura and Fukamachi, 2004), which results in cold summer conditions in Northern Japan. An example is in summer of 1993, when the frequency of the OH increased during July and August. Figure 8-6 shows a surface weather chart for the 21st July 1993 from Nakamura and Fukamachi. (2004). The figure shows the southward extension of the high-pressure system. The presence of the OH over Hokkaido resulted in colder than average conditions. Average temperature in July and August from the Hiroo weather station is 16.2 and 18.5°C (based on temperature data from between 1958 and 2014). In 1993, temperatures were 13.5 and 16.9°C, respectively. July temperatures were therefore 2.7°C lower than average and August was 1.6°C lower than average. Some locations have observed temperatures lowering as much as 5°C below normal during years when the OH increased in frequency. Similarly to the EASM, the intensity of the OH is also influenced by the positive phase of the AO (Ogi et al., 2004).

When the OH intensifies and moves further south, it prevents the northward shift of the NPSH during summer (Yafei et al., 2003, Park and Ahn, 2014). This is demonstrated in Figure 8-6. The OH is a blocking high (Park and Ahn, 2014); when the blocking frequency increases (positive blocking years), the OH enhances and the NPSH weakens (Nakamura and Fukamachi, 2004, Park and Ahn, 2014). As a result, cold summers occur in Hokkaido due to the boundary where the warm Pacific air meets the cold polar air being located further south. When the polar front is located further south, the influence of the Pacific air-mass is reduced in Hokkaido and the influence of the polar air-mass increases, which will record lower δD_{HPW} values in the Lake Toyoni sedimentary record. Whereas, when the boundary is located further north, the influence of the Pacific air-mass

is increased and higher δD_{HPW} values will be recorded in the Lake Toyoni sedimentary record.

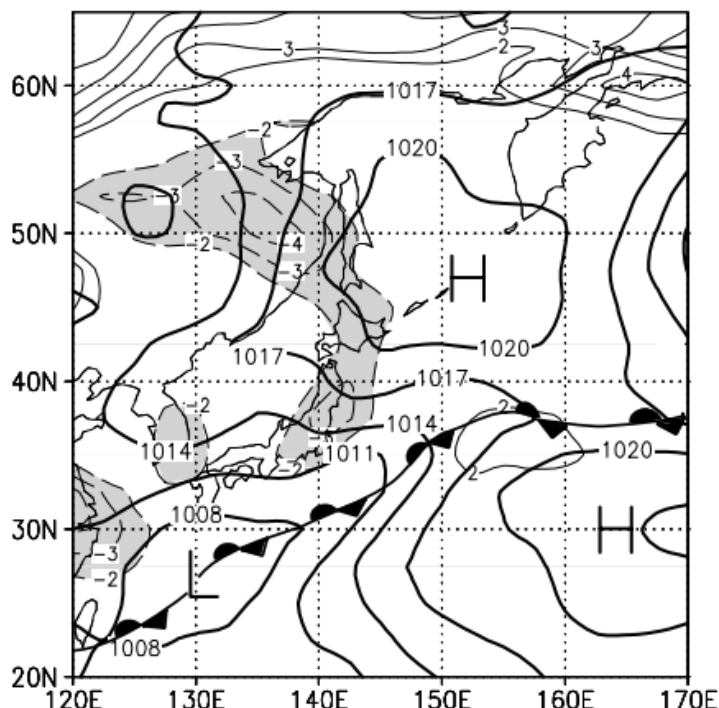


Figure 8-6: A surface weather chart from 21st July 1993 in Japan based on the NCEP/NCAR reanalyses (Figure from: Nakamura and Fukamachi, 2004). The polar front is the toothed line between the high-pressure system to the North - OH) and the high-pressure system to the South (NPSH). The figure shows the OH covering a large part of Hokkaido, preventing the NPSH from moving north. The polar front therefore remained further south than usual and prevented the influence of monsoon precipitation during this summer. Rainfall is therefore associated with the OH rather than the NPSH when the OH intensifies and moves south.

8.2.3.3 Sub-polar continental air-mass (low δD values)

Another sub-polar air-mass contributing to low δD values in the down-core sedimentary record of Lake Toyoni is associated with the EAWM from the SibH pressure system. Precipitation during winter has the lowest δD values due to the formation at high latitudes and also the low temperatures during this season. When the snow melts in spring, plants leafing out at this time can use water from the spring melt. This water will contribute to soil moisture and groundwater, which plants can use during photosynthesis.

The variability of the EAWM depends on the extent of the SibH, Aleutian Low and subtropical westerly jet-stream (Ha et al., 2012). The strength of the SibH is influenced by the AO, with an increase in intensity occurring when the AO is in

its negative phase (Gong et al., 2001, Jhun and Lee, 2004b). Therefore, when the NAO/AO is negative and the EAWM enhances; lower δD_{HPW} values will be recorded in the Lake Toyoni sedimentary record.

8.2.4 Summary

To better understand the hydrological variability of Hokkaido, we present a reconstruction of hydrology from Lake Toyoni spanning the past millennium. In Northern Japan, the δD_{PRECIP} precipitation reflects temperature and the source of the precipitation. Hokkaido is influenced by sub-polar and sub-tropical air-masses, which is ultimately controlled by the EAM and the OH. The δD values for the leaf waxes are an indicator of past changes in the EAM and the OH over the past 1000 years. Higher δD_{HWP} values suggest an increased influence from the Pacific Ocean resulting in warm and wet conditions. The increased Pacific Ocean influence is related to the strength of the NPSH, which also drives the intensity of the EASM (a strengthened NPSH resulting in a strengthened EASM and vice versa). Therefore high δD_{HPW} values suggest an enhancement of the EASM. Lower values, on the other hand, represent [1] an intensification of the EAWM, [2] a reduction in the influence from the EASM, [3] an increased influence from sub-polar air-masses from the OH.

The down-core record of the δD_{HPW} therefore provides a record of EAM variability of the past 1000 years. The specific aims of this chapter are:

1. To determine how δD_{HPW} differ in different plant types under the same precipitation at a single site.
2. To determine the apparent fractionation between δD_{PRECIP} and the δD_{HPW} .
3. To determine if solar irradiance is a key driver of EAM variability in Northern Japan.
4. To determine the main teleconnections (e.g. NAO/PDO/ENSO) driving EAM variability.

8.3 Results

8.3.1 δD values of vegetation samples

Eleven vegetation samples were collected and analysed for their δD values. We found that the δD C₂₇ *n*-alkane varied from -225‰ to -146 ‰ with an average value of -168‰, the δD C₂₉ *n*-alkane varied from 227‰ to 153‰ with an average value of -183‰ and the δD C₃₁ *n*-alkane varied from 210‰ to -150‰ with an average value of -175‰.

Table 8-1: δD values of *n*-alkanes extracted from leaf samples in the catchment of Lake Toyoni (SD=standard deviation). Duplicate analysis were carried out to obtain the standard deviation.

Species name	δD C ₂₇	SD	δD C ₂₉	SD	δD C ₃₁	SD
Cherry	-148	2	-153	3	-150	5
Maple	-178	2	-189	3	-175	1
Oak	-174	2	-179	3	-172	1
Ash			-207	2	-208	1
Birch					-158	1
Prunus	-146	1	-154	3	-152	1
Mulberry	-161	0	-200	0	-177	0
Fraxinus	-163	0	-188	3	-188	5
Bamboo	-225	0	-227	7	-210	1
Fern	-166	0	-175	10	-181	0
Hippocastanaceae acsculus	-156	4	-156	1	-152	0

8.3.2 δD values of down-core *n*-alkanes

A Pearson correlation was used to test the correlation between δD C₂₇, δD C₂₉ and δD C₃₁. When α values are lower than 0.02 the correlation is significant. All values are below 0.02 (highlighted in bold in Table 1), confirming that the δD values of the C₂₇, C₂₉ and C₃₁ are all significantly correlated (Table 1). The highest correlation was between the C₂₉ and C₃₁ (0.91), followed by C₂₇ and C₂₉ (0.84) and the lowest correlation was between the C₂₇ and C₃₁ (0.81). Based on the strong significant correlation, an average of the δD C₂₇, C₂₉ and C₃₁ is used for the discussion of the results.

Table 8-2: Pearson correlations between δD C₂₇, δD C₂₉ and δD C₃₁. Bonferroni correction for multiple pair-wise comparisons lowered the α value to 0.02 ($\alpha=0.05/3=0.02$). Pair-wise relationship (n= 3).

	δD C ₂₇	δD C ₂₉	δD C ₃₁
δD C ₂₇		1.93E-16	2.42E-14
δD C ₂₉	0.84		1.77E-23
δD C ₃₁	0.81	0.91	

Each sample was run three times on the GC-IRMS and the average values for the δD C₂₇, δD C₂₉ and δD C₃₁ are present in Figure 8-7. An average of the C₂₇, C₂₉ and C₃₁ is also presented in Figure 8-7. The results from the averaged C₂₇, C₂₉ and C₃₁ δD values are termed δD_{HPW} . The results show that the δD_{HPW} values are variable between 1082 and 1273AD, with a large decrease to -202‰ at 1156AD. δD_{HPW} rise in 1361AD to the highest values recorded in the sedimentary record (-169‰), followed by a sharp decrease to -196‰ in 1376AD, where values continued to decrease to -207‰ in 1446AD. δD_{HPW} values increase to -178‰ in 1615AD, followed by a sharp decrease to the lowest values recorded in the record (-209‰) in 1684AD and remained low (~-200‰) till 1703AD where δD_{HPW} values gradually increase to -175‰ in 1820AD. δD_{HPW} values decreased and remained at -192‰ between 1850 and 1879AD where δD_{HPW} values increased to -177‰ in 1925AD and δD_{HPW} values generally decrease to the present day.

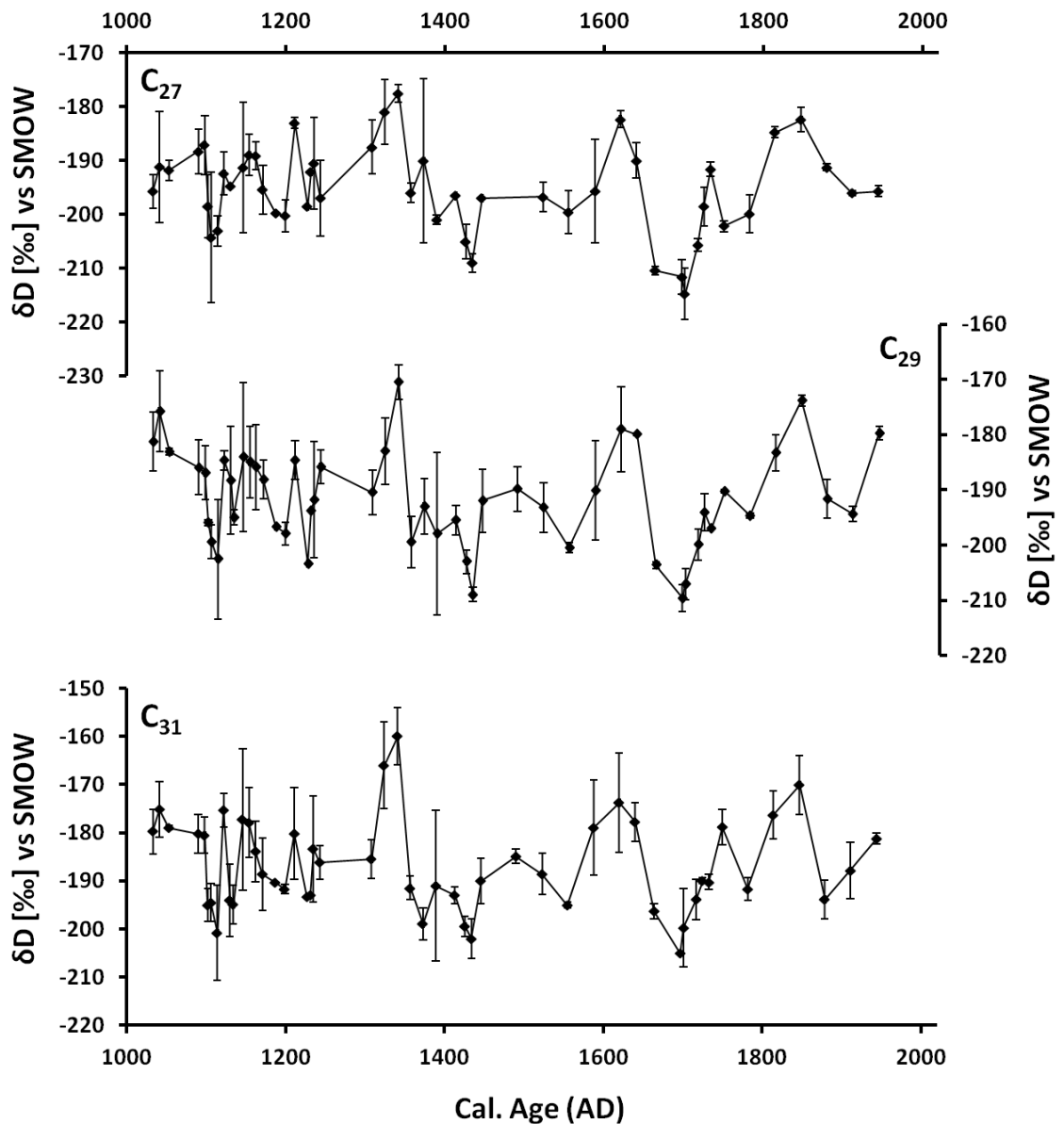


Figure 8-7: Variations in the δD C_{27} , δD C_{29} and δD C_{31} over the past 1000 years from Lake Toyoni, Japan. Error bars represent the (SD=standard deviation). Triplicate analysis were carried out to obtain the standard deviation.

8.4 Discussion

8.4.1 δD_{HPW} in the catchment surrounding Lake Toyoni

Modern vegetation samples were collected from the catchment of Lake Toyoni in order to evaluate how the δD_{HPW} differ in different plant types under the same precipitation in the catchment of Lake Toyoni. We found that the δD C_{27} *n*-alkane varied from -225‰ to -146 ‰ with an average value of -168‰, the δD C_{29} *n*-alkane varied from 227‰ to 153‰ with an average value of -183‰ and the δD C_{31} *n*-alkane varied from 210‰ to -150‰ with an average value of -175‰.

The results show that the δD of different plant types differs in a single catchment, despite the precipitation in the catchment being the same for all plants. For example, the δD values of the C_{27} , C_{29} and C_{31} *n*-alkanes are 80‰, 74‰ and 60‰, respectively. Although these differences appear high, Hou et al. (2008) also found large differences (as much as 70‰) in the δD_{HPW} values in vegetation samples collected from Blood pond, Massachusetts. A suggested reason for the differences between the δD of different plant types is that different source water being utilised due to different depths of roots. Rooted plants are not as influenced by soil evaporation (Feakins and Sessions, 2010), compared to swallow-rooted grasses (Smith and Freeman, 2006).

For example, some roots are deep into the ground are not as influenced by soil evaporation (Feakins and Sessions, 2010), whilst others are shallow, the difference in depth is reflected in the δD values; with less depleted δD values in shallow soil due to evaporation (Barnes and Turner, 1998, Smith and Freeman, 2006). Another reason for differences in the δD_{HPW} from different plants is due to differences in evapotranspiration. For example, some plants are taller and in direct sunlight (resulting in more evapotranspiration), whereas others are smaller (e.g. Fern) and are shaded by the larger trees (resulting in less evapotranspiration (Hou et al., 2008)). However, given the small data set (eleven leaf samples), we are unable to determine the key factors driving the differences in the δD_{HPW} .

Although we cannot pin point the exact reason for the differences in the δD of individual plant waxes, the results clearly indicate that the apparent fractionation between δD_{HPW} and δD_{PRECIP} is not constant for different plant types; therefore, changes in the δD_{HPW} may be influenced by changes in vegetation type. However, we suggest that significant changes in vegetation are minor over the past 1000 years in this catchment. Further evidence for this that the ACL values do not show any major changes during the past 1000 years (Chapter 4) which is an indication of vegetation change. Therefore the δD_{HPW} in the sedimentary record of Lake Toyoni represents a mixture of all the different δD of different plant types.

Despite inter-species differences influencing the primary δD_{PRECIP} signal preserved in the δD_{HPW} , the δD_{HPW} has been successfully used to provide reliable

hydrological reconstructions (Schefuss et al., 2005, Kuechler et al., 2013, Feakins et al., 2014, Fornace et al., 2014, e.g. Aichner et al., 2015). This suggests that although it is important to account for factors that can contribute to differences between the δD_{PRECIP} and δD_{HPW} , the offset may not be as large in the sedimentary record in comparison to the modern environment, especially when large shifts in vegetation have not been experienced. A potential reason for this is that lakes, such as Lake Toyoni, integrate the δD signal from all living plants in the catchment resulting in an average value for the system.

8.4.2 Apparent fractionation between precipitation and leaf wax

In this study, the fractionation between δD_{PRECIP} and the δD_{HPW} was calculated based on subtracting the modern core top C_{29} δD_{HPW} value (-194‰) from the annual average δD_{PRECIP} values from the OIPC data (-65‰). This assumes that plants are using mean annual precipitation. This results in an apparent fractionation value of -130‰.

$$\text{Fractionation} = \text{modern } \delta D_{\text{HPW}} (194\text{‰}) - \text{average annual } \delta D_{\text{PRECIP}} (-65\text{‰})$$

A fractionation value of -129‰ is reasonable given that Sachse et al. (2012) found that the C_{29} *n*-alkane for terrestrial C_3 plants has a fractionation value of $-149 \pm 28\text{‰}$ ($n = 47$) and $-134 \pm 28 \text{‰}$ ($n = 53$) for C_4 plants. In Figure 8-8, we present the fractionation corrected δD_{HPW} (referred to as $\delta D_{\text{HPW-COR}}$) values, which are simply the δD_{HPW} values subtracted by the apparent fraction (-129‰). This allows us to put the 1000-year sedimentary δD_{HPW} values in the context of modern precipitation values. The ($\delta D_{\text{HPW-COR}}$) estimations fall within a range of -79 to -39‰, which is similar to the range of modern precipitation values (-82 to -50‰). In order to evaluate changes in moisture source (EAWM versus the EASM) over the past 1000 years, changes in moisture source over the past 1000 years, average δD_{PRECIP} values from August-September (EASM precipitation) and December-February (EAWM precipitation) were determined. δD_{PRECIP} values in August and September (EASM precipitation) ranged from -55 to -50‰, whereas δD values from December-February (EAWM precipitation) ranged from -82 to -72‰. We have chosen threshold values of -55‰ and -72‰ to define intense EASM and EAWM, respectively (Figure 8-8). Values higher than -55‰ are interpreted as

an intensification of the EASM and values lower than -72‰ are interpreted as an intensification of the EAWM (Figure 8-8). Based on this, the EAWM intensified briefly $\sim 1434\text{AD}$ and $1670\text{-}1700\text{AD}$ and the EASM intensified $1030\text{-}1050\text{AD}$, $1324\text{-}1341\text{AD}$, $1588\text{-}1640\text{AD}$ and $1814\text{-}1847\text{AD}$.

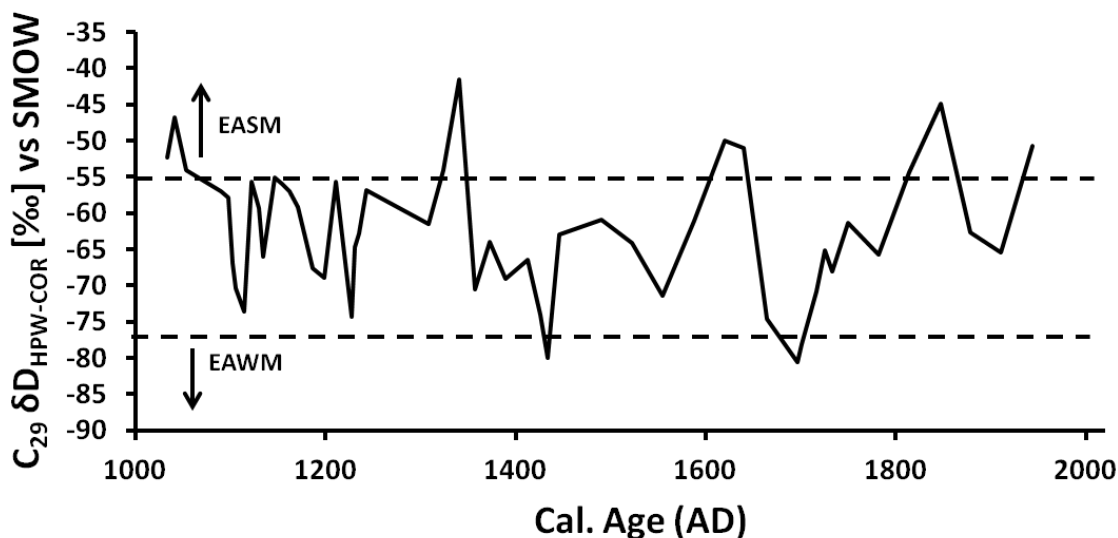


Figure 8-8: The fractionation corrected (-130‰) δD_{HPWCOR} values to show the δD_{PRECIP} over the past 1000 years in Hokkaido, Japan. Values range from -79 to -39‰ . Values above -55‰ (highlighted with dotted line) suggest an intensification of the EASM. Values below -72‰ (highlighted with a dotted line) suggest an intensification of the EAWM.

The use of δD_{HPWCOR} to record changes in moisture source is dependent on the assumption that the *n*-alkanes in Lake Toyoni are from the surrounding catchment. It is possible that *n*-alkanes could be transported via the EAWM winds to this site. Research on biomarkers from snow samples in Sapporo, Hokkaido shows evidence for long-range atmospheric transport of organic matter derived from higher plant waxes by the EAWM is possible (Yamamoto et al., 2011). However, the catchment of Lake Toyoni is surrounded by dense vegetation, which suggests that most of the *n*-alkanes in Lake Toyoni originate from the catchment area.

8.4.3 δD_{HPW} as a proxy for EAM variability

8.4.3.1 Solar activity and the EAM

The EAM is driven by seasonal changes in the heating contrast between the Pacific Ocean and the Asian continent and the pressure systems associated with these systems (mainly the SibH in winter and the NPSH in summer). Although cooling results in high-pressure systems (e.g., the SibH), high-pressure systems during summer can be intensified due to increased temperature contrast between the East Asian continent and the NW Pacific (e.g. the NPSH).

During summer, the thermal contrast between the Asian continent and the North Pacific ocean is defined as the Asian-Pacific Oscillation (APO) Index (Figure 8-9), which has a close link to changes in Northern Hemisphere air temperatures and also solar activity (Zhou et al., 2009c). Significantly, the APO index and solar activity both share 90-year and 11-year periodic oscillations (Zhou et al., 2009c), which further confirms the fundamental link between solar irradiance and the APO index.

Solar activity is a forcing for the APO index, because increased solar activity heats the land faster than the ocean causing increased thermal contrast between land and sea, and hence increased solar irradiance contributes towards higher APO index values. When the temperature contrast increases during summer (high APO index), the low-pressure system over the Asian continent becomes stronger, which intensifies the NPSH resulting in a northward movement of the NPSH (Zhou et al., 2011). The movement of this high-pressure system results in an increased influence of the southwesterly monsoonal winds from the Pacific Ocean to Hokkaido. There is therefore a link between the positive summer APO index and the intensity of the EASM in the modern day. To establish if there is relationship between land-sea thermal contrast and changes in moisture source to Hokkaido over the past 1000 years, the δD_{HPW} record is compared to the APO index from Zhou et al. (Zhou et al., 2009c). The APO index is related to surface air temperatures in the mid-latitudes of Asia and sea surface temperatures (SSTs) in the extratropical North Pacific therefore the APO index was reconstructed using reconstructions of temperatures in the eastern Asian land and the Pacific SST (Zhou et al., 2009c). APO values are generally

high between 1000-1400AD. During this time period the EASM intensified several times (e.g. 1030-1050AD and 1324-1341AD). The EASM also increased between 1588 and 1640AD, which is associated with a significant change from negative to positive APO values. The EASM intensified again between 1814 and 1847AD, which is associated with positive APO values. This confirms that strong EASM time periods occur during time periods of positive APO index values, which suggests a link between solar irradiance and the EAM at our site also.

The link between increased solar irradiance and a stronger EASM is also well documented (Dykoski et al., 2005, Wang et al., 2005, Xiao et al., 2006, Liu et al., 2009b, He et al., 2013, Sagawa et al., 2014). The influence of solar activity on the EAM is based on amplified solar radiation causing increased warming the land over middle and high latitudes compared to lower latitudes (Zhou et al., 2011). In addition, land warms at a faster rate than oceans promoting a temperature different between the land and ocean (Zhou et al., 2011). Moist air is transported from the ocean to the land resulting in warm and wet conditions. When solar activity decreases, there is less heating of the land resulting in a higher-pressure system developing over Siberia and as a result the EAWM strength increases (Kim et al., 2013).

To establish the relationship between solar activity and the EAM in Hokkaido, the δD_{HPW} record is compared to Bard et al. (2000). This record is based on the production rates of cosmogenic nuclides (^{14}C and ^{10}Be) from an ice core record at the South Pole (Bard et al., 2000). Chapter 4 describes how the production rates of cosmogenic nuclides record solar irradiance; briefly, lower production rates occur during high solar irradiance due to the increased influence of magnetic fields of solar winds, which deflect proportions of the charged cosmic particles. The record of solar irradiance from Bard et al. (2000) over the past 1000 years is presented in Figure 8-9.

We compared the EAM record, as inferred from δD_{HPW} , at Lake Toyoni and the variation of solar activity during the last 1000 years (Figure 8-9). Based on the above discussion, we would expect high solar radiation to drive the intensity of the EASM and low solar radiation to drive the intensity of the EAWM. The results show a clear relationship between the δD_{HPW} values at Lake Toyoni and the solar

activity over the past 1000 years (Figure 8-9); less depleted δD_{HPW} (suggesting enhanced EASM) generally corresponds to higher solar irradiance, whereas more depleted δD_{HPW} (suggesting enhanced EAWM) correlates to lower solar irradiance. The lowest δD_{HPW} values corresponded to the Spörer minimum (1402-1516AD). All time periods associated with low δD_{HPW} values corresponded with minima including; the Wolf (1280-1350AD), the Maunder (1645-1715AD) and the Dalton (1770-1820AD) minima. The similarity between the δD_{HPW} record and the solar irradiance record suggests that they vary together over the past 1000 years (Figure 8-9) suggesting that solar activity is a key control on the EAM in Hokkaido, Japan.

Although there are generally high δD_{HPW} values during the MWP, the relationship between high solar irradiance and high δD_{HPW} values is not as pronounced during the MWP. This suggests that there is an influence of the (1) EAWM, (2) or the sub-arctic maritime precipitation (e.g. the OH). The δD_{HPW} values during the MWP do not record values lower than -72‰ (threshold for EAWM intensification). This suggests that the MWP also has an influence from the OH, rather than the EAWM, during this time period. This suggests that solar irradiance or another climate driver, further discussed in following section, also intensified the OH as well as the NPSH during this time period. This resulted in a strong influence from the Pacific Ocean as well as from the Okhotsk Sea during this time period.

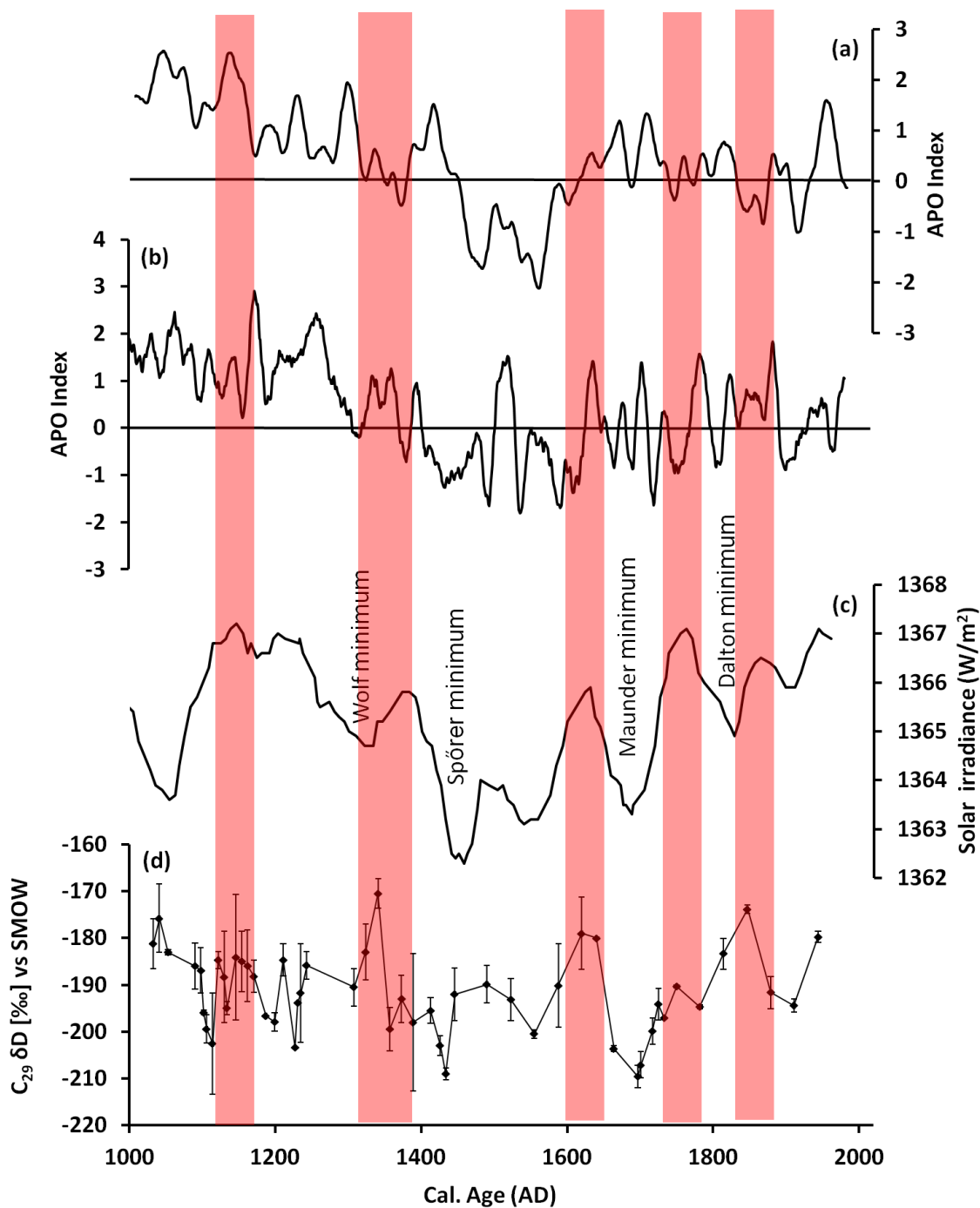


Figure 8-9: Variations in δD_{HPW} compared with the APO index and solar irradiance over the past 1000 years. (a) Reconstructed summer APO index by Zhou et al., (2011a). (b) APO index simulated by the FGOALS_gi model (Man and Zhou, 2011) by Zhou et al., (2011b). Both (a) and (b) are normalised and are a 31 year running mean. (c) Solar Irradiance (w/m^2) by Bard et al., (2000) and (d) the variations in $C_{29} \delta D_{HPW}$ from Lake Toyoni, Japan (present study).

8.4.3.2 Teleconnections

The forcing mechanism of small changes in solar activity on the EAM system is complex. It is likely that other factors (e.g. teleconnections) may amplify/dampen the solar irradiance signal, and in turn affect the variability in

the EAM (e.g the PDO, NAO/AO and ENSO). In order to evaluate the influence of these teleconnections on the down-core reconstruction of the EAM variability, the down-core record of the δD_{HPW} from Lake Toyoni is compared with a PDO (MacDonald and Case, 2005), NAO (Trouet et al., 2009) and ENSO (Yan et al., 2011a) reconstructions. Information on how the indices were reconstructed was outlined in Chapter 5.

8.4.3.2.1 EAWM

The EAWM intensified twice based on δD_{HPW} data; ~1434AD and 1670-1700AD (highlighted in grey in Figure 8-10). Based on these findings, the PDO does not have a strong influence on the intensity of the EAWM (Figure 8-10a). The NAO, on the other hand, may be linked to the intensity of the EAWM. The two EAWM intensifications (~1434AD and 1670-1700AD) both occurred during time periods when the NAO shifted from a positive to a negative phase (Figure 8-10b). However, the strongest control on the intensity of the EAWM is ENSO. It was found that the intensity of the EAWM corresponds to the positive ENSO index (La Niña conditions). The influence of La Niña on the EAWM was also noted in modern climate data from Hiroo weather station (Chapter 2). During La Niña events, the occurrence of East Asian cold surges increases and also the strength of the northerlies increases (Zhang et al., 1997), this triggers a decrease in temperature in East Asia and hence a stronger EAWM.

8.4.3.2.2 EASM

The EASM intensified 1030-1050, 1324-1341, 1588-1640 and 1814-1847AD based on the down-core δD_{HPW} data (highlighted in red; Figure 8-10). Based on these findings, the EASM occurs during both positive and negative phases of the PDO (Figure 8-10a) and NAO (Figure 8-10b). A strong control on the intensity of the EASM is ENSO. It was found that low ENSO index values (El Niño conditions) resulted in strong EASM. A connection between ENSO and the EASM was also noted in modern climate data from Hiroo weather station (Chapter 2). It was found that a strong EASM occurs during the mature phase of El Niño, rather than the developing year. The EAM record, based on δD_{HPW} data, therefore further confirms the relationship between El Niño and EASM on timescales exceeding instrumental data

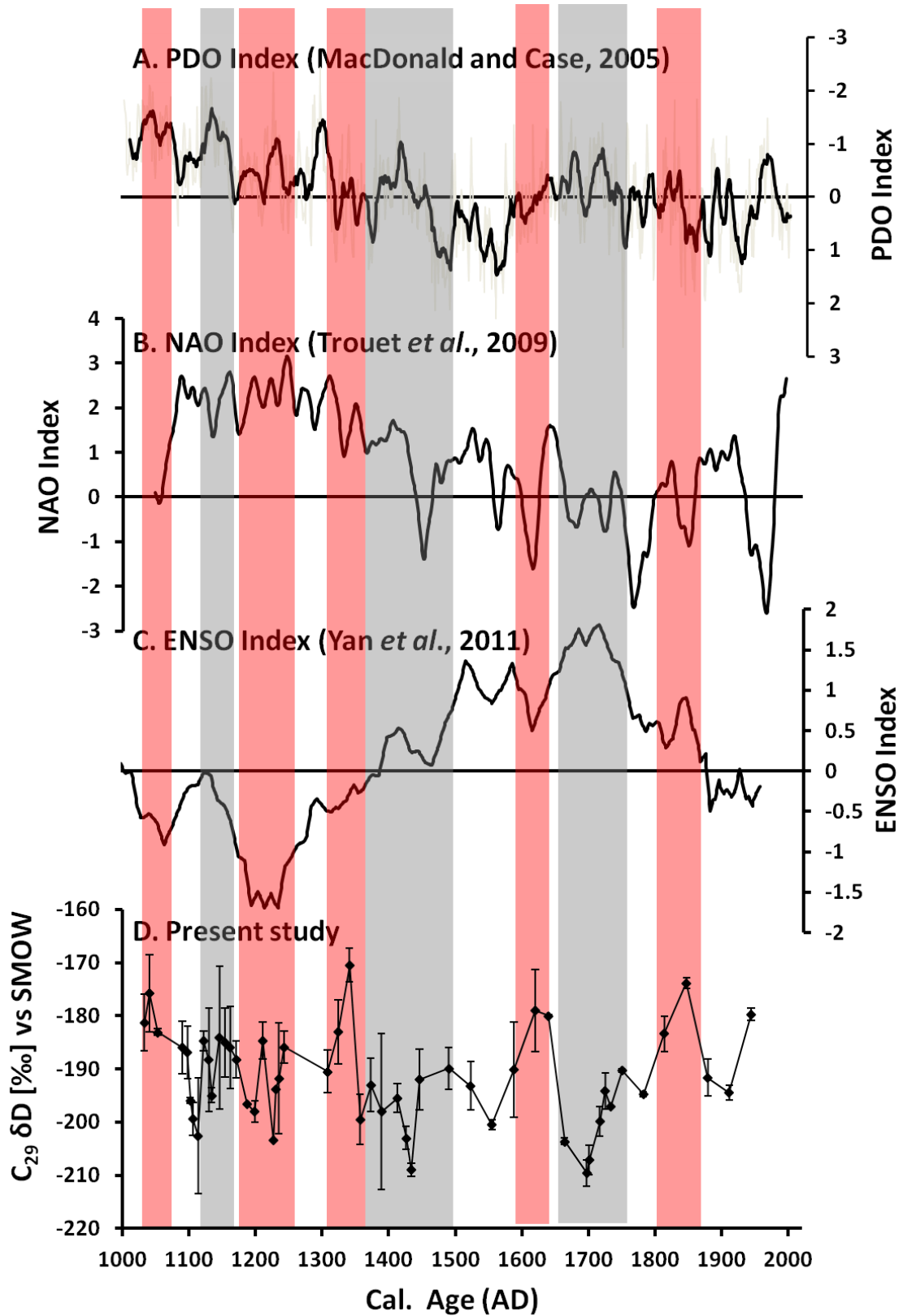


Figure 8-10: Variations in the δD_{HPW} record compared with teleconnections; A. PDO index by Macdonald and Case (2009) (scale inverted), B. the NAO index by Trouet et al. (2009), C. ENSO Index by Yan et al. (2011), D. the down-core variations in the δD_{HPW} values (present study). Grey bars highlights time periods identified as strong EAWM time periods and red bars highlights time periods identified as strong EASM time periods.

8.4.4 Hydrological variability in Hokkaido during the MWP and LIA

8.4.4.1 δD_{HPW} during the MWP

The MWP is defined here as 1000-1350AD because this time period is associated with higher than average δD_{HPW} values. The MWP (1000-1350AD) is characterised by high solar irradiance and positive APO index values (Figure 8-9). The teleconnections affecting this time period are negative PDO, positive NAO and El Niño conditions (Figure 8-10). High solar irradiance, positive APO index values and El Niño conditions were all identified to contribute towards a stronger EASM in the previous sections. The strong EASM during the MWP has been documented in many East Asian palaeo-climate studies (e.g. Hu et al., 2008; Figure 8-11). Zhou et al. (2011) also suggested that the EASM was in fact at its the strongest during this time period over the past 1000 years. Within Japan, previous studies have found that the MWP in Japan is characterised by warm and wet climate (Yamada et al., 2010), suggesting the increased intensity of the EASM during the MWP influenced Japan.

A strong EASM during the MWP would result in the northward movement of the NPSH, which would expose Hokkaido to an increased influence from air-masses originating from the Pacific Ocean and hence record higher δD_{HPW} values. Corresponding to stronger EASM during the MWP, we would therefore expect to see high δD_{HPW} values throughout this time period. Although δD_{HPW} values are generally increased during this time period in the Lake Toyoni down-core sedimentary record (Figure 8-7), the MWP is also characterised by considerable variability. Moreover, compared to the relationship between solar irradiance and δD_{HPW} values in the rest of the record, the relationship during the MWP is less pronounced. A suggested reason for this is that the OH was also enhanced during this time period and acted as a barrier for the northward movement of the strengthened NPSH and dampened the influence of the EASM in Hokkaido (e.g. Nakamura and Fukamachi, 2004) (Figure 8-6).

Evidence that suggests that the OH was enhanced during the MWP is the increased thermal contrast and the positive phase of the NAO/AO during this time. In the same way that the increased thermal contrast positively influences the strength of the NPSH, it also influences the strength of the OH (Nakamura

and Fukamachi, 2004). Therefore, the influence of land-sea thermal contrast can positively influence both the EASM intensity as well as the OH intensity and for the Hokkaido region; it appears that the OH had a stronger influence on climate during the MWP.

In addition to increased land-sea thermal contrast, the strength of the OH (Ogi et al., 2004) and the EASM (Gong and Ho, 2003, Lee and Park, 2015) are also both influenced by the positive phase of the NAO/AO. When the NAO/AO is in its positive phase, there is northward shift of westerly jet stream during summer, which causing an increase in the intensity of the EASM (Lee and Park, 2015). As a result, the positive NAO/AO (Figure 8-10) and APO index values (Figure 8-9) create conditions for an intensified OH, as well as, a strong EASM, which can work against each other in their climate forcing mechanisms.

8.4.4.2 δD_{HPW} during the LIA

In comparison to the high solar irradiance and high APO index values during the MWP, the LIA is characterised by relatively low solar irradiance and low APO index values (Figure 8-9). This is reflected in more depleted δD_{HPW} values for the most part of the LIA (Figure 8-9) and suggests that the polar air-masses (from the EAWM and OH) dominated the moisture supply to Hokkaido in comparison to the influence of the EASM (an exception being ~1600AD, which is further discussed in Section 1.5.4.3.3). There are two time periods with enhanced EAWM intensity are recorded in the Lake Toyoni sedimentary record ($\delta D_{HPW-COR}$ values $<72\text{‰}$; Figure 8-8). Both time periods are associated with solar minima events, namely the Spörer minimum and the Maunder Minimum (Figure 8-9). The presence of two cold events within the LIA has been identified in other Japanese records (e.g. Adhikari and Kumon, 2001; Yamada et al., 2010). The timing of the cooling events is slightly different in all records; the timings roughly correspond to the 15th century and 18th century. The timings of these cold events are consistent with the timing of EASM weakening, as documented in high $\delta^{18}O$ values in Heshang stalagmite (Figure 8-11; Hu et al., 2008), suggesting a potential inverse relationship between the EASM and the EAWM (further discussed in section 8.4.7).

8.4.4.2.1 15TH century cooling

The first intensification of the EAWM during the LIA occurs directly at the onset of the LIA and is associated with the Spörer minima. The cooling at the onset of the LIA was abrupt based on the δD_{HPW} values from Lake Toyoni (Figure 8-7). The abrupt change is associated with a distinct decrease in solar activity to the lowest values of solar irradiance recorded over the past 1000 years (Figure 8-9) and a shift to the negative phase of the NAO/AO and positive phase of the PDO (Figure 8-10). Solar forcing can cause a shift in the NAO/AO patterns, with increases in solar forcing resulting in a positive AO phase and decreased solar forcing causes shifts to a negative AO phase (Shindell et al., 2001). The dramatic decrease in solar activity during this time period have may resulted in a shift to a negative NAO/AO phase, as well, which results in a decrease in the EASM intensity and an increase in the EAWM (Lee and Park, 2015). Within the Lake Toyoni sedimentary record, all shifts to negative NAO/AO time periods are associated with low δD_{HPW} values (highlighted with grey bars in Figure 8-10). This suggests that the negative phase of the AO strongly influences the intensity of the EAWM at this site.

8.4.4.2.2 18th century cooling

The second intensification of the EAWM ($\delta D_{HPW-COR}$ values $<72\%$; Figure 8-8) occurred during the Maunder minima (Figure 8-9). The lowest δD_{HPW} values in the down-core sedimentary record are recorded during this time. Significantly, D'Arrigo et al. (1997) also found the lowest value in the record for a ring-width chronology of Kashiwa oak for north coastal Hokkaido occurred in 1784AD (D'Arrigo et al., 1997). Larger ring-widths occur when the growth of the trees increase, which is related to warm early summers. Smaller ring-widths therefore occur when summers are cold, providing further evidence for cold conditions during this time period. In addition, Yamada et al. (2010) also found a large increase in coarse-grained input into lakes Ni-no-Megata and San-no-Megata, Northern Japan, which was interpreted as a EAWM signal. This provides further evidence for an enhanced EAWM in Hokkaido during this time.

Similar to the 15th century cooling, the 18th century cooling is also associated with the positive phase of the PDO and the negative phase of the NAO/AO. However, the magnitude of these shifts in the PDO and the NAO/AO are much smaller during the 18th century cooling in comparison to the 15th century cooling, despite δD_{HPW} values during the 18th century being lower. It is suggested that other forcing mechanisms in addition to the PDO and the NAO/AO are responsible for the extremely low values during this time period. For instance, the very low δD_{HPW} values within this time period may be associated with volcanic eruptions in Japan and Iceland during the 1700's (after Davi et al., 2002). The cooling associated with volcanic eruptions and low solar irradiance may have prevented the northward movement of the NPSH and therefore the influence of the EASM is reduced, or even absent, during this time period. In addition to volcanic eruptions during the Maunder minimum, the glaciers advanced to their maximum extent in the southeastern Tibetan Plateau (Xu et al., 2012). The presence of increased glaciated conditions positively influences the intensity of the EAWM through a southward shift in the latitudinal position of the SibH (Chen and Huang, 1998). This suggests that the stronger EAWM during this time period brought cold air from the intensified SibH towards Hokkaido.

8.4.4.2.3 17th century warming

The cold conditions associated with the LIA were disturbed by an intensification of the EASM leading into the 1600's ($\delta D_{HPW-COR}$ values $>-55\%$; Figure 8-8). This time period is also associated with a solar maximum and a switch from negative to positive APO index values. This switch from negative to positive APO index values provides further evidence for the influence of increased land-sea thermal contrast resulting in a stronger NPSH. The increased strength of this high-pressure system allowed Hokkaido to come under the influence of the EASM, and hence record higher δD_{HPW} values. Unlike the MWP, the OH did not block the movement of the NPSH at this time, possibly as a result of the lower NAO/AO index values compared to the MWP values. The climate at this time in Hokkaido was characterised by warm and wet conditions as a result of an enhanced EASM.

A warm event was also found within the LIA based on alkenone-derived temperature reconstructions from two lake records (Lake Gahai and Lake Suga) on the northern Tibetan Plateau (He et al., 2013). This warm event was between

1590 and 1650AD, which is similar in timing to the warming event at Lake Toyoni. He et al. (2013) found a strong relationship between temperature changes at solar activity on the northern Tibetan Plateau. This provides further evidence to suggest the warming in Hokkaido was associated with high solar irradiance values during this time period. We found a strong control of the EASM was El Niño (previous section). During the intensification of the EASM ~1600's, we find that the ENSO index decreases; suggesting more El Niño occurrences. In addition to ENSO, a potential mechanism for the EASM intensifying during this particular time period may be associated with the switch from a positive PDO to a negative PDO (Figure 8-10). When the PDO is in its negative phase, the NPSH intensifies (Tsuji et al., 2008) resulting in an increased influence from the southerly monsoonal winds in Hokkaido from the Pacific Ocean (high δD_{HPW} values).

8.4.5 Post 1800 AD

The time period between 1800-present is characterised by a strong EASM between 1814 and 1847AD (less depleted δD_{HPW} values). The time period between 1814 and 1847AD is associated with a strong EASM ($\delta D_{HPW-COR}$ values $> -55\%$; Figure 8-8). This strong EASM is also documented in other EASM records (Figure 8-12). Suggested reasons for the intensification during this time period are (1) a decrease in ENSO index values (more El Niño conditions) and (2) positive APO values. Both of these factors were identified to contribute towards a strong EASM.

8.4.6 Short core TY11

We also have δD_{HPW} values for the shot core taken in 2011 (TY11). This sediment core, however, does not have an age model and is therefore discussed against depth. Overall, the δD_{HPW} values from the short core records a decrease in the EASM intensity, however, there was a brief intensification between 4-2cm (Figure 8-11). Particularly there was a weakening between 1963 (2cm) and present (0cm). Temperatures over the past ~50 years have increased as a result of human-induced climate change. We might expect that the EASM would in fact

increase in intensity due to the warmer conditions (Xu et al., 2006); however, the EASM has weakening during this time (Xu et al., 2006, Ding et al., 2008, Hu et al., 2008, Zhu et al., 2012). The weakening of the EASM during this time period has been attributed to [1] a weakening of southwesterly winds due to human-induced increased temperatures (emissions of greenhouse gases; [GHG]) (Zhu et al., 2012) and [2] cooling over south central China as a result of air pollution and warming over the western North Pacific Ocean (Xu et al., 2006). Given that the emissions of GHGs and also increased air pollution are as a result of human activities, it is suggested that the weakening of the EASM during this time period is as a result of anthropogenic-induced climate change. Conversely, Dabang and Huijun. (2005) suggested that the weakening of the EASM during this time period is a result of natural variability rather than anthropogenic warming. If the weakening of the EASM is due to anthropogenic-induced climate change, there will have future implications as greenhouse gases and air pollution continue to increase.

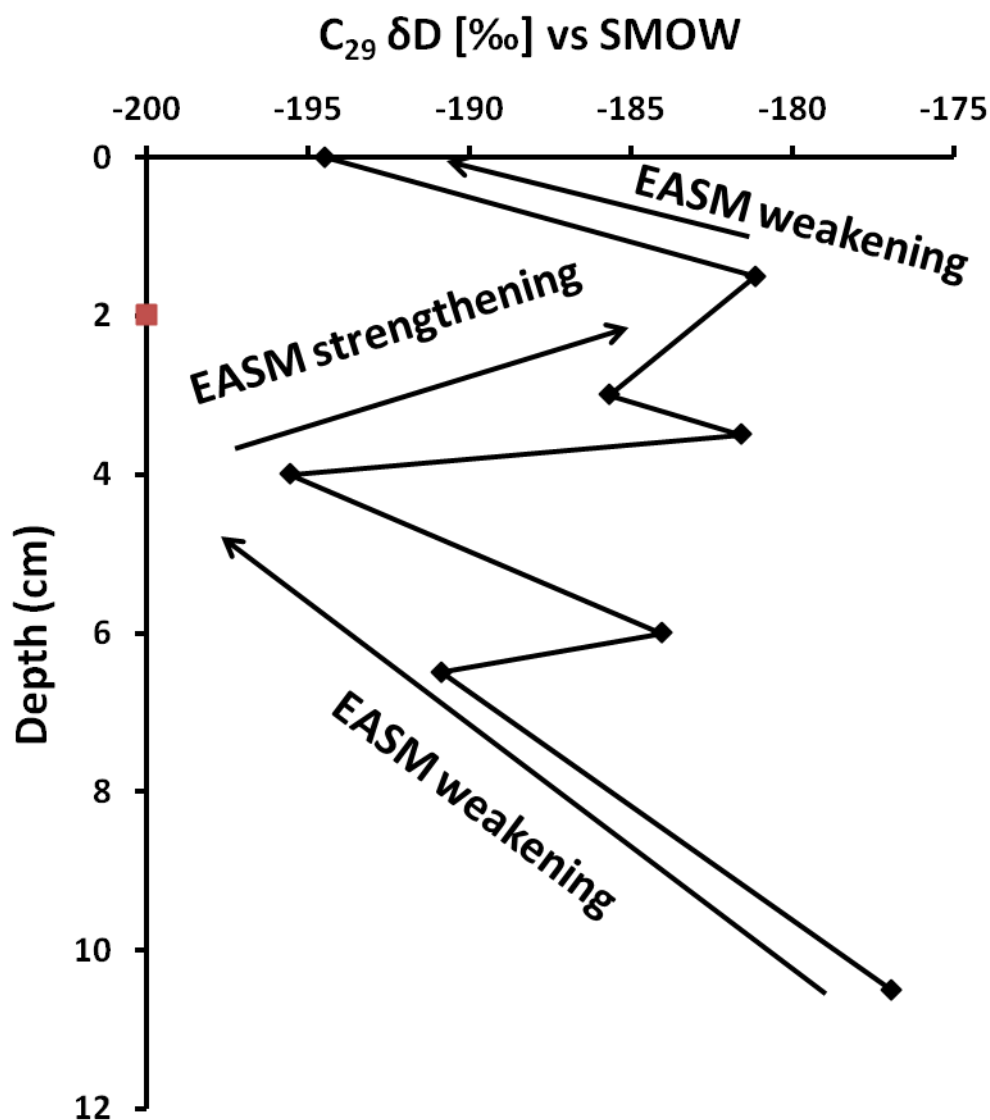


Figure 8-11: Variations in the $\delta D C_{29}$ from short core (TY11) from Lake Toyoni, Japan. Red dot represents Pu dating at 2cm giving a date of 1963.

8.4.7 Relationship between the EASM and the EAWM

The relationship between the EASM and the EAWM is currently poorly understood. Whilst some researchers' suggest that the EASM and the EAWM are inversely connected, e.g. a strong EASM occurs when the EAWM weakens and vice versa (Liu et al., 2009b, Sagawa et al., 2014), others suggest that there is no inverse relationship between the EASM and the EAWM, e.g. a strong EASM and strong EAWM occur together and a weak EASM and weak EAWM occur together (Yan et al., 2011b). In order to investigate the relationship between the EASM and the EAWM, we compared the δD_{HPW} record with EASM and EAWM records.

The δD_{HPW} record was firstly compared with EASM records of Hu et al. (2008) and Yamada et al. (2016) (Figure 8-10). There is a clear resemblance between the records from Heshang stalagmite and Lake Toyoni. A key finding when comparing the δD_{HPW} record from Lake Toyoni to Heshang stalagmite is that when the $\delta^{18}O$ values increase (highlighted with grey bars in Figure 8-12), suggesting a weakening in the EASM, we find an intensification of the EAWM record at the same time ($\delta D_{HPW-COR}$ values $<72\%$; Figure 8-8). This provides strong evidence for an inverse relationship between the EASM and the EAWM, at least during these time periods. Based on the evidence of the consistency in the timing between the intensification of the EAWM (once during the MWP and twice during the LIA) in the Lake Toyoni record and the timing of the weakening of the EASM in the Heshang stalagmite record, we provide further evidence to support the idea that a weakening of the EASM results in a strengthening of the EAWM.

To provide further evidence for the relationship between the EASM and the EAWM, we compared the δD_{HPW} record with a reconstruction of the SibH by Meeker and Mayewski. (2002; Figure 8-12). The EAWM is controlled by the intensity of the SibH therefore by comparing the δD_{HPW} record with reconstruction by Meeker and Mayewski. (2002), we can investigate the relationship between the EASM and the EAWM. The record shows that time periods identified as strong EASM time periods (less depleted δD_{HPW} values) occurred when there was a weak EAWM (low SLP values). This suggests that a weakening of the intensity of EAWM has a positive influence on the strengthening of the EASM. It was therefore found that there appears to be an inverse relationship between the EASM and the EAWM over the past 1000 years at this site.

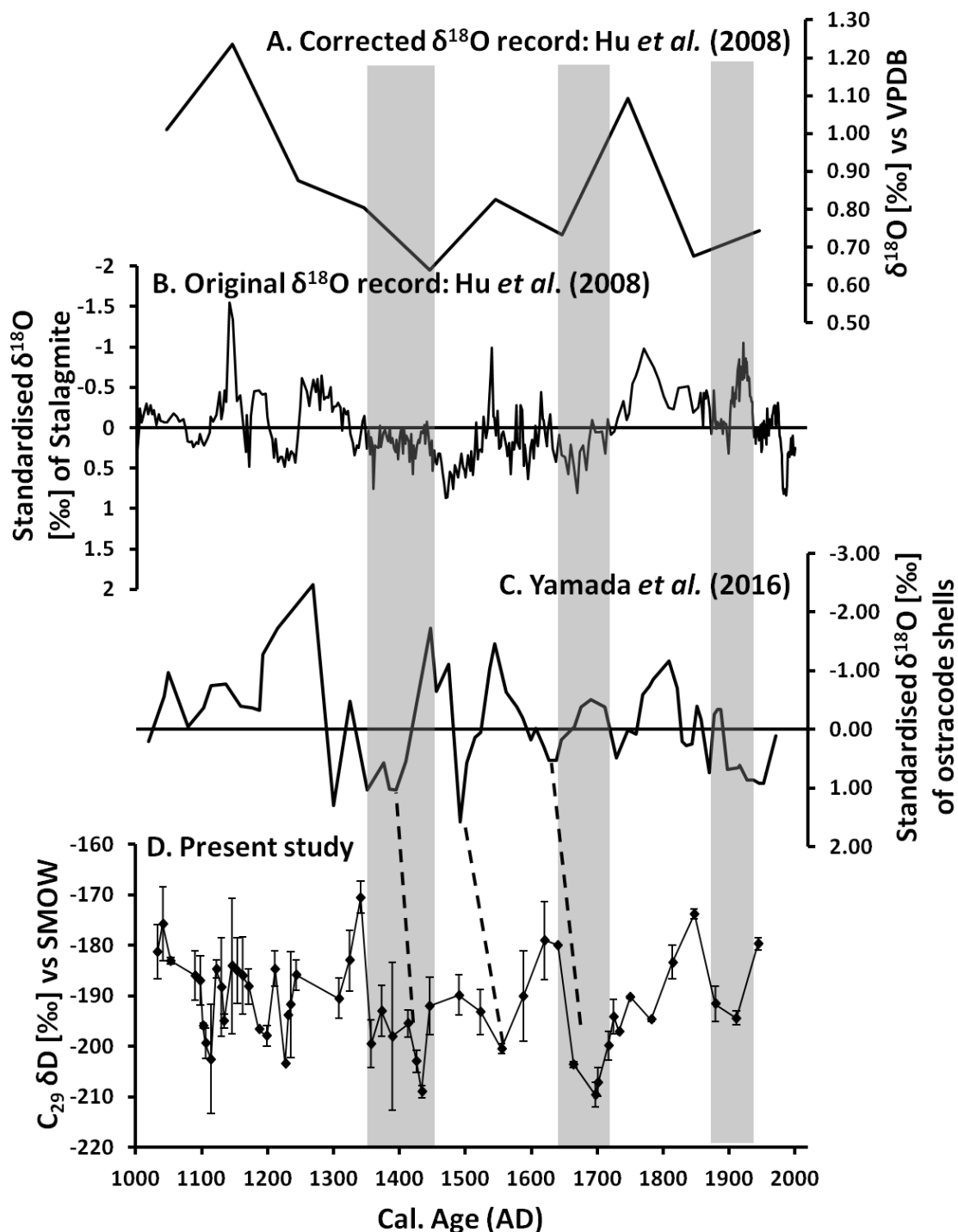


Figure 8-12: Comparison of the normalised δD_{HPW} variations over the past 1000 years with EASM records. A: The corrected Hersheng stalagmite record (Hu et al., 2008), B: the original $\delta^{18}O$ values from the Heshang stalagmite (Hu et al., 2008) (Note: values have been normalised and the axis is also reversed to show the EASM all going in same direction), C: The bottom graph is the normalised δD_{HPW} variations over the past 1000 years (present study). Grey shading indicates time periods when the EASM weakened based on the corrected Hersheng stalagmite record (Hu et al., 2008) (graph A).

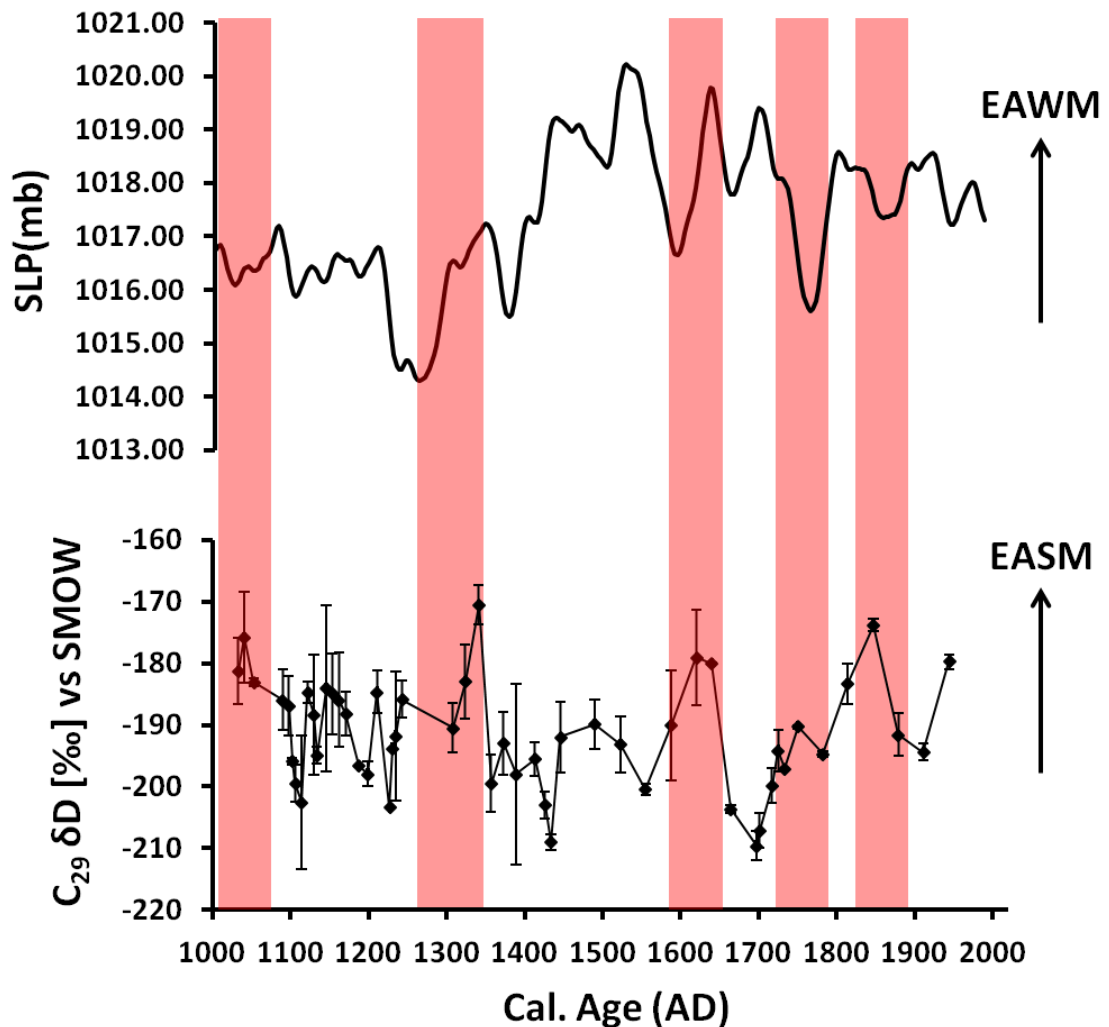


Figure 8-13: Comparison of the δD_{HPW} variations over the past 1000 years with the intensity of the SibH. Top graph: SibH reconstruction by Meeker and Mayewski. (2002). Bottom graph: δD_{HPW} variations over the past 1000 years (present study). Red shading indicates time periods when the EASM strengthened based on the findings from this study.

8.5 Conclusions

The δD_{HPW} preserved in sedimentary record of Lake Toyoni provides a unique archive of the source of precipitation (and hence the EAM) in Hokkaido and the competing influences of solar irradiance and teleconnections (e.g. ENSO/PDO/AO) over the past 1000 years. We find that the EAM intensity shows a clear resemblance to changes in solar irradiance with the EASM increasing in intensity during solar maxima and the EAWM increasing in intensity during solar minima. In addition, we found that the EAWM was strongly influenced by El Niño conditions and the EAWM was influenced by the negative phase of the NAO/AO.

The high solar irradiance and positive AO (NAO) during the MWP resulted in key conditions for an intensified EASM, as well as, a strong OH. Although the EASM was strong during this time period, the presence of the intensified OH during the MWP resulted in a reduced influence of the EASM in Hokkaido compared to other records within in the EAM domain. Within the LIA, the EAWM enhanced in the 15th century and the 18th century associated with the time periods of the Spörer Minimum and the Maunder Minimum, respectively. The cooling during the LIA was disturbed with an enhancement of the EASM leading in the 1600's. The increased influence of the EASM during this time is likely associated with the negative phase of the PDO enhancing the strength of the NPSH. The EASM was strong between 1814-1847AD. Over the past ~50 years, we found a decrease in the intensity of the EASM and attributed this change as a result of human-induced climate change.

The δD_{HPW} record was compared with an EASM record from $\delta^{18}O$ record from Heshang stalagmite (Hu et al., 2008) and a SibH (and hence EAWM intensification) reconstruction by Meeker and Mayewski. (2000) to establish if a relationship exists between the EASM and the EAWM. It was found that when the EAWM was enhanced in the Lake Toyoni record, the $\delta^{18}O$ record from Heshang stalagmite recorded a weakening in the EASM, suggesting a possible inverse relationship between the two EAM systems during these time periods. We also found that the EASM intensified when the SibH (and hence EAWM) weakened, providing further evidence for a possible inverse relationship between the EASM and the EAWM over the past 1000 years.

Synthesis

9.1 Summary

Two atmospheric circulation systems, the Westerlies and the East Asian monsoon (EAM), play a key role in East Asian climate variability. However, the interactions between the Westerlies and the EAM over the past 1000 years remain unclear. In particular, there is debate about the relationship between the East Asian Summer Monsoon (EASM) and the East Asian Winter Monsoon (EAWM); some suggest that the two subsystems are inversely correlated (Liu et al., 2009b, Sagawa et al., 2014), whilst others suggest that they are not (Yan et al., 2011b). In addition, some studies in Japan group the intensification of the Westerlies and the EAWM together (e.g. Yamada and Fukusawa, 1999, Yamada, 2004). A comparison of multi-proxy investigations is necessary to develop reconstructions of the intensity changes and teleconnections between the Westerlies and EAM systems in Asia. The key objective of this thesis therefore was to reconstruct past climatic and hydrologic variability in East Asia using a multi-proxy approach from Lake Toyoni. This variability is controlled by the two key atmospheric systems; the Westerlies and the EAM, so the present study develops multi-proxy reconstructions to determine past climatic and hydrologic variability in Japan over the past 1000 years and aid in understanding the effects of the EAM and the Westerlies independently and interactively.

The EAM is divided into two sub-systems; the East Asia Summer monsoon (EASM) and the East Asian winter monsoon (EAWM). The EASM intensity can be directly represented by precipitation and temperature in Hokkaido, Japan: stronger (weaker) EASM circulation carries more (less) water vapour from the Pacific Ocean, resulting in higher (lower) precipitation and warmer (colder) temperatures (as previously demonstrated in chapter 2). In turn, warm and wet conditions positively influence lake productivity. The EASM was therefore investigated using; incoherent/ coherent (Inc/Coh) ratio as a precipitation proxy (Chapter 4), Silica/Rubidium (Si/Rb) and Carbon/Nitrogen (C/N) ratios as a productivity indicators (Chapter 4) and alkenones as a summer lake surface temperature (LST) proxy (Chapter 7). The EAWM intensity can be directly represented by coarse-grained aeolian input into Lake Toyoni and was investigated using the Titanium/Rb (Ti/Rb) as a proxy for aeolian input in combination with grain size analysis (Chapter 5). Similarly, the Westerlies intensity can be directly represented by fine-grained aeolian input into Lake Toyoni and was investigated using the Ti/Rb as a proxy for aeolian input in combination with grain size analysis (Chapter 5). Although all three climate modes are investigated independently from one other, the final chapter (Chapter 8) reports on the hydrogen stable isotopic values (δD) of *n*-alkanes derived from higher plant waxes (δD_{HPW}) over the past 1000 years, which provides information on the EASM and the EAWM. The multi-proxy findings are discussed in relation to each other, global climate variability and the controlling climate driver mechanisms. The presence of globally recognised events; namely the Medieval Warm Period (MWP) and the Little Ice Age (LIA) suggests that the climate in Hokkaido responded to global climate fluctuations. Over the past ~1000 years, global climate variability was driven by variations in volcanic forcing along with the variability of climate modes such as El Niño-Southern Oscillation (ENSO) and the North Atlantic Oscillation (NAO)/Arctic Oscillation (AO) (Jones et al., 2001). The findings from this study are therefore discussed in relation to global climate records.

9.2 Dominant climate modes over the past 1000 years

9.2.1 Climate modes during the MWP (1050-1350AD)

Multi-proxy climate and hydrological reconstructions reveal that the MWP (1000-1350 AD) in Hokkaido was characterised by high productivity (as inferred from high Si/Rb and low C/N ratios; Chapter 4), increased precipitation (as inferred from high Inc/Coh ratios; Chapter 4), increased summer LST (as inferred from alkenone-based LST reconstructions; Chapter 7), which suggests that it was strongly influenced by the EASM. In contrast, the EAWM was weakened during the MWP as inferred from a decrease in coarse grain size sediments and a decrease in Ti/Rb ratio values; Chapter 5. An intensification of the EASM and a weakening of the EAWM are further supported by a slight increase in δD_{HPW} values during this time period (Chapter 8).

Within the MWP, there was also an intensification of the Westerlies during the MWP between 1050-1122AD and 1277-1308AD, which is clearly defined by the combined evidence of increased fine-grained aeolian input (Chapter 5) and low δD_{HPW} values (Chapter 8). The Westerlies transport cold, dry air towards Japan and hence more depleted δD_{HPW} values that reflect the enhancement of the Westerlies during this time period.

9.2.2 Climate modes during the LIA (1360-1850AD)

The EASM- and Westerlies-dominated MWP came to an abrupt end ~1350AD in Hokkaido, Japan, and was followed by the colder conditions of the LIA (1350-1850AD). The LIA is split and discussed in two separate time periods below; the early LIA (13650-1600AD) and the late LIA (1600-1850AD).

9.2.2.1 Early LIA (1360-1580AD)

The onset of the LIA is characterised by an abrupt change in the EAM system. Morrill et al. (2003) also suggested that ~1350AD was the most prominent abrupt change in the EASM intensity over the past 4000 years based on a moving t-test calculation of a compilation of 36 palaeo-climate records. Since this publication, Lee and Park. (2015) also found an abrupt change in the EASM during this time period and attributed this as monsoon failure.

We find that the climate during the early LIA is driven by an intensification of the EAWM (1350-1600AD), as inferred from an increase in coarse-grained aeolian input (Figure 9-1). However, a brief period of EAWM weakening and an intensification of the Westerlies occurred between 1450-1520AD. In addition to a strong EAWM, the EASM weakened as inferred from a decrease in productivity (as inferred from low Si/Rb and high C/N ratio values), a decrease in precipitation (as inferred from low Inc/Coh ratio values) and an abrupt drop in summer LST (as inferred from alkenone-based temperature reconstructions). The intensification of the EAWM and a weakening of the EASM are further reflected in the more depleted δD_{HPW} values (Figure 9-1). Based on the multi-proxy reconstructions, we provide further evidence for an abrupt change in the EASM, suggesting monsoon failure during this time period.

9.2.2.2 Late LIA (1600-1850AD)

Although the EAWM was a dominant climate driver during the early LIA, its influence on the late LIA was reduced. In contrast, a mixture of the EASM (highlighted in red; Figure 9-1) and the EAWM (highlighted in grey; Figure 9-1) play key roles in determining the climate in Hokkaido during this period. The start of the late LIA (1600-1640AD) is associated with an enhancement of the EASM based on a sharp decrease in C/N ratio values and an increase in Si/Rb ratio values suggesting an increase in productivity (Figure 9-1). In addition, water temperatures (as inferred from alkenone-based reconstructions) show warming and high δD_{HPW} values provide further evidence for the enhancement of the EASM. (Figure 9-1). The aeolian record shows an increase in Ti/Rb ratio values and coarse-grained sediments. In other sections of the record, we interpret this as an intensification of the EAWM. However, we suggest that the EAWM was not enhanced during this time period based on the presence of a visible tephra layer in this section of the core. Volcanic ash contains Ti and therefore the high Ti/Rb values can be explained by the presence of volcanic ash. The presence of coarse-grained sediments is potentially from an increase in run-off into the lake under an enhanced EASM climate. Further evidence for increased rainfall during this time period is based on increased Inc/Coh values (Figure 9-1); a proxy for organic matter and hence run-off into Lake Toyoni.

The EASM also intensified between 1800AD and 1850AD based on warmer LST conditions (as inferred from alkenone-based reconstructions), increased precipitation (Inc/Coh ratio values) and increased δD_{HPW} values. At the same time, there is evidence for a significant decrease in the EAWM, as inferred from low Ti/Rb ratio values (Figure 9-1).

In between the two enhancements of the EASM during the LIA, the EAWM enhanced (1640-1780AD), as inferred from a reduction in the δD_{HPW} values. This time period was initially interpreted as an intensification of the Westerlies (Chapter 5), however, the more depleted δD_{HPW} values and a slight increase in coarse-grained aeolian input (increased Ti/Rb ratio values) (Figure 9-1). An enhancement of the EAWM brings cold air-mass towards Japan during winter and also results in colder summer temperatures based on the instrumental data (1958-2014AD; Chapter 2). Although the instrumental data suggests that strong EAWM time periods are associated with a decrease in summer temperatures (Chapter 2), the summer LST's do not show a decrease in temperatures associated with the intensification of the EAWM. A suggested reason for this will be provided in this discussion.

9.2.3 Climate modes 1850-1950AD

Climate during the 1850-1950AD appears to be driven mainly by the Westerlies based on presence of fine-grained sediments in this section of the record. The EASM was also active based on increased precipitation (increased Inc/Coh ratio values) and warm alkenone-based LST (Figure 9-1).

9.2.4 Short core

There are no XRF data for TY11, therefore the wind patterns cannot be determined. However, we do find a dramatic increase in productivity (lower C/N ratios) suggesting that a change in environmental conditions occurred during this time. The δD_{HPW} data record relatively high values with a decreasing trend. This suggests that the EAWM intensified and/or the EASM weakened. The dramatic decrease in the C/N ratios, however, does not reflect an increase in the EAWM/weakening of the EASM, because an increase in productivity in the rest of the record is indicative of the intensification of the EASM. We suggest that the

C/N ratios in this section of the record are responding to human-induced environmental change rather than climate-induced environmental change. The population in Hokkaido increased substantially over the past 100 years. Accompanying this increased population, there was an increase in building activity and agriculture activity. As a result of these activities, an increase in nutrients into the lake may have temporarily increased the productivity in the lake. This hypothesis is supported by the fact that an increase in productivity would result in anoxic sediments, which would stimulate a large increase in bacterial growth in the sediments with C/N ratio values lower than 4 (Lamb et al., 2006). Further evidence for bacterial degradation are the low CPI values during this time period.

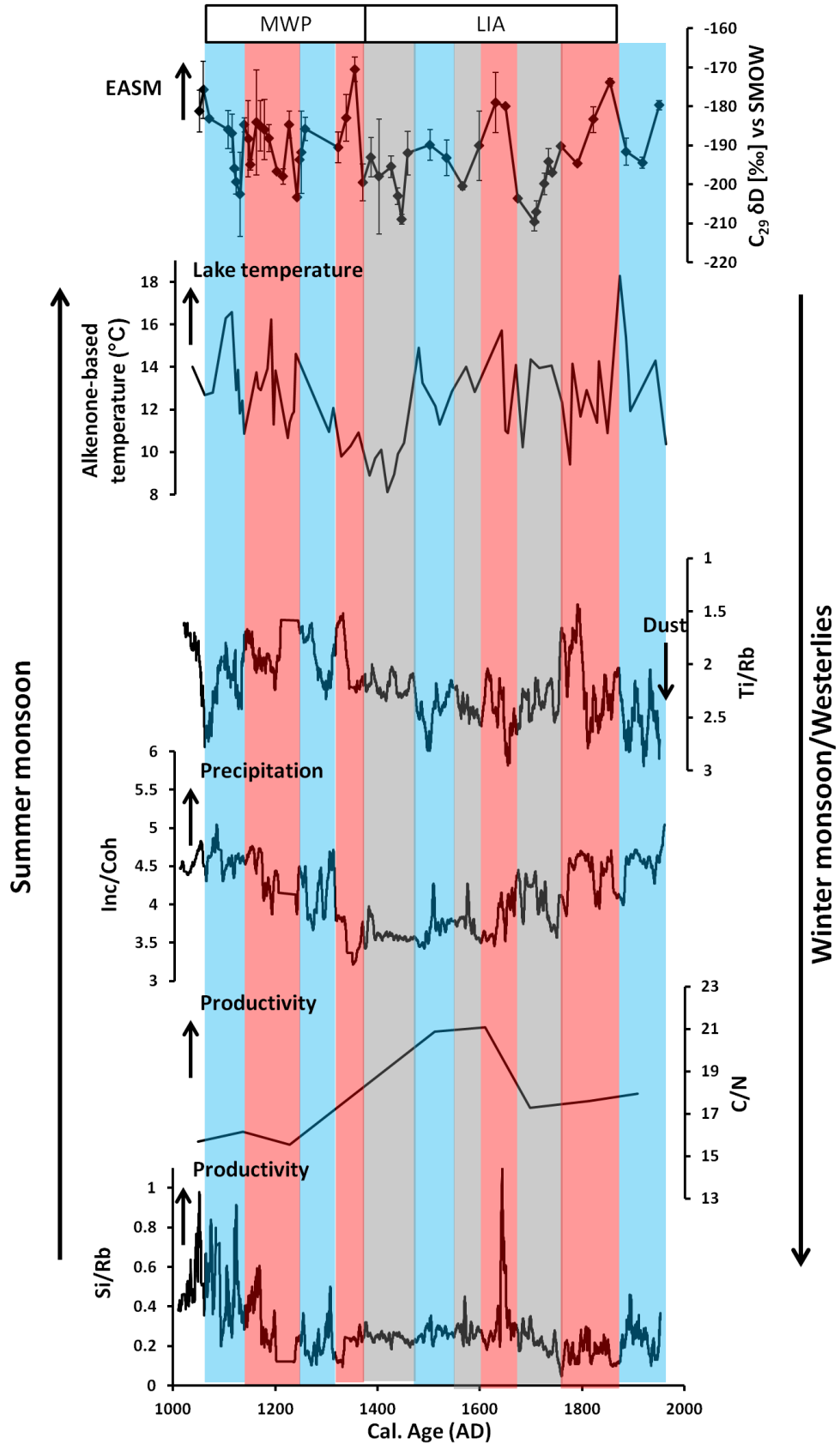


Figure 9-1: Multi-proxy climate reconstructions from Lake Toyoni over the past 1000 years. From top to bottom; δD_{HPW} as a proxy for temperature and source of precipitation, alkenones as a LST proxy, Ti/Rb as an aeolian input proxy, Inc/Coh ratio as a precipitation proxy, C/N ratio and Si/Rb ratio as productivity proxies. Higher values on graphs indicate a stronger EASM (highlighted in red) and lower values indicate a stronger EAWM (highlighted in grey) and/or Westerlies input (highlighted in blue).

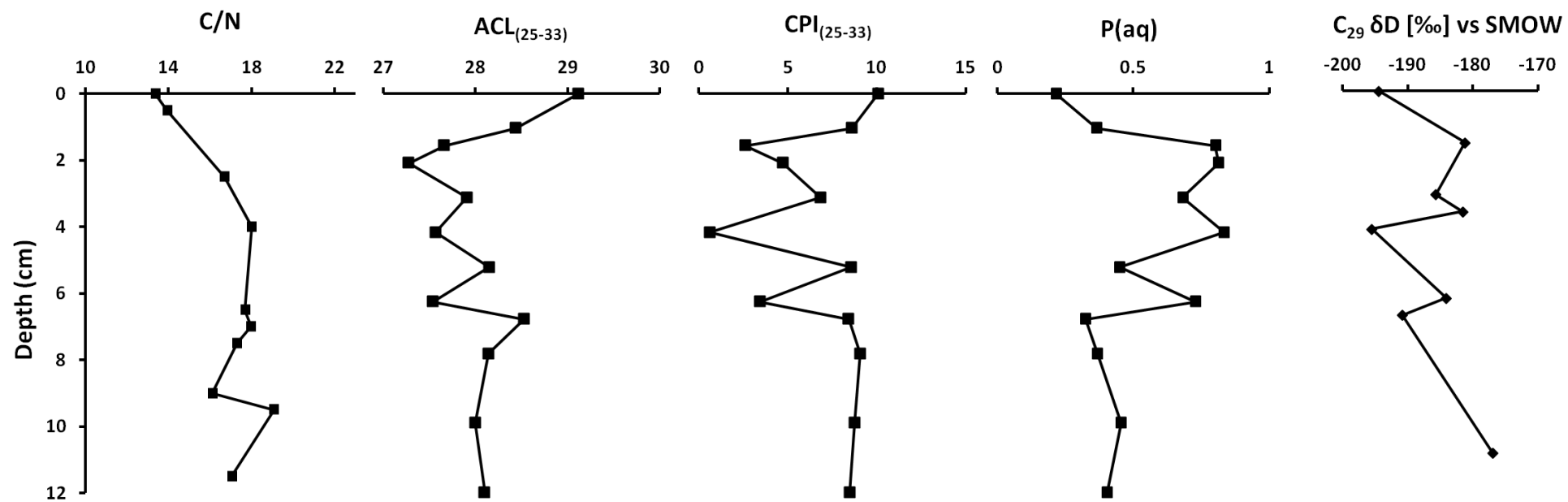


Figure 9-2: Downcore variations in C/N, ACL, CPI, P(aq) and δD_{HPW} from TY11.

9.3 Potential climate drivers of EASM intensification

Multi-proxy reconstructions from Lake Toyoni, Japan, show that the EASM was generally stronger during the MWP and the late LIA and weaker during the early LIA. However, there is a large degree of variability of the EASM within both the MWP and the LIA. Particular intensifications of the EASM occurred 1122-1277AD, 1308-1350AD, 1600-1640AD and 1800-1850AD.

9.3.1 The EASM and the NAO/AO

A teleconnection known to significantly influence climate in Hokkaido is the AO (Tsuji et al., 2008). The temperature patterns of the NAO and the AO are well connected (Thompson and Wallace, 1998) therefore we will use the NAO index by Trouet et al. (2009) to represent the AO in this study (after Lee and Park, 2015), because a record of the AO over the past 1000 years is not available (Figure 9-3). The positive phase of the NAO/AO persists for the entire MWP (Figure 9-3), which has been interpreted as a response to high solar forcing during this time period and was a driving factor for the warm MWP conditions (Trouet et al., 2009). A shift to the negative phase occurred at the onset of the LIA, which was characterised by weaker NAO phases. Similarly to the MWP, the positive phase of the AO has also been suggested as a link to the observed warming over the past 30 years in mid- to high-latitudes (Thompson et al., 2000). Within Asia, the positive phase of the AO also has a significant influence on the northward movement of the East Asian Subtropical Jet (EASJ), resulting in a strong EASM (Lee and Park, 2015). Our records show that the EASM is generally stronger when the NAO/AO is in its positive phase, providing further evidence for the link between the positive NAO and the EASM.

9.3.2 The EASM and the PDO

Hokkaido is adjacent to the North Pacific, and is therefore sensitive to SST anomalies that are influenced by the PDO. Therefore another teleconnection known to significantly influence the EASM is the PDO (Tsuji et al., 2008). Significantly, Schwing et al. (2003) investigated the decadal changes in the NAO and the PDO post 1900AD and suggested they are teleconnected on decadal

scales. Over the past 1000 years, there also appears to be a relationship between the positive NAO/AO and the negative PDO and vice versa (Figure 9-3). We find that the EASM generally intensifies during time periods associated with the negative PDO. Tsuji et al. (2008) also found that relative humidity increased when the PDO was in its negative phase due to the intensification of the North Pacific High. Furthermore, we investigated the phase of the PDO and its relationship with temperature and precipitation using modern day meteorological data (presented in Chapter 2) and found that the negative phase of the PDO resulted in wet conditions in June and September, which is associated with a strong EASM. In addition to the modern day meteorological weather data, the down-core sedimentary record also shows a strong relationship between the negative phase of the PDO and a strong EASM. The connection between the EASM and the negative PDO was particularly clear during the MWP ~1000-1300AD, which is associated with a persistent negative phase of the PDO. An exception is the intensification of the EASM ~1300AD, which occurred despite a positive phasing of the PDO. This suggests that the NAO is a stronger control on the EASM than the PDO.

9.3.3 The EASM and ENSO

The strongest control on the EASM, however, appears to be ENSO. We find that the EASM intensifies during El Niño conditions and also when there is a decrease in La Niña conditions (Figure 9-3). The ENSO reconstruction (Yan et al., 2011a) over the past 2000 years is based on precipitation records from Indo-Pacific and Galapagos. The Indonesian rainfall was derived from a salinity reconstruction based on planktonic-foraminifera $\delta^{18}\text{O}$ and the magnesium/calcium (Mg/Ca) ratio (Oppo et al., 2009). The precipitation variability in the Galapagos is derived from a lake level reconstruction which is based on the grain size data from the Lago El Junco sediment core (Conroy et al., 2008). The Southern Oscillation Index (SOI) is positively correlated with precipitation over the Indo-Pacific warm pool, and negatively correlated with precipitation over the eastern and mid-tropical Pacific. As a result, ENSO can be reconstructed by the difference between these precipitation records (Yan et al., 2011a).

The connection between El Niño and the EASM has resulted in contradictory theories. Some studies suggest that El Niño conditions results in a weaker EASM (e.g. Chen et al., 2015a), whilst others suggest that that El Niño events are

consistent with a strong EASM (e.g. Zhang et al., 1996, Wang et al., 2003, Hong et al., 2005). A suggested reason for the weakening of the EASM in response to El Niño conditions is provided by Chen et al. (2015). Chen et al. (2015) suggested that that the warming in the eastern Pacific Ocean induces an eastward propagating Kelvin wave resulting in warm western Pacific Ocean temperatures during El Niño (Chiang and Sobel, 2002, Xie et al., 2009), that weaken the land-sea thermal contrast and in turn weakens the Asian monsoon (Chen et al., 2015a). However, Wang et al. (2000) suggest that the resultant warming in the central Pacific in response to El Niño conditions plays a key role in cooling the western Pacific. Cooling in the western Pacific in turn provides key conditions for the development of the NPSH, which is a dominant control on the EASM (Wang et al., 2013a). Furthermore, Wang et al. (2001) found that the response of the intensification of the EASM to El Niño events occurred in the summer following the event. The authors found that the WPSH extends unusually westward in the summer following El Niño, which results in a strong EASM. We found a distinct relationship between the years following El Niño events and the intensification of the EASM in the instrumental record (Chapter 2). Significantly, in the years following the mature phase of El Niño, we find that precipitation at our site increases in June (Baiu precipitation) and August (Shurin precipitation); which is associated with EASM precipitation. We therefore suggest that El Niño positively influences the EASM in Hokkaido via its influence on the development and position of the WPSH (after Wang et al., 2001).

9.3.4 The intensification of the EASM and global climate variability

Our study confirms that the EASM is significantly influenced by global climate drivers (e.g. NAO/AO and ENSO). To further define the link between global and East Asian climate variability, we compare our records with:

1. A record of CO₂ (Frank et al., 2010; Figure 9-3). The record is based on a combination of proxy-based temperature reconstructions and CO₂ data from three ice-core records from Antarctica. Higher (lower) values suggest an increase (decrease) in atmospheric CO₂ levels.
2. A record of dust input to the Arctic (Meeker and Mayewski, 2002) (Figure 9-4). As discussed in previous chapter, the reconstruction is based on non

sea-salt potassium content in a Greenland ice core. Potassium within the ice-core is interpreted as dust input from central Asia when the SibH intensified (Meeker and Mayewski, 2002). An increase in the SibH (increase Sea Level Pressure [SPL] values Figure 9-3) suggests an increase in dust transport from Asia to Greenland.

3. A Norwegian glacial retreat record (Bakke et al., 2005) (Figure 9-4). The record is based on bulk density of glaciolacustrine sediments retrieved from two glacier-fed lakes and a peat bog north of the ice cap. Low bulk density values suggest increased organic sediments and high bulk density values suggest fine-grained poorly sorted minerogenic sediments. A correlation ($r^2=0.86$) was noted between bulk density and the temperature-precipitation equilibrium-line altitude (TP-ELA). A regression model was then used to transfer the bulk density record to TP-ELA values.
4. A Northern Hemisphere temperature record (Mann and Jones, 2003) (Figure 9-4) based on a compilation of 23 temperature reconstructions from 8 distinct regions, including records from different seasons, latitudes (e.g. tropical to polar environments) and includes both marine and terrestrial records. The reconstruction is consistent with previous reconstructions and model simulations of Northern Hemisphere mean temperatures over the past millennium within estimated uncertainties providing a reliable record of Northern Hemisphere temperature variability over the past 1000 years to compare with palaeo-climate reconstructions from Lake Toyoni.

Previous studies have provided evidence that the EASM responds to Northern Hemisphere climate (Guo et al., 1996, Morrill et al., 2003, Wang et al., 2005, Porter and Weijian, 2006, Wang et al., 2008c, Sun et al., 2012). The intensification of the EASM in Hokkaido is usually associated with notable decreases in dust input to the Arctic (Meeker and Mayewski, 2002), global warming (Mann and Jones, 2003) and glacial retreat (Bakke et al., 2005) (Figure 9-4), supporting the theory that the EASM responds to Northern Hemisphere climate. During warmer climates, there is a decrease in sea-ice extent, snow accumulation and a retreat in glaciers. The reduction in sea-ice and snow accumulation results in a stronger EASM (Tao et al., 2004, Zhao et al., 2004). A

suggested reason for this is that a decrease (increase) in snow cover results in warmer (colder) land temperatures over the Tibetan Plateau, which enhances (reduces) the land-sea temperature gradient and results in a strong (weak) EASM (Wu and Qian, 2003).

9.4 Potential climate drivers of EAWM intensification

A strong EAWM is defined as strong northerly winds, cold temperatures on the Asian continent and warm SST in the tropical western Pacific Ocean (Chen et al., 2000, Wang and Chen, 2014). Cold continental and warm oceanic conditions results in a high pressure system over the continent (e.g. the Siberian high; [SibH]) and a low pressure system over the adjacent ocean and hence a strong land-sea thermal contrast. A strong EAWM occurs when there is a strong SibH (Ding, 1990, Zhang et al., 1997, Wu et al., 2006a), the Ural-Siberian blocking increases (Cheung et al., 2012) and cold surges increase resulting in strong northerly winds, colder winter temperatures and increased snow cover in East Asia (Wen et al., 2009, Sun et al., 2010, Wang et al., 2011, Li and Wang, 2012).

Although Lake Toyoni is not located on the Asian continent, our study shows that the site is sensitive to changes in the EAWM. Multi-proxy reconstructions from Lake Toyoni, Japan, show that the EAWM was generally weak during the MWP and stronger during the LIA; in particular during the early LIA (1350-1450AD, 1520-1600AD and 1640-1780AD). Various teleconnections (e.g. AO and ENSO) can amplify/dampen these components resulting in a stronger/weaker EAWM. The relationship between teleconnections and the EAWM is now further discussed in relation to our findings from Lake Toyoni.

9.4.1 Impacts of the NAO/AO

We find that the EAWM (highlighted in grey Figure 9-2) is more associated with the negative phase of the NAO/AO than the positive phase of the NAO (Figure 9-3). The relationship between the EAWM and the AO was investigated in Chapter 2 using instrumental data from Hiroo weather station and shows a clear link between the EAWM intensification and the negative phase of the AO.

Other studies show that the intensity of the EAWM is related to the strength of the SibH (Ding, 1990, Zhang et al., 1997, Wu et al., 2006a), which refers to the

semi-permanent pressure system that accumulates cold, dry air in northeastern Siberia. In turn, a strong SibH closely relates to the negative phase of the AO (Gong et al., 2001) and hence the negative phase of the AO has a distinct influence on the strength of the EAWM. The mechanism behind the influence of the AO on the EAWM is due to the difference in pressure between high and low latitudes. When the AO is in its negative phase there is high pressure in the high latitudes and low pressure in the lower latitudes resulting in an advection of polar air mass to more southerly locations (Hurrell, 1995, Thompson and Wallace, 1998). An increase in cold air-masses in Asia increases snow and ice cover extent. Snow and ice extent also influence the strength of the SibH, and in turn the EAWM. Increased snow and ice increases the albedo, reduces the amount of solar radiation absorbed and lowers air temperatures, creating an enhanced SibH.

9.4.2 Impacts of ENSO

In addition to the NAO/AO, variability of ENSO is also an important forcing of the intensity of the EAWM. Notably, the intensification of the EAWM occurred contemporaneous with a change in ENSO conditions; from a dominant El Niño phase during the MWP to a dominant La Niña phase during the LIA. The consistency in the timing of a change of La Niña conditions and the enhanced EAWM suggests a relationship between ENSO and the EAWM system (Figure 9-3). All intensifications of the EAWM occur when there are increased La Niña years. This relationship between ENSO and the EAWM has been found in previous studies (Tomita and Yasunari, 1996, Zhang et al., 1996, Chen et al., 2000, Chen et al., 2013, Chen et al., 2014, Wang and Chen, 2014). A suggested reason for La Niña positively influencing the EAWM is due to the correlation between ENSO and the inter-annual variation of winter northerlies and cold surges near the South China Sea (Zhang et al., 1997). La Niña conditions result in cooling over the equatorial Eastern Pacific; however, the western Pacific is not influenced by this cooling and therefore remains warm during La Niña conditions (Chen et al., 2000). During La Niña events, the occurrence of East Asian cold surges and the strength of the northerlies increase (Zhang et al., 1997). This triggers a decrease in temperature in East Asia, resulting in a large land-sea thermal contrast during La Niña episodes and a movement of air from the Asian continent towards Japan. In the instrumental record (1958-2014AD; Chapter 2), we find that the intensification of the EAWM is associated with a decrease in summer

temperatures. The relationship between low summer temperatures (as inferred from alkenone-based LST's) and the EAWM intensification is demonstrated between 1350-1450AD in the sedimentary record. However, the EAWM intensification between 1520-1600AD and 1640-1780AD do not show a decrease in summer temperature (highlighted in grey in Figure 9-1). This is likely due to the strong La Niña episodes during these time periods, particularly associated with the EAWM intensification between 1640 and 1780AD. In the instrumental data we find that La Niña episodes are associated with slightly warmer summer temperatures (Chapter 2). As a result, La Niña episodes influence the intensity of EAWM (recorded as low δD_{HPW} values at Lake Toyoni) resulting in cold winters with heavy snowfall. However, summer temperatures remain high (as inferred from alkenone-based temperature reconstructions) during the La Niña years. In comparison, the summer temperatures are low during the EAWM intensification between 1350-1450AD. This time period is also associated with a change from the positive to the negative phase of the PDO (Figure 9-3). Previous studies have suggested that the influence of ENSO on the EAWM is weak during the positive phase of the PDO and strong during the negative phase of the PDO (Wang et al., 2008a). If this is the case, the reconstructed shift from a positive phase to a negative phase of the PDO ~1350AD may be an important reason behind the strong response of the EAWM to La Niña conditions. This time period is also associated with an abrupt change in the EASM in other records (Morrill et al., 2003, Lee and Park, 2015) therefore we suggest that the influence of the phase change of the PDO combined with a change from El Niño to La Niña conditions may have resulted in monsoon failure in this region.

9.4.3 The intensification of the EAWM and global climate variability

The abrupt intensification of the EAWM (increased input of coarse-grained dust) occurred ~1350AD; whereas, the decrease in global temperature occurred ~1430AD (Mann and Jones, 2003) (Figure 9-4). We find that the EAWM intensified ~80 years before a decrease in global temperatures (Figure 9-4). Although the timing may be influenced by errors in the age model, for example, the error on the age model at 1360AD is between 1491-1213AD. However, we suggest that there is potentially a relationship between the strengthened EAWM over East Asia and the initiation and also intensification of Northern Hemisphere cooling. Our hypothesis is that an increase in the EAWM increases input of dust transport

to the Pacific and the Arctic Ocean will result in increased iron input into the Pacific and Arctic Oceans, which is an essential and often limiting nutrient, resulting in increased phytoplankton production. Increasing phytoplankton production will act as a natural sink for carbon dioxide from the atmosphere and hence result in cooler climate conditions in the Northern hemisphere. In addition, previous studies also suggest that the biological pump is also more efficient during colder climates due to the complete consumption of nutrients by algae in locations where a large supply usually goes unutilised (Sigman and Boyle, 2000). This is supported by increased dust levels in the Greenland ice core (Meeker and Mayewski, 2002) during the intensification of the EAWM (~1350AD) increased (Figure 9-5).

Increased dust input will result in cooling in the Northern Hemisphere, which would then lead to a positive feedback loop between the EAWM and temperatures in the Northern hemisphere. For example, cooling in the high latitudes of the North Atlantic ocean, produce more extensive glacial conditions, which positively influences the intensity of the EAWM through a southward shift in the latitudinal position of the SibH pressure system (Chen et al., 1999b). The reconstruction of the SibH shows significant intensification during this time period, providing further evidence and winter temperature reconstructions based on historical documents by Ge et al. (2003) also show significant cooling. On the other hand, another reason for the cold temperatures ~1450AD may be due to the strong volcanic eruptions in 1453AD (Crowley, 2000) and low solar activity (Bard et al., 2000). Based on climate models, 41-64% of temperature variability over the past 1000 years is attributed to changes in solar irradiance and volcanism (Crowley, 2000). However, the subsequent intensification of the EAWM (1550-1580-AD) also occurred before Northern Hemisphere cooling and resulted in a decrease in temperatures. Although we suggest a possible connection between the intensification of the EAWM leading Northern Hemisphere cooling, the relationship between the timing of the EAWM and Northern Hemisphere cooling needs further investigation to determine the leads and lags between the EAWM and Northern Hemisphere cooling.

The transition between the MWP and the LIA (~1350AD) is associated with a time period of EAWM intensification. In addition to this change in atmospheric

processes, this transition period was also associated with changes in oceanic processes. For example, Bianchi and McCave (1999) use centennial-scale, Holocene-long North Atlantic sediment records of sortable silt that provides information of the strength of bottom currents, which were reduced during this time period (Bianchi and McCave, 1999). This suggests that the Atlantic Meridional Overturning Circulation (AMOC) was reduced and suggests that a possible connection exists between the AMOC and the EAM system. The connection between the AMOC and the EAM system has been previously studied by Sun et al. (2012). The authors suggested that the AMOC is a driver of abrupt changes in the EAWM and EASM systems using a coupled climate model simulation. When the AMOC was reduced, the heat transport northward is also reduced, which in turn results in the expansion of sea-ice conditions in the North Pacific and the Atlantic (Sun et al., 2012). In association with the cooling in the North Atlantic, there is a southward shift of the Intertropical Convergence Zone (ITCZ), significant strengthening of the EAWM and a weakening of the EASM (Sun et al., 2012). We see this expressed at Lake Toyoni as a cold time period.

9.5 Potential climate drivers of Westerlies intensification

Similar to the EAWM, an intensification of the Westerlies brings a cold air mass to Hokkaido (Fukusawa, 1999). The annual cycle of the Westerlies described by Kuang and Zhang (2005) and Lim and Matsumoto (2008) shows that the Westerlies influence the study site in July during their northward migration and in September during their southward migration. Multi-proxy reconstructions from Lake Toyoni, Japan, show that the Westerlies intensified at the study site between 1050-1122, 1277-1308, 1450-1520 and 1880-1945AD. We find that an enhancement of the Westerlies is often associated with increasing solar irradiance.

9.5.1 Impact of the NAO/AO

The AO is a measure of the strength of the polar vortex (stronger during the positive phase and weaker during the negative phase). Our results show that the Westerlies are enhanced when the NAO/AO is in its positive phase. The relationship between the positive phase of the NAO/AO and the Westerlies has been suggested in previous studies (e.g. Hurrell, 1995, Lee and Zhang, 2011). In

addition to the enhancement of the Westerlies during the positive phase of the NAO, the Westerlies are also located further north (Lee and Zhang, 2011). We suggest that when the Westerlies are located further south during the negative phase of the NAO, they do not influence our site to the same degree as during the positive phase of the NAO, when the Westerlies migrate northwards and their influence on this site is greatly increased. The southern migration of the Northern Hemisphere (NH) Westerlies has also been noted during the Last Glacial Maximum (LGM) (Ono and Irino, 2004). Accompanying the shift in the Westerlies during this time period is the EASJ, which shifted by around 3-5° of latitude during the LGM (Ono and Irino, 2004). The latitudinal shift of the Westerlies is demonstrated in Figure 9-5 (positive NAO/AO in Box A and B and the negative phase of the NAO/AO in Box C and D).

The accompanied shift in the EASJ with the Westerlies is responsible for the high summer temperatures (based on alkenone-temperature reconstructions) often recorded during time periods of strong Westerlies (highlighted in blue Figure 9-1). An enhancement of the Westerlies, like the EAWM, also results in an increase in cold air-masses to Hokkaido (Fukusawa, 1999), and hence low δD_{HPW} values. However, unlike the enhancement of the EAWM, we find that an enhancement of the Westerlies does not necessarily accompany cold summer temperatures. In fact, as previously stated, time periods associated with an enhancement of the Westerlies (increased in fine-grained dust and more depleted δD_{HPW} values) are also associated with slightly warmer summer temperatures due to the northward position of the EASJ. The northward location of the EASJ results in a stronger EASM and hence warmer summer temperatures (Figure 9-5).

The findings from the present study, therefore, show that there are strong differences between the climate in Hokkaido when the EAWM and the Westerlies are enhanced. This is significant because previous studies have grouped the EAWM and the Westerlies to occur in sync with one another (e.g. Yamada and Fukusawa, 1999, Yamada, 2004), whereas we find that although these systems both bring cold air-mass to Japan, they behave independently from each other and the mechanisms responsible for their intensification are fundamentally different. For example, a key difference is the phase of the NAO/AO. When the

AO is positive, the Westerlies are enhanced and located further north and the EAWM is weakened (Figure 9-5). On the other hand, when the AO is negative, the Westerlies are weaker, which strengthens the advection of polar air southward, resulting in a cooler air temperatures (Hurrell, 1995, Thompson and Wallace, 1998) and a stronger SibH (Gong et al., 2001). The EAWM is therefore intensified and moves further south (Figure 9-5).

9.5.2 Impact of ENSO

Unlike the phase of the NAO/AO, ENSO is not a strong an influence on the intensity of the Westerlies, since they are intensified during both El Niño and La Niña. However, we suggest that ENSO has an influence on the location (e.g. latitude) of the Westerlies. For example, we find that when there is a positive phase of the NAO/AO and the Westerlies are intensified and there is also El Niño conditions (e.g ~1200AD), the northern limit of the Westerlies is extended (Box A; Figure 9-5). During time periods when there is La Niña conditions and a positive phase of the NAO/AO, the Westerlies are located slightly south compared to time periods with El Niño conditions and a positive phase of the NAO/AO (box B; Figure 9-5). We find that the Westerlies are located directly over our study site during these time periods and have a very strong influence on the climate in Hokkaido. During the negative phase of the NAO/AO, the influence of the Westerlies at Lake Toyoni is weakened regardless of the state of ENSO (Figure 9-5).

9.5.3 The Westerlies and global climate variability

The moisture source for the Westerlies is the Atlantic Ocean. When the NAO is in its positive phase and the Westerlies intensify, there is an increased transport of a warm and moist maritime air-mass over Northern Europe and Scandinavia and hence there are warm and wet conditions in this location (Hurrell and Loon, 1997). On the other hand, Southern Europe and the Mediterranean experiences dry conditions under a positive NAO phase (Hurrell and Loon, 1997). As a result, we find that time periods associated with an intensification of the Westerlies are also associated with a retreat of glaciers in Norway (Figure 9-4) due to the increased transport of the warm, maritime air-mass via the Westerlies. The Westerlies therefore link the climates of the North Atlantic and Northern Japan.

We also find that the enhancement of the Westerlies is associated with an increase in carbon dioxide (CO₂) levels (Figure 9-4). There are two possible reasons for the elevated CO₂ levels during these time periods; firstly, the strengthened Westerlies promoted the release CO₂ or secondly, the release of CO₂ (and hence warming) increased the strength of the Westerlies. In the Southern Hemisphere, the poleward movement of the Westerlies promoted upwelling and the release of CO₂ from the ocean (Anderson et al., 2009, Toggweiler, 2009). We suggest that the stronger winds during time periods when the Westerlies intensified may have also promoted ocean upwelling in the Northern Hemisphere and hence the release of old carbon. This has implications for future climate variability because it may accerate warming in this region.

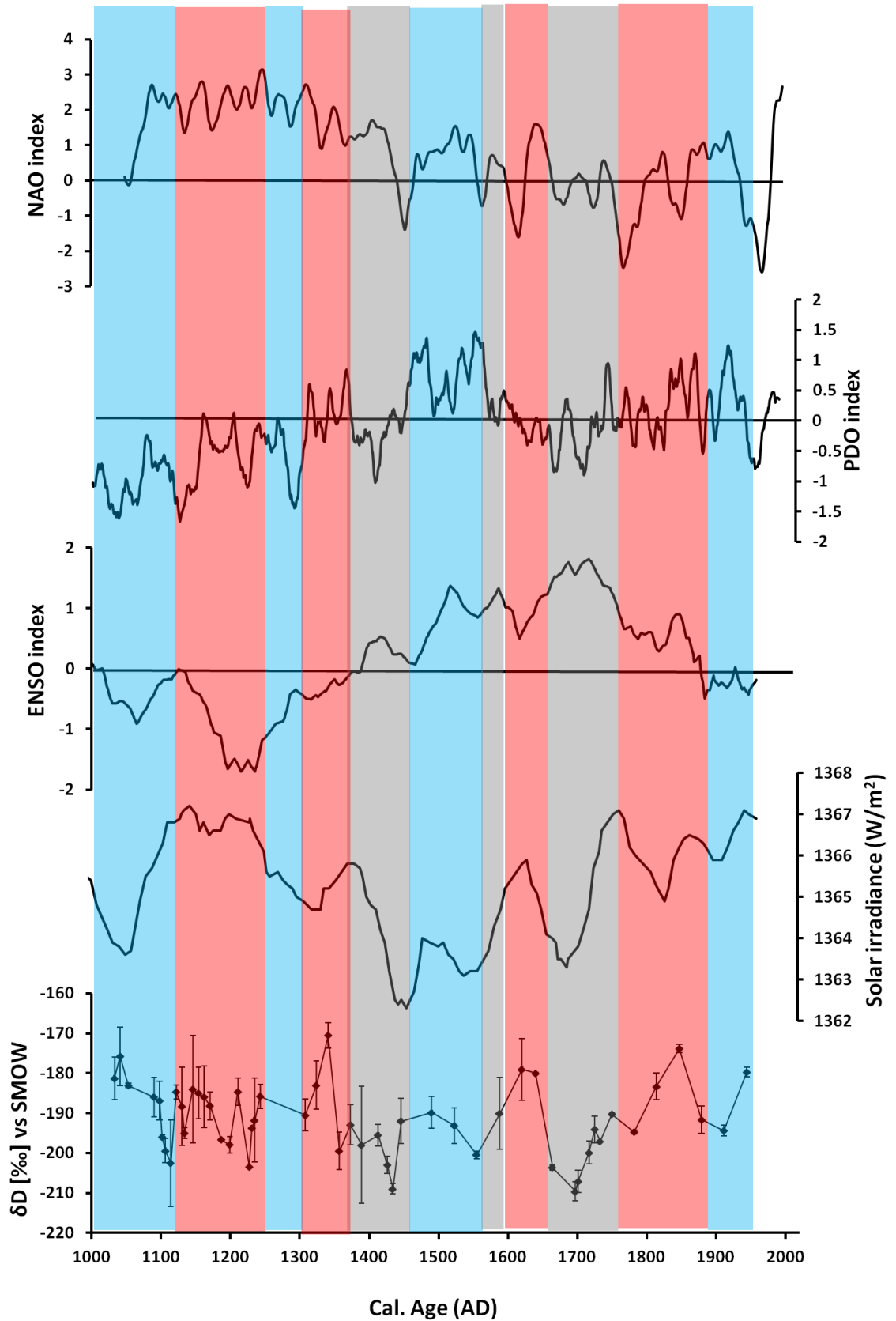


Figure 9-3: Variations in δD_{HPW} compared with global climate modes. From top to bottom the NAO index by Trouet et al. (2009), the PDO index by (MacDonald and Case, 2005), ENSO index reconstruction (Yan et al., 2011a); high values are La Niña and low values are El Niño, Solar Irradiance (w/m^2) by Bard et al. (2000) and the variations in δD_{HPW} from Lake Toyoni, Japan (present study).

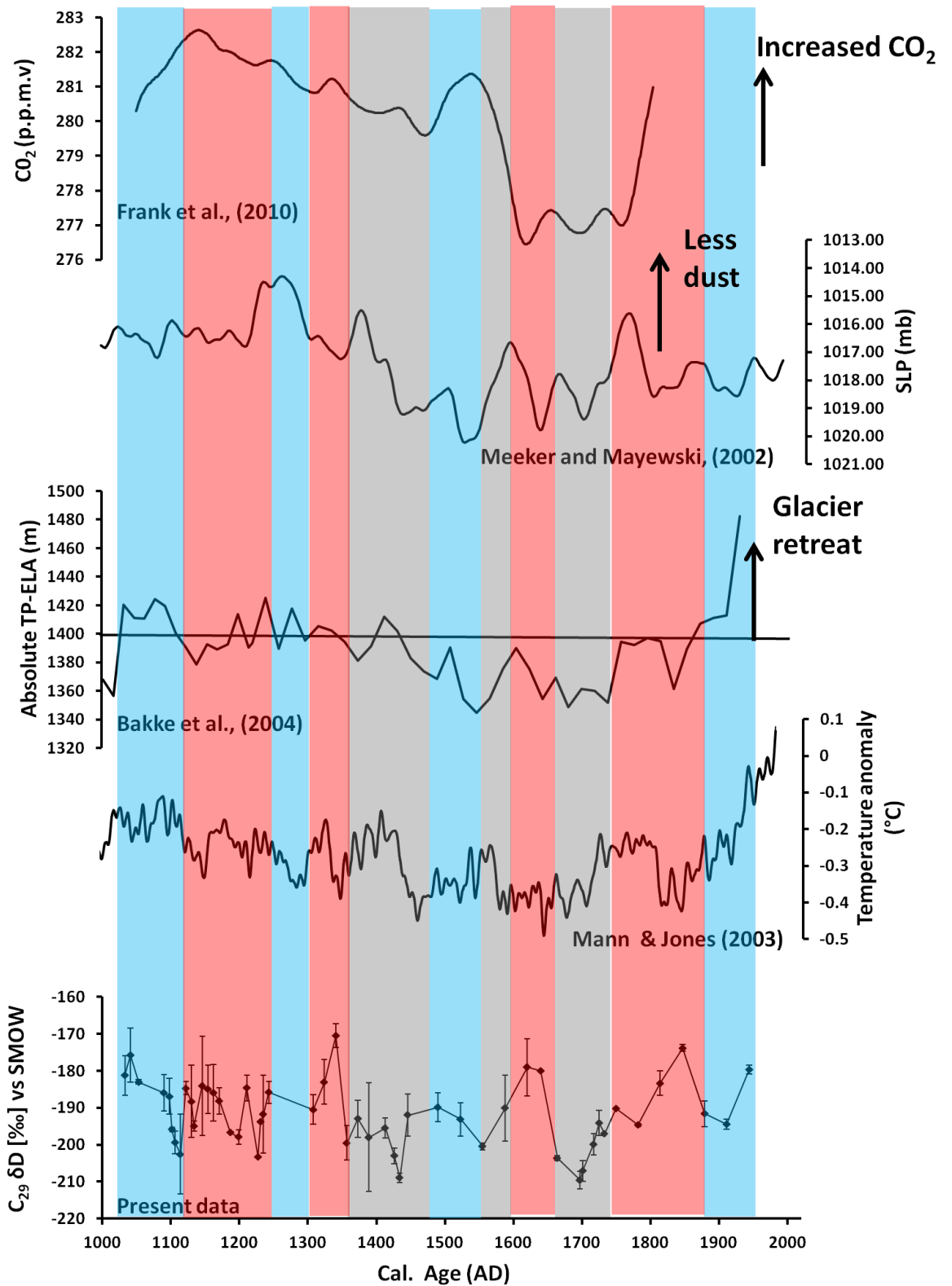


Figure 9-4: Variations in δD_{HPW} compared with global climate reconstructions. Going from top to bottom; a CO_2 record (50-year smoothed) (Frank et al., 2010), a dust record from a Greenland ice-core (Meeker and Mayewski, 2002), a glacier advance and retreat record (Bakke et al., 2005), a Northern Hemisphere surface temperature reconstruction (Mann and Jones, 2003) and the present δD_{HPW} data.

9.6 Combined impacts of the NAO/AO and ENSO

ENSO and the NAO/AO have been identified as key drivers of both global and regional climate variability. We find that ENSO and NAO/AO separately influence the EAM and the Westerlies in Hokkaido, as previously discussed. The combined influence of ENSO and the NAO/AO is now discussed in relation to the climate in Hokkaido.

ENSO and the NAO/AO are in-phase when El Niño and the positive phase of the NAO/AO are combined (referred to as the positive in-phase; Box A, Figure 9-5) and when La Niña and the negative phase of the NAO/AO are combined (referred to as the negative in-phase; Box D, Figure 9-5). ENSO and the NAO/AO are out of phase when Niño and the positive phase of the AO are combined Box B, Figure 9-5) or when La Niña and the positive phase of the NAO/AO are combined (Box C, Figure 9-5). The combined link between the NAO/AO and ENSO on the EAWM has been previously investigated by Cheung & Zhou. (2012). Cheung & Zhou. (2012) found a distinct relationship when the AO and ENSO were negative in-phase and the intensity of the EAWM. When the AO and ENSO were negative (positive) in-phase, they found that the SibH was stronger (weaker), the air-temperatures were lower (higher) in East Asia and there was more (less) Ural-Siberian blocking and hence a stronger (weaker) EAWM. Our results also show a clear relationship between the combined relationship of the NAO/AO and ENSO and the intensity of the EASM, EAWM and the Westerlies. We find that when the NAO/AO and ENSO are positive in-phase (e.g. positive AO and El Niño), the EAWM, the EASM limit and the EAJS is located further north and as a result there is a stronger EASM, weakening of the EAWM and the Westerlies are located further north (Box A, Figure 9-5). We also find that when the NAO/AO and ENSO are negative in-phase (e.g. negative AO and La Niña; box D, Figure 9-5) the EAWM, the EASM limit and the EAJS is located further south resulting in a weaker EASM, stronger EAWM and the Westerlies being located further south and hence not influencing the higher latitudes of Japan such as Hokkaido. When ENSO and the NAO/AO are out of phase (e.g. La Niña and positive phase of the NAO/AO), the EAWM, the EASM limit and the EAJS is located to the north however not as far north as when ENSO and NAO/AO are positive in-phase (box A, Figure 9-5). ENSO and the NAO/AO are also out of phase when there are El Niño and the

negative phase of the NAO/AO (Box C, Figure 9-5), during these time periods the EAWM the EASM limit and the EAJS is located slightly south of the study site and therefore the influence of the EAWM is stronger than the EASM during these time periods.

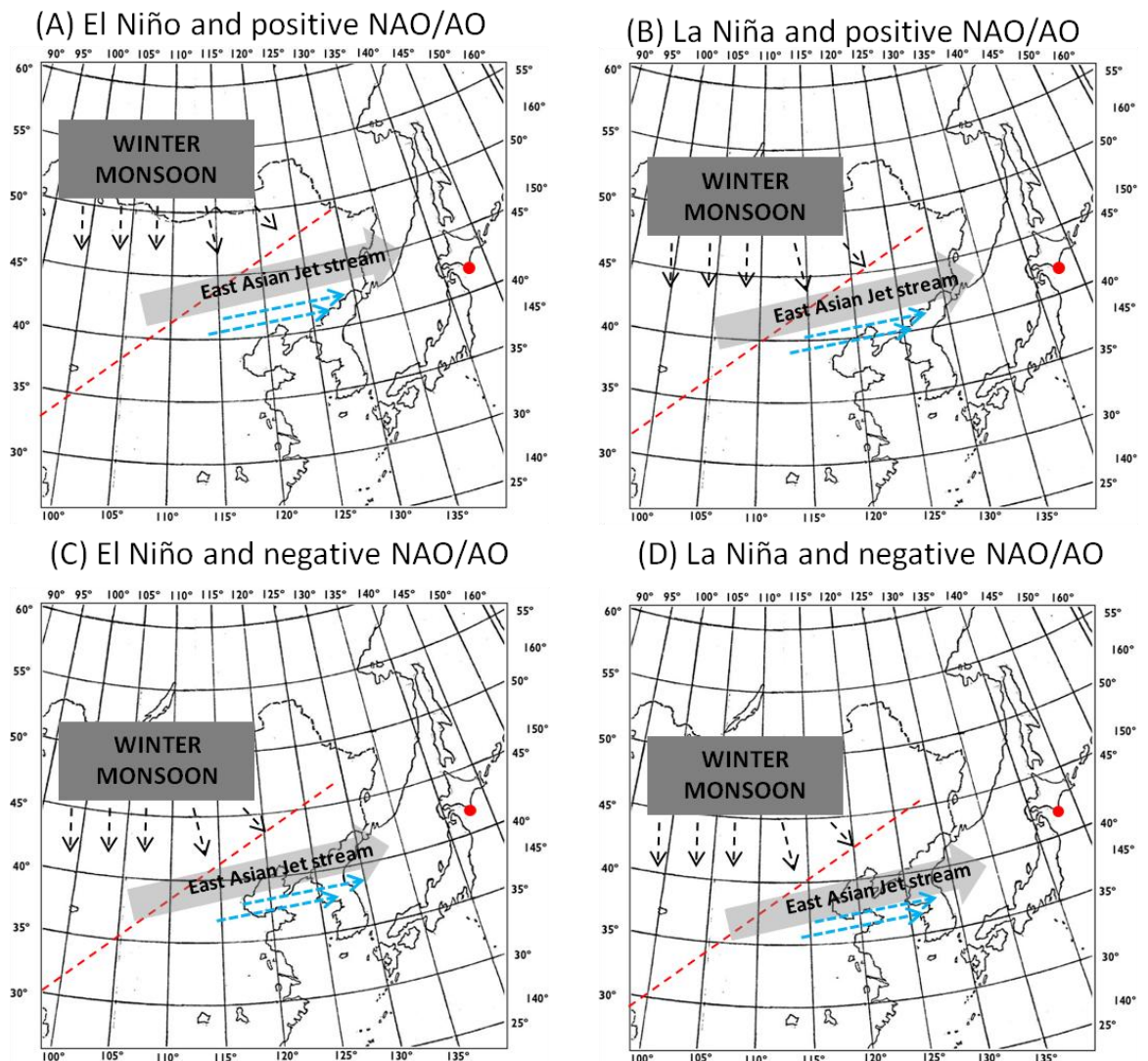


Figure 9-5: Schematic diagram of the combined influence of ENSO and the NAO/AO. Box A represents El Niño and the positive phase of the NAO/AO; during these time periods the EAWM, the EASM limit and the EAJS is located further north. Box B represents La Niña and positive phase of the NAO/AO; during these time periods the EAWM, the EASM limit and the EAJS is located to the north however not as far north as box A conditions. Box C represents El Niño and the negative phase of the NAO/AO; during these time periods the EAWM the EASM limit and the EAJS is located slightly south of the study site. Box D represents La Niña and negative phase of the NAO/AO; during these time periods the EAWM, the EASM limit and the EAJS is located further south. The Blue dotted lines represent the Westerlies, red dotted line represents the EASM limit and the red dot represents Lake Toyoni (study site).

9.7 Solar irradiance and climate variability in Hokkaido

Our multi-proxy climate records show strong similarities to global temperature reconstructions suggesting a relationship between global temperature and Asian climate variability. However, our records follow solar variability more closely than global temperature suggesting that climate variability in Hokkaido responds

more strongly to changes in solar irradiance than global temperature. The link between solar irradiance and global temperature is not clear in the published literature. For example, a recent study suggested that the influence of solar forcing on global climate is minor (Schurer et al., 2014), whereas, a climate model study suggest that 41-64% of Northern Hemisphere temperature variability over the past 1000 years is attributed to changes in solar irradiance, as well as, volcanism (Crowley, 2000). However, the mechanisms involved in the influence of solar irradiance and global climate is currently not fully understood. The amount of change in solar irradiance is relatively small for the large scale temperature recorded and therefore changes in solar irradiance therefore must influence feedback loops, which amplify climate changes and transmit them globally.

We find a strong relationship between solar irradiance and the EAM and the Westerlies at our site. The link between increased solar irradiance and the EAM is well documented in previous studies (e.g. Dykoski et al., 2005, Wang et al., 2005, Xiao et al., 2006, Liu et al., 2009b, He et al., 2013, Sagawa et al., 2014). Similar to their findings, we found that the EAWM increased in intensity during low solar irradiance and the EASM and increased in intensity when solar irradiance increased (Figure 9-3). We also found a connection between increases in solar irradiance and the intensification of the Westerlies.

It is possible that the strong relationship between solar irradiance and climate variability in Hokkaido is due to the influence for solar activity on the EASJ. A modelling study revealed that during time periods of increased solar irradiance, the stratosphere becomes warmer and this causes a broadened and weakened Hadley cell and a poleward shift in the midlatitude Ferrel cell and EASJ, (Haigh, 1996, Haigh, 1999). The movement of the EASJ influences both the EAM and also the Westerlies, as previously discussed. A poleward shift in the EASJ increases the intensity of the EASM in Hokkaido resulting in warmer and wetter conditions. In addition, the westerlies are therefore positioned over Hokkaido and can influence the study site. Conversely, a southward migration of the EASJ during low solar activity increases the influence of northerly air-mass to the study site and hence an intensification of the EAWM. The broadened and weakened Hadley cell and poleward movement of the mid-latitude Ferrel Cell during high solar irradiance also occurs during El Niño conditions, which also has a positive impact

on the EASM. A poleward movement of the Ferrel Cell will result in strong advection of warm air and hence warmer conditions.

In addition to the effect of stratosphere warming on the EASJ, the warming associated with increased solar irradiance also results in an increase in land-sea thermal contrast. The EAM is driven by seasonal changes in the heating contrast between the Pacific Ocean and the Asian continent and the pressure systems associated with these systems (mainly the SibH in winter and the NPSH in summer). The thermal contrast between the Asian continent and the North Pacific Ocean is defined as the Asian-Pacific Oscillation (APO) Index, which has a close link to changes in Northern Hemisphere air temperatures and also solar activity (Zhou et al., 2011). Solar activity is a forcing for the APO index, because increased solar activity heats the land faster than the ocean causing increased thermal contrast between land and sea, and hence increased solar irradiance contributes towards higher APO index values. When the temperature contrast increases during summer (high APO index), the low-pressure system over the Asian continent becomes stronger, which intensifies the high-pressure system over the NW Pacific that then migrates further north (Zhou et al., 2011). The movement of this high-pressure system results in an increased influence of the southwesterly monsoonal winds from the Pacific Ocean to Hokkaido. The influence of solar activity on the land-sea thermal contrast is based on amplified solar radiation causing increased warming the land over middle and high latitudes compared to lower latitudes (Zhou et al., 2011). In addition, land warms at a faster rate than oceans promoting a temperature different between the land and ocean (Zhou et al., 2011). Moist air is transported from the ocean to the land resulting in warm and wet conditions in Hokkaido, which enhances the influence of the EASM in this region. When solar activity decreases, there is less heating of the land resulting in a higher-pressure system developing over Siberia and as a result the EAWM strength increases (Kim et al., 2013). The findings are supported by model simulations of the decadal-centennial variations of the EASM over the past 1000 years (Man et al., 2012). The model was driven by reconstructions of solar irradiance changes and they found that the land-sea thermal contrast change caused by the effective radioactive forcing leads to variability in the EASM. During high solar irradiance, there is a “warmer land-colder ocean” anomaly pattern and southerly wind patterns, which this results in

a strong EASM. Although the ocean does not cool during higher solar irradiance, the magnitude of warmer is weaker than that over the land, so the land-sea thermal contrast increases (Man et al., 2012). During low solar irradiance, there is a “colder land-warmer ocean” anomaly pattern and northerly wind patterns, resulting in a weak EASM (Man et al., 2012). Similarly to time period of high solar irradiance, low solar irradiance does not cause warming of the ocean but rather the magnitude of cooling is larger over the land (Man et al., 2012).

Another potential influence of changes in solar irradiance and climate in Hokkaido is based on the influence of solar irradiance on teleconnections. The influence of the sun on a global level is significantly lower than region level (Shindell et al., 2001). A key reason for this is due to the effect of solar irradiance on the NAO/AO (Shindell et al., 2001, Boberg and Lundstedt, 2002). Changes in solar forcing can cause shifts in the NAO/AO patterns, with increases in solar forcing resulting in a positive AO phase and decreased solar forcing causes shifts to a negative AO phase (Shindell et al., 2001). We found in this study that the NAO/AO has an influence on the Westerlies, the EAWM and to a lesser degree the EASM. A decrease in solar activity causes a shift to negative phase of the NAO/AO, which enhances the EAWM. On the other hand, an increase in solar irradiance causes a shift to a positive NAO phase and hence enhances the Westerlies.

9.8 Summary

Table 9-1: Summary table of the key drivers of the EASM, EAWM and Westerlies intensification in Hokkaido, Japan.

	Key drivers
EASM intensification	Positive phase of the NAO/AO, negative phase of the PDO, and El Niño conditions.
EAWM intensification	Negative phase of the NAO/AO and La Niña conditions.
Westerlies intensification	Positive phase of the NAO/AO

9.9 Conclusions

In this study, we generated and reported on multi-proxy climate reconstructions from Lake Toyoni, Japan, which documents both the Westerlies and also the EAM over the past 1000 years. This is a key time period as it is associated with two globally recognised climate events; the MWP and the LIA that are frequently used to understand the effects of climate extremes at local and global scales. During the MWP, we find that the EASM dominated and the EAWM was suppressed based on higher, precipitation, productivity and low dust input. During the LIA, the influence of the EAWM dominated; prominent dust rich intervals and low δD_{HPW} and productivity reflect an intensified EAWM input. The EASM and the Westerlies also intensified during the LIA.

A key finding from this study is that there is an anti-phase relationship between the EASM and the EAWM (e.g. the intensification of the EASM and weakening of the EAWM and vice versa) and that the EAWM and the Westerlies vary independently from each other, rather than coincide as previously suggested in other studies.

This study also provides insights on the teleconnections influencing the climate modes in Hokkaido (e.g. the EAM and the Westerlies). It is evident that the EASM is greatly influenced by position and intensity of the WPSH and El Niño events. When there is warming in the Western Pacific, e.g. during El Niño events, the WPSH shifts westward and as a result impacts the amount of monsoon precipitation in Hokkaido. The EAWM, on the other hand, is greatly influenced by La Niña events. The intensity of the EAWM is controlled by the negative phase of the AO and the intensity of the SibH, which in turn is regulated by the extent of Arctic ice. The Westerlies, on the other hand, are mainly controlled by the AO/NAO. During the positive phase of the NAO, the Westerlies are stronger and located further north and play a significant role in the climate of Hokkaido.

ENSO and the NAO/AO have been identified as key drivers of global climate variability. We find that ENSO and the NAO/AO also significantly influence the local climate of Hokkaido. The combined impacts of ENSO and the NAO/AO show that when ENSO and the NAO/AO are in phase (e.g. NAO/AO- La Niña and NAO/AO+ El Niño), the climate behaves in a predictable way. For example, when

during NAO/AO- La Niña conditions, the EAWM intensifies, the EASM weakens and there are also weak Westerlies. The SibH intensifies and migrates further south, which increases blocking and cold surges. As a result, the EAWM and the EASM limit migrate south. This forces the weakened Westerlies to also migrate south. As a result, there is cold winter and summer temperatures, low summer rainfall in this region. In the opposite case, NAO/AO+ El Niño, we find that the EAWM weakens, the EASM intensifies and the Westerlies are also stronger. The Northern limit of the EASM migrates north and Hokkaido becomes under the influence of the North Pacific High. At the same time, the Ferrel Cell is activated by the active Hadley Cell in El Niño years and strong Westerlies inhibit the intensification of the SibH. The combination of the weakened SibH and the warming associated with the northward movement of the EASM results in a weak EAWM. Therefore the inverse relationship between the EAWM and the EASM occurs when the NAO/AO and ENSO are in phase with each other; with a strong EAWM and weak EASM occurring when there is NAO/AO- La Niña conditions and a weak EAWM and strong EASM occurring when there is NAO/AO+ El Niño conditions. The climate conditions when the NAO/AO and ENSO are out of phase results in less predictable climate conditions. We find that a combination of La Niña and positive phase of the NAO/AO conditions results in the EAWM, the EASM limit and the EAJS is located to the north however not to the same extent as when El Niño and the NAO/AO are positive in-phase. El Niño and the negative phase of the NAO/AO results in the EAWM, the EASM limit and the EAJS being located slightly south of the study site.

10

Conclusions and future work

The EAM drives changes in temperature and precipitation in East Asia via the changes in ocean-atmospheric system. The EAM also has a strong interaction with other ocean-atmospheric systems including the ENSO, NAO/AO and the PDO. The intensity of the EAM has not been constant over the past 1000 years and this has led to significant climate variability during this time period. In order to understand future climate change better, especially under a global warming scenario, it is necessary to have an understanding of how and why the natural climate has varied in the past.

The general aim of this thesis was to test the hypothesis:

The climate in Northern Japan was strongly influenced by the intensity of the EAM (EASM and the EAWM) and the Westerlies over the past 1000 years.

Climate variability was reconstructed using a multi-proxy approach from a sediment core taken from Lake Toyoni. The multi-proxy study is the most comprehensive and high-resolution, organic biomarker based study of climate change in Northern Japan over the past 1000 years. To compliment the biomarker based paleo-environmental reconstruction, the sediment core (TY09) was also XRF scanned to provide information on terrestrial and biological processes in Lake Toyoni. In addition to Lake Toyoni being located on the northern boundary of the limit of the EASM and hence being sensitive to the intensification of the EASM

Lake Toyoni. In addition, Lake Toyoni is also not influenced by the ISM, whereas other records of the EASM have this complication. Furthermore, Lake Toyoni also provides a key location for investigating the variability of the EAM because of the following reasons:

1. Lake Toyoni seasonally stratifies resulting in anoxic conditions in the sediments, resulting in preservation of organic matter. (Chapter 4)
2. Lake Toyoni is a hydrological closed lake and therefore is strongly influenced by terrestrial input via wind rather than fluvial input. The EAWM transports coarse-grained dust towards Hokkaido, therefore, investigations of the particle size variability in the sedimentary record provides valuable information on the EAWM (Chapter 5).
3. The surface temperatures of Lake Toyoni correspond to air-temperature; which in turn is driven by changes in the EAM. Therefore temperature reconstruction of Lake Toyoni provides information on past air temperatures and hence the EAM over the past 1000 years (Chapter 7). In order to study and develop the use of the alkenone biomarker in Lake Toyoni, we also completed DNA analysis to determine the identity of the alkenone producer(s) in Lake Toyoni (Chapter 6).
4. The catchment surrounding Lake Toyoni is densely covered in vegetation. The vegetation in the catchment uses environmental water (precipitation and snow-melt), which is supplied via the EAM. The D/H of higher plant waxes preserved in Lake Toyoni therefore provides information on the variability of the EAM over the past 1000 years (Chapter 8).

By combining the data generated from XRF, alkenone palaeothermometry and the $\delta D_{(HPW)}$ reconstructions, we provide valuable information on the EAM and the Westerlies, including; the timing of intensification and weakening, the teleconnections influencing them and the relationship between them. During the Medieval Warm Period (MWP), we find that the EASM dominated and the EAWM was suppressed, whereas, during the Little Ice Age (LIA), the influence of the EAWM dominated with time periods of increased EASM and Westerlies intensification. The key findings were that the El Niño Southern Oscillation

(ENSO) significantly influenced the EAM; a strong EASM occurred during El Niño conditions and a strong EAWM occurred during La Niña. The North Atlantic Oscillation, on the other hand, was a key driver of the Westerlies intensification; strengthening of the Westerlies during a positive NAO phase and weakening of the Westerlies during a negative NAO phase. Another key finding from this study is that our data support an anti-phase relationship between the EASM and the EAWM (e.g. the intensification of the EASM and weakening of the EAWM and vice versa) and that the EAWM and the Westerlies vary independently from each other, rather than coincide as previously suggested in other studies. In the following section the main results of this PhD research are summarised. In addition we also discuss further work, which has arisen as a result of this study.

10.1 Chapter 4: Decadal-resolved terrestrial and biological input into Lake Toyoni.

The aim of this chapter was to determine palaeoproductivity variability over the past 1000 years in Lake Toyoni. Productivity variability over the past 1000 years was determined using a multi-proxy approach including; MS (proxy for magnetite preservation), Si/Rb (proxy for diatom productivity), Inc/Coh (proxy for OM), and molecular composition of n-alkanes; CPI, ACL and Paq (proxies for source of n-alkanes, temperature and productivity, respectively). The key findings were:

1. High productivity during the Medieval Warm Period (MWP) (~1000-1300AD) based on; low magnetic susceptibility and high OM content of sediments was high suggesting strong thermal stratification and hence warm conditions. High Si/Rb suggesting increased productivity and high Inc/Coh suggesting increased precipitation. The combined results suggest a weakening of the East Asian Winter Monsoon (EAWM) and intensification of the East Asia Summer Monsoon (EASM) during the MWP.
2. Low productivity during the early Little Ice Age (LIA) (1300-1600AD) as inferred from a decrease in productivity (as inferred from low Si/Rb and high C/N ratio values). The combined results suggest increased ice-cover on the lake due to the strengthening of the EAWM. The increased ice-cover reduces the time period of the bloom in the lake and hence reducing productivity. The late LIA (1600-1800AD) was characterised by

higher productivity than the early LIA based on an enhancement a sharp decrease in C/N ratio values and an increase in Si/Rb ratio values suggesting an increase in productivity (Figure 9-1), which is attributed to a change in the Pacific Decadal Oscillation (PDO) from positive to negative. The negative phase of the PDO is characterised by wetter conditions in Hokkaido, which promotes productivity in the lake through increased run-off.

3. Evidence of an abrupt population increase in Hokkaido (~1870AD). We found that the rapid environmental change over the past 100 years was consistent with the significant population change in Hokkaido at the same time. We suggested that the increased nutrients, associated with an increase in human activity, led to an increase in aquatic production in the lake (e.g. submerged and floating macrophytes and also algae). In turn, an increase in productivity resulted in anoxic sediments and stimulated a large increase in bacterial growth in the sediments.

10.2 Chapter 5: Assessing the contribution of dust from global (Westerlies) and regional (EAWM) wind patterns

The aim of this chapter was to determine the contribution of dust from global (Westerlies) and regional (EAWM) wind patterns. The contribution of dust into Lake Toyoni was determined by the Ti/Rb proxy. The contribution from the Westerlies and the EAWM was separated based on the fact that the grain size of the dust would be fine and coarse, respectfully. The main findings were:

1. The EAWM increased in intensity between 1450-1500AD and 1550-1650AD. The intensity of the EAWM was controlled by temperature in the source regions as well as the strength of the Siberian high (SibH). When the SibH was strong and temperatures were colder, the EAWM intensified, bringing more coarse-grained sediments to Lake Toyoni. The EAWM weakened between 1700-1800AD, which was also associated with a decrease in the intensity of the SibH.

2. The Westerlies increased between 1050-1135AD during the MWP, between 1500-1550AD during the LIA and between 1800-1920AD during the CWP, which are all associated with the positive phase of the NAO/AO.

10.3 Chapter 6: 18S rDNA analysis of the alkenone producer(s) in Lake Toyoni

The aim of this chapter was to identify the alkenone producer(s) in Lake Toyoni using 18S rDNA analyses of planktonic, phototrophic algae that are preserved in the surface sediment. The key findings were

1. Phylogenetic analyses of the rDNA sequences suggest that alkenones are produced by a single haptophyte species within the class Prymnesiophyceae (order Isochrysidales). This species represent a new taxon of haptophyte algae that occupies a phylogenetic clade with the BrayaSø Greenland lake haptophyte, which is distinct from the well-studied marine alkenone producers *Emiliana huxleyi*, *Gephyrocapsa oceanica* and coastal alkenone producers *Isochrysis galbana* and *Chrysothila lamellosa*.
2. The Lake Toyoni alkenone-producer shares a distinct phylotype with a haptophyte reported from water filter samples collected in Lake BrayaSø, Greenland (D'Andrea et al., 2006; DOI: 10.1029/2005JG000121). Similarity between the 18S rDNA sequences from Lake Toyoni and Lake BrayaSø provides a basis for applying the Greenland lake temperature calibration.

10.4 Chapter 7: Alkenone-based temperature reconstructions from Lake Toyoni

The aim of this chapter was to reconstruct past water temperatures over the past 1000 years from Lake Toyoni Japan. The key findings were:

1. Surface water temperatures in Lake Toyoni correspond to air temperatures therefore the alkenone-based temperatures from Lake Toyoni reflect changes in air-temperatures and hence variability of the EAM and the NAO/AO. The similarities between the alkenone-based

temperature reconstruction and published records on the EASM provide evidence for Lake Toyoni recording a strong EAM signal and is also influenced by the phase of the NAO/AO.

2. Temperatures during MWP were generally warm and the EASM was intense, whereas, the onset of the LIA recorded a distinct cooling event, which has been attributed to monsoon failure. As a result of the monsoon failure during this time period, the conditions were very cold and dry during summer in Hokkaido. The later part of the LIA (1470-1800AD) was characterised by warmer temperatures compared to the onset of the LIA. The past 200 years is characterised by warming in the 1800's and a decrease in temperature towards modern day temperatures. It is suggested that the EASM has weakening over the past 100 years in Hokkaido, Japan; possibly as a result of human-induced climate change.
3. We found evidence for strong relationship between the frequency of famines and temperature in Japan. During time periods with cold summers, the frequency of famines in Japan increases. This demonstrates that natural forcing mechanisms, without modern human activities, can also lead to strong climate variability and also strongly influence society through agriculture loss.

10.5 Chapter 8: Hydrogen isotopic composition of higher plant waxes in the catchment and down-core sedimentary records of Lake Toyoni

The aim of this chapter was determine the controlling factors on the hydrogen stable isotopic values (δD) of *n*-alkanes derived from higher plant waxes (δD_{HPW}) in the catchment of Lake Toyoni and reconstruct hydrological variability over the past 1000 years. The main results were:

1. The δD_{HPW} are primarily controlled by the δD of the source water taken up by the plant during photosynthesis. As a result the δD_{HPW} proxy has been successfully used to reconstruct the δD of precipitation (δD_{PRECIP}). The δD_{PRECIP} in Hokkaido is controlled by temperature and the source of the precipitation, which in turn is controlled by the EAM. During winter, temperatures are low and the source of the precipitation is from the Asian

continent; this results in low δD_{HPW} values. During summer, temperatures are high and the source of the precipitation is from the Pacific Ocean; this results in high δD_{HPW} values. The difference between summer and winter δD_{PRECIP} values is large; average summer δD_{PRECIP} values are -52.5‰ and average winter δD_{PRECIP} values are -77‰ . This large difference in δD_{PRECIP} values (24.5‰) allows the contribution from the EASM (higher δD_{HPW} values) and the EAWM (lower δD_{HPW} values) to be separated in the down-core sedimentary record.

2. The apparent fractionation between δD_{PRECIP} and the δD_{HPW} was calculated to be -130‰ . Based on the large difference between summer and winter δD_{PRECIP} values, we suggested that values above -55‰ were an intensification of the EASM and values below -72‰ were an intensification of the EAWM. Based on this, the EAWM intensified briefly $\sim 1156\text{AD}$, $1438\text{-}1446\text{AD}$ and $1655\text{-}1688\text{AD}$ and the EASM intensified $1082\text{-}1141\text{AD}$, $\sim 1163\text{AD}$, $\sim 1192\text{AD}$, $\sim 1244\text{AD}$, $1347\text{-}1361\text{AD}$, $1615\text{-}1633\text{AD}$, $1791\text{-}1820\text{AD}$, $\sim 1925\text{AD}$ and $1954\text{-}1963\text{AD}$.
3. The EAM intensity shows a clear resemblance to changes in solar irradiance; with the EASM increasing in intensity during solar maxima and the EAWM increasing in intensity during solar minima. In addition, we found that the EASM was strongly influenced by El Niño conditions and the EAWM was influenced by the negative phase of the NAO/AO. An inverse relationship exists between the EASM and the EAWM; when the EASM intensifies, the EAWM weakens and vice versa. This is likely caused by the variations in solar irradiance
4. High solar irradiance and positive AO (NAO) during the MWP resulted in key conditions for an intensified EASM, as well as, a strong Okhotsk High. Although the EASM was strong during this time period, the presence of the intensified OH during the MWP resulted in a reduced influence of the EASM in Hokkaido compared to other records within in the EAM domain.
5. Within the LIA, the EAWM enhanced in the 15th century and the 18th century associated with the time periods of the Spörer Minimum and the Maunder Minimum, respectively. The cooling during the LIA was disturbed

with an enhancement of the EASM leading in the 1600's. The increased influence of the EASM during this time is likely associated with the negative phase of the PDO enhancing the strength of the North Pacific Subtropical High (NPSH).

6. Over the past 200 years, the EASM was strong between 1800-1820AD and 1900-1963AD and slightly weaker between 1820-1900AD. Over the past ~50 years, we found a decrease in the intensity of the EASM and attributed this change as a result of human-induced climate change.

10.6 Future work

This research could be further developed in a number of ways:

The present study uses a temperature calibration by D'Andrea et al. (2011) based on the fact that the alkenone producer in Lake Toyoni is the same as the alkenone producer in Greenland lakes. To improve this calibration, a site-specific calibration can be developed filtering the water column for alkenones and recording the temperature of the water column at the same time. In addition, filter samples from Lake Toyoni would also determine the timing of alkenone production in the lake. This was initially a key objective for the current PhD research, and filter samples were taken on a monthly basis from 0m, 5m, 10m and 15m in Lake Toyoni. However, only 1L of water was filtered and the alkenone concentrations were too low to be detected. A filtering campaign at Lake Toyoni, in order to develop a site-specific temperature calibration for Lake Toyoni and to determine the timing of alkenone production, would improve the temperature reconstruction at this site. Following on from a site-specific calibration at Lake Toyoni, a species specific calibration can also be developed using culturing. This is partly in progress by Prof. Yoshihiro Shiraiwa at the life and environmental sciences department at Tsukuba University, Japan.

In addition, we found that there was an inverse relationship between the EASM and the EAWM and also that the EAWM and the Westerlies were distinct from each other. We also identified that ENSO exerted a key control on the EAM and

that NAO influences the intensity of the Westerlies. Based on the findings from this research, we developed a schematic diagram of the combined influence of ENSO and the NAO/AO on the EAM and the Westelies in Hokkaido, Japan. Following on from this study, modelling simulations will provide further clarification on the combined influence of ENSO and the NAO in Japan and also further afield.

10.7 Future implications

A key finding of this thesis was that solar irradiance is a key driving force in the climate in Hokkaido, Japan. However, the current solar forcing is decreasing in the Northern Hemisphere. Based on the findings in this work, we would expect a strengthening of the EAWM or/and a weakening of the EASM. The IPCC report found that the EASM and the EAWM have both experienced inter-decadal scale weakening since the 1970's. The IPCC report has also found that temperature has increased in Asia, and will continue to rise, due to anthropogenic induced warming. Therefore an understanding on how anthropogenic induced warming in Asia will influence the EAM and Westerlies in the future is required.

Another key finding in this thesis was that the positive phase of the NAO strengthened the Westerlies. We also suggested that the stronger winds during time periods when the Westerlies intensified may have also promoted ocean upwelling in the Northern Hemisphere and hence the release of old carbon. This has implications for future climate variability because climate models project that there will be more occurrences of the positive phase of the NAO in the future. Furthermore, the Intergovernmental Panel on Climate Change (IPCC, 2013; chapter 11) predict with *medium confidence* that the Westerlies will shift polewards in the twenty-first century based on climate models (Yin, 2005). This suggests that there will be an enhancement of the Westerlies in the future.

10.8 Concluding remarks

This thesis research represents a detailed multi-proxy, multi-disciplinary, paleo-climate study from Lake Toyoni, Hokkaido, Japan. All proxies, to a certain degree, have uncertainties associated with them due to the degree of preservation in palaeo-climate archives and also due to complications with other environmental factors. The use of a combination of proxies across a range of disciplines when addressing questions relating to past climate variability reduces these uncertainties. A multi-proxy approach revealed how productivity (Chapter 4) and wind patterns (Chapter 5) varied over the past 1000 years. In addition, the use of a proxy from another discipline (molecular biology) provided information on the identity of alkenone producer within Lake Toyoni (Chapter 6), which ultimately improved the applicability of alkenone-based temperature reconstructions from this site (Chapter 7). Furthermore, the isotopic composition of higher plant waxes provided key information on hydrological variability over the past 1000 years (Chapter 8).

List of references

- ADHIKARI, D. & KUMON, F. (2001) Climatic changes during the past 1300 years as deduced from the sediments of Lake Nakatsuna, central Japan. *Limnology*, 2, 157-168.
- AICHNER, B., FEAKINS, S., LEE, J., HERZSCHUH, U. & LIU, X. (2015) High-resolution leaf wax carbon and hydrogen isotopic record of the late Holocene paleoclimate in arid Central Asia. *Climate of the Past*, 11, 619-633.
- ALTSCHUL, S., MADDEN, T., SCHAFFER, A., ZHANG, J., ZHANG, Z., MILLER, W. & LIPMAN, D. (1997) Gapped BLAST and PSI-BLAST: a new generation of protein database search programs. *Nucleic Acids Res*, 25, 3389 - 3402.
- AN, C.-B., ZHAO, J., TAO, S., LV, Y., DONG, W., LI, H., JIN, M. & WANG, Z. (2011) Dust variation recorded by lacustrine sediments from arid Central Asia since ~ 15 cal ka BP and its implication for atmospheric circulation. *Quaternary Research*, 75, 566-573.
- AN, Z. (2000) The history and variability of the East Asian paleomonsoon climate. *Quaternary Science Reviews*, 19, 171-187.
- ANDERSON, R., ALI, S., BRADTMILLER, L., NIELSEN, S., FLEISHER, M., ANDERSON, B. & BURCKLE, L. (2009) Wind-driven upwelling in the Southern Ocean and the deglacial rise in atmospheric CO₂. *Science*, 323, 1443-1448.
- AO, H., DENG, C., DEKKERS, M. J. & LIU, Q. (2010) Magnetic mineral dissolution in Pleistocene fluvio-lacustrine sediments, Nihewan Basin (North China). *Earth and Planetary Science Letters*, 292, 191-200.
- AONO, Y. & KAZUI, K. (2008) Phenological data series of cherry tree flowering in Kyoto, Japan, and its application to reconstruction of springtime temperatures since the 9th century. *International Journal of Climatology*, 28, 905-914.
- ARAGUÀS-ARAGUÀS, L., FROELICH, K. & ROZANSKI, K. (1998) Stable isotope composition of precipitation over southeast Asia. *Journal of Geophysical Research: Atmospheres*, 103, 28721-28742.
- AUSTIN, J. A. & COLMAN, S. M. C. L. (2007) Lake Superior summer water temperatures are increasing more rapidly than regional air temperatures: A positive ice-albedo feedback. *Geophysical Research Letters*, 34, n/a-n/a.
- BAKKE, J., NESJE, A. & DAHL, S. O. (2005) Utilizing physical sediment variability in glacier-fed lakes for continuous glacier reconstructions during the Holocene, northern Fjellfonna, western Norway. *The Holocene*, 15, 161-176.
- BARD, E., RAISBECK, G., YIOU, F. O. & JOUZEL, J. (2000) Solar irradiance during the last 1200 years based on cosmogenic nuclides. *Tellus B*, 52.
- BARNES, C. J. & TURNER, J. V. (1998) *Isotopic exchange in soil water*, Elsevier: Amsterdam.
- BENDLE, J. & ROSELL-MELÉ, A. (2004) Distributions of UK37 and UK'37 in the surface waters and sediments of the Nordic Seas: Implications for paleoceanography. *Geochemistry, Geophysics, Geosystems*, 5.
- BENDLE, J., ROSELL-MELÉ, A. & ZIVERI, P. (2005) Variability of unusual distributions of alkenones in the surface waters of the Nordic seas. *Paleoceanography*, 20.
- BENDLE, J. A. P., ROSELL-MELÉ, A., COX, N. J. & SHENNAN, I. (2009) Alkenones, alkenoates, and organic matter in coastal environments of NW Scotland:

- Assessment of potential application for sea level reconstruction. *Geochem Geophys Geosy*, 10.
- BIANCHI, G. G. & MCCAIVE, I. N. (1999) Holocene periodicity in North Atlantic climate and deep-ocean flow south of Iceland. *Nature*, 397, 515-517.
- BILLON, G., OUDDANE, B., RE COURT, P. & BOUGHRIET, A. (2002) Depth Variability and some Geochemical Characteristics of Fe, Mn, Ca, Mg, Sr, S, P, Cd and Zn in Anoxic Sediments from Authie Bay (Northern France). *Estuarine, Coastal and Shelf Science*, 55, 167-181.
- BITTNER, L., GOBET, A., AUDIC, S., ROMAC, S., EGGE, E. S., SANTINI, S., OGATA, H., PROBERT, I., EDVARSEN, B. & DE VARGAS, C. (2012) Diversity patterns of uncultured Haptophytes unravelled by pyrosequencing in Naples Bay. *Molecular Ecology*, 22, 87-101.
- BLOTT, S. & PYE, K. (2001) Gradstat: A grain size distribution and statistics package for the analysis of unconsolidated sediments *Earth Surface Processes and Landforms*, 26, 1237-1248.
- BOBERG, F. & LUNDSTEDT, H. (2002) Solar wind variations related to fluctuations of the North Atlantic Oscillation. *Geophysical Research Letters*, 29.
- BONSAL, B. R., PROWSE, T. D., DUGUAY, C. R. & LACROIX, M. P. (2006) Impacts of large-scale teleconnections on freshwater-ice break/freeze-up dates over Canada. *Journal of Hydrology*, 330, 340-353.
- BRASSELL, S. C. & DUMITRESCU, M. (2004) Recognition of alkenones in a lower Aptian porcellanite from the west-central Pacific. *Organic Geochemistry*, 35, 181-188.
- BRASSELL, S. C., EGLINTON, G., MARLOWE, I. T., PFLAUMANN, U. & SARNTHEIN, M. (1986) Molecular stratigraphy: a new tool for climatic assessment. *Nature*, 320, 129-133.
- BRAY, E. E. & EVANS, E. D. (1961) Distribution of n-paraffins as a clue to recognition of source beds. *Geochimica et Cosmochimica Acta*, 22, 2-15.
- BURNETT, A. P., SOREGHAN, M. J., SCHOLZ, C. A. & BROWN, E. T. (2011) Tropical East African climate change and its relation to global climate: A record from Lake Tanganyika, Tropical East Africa, over the past 90+ kyr. *Palaeogeography, Palaeoclimatology, Palaeoecology*, 303, 155-167.
- BURT, W. J., THOMAS, H., FENNEL, K. & HORNE, E. (2013) Sediment-water column fluxes of carbon, oxygen and nutrients in Bedford Basin, Nova Scotia, inferred from ^{224}Ra measurements. *Biogeosciences*, 10, 53-66.
- CALANCHI, N., CATTANEO, A., DINELLI, E., GASPAROTTO, G. & LUCCHINI, F. (1998) Tephra layers in Late Quaternary sediments of the central Adriatic Sea. *Marine Geology*, 149, 191-209.
- CASTAÑEDA, I. S. & SCHOUTEN, S. (2011) A review of molecular organic proxies for examining modern and ancient lacustrine environments. *Quaternary Science Reviews*, 30, 2851-2891.
- CHEN, F., XU, Q., CHEN, J., BIRKS, H. J. B., LIU, J., ZHANG, S., JIN, L., AN, C., TELFORD, R. J. & CAO, X. (2015a) East Asian summer monsoon precipitation variability since the last deglaciation. *Scientific reports*, 5.
- CHEN, F. H., BLOEMENDAL, J., WANG, J. M., LI, J. J. & OLDFIELD, F. (1997) High-resolution multi-proxy climate records from Chinese loess: evidence for rapid climatic changes over the last 75 kyr. *Palaeogeography, Palaeoclimatology, Palaeoecology*, 130, 323-335.
- CHEN, J., AN, Z., WANG, Y., JI, J., CHEN, Y. & LU, H. (1999a) Distribution of Rb and Sr in the Luochuan loess- paleosol sequence of China during the last 800 ka. *Science in China Series D: Earth Sciences*, 42, 225-232.
- CHEN, J., CHEN, F., FENG, S., HUANG, W., LIU, J. & ZHOU, A. (2015b) Hydroclimatic changes in China and surroundings during the Medieval

Climate Anomaly and Little Ice Age: spatial patterns and possible mechanisms.

- CHEN, M.-T. & HUANG, C.-Y. (1998) Ice-volume forcing of winter monsoon climate in the South China Sea. *Paleoceanography*, 13, 622-633.
- CHEN, M.-T., WANG, C.-H., HUANG, C.-Y., WANG, P., WANG, L. & SARNTHEIN, M. (1999b) A late Quaternary planktonic foraminifer faunal record of rapid climatic changes from the South China Sea. *Marine Geology*, 156, 85-108.
- CHEN, W., HANS- F, G. & HUANG, R. (2000) The interannual variability of East Asian Winter Monsoon and its relation to the summer monsoon. *Advances in Atmospheric Sciences*, 17, 48-60.
- CHEN, W., LAN, X., WANG, L. & MA, Y. (2013) The combined effects of the ENSO and the Arctic Oscillation on the winter climate anomalies in East Asia. *Chinese Science Bulletin*, 58, 1355-1362.
- CHEN, Z., WU, R. & CHEN, W. (2014) Distinguishing interannual variations of the northern and southern modes of the East Asian winter monsoon. *Journal of Climate*, 27, 835-851.
- CHENG, H., EDWARDS, R. L., BROECKER, W. S., DENTON, G. H., KONG, X., WANG, Y., ZHANG, R. & WANG, X. (2009) Ice age terminations. *Science*, 326, 248-252.
- CHEUNG, H. N., ZHOU, W., MOK, H. Y. & WU, M. C. (2012) Relationship between Ural-Siberian blocking and the East Asian winter monsoon in relation to the Arctic Oscillation and the El Niño-Southern Oscillation. *Journal of Climate*, 25, 4242-4257.
- CHIANG, J. C. & SOBEL, A. H. (2002) Tropical tropospheric temperature variations caused by ENSO and their influence on the remote tropical climate*. *Journal of Climate*, 15, 2616-2631.
- CHIKARAISHI, Y. & NARAOKA, H. (2003) Compound-specific δD - $\delta^{13}C$ analyses of n-alkanes extracted from terrestrial and aquatic plants. *Phytochemistry*, 63, 361-371.
- CHIKARAISHI, Y., NARAOKA, H. & POULSON, S. R. (2004) Hydrogen and carbon isotopic fractionations of lipid biosynthesis among terrestrial (C3, C4 and CAM) and aquatic plants. *Phytochemistry*, 65, 1369-1381.
- CHU, G., LIU, J., SUN, Q., LU, H., GU, Z., WANG, W. & LIU, T. (2002) The 'Mediaeval Warm Period' drought recorded in Lake Huguangyan, tropical South China. *The Holocene*, 12, 511-516.
- CHU, G., SUN, Q., LI, S., LIN, Y., WANG, X., XIE, M., SHANG, W., LI, A. & YANG, K. (2013) Minor element variations during the past 1300 years in the varved sediments of Lake Xiaolongwan, north-eastern China. *GFF*, 135, 265-272.
- CHU, G., SUN, Q., LI, S., ZHENG, M., JIA, X., LU, C., LIU, J. & LIU, T. (2005) Long-chain alkenone distributions and temperature dependence in lacustrine surface sediments from China. *Geochimica et Cosmochimica Acta*, 69, 4985-5003.
- CHU, G., SUN, Q., WANG, X., LIU, M., LIN, Y., XIE, M., SHANG, W. & LIU, J. (2011) Seasonal temperature variability during the past 1600 years recorded in historical documents and varved lake sediment profiles from northeastern China. *The Holocene*, 0959683611430413.
- CONROY, J. L., OVERPECK, J. T., COLE, J. E., SHANAHAN, T. M. & STEINITZ-KANNAN, M. (2008) Holocene changes in eastern tropical Pacific climate inferred from a Galápagos lake sediment record. *Quaternary Science Reviews*, 27, 1166-1180.
- COOLEN, M. J. L., MUYZER, G., RIJPSTRA, W. I. C., SCHOUTEN, S., VOLKMAN, J. K. & SINNINGHE DAMSTÁ, J. S. (2004a) Combined DNA and lipid analyses

- of sediments reveal changes in Holocene haptophyte and diatom populations in an Antarctic lake. *Earth and Planetary Science Letters*, 223, 225-239.
- COOLEN, M. J. L., MUYZER, G., RIJPSTRA, W. I. C., SCHOUTEN, S., VOLKMAN, J. K. & SINNINGHE DAMSTÉ, J. S. (2004b) Combined DNA and lipid analyses of sediments reveal changes in Holocene haptophyte and diatom populations in an Antarctic lake. *Earth and Planetary Science Letters*, 223, 225-239.
- COOLEN, M. J. L., MUYZER, G., RIJPSTRA, W. I. C., SCHOUTEN, S., VOLKMAN, J. K. & SINNINGHE DAMSTÉ, J. S. (2004c) Combined DNA and lipid analyses of sediments reveal changes in Holocene haptophyte and diatom populations in an Antarctic lake. *Earth and Planetary Science Letters*, 223, 225-239.
- COSFORD, J., QING, H., EGLINGTON, B., MATTEY, D., YUAN, D., ZHANG, M. & CHENG, H. (2008) East Asian monsoon variability since the Mid-Holocene recorded in a high-resolution, absolute-dated aragonite speleothem from eastern China. *Earth and Planetary Science Letters*, 275, 296-307.
- CRANWELL, P. (1973) Chain-length distribution of n-alkanes from lake sediments in relation to post-glacial environmental change. *Freshwater Biology*, 3, 259-265.
- CRANWELL, P. A. (1985) Long-chain unsaturated ketones in recent lacustrine sediments. *Geochimica et Cosmochimica Acta*, 49, 1545-1551.
- CRANWELL, P. A., EGLINTON, G. & ROBINSON, N. (1987) Lipids of aquatic organisms as potential contributors to lacustrine sediments—II *Organic Geochemistry*, 11, 513-527.
- CROUDACE, I. W., RINDBY, A. & ROTHWELL, R. G. (2006) ITRAX: description and evaluation of a new multi-function X-ray core scanner. *Geological Society, London, Special Publications*, 267, 51-63.
- CROWLEY, T. J. (2000) Causes of Climate Change Over the Past 1000 Years. *Science*, 289, 270-277.
- D'ANDREA, W. J. & HUANG, Y. (2005) Long chain alkenones in Greenland lake sediments: Low $\delta^{13}\text{C}$ values and exceptional abundance. *Organic Geochemistry*, 36, 1234-1241.
- D'ANDREA, W. J., HUANG, Y., FRITZ, S. C. & ANDERSON, N. J. (2011) Abrupt Holocene climate change as an important factor for human migration in West Greenland. *Proceedings of the National Academy of Sciences of the United States of America*, 108, 9765-9769.
- D'ANDREA, W. J., LAGE, M., MARTINY, J. B. H., LAATSCH, A. D., AMARAL-ZETTLER, L. A., SOGIN, M. L. & HUANG, Y. (2006) Alkenone producers inferred from well-preserved 18S rDNA in Greenland lake sediments. *J. Geophys. Res.*, 111, G03013.
- D'ANDREA, W. J., VAILLENCOURT, D. A., BALASCIO, N. L., WERNER, A., ROOF, S. R., RETELLE, M. & BRADLEY, R. S. (2012) Mild Little Ice Age and unprecedented recent warmth in an 1800 year lake sediment record from Svalbard. *Geology*, 40, 1007-1010.
- D'ARRIGO, R., VILLALBA, R. & WILES, G. (2001) Tree-ring estimates of Pacific decadal climate variability. *Climate Dynamics*, 18, 219-224.
- D'ARRIGO, R. D., YAMAGUCHI, D. K., WILES, G. C., JACOBY, G. C., OSAWA, A. & LAWRENCE, D. M. (1997) A kashiwa oak (*Quercus dentata*) tree-ring width chronology from northern coastal Hokkaido, Japan. *Canadian journal of forest research*, 27, 613-617.
- DABANG, J. & HUIJUN, W. (2005) Natural interdecadal weakening of East Asian summer monsoon in the late 20th century. *Chinese Science Bulletin*, 50, 1923-1929.
- DANSGAARD, W. (1964) Stable isotopes in precipitation. *Tellus*, 16, 436-468.

- DASCH, E. J. (1969) Strontium isotopes in weathering profiles, deep-sea sediments, and sedimentary rocks. *Geochimica et Cosmochimica Acta*, 33, 1521-1552.
- DAVI, N., D'ARRIGO, R., JACOBY, G., BUCKLEY, B. & KOBAYASHI, O. (2002) Warm-Season Annual to Decadal Temperature Variability for Hokkaido, Japan, Inferred from Maximum Latewood Density and Ring Width Data. *Climatic Change*, 52, 201-217.
- DE LEEUW, J. W., V.D. MEER, F. W., RIJPSTRA, W. I. C. & SCHENCK, P. A. (1980) On the occurrence and structural identification of long chain unsaturated ketones and hydrocarbons in sediments. *Physics and Chemistry of the Earth*, 12, 211-217.
- DE VARGAS, C., AUBRY, M. P., PROBERT, I. & YOUNG, J. (2007) Origin and evolution of coccolithophores: from coastal hunters to oceanic farmers. *Evolution of Aquatic Photoautotrophs, Elsevier Academic, New York* 251-281.
- DEARING, J. A., ELNER, J. K. & HAPPEY-WOOD, C. M. (1981) Recent sediment flux and erosional processes in a Welsh upland lake-catchment based on magnetic susceptibility measurements. *Quaternary Research*, 16, 356-372.
- DELAYGUE, G. & BARD, E. (2011) An Antarctic view of Beryllium-10 and solar activity for the past millennium. *Climate Dynamics*, 36, 2201-2218.
- DENYS, L. (2010) Incomplete Spring Turnover in Small Deep Lakes in SE Michigan. *McNair Scholars Research Journal*, 2, 10.
- DIAZ, R. J. (2001) Overview of Hypoxia around the World. *Journal of Environmental Quality*, 30, 275-281.
- DING, Y. (1990) Build-up, air mass transformation and propagation of Siberian high and its relations to cold surge in East Asia. *Meteorology and Atmospheric Physics*, 44, 281-292.
- DING, Y., LIU, Y., LIANG, S., MA, X., ZHANG, Y., SI, D., LIANG, P., SONG, Y. & ZHANG, J. (2014) Interdecadal variability of the East Asian winter monsoon and its possible links to global climate change. *Journal of Meteorological Research*, 28, 693-713.
- DING, Y., WANG, Z. & SUN, Y. (2008) Inter-decadal variation of the summer precipitation in East China and its association with decreasing Asian summer monsoon. Part I: Observed evidences. *International Journal of Climatology*, 28, 1139-1161.
- DUAN, Y. & XU, L. (2012) Distributions of n-alkanes and their hydrogen isotopic composition in plants from Lake Qinghai (China) and the surrounding area. *Applied geochemistry*, 27, 806-814.
- DUCE, R. A., UNNI, C. K., RAY, B. J., PROSPERO, J. M. & MERRILL, J. T. (1980) Long-Range Atmospheric Transport of Soil Dust from Asia to the Tropical North Pacific: Temporal Variability. *Science*, 209, 1522-1524.
- DYKOSKI, C. A., EDWARDS, R. L., CHENG, H., YUAN, D., CAI, Y., ZHANG, M., LIN, Y., QING, J., AN, Z. & REVENAUGH, J. (2005) A high-resolution, absolute-dated Holocene and deglacial Asian monsoon record from Dongge Cave, China. *Earth and Planetary Science Letters*, 233, 71-86.
- EDVARSEN, B., EIKREM, W., GREEN, J. C., ANDERSEN, R. A., MOON-VAN DER STAAY, S. Y. & MEDLIN, L. K. (2000) Phylogenetic reconstructions of the Haptophyta inferred from 18S ribosomal DNA sequences and available morphological data. *Phycologia*, 39, 19-35.
- EGLINTON, G. & HAMILTON, R. (1963) The distribution of alkanes. *Chemical plant taxonomy*, 187, 217.
- EGLINTON, G. & HAMILTON, R. J. (1967) Leaf epicuticular waxes. *Science*, 156, 1322-1335.

- EGLINTON, T. I. & EGLINTON, G. (2008) Molecular proxies for paleoclimatology. *Earth and Planetary Science Letters*, 275, 1-16.
- ELTGROTH, M. L., WATWOOD, R. L. & WOLFE, G. V. (2005) production and cellular localization of neutral long-chain lipids in the haptophyte algae *Isochrysis galbana* and *Emiliana huxleyi*. *Journal of Phycology*, 41, 1000-1009.
- EPSTEIN, B. L., D'HONDT, S. & HARGRAVES, P. E. (2001) The possible metabolic role of C37 alkenones in *Emiliana huxleyi*. *Organic Geochemistry*, 32, 867-875.
- FEAKINS, S. J., KIRBY, M. E., CHEETHAM, M. I., IBARRA, Y. & ZIMMERMAN, S. R. (2014) Fluctuation in leaf wax D/H ratio from a southern California lake records significant variability in isotopes in precipitation during the late Holocene. *Organic Geochemistry*, 66, 48-59.
- FEAKINS, S. J. & SESSIONS, A. L. (2010) Controls on the D/H ratios of plant leaf waxes in an arid ecosystem. *Geochimica et Cosmochimica Acta*, 74, 2128-2141.
- FERNÁNDEZ, E., BALCH, W. M., MARAÑÓN, E. & HOLLIGAN, P. M. (1994) High rates of lipid biosynthesis in cultured, mesocosm and coastal populations of the coccolithophore *Emiliana huxleyi*.
- FERRAT, M., WEISS, D. J., STREKOPYTOV, S., DONG, S., CHEN, H., NAJORKA, J., SUN, Y., GUPTA, S., TADA, R. & SINHA, R. (2011) Improved provenance tracing of Asian dust sources using rare earth elements and selected trace elements for palaeomonsoon studies on the eastern Tibetan Plateau. *Geochimica et Cosmochimica Acta*, 75, 6374-6399.
- FICKEN, K. J., LI, B., SWAIN, D. L. & EGLINTON, G. (2000) An n-alkane proxy for the sedimentary input of submerged/floating freshwater aquatic macrophytes. *Organic Geochemistry*, 31, 745-749.
- FORNACE, K. L., HUGHEN, K. A., SHANAHAN, T. M., FRITZ, S. C., BAKER, P. A. & SYLVA, S. P. (2014) A 60,000-year record of hydrologic variability in the Central Andes from the hydrogen isotopic composition of leaf waxes in Lake Titicaca sediments. *Earth and Planetary Science Letters*, 408, 263-271.
- FRANK, D. C., ESPER, J., RAIBLE, C. C., BUNTGEN, U., TROUET, V., STOCKER, B. & JOOS, F. (2010) Ensemble reconstruction constraints on the global carbon cycle sensitivity to climate. *Nature*, 463, 527-530.
- FROEHLICH, K., GIBSON, J. & AGGARWAL, P. (2001) Deuterium excess in precipitation and its climatological significance. *Study of Environmental Change Using Isotope Techniques. Proc. Intern. Conf. Citeseer*.
- FUKUSAWA, H. (1999) Varved Lacustrine Sediments in Japan:Recent Progress. *The Quaternary Research (Daiyonki-Kenkyu)*, 38, 237-243.
- GAGOSIAN, R. B. & PELTZER, E. T. (1986) The importance of atmospheric input of terrestrial organic material to deep sea sediments. *Organic Geochemistry*, 10, 661-669.
- GE, Q., HAO, Z., ZHENG, J. & SHAO, X. (2013) Temperature changes over the past 2000 yr in China and comparison with the Northern Hemisphere. *Climate of the Past*, 9, 1153-1160.
- GE, Q., ZHANG, X., HAO, Z. & ZHENG, J. (2011) Rates of temperature change in China during the past 2000 years. *Science China Earth Sciences*, 54, 1627-1634.
- GEBHARDT, A., FRANCKE, A., KÜCK, J., SAUERBREY, M., NIESSEN, F., WENNRICH, V. & MELLES, M. (2013) Petrophysical characterization of the lacustrine sediment succession drilled in Lake El'gygytgyn, Far East Russian Arctic. *Climate of the Past*, 9, 1933-1947.

- GHANBARI, R. N., BRAVO, H. R., MAGNUSON, J. J., HYZER, W. G. & BENSON, B. J. (2009) Coherence between lake ice cover, local climate and teleconnections (Lake Mendota, Wisconsin). *Journal of Hydrology*, 374, 282-293.
- GIGER, W., SCHAFFNER, C. & WAKEHAM, S. G. (1980) Aliphatic and olefinic hydrocarbons in recent sediments of Greifensee, Switzerland. *Geochimica et Cosmochimica Acta*, 44, 119-129.
- GODDARD, L. (2014) Heat hide and seek. *Nature Climate Change*, 4, 158-161.
- GONG, D.-Y. & HE, X.-Z. (2002) Interdecadal change in Western Pacific Subtropical High and climatic effects. *Journal of Geographical Sciences*, 12, 202-209.
- GONG, D.-Y., WANG, S.-W. & ZHU, J.-H. (2001) East Asian Winter Monsoon and Arctic Oscillation. *Geophysical Research Letters*, 28, 2073-2076.
- GONG, D. Y. & HO, C. H. (2003) Arctic oscillation signals in the East Asian summer monsoon. *Journal of Geophysical Research: Atmospheres*, 108.
- GUO, Z., LIU, T., GUIOT, J., WU, N., LÜ, H., HAN, J., LIU, J. & GU, Z. (1996) High frequency pulses of East Asian monsoon climate in the last two glaciations: link with the North Atlantic. *Climate Dynamics*, 12, 701-709.
- GUYARD, H., CHAPRON, E., ST-ONGE, G., ANSELMETTI, F. S., ARNAUD, F., MAGAND, O., FRANCUS, P. & MÉLIÈRES, M.-A. (2007) High-altitude varve records of abrupt environmental changes and mining activity over the last 4000 years in the Western French Alps (Lake Bramant, Grandes Rousses Massif). *Quaternary Science Reviews*, 26, 2644-2660.
- HA, K.-J., HEO, K.-Y., LEE, S.-S., YUN, K.-S. & JHUN, J.-G. (2012) Variability in the East Asian Monsoon: a review. *Meteorological Applications*, 19, 200-215.
- HABERLE, S. G. & LUMLEY, S. H. (1998) Age and origin of tephras recorded in postglacial lake sediments to the west of the southern Andes, 44 S to 47 S. *Journal of Volcanology and Geothermal Research*, 84, 239-256.
- HAIGH, J. D. (1996) The impact of solar variability on climate. *Science*, 272, 981-984.
- HAIGH, J. D. (1999) Modelling the impact of solar variability on climate. *Journal of Atmospheric and Solar-Terrestrial Physics*, 61, 63-72.
- HALLETT, D. J., MATHEWES, R. W. & FOIT JR, F. F. (2001) Mid-Holocene Glacier Peak and Mount St. Helens We Tephra Layers Detected in Lake Sediments from Southern British Columbia Using High-Resolution Techniques. *Quaternary Research*, 55, 284-292.
- HAO, Z., ZHENG, J., ZHANG, X., LIU, H., LI, M. & GE, Q. (2016) Spatial patterns of precipitation anomalies in eastern China during centennial cold and warm periods of the past 2000 years. *International Journal of Climatology*, 36, 467-475.
- HARADA, N., SATO, M., OGURI, K., HAGINO, K., OKAZAKI, Y., KATSUKI, K., TSUJI, Y., SHIN, K.-H., TADAI, O., SAITOH, S.-I., NARITA, H., KONNO, S., JORDAN, R. W., SHIRAIWA, Y. & GREBMEIER, J. (2012) Enhancement of coccolithophorid blooms in the Bering Sea by recent environmental changes. *Global Biogeochemical Cycles*, 26, n/a-n/a.
- HARADA, N., SHIN, K. H., MURATA, A., UCHIDA, M. & NAKATANI, T. (2003) Characteristics of alkenones synthesized by a bloom of *emiliania huxleyi* in the Bering Sea. *Geochimica et Cosmochimica Acta*, 67, 1507-1519.
- HE, Y., LIU, W., ZHAO, C., WANG, Z., WANG, H., LIU, Y., QIN, X., HU, Q., AN, Z. & LIU, Z. (2013) Solar influenced late Holocene temperature changes on the northern Tibetan Plateau. *Chinese Science Bulletin*, 58, 1053-1059.

- HERBERT, T. D., EDITORS-IN-CHIEF: HEINRICH, D. H. & KARL, K. T. (2003) 6.15 - Alkenone Paleotemperature Determinations. *Treatise on Geochemistry*. Oxford, Pergamon.
- HO, C.-H., BAIK, J.-J., KIM, J.-H., GONG, D.-Y. & SUI, C.-H. (2004) Interdecadal changes in summertime typhoon tracks. *Journal of Climate*, 17, 1767-1776.
- HONG, Y., HONG, B., LIN, Q., SHIBATA, Y., HIROTA, M., ZHU, Y., LENG, X., WANG, Y., WANG, H. & YI, L. (2005) Inverse phase oscillations between the East Asian and Indian Ocean summer monsoons during the last 12 000 years and paleo-El Niño. *Earth and Planetary Science Letters*, 231, 337-346.
- HOU, J., D'ANDREA, W. J. & HUANG, Y. (2008) Can sedimentary leaf waxes record D/H ratios of continental precipitation? Field, model, and experimental assessments. *Geochimica et Cosmochimica Acta*, 72, 3503-3517.
- HOU, J., D'ANDREA, W. J., MACDONALD, D. & HUANG, Y. (2007) Hydrogen isotopic variability in leaf waxes among terrestrial and aquatic plants around Blood Pond, Massachusetts (USA). *Organic Geochemistry*, 38, 977-984.
- HU, C., HENDERSON, G. M., HUANG, J., XIE, S., SUN, Y. & JOHNSON, K. R. (2008) Quantification of Holocene Asian monsoon rainfall from spatially separated cave records. *Earth and Planetary Science Letters*, 266, 221-232.
- HUANG, R.-H. & ZHOU, L.-T. (2002) Research on the characteristics, formation mechanism and prediction of severe climatic disasters in China. *Journal of Natural Disasters*, 11, 1-9.
- HUANG, R., CHEN, J. & HUANG, G. (2007) Characteristics and variations of the East Asian monsoon system and its impacts on climate disasters in China. *Advances in Atmospheric Sciences*, 24, 993-1023.
- HUANG, R., GU, L., XU, Y.-H., ZHANG, Q., WU, S. & CAO, J. (2005) Characteristics of the interannual variations of onset and advance of the East Asian summer monsoon and their associations with thermal states of the tropical western Pacific. *Chinese J. Atmos. Sci.*, 29, 20-36.
- HUANG, R., ZHANG, R. & YAN, B. (1999) Progresses in the studies on the interannual variability of East Asian climate system and problems to be studied further. *Basic Research in China*, 2, 66-73.
- HUANG, R., ZHOU, L. & CHEN, W. (2003) The progresses of recent studies on the variabilities of the East Asian monsoon and their causes. *Advances in Atmospheric Sciences*, 20, 55-69.
- HURRELL, J. W. (1995) Decadal trends in the North Atlantic Oscillation: regional temperatures and precipitation. *Science*, 269, 676-679.
- HURRELL, J. W., KUSHNIR, Y., OTTERSEN, G. & VISBECK, M. (2003) The North Atlantic Oscillation: climate significance and environmental impact.
- HURRELL, J. W. & LOON, H. (1997) Decadal Variations in Climate Associated with the North Atlantic Oscillation. IN DIAZ, H. F., BENISTON, M. & BRADLEY, R. S. (Eds.) *Climatic Change at High Elevation Sites*. Dordrecht, Springer Netherlands.
- IGARASHI, Y., YAMAMOTO, M. & IKEHARA, K. (2011) Climate and vegetation in Hokkaido, northern Japan, since the LGM: Pollen records from core GH02-1030 off Tokachi in the northwestern Pacific. *Journal of Asian Earth Sciences*, 40, 1102-1110.

- INNES, H. E., BISHOP, A. N., FOX, P. A., HEAD, I. M. & FARRIMOND, P. (1998) Early diagenesis of bacteriohopanoids in Recent sediments of Lake Pollen, Norway. *Organic Geochemistry*, 29, 1285-1295.
- ISHIWATARI, R., HIRAKAWA, Y., UZAKI, M., YAMADA, K. & YADA, T. (1994) Organic geochemistry of the Japan Sea sediments-1: Bulk organic matter and hydrocarbon analyses of Core KH-79-3, C-3 from the Oki Ridge for paleoenvironment assessments. *Journal of Oceanography*, 50, 179-195.
- JHUN, J.-G. & LEE, E.-J. (2004a) A New East Asian Winter Monsoon Index and Associated Characteristics of the Winter Monsoon. *Journal of Climate*. American Meteorological Society.
- JHUN, J. G. & LEE, E. J. (2004b) A new East Asian winter monsoon index and associated characteristics of the winter monsoon. *Journal of Climate*, 17, 711-726.
- JIN, Z., CAO, J., WU, J. & WANG, S. (2006) A Rb/Sr record of catchment weathering response to Holocene climate change in Inner Mongolia. *Earth Surface Processes and Landforms*, 31, 285-291.
- JIN, Z., WANG, S., SHEN, J., ZHANG, E., LI, F., JI, J. & LU, X. (2001) Chemical weathering since the Little Ice Age recorded in lake sediments: a high-resolution proxy of past climate. *Earth Surface Processes and Landforms*, 26, 775-782.
- JOHNSON, T. C., BROWN, E. T., MCMANUS, J., BARRY, S., BARKER, P. & GASSE, F. O. (2002) A High-Resolution Paleoclimate Record Spanning the Past 25,000 Years in Southern East Africa. *Science*, 296, 113-132.
- JONES, P. D., OSBORN, T. J. & BRIFFA, K. R. (2001) The Evolution of Climate Over the Last Millennium. *Science*, 292, 662-667.
- KARLSSON, J., BYSTROM, P., ASK, J., ASK, P., PERSSON, L. & JANSSON, M. (2009) Light limitation of nutrient-poor lake ecosystems. *Nature*, 460, 506-509.
- KATSUKI, K., SETO, K., NOGUCHI, T., SONODA, T. & KIM, J. (2012) Effects of regional climate changes on the planktonic ecosystem and water environment in the frozen Notooro Lagoon, northern Japan. *Marine environmental research*, 81, 83-89.
- KAWAMURA, K., ISHIMURA, Y. & YAMAZAKI, K. (2003) Four years' observations of terrestrial lipid class compounds in marine aerosols from the western North Pacific. *Global Biogeochemical Cycles*, 17, 1003.
- KELLEY, J., BOND, L. & BEASLEY, T. (1999) Global distribution of Pu isotopes and ²³⁷Np. *Science of the Total Environment*, 237, 483-500.
- KEMP, A. E. (1996) Laminated sediments as palaeo-indicators. *Geological Society, London, Special Publications*, 116, vii-xii.
- KETTERER, M. E., HAFER, K. M., LINK, C. L., KOLWAITE, D., WILSON, J. & MIETELSKI, J. W. (2004) Resolving global versus local/regional Pu sources in the environment using sector ICP-MS. *Journal of analytical atomic spectrometry*, 19, 241-245.
- KIM, Y., KIM, K.-Y. & JHUN, J.-G. (2013) Seasonal evolution mechanism of the East Asian winter monsoon and its interannual variability. *Climate Dynamics*, 41, 1213-1228.
- KIMURA, J. C. (1966) The beginning and end of the Shurin season of Japan.
- KITAGAWA, H. & MATSUMOTO, E. (1995) Climatic implications of $\delta^{13}\text{C}$ variations in a Japanese cedar (*Cryptomeria japonica*) during the last two millenia. *Geophysical Research Letters*, 22, 2155-2158.
- KITAYAMA, S., ISHII, K., IMADA, T., TAKEMURA, K. & RAMASWAMY, J. (2006) Voluntary settlement and the spirit of independence: Evidence from Japan's" northern frontier.". *Journal of personality and social psychology*, 91, 369.

- KNIGHT, J. (1997) On the Extinction of the Japanese Wolf. *Asian Folklore Studies*, 56, 129-159.
- KORTE, M. & CONSTABLE, C. G. C. Q. H. (2005) Continuous geomagnetic field models for the past 7 millennia: 2. CALS7K. *Geochemistry, Geophysics, Geosystems*, 6, n/a-n/a.
- KOTILAINEN, A., VALLIUS, H. & RYABCHUK, D. (2007) Seafloor anoxia and modern laminated sediments in coastal basins of the eastern Gulf of Finland, Baltic Sea. *Holocene sedimentary environment and sediment geochemistry of the eastern Gulf of Finland, Baltic Sea. Geological Survey of Finland, Special Paper*, 45, 49-62.
- KUANG, X. & ZHANG, Y. (2005) Seasonal variation of the East Asian subtropical westerly jet and its association with the heating field over East Asia. *Advances in Atmospheric Sciences*, 22, 831-840.
- KUECHLER, R., SCHEFUß, E., BECKMANN, B., DUPONT, L. & WEFER, G. (2013) NW African hydrology and vegetation during the Last Glacial cycle reflected in plant-wax-specific hydrogen and carbon isotopes. *Quaternary Science Reviews*, 82, 56-67.
- KYLANDER, M. E., LIND, E. M., WASTEGÅRD, S. & LÖWEMARK, L. (2012) Recommendations for using XRF core scanning as a tool in tephrochronology. *The Holocene*.
- LARRASOÑA, J. C., ROBERTS, A. P. & ROHLING, E. J. (2008) Magnetic susceptibility of eastern Mediterranean marine sediments as a proxy for Saharan dust supply? *Marine Geology*, 254, 224-229.
- LEE, B.-S. (1974) A synoptic study of the early summer and autumn rainy season in Korea and in East Asia.
- LEE, H. & ZHANG, D. (2011) Relationship between NAO and drought disasters in northwestern China in the last millennium. *Journal of Arid Environments*, 75, 1114-1120.
- LEE, K. E. & PARK, W. (2015) Initiation of East Asia monsoon failure at the climate transition from the Medieval Climate Anomaly to the Little Ice Age. *Global and Planetary Change*, 128, 83-89.
- LEINEN, M., CWIENK, D., HEATH, G. R., BISCAYE, P. E., KOLLA, V., THIEDE, J. R. & DAUPHIN, J. P. (1986) Distribution of biogenic silica and quartz in recent deep-sea sediments. *Geology*, 14, 199-203.
- LI, B., NYCHKA, D. W. & AMMANN, C. M. (2010) The Value of Multiproxy Reconstruction of Past Climate. *Journal of the American Statistical Association*, 105, 883-895.
- LI, F. & WANG, H. (2012) Predictability of the East Asian winter monsoon interannual variability as indicated by the DEMETER CGCMS. *Advances in Atmospheric Sciences*, 29, 441-454.
- LI, J., PHILIP, R. P., PU, F. & ALLEN, J. (1996) Long-chain alkenones in Qinghai Lake sediments. *Geochimica et Cosmochimica Acta*, 60, 235-241.
- LIM, J. & MATSUMOTO, E. (2008) Fine aeolian quartz records in Cheju Island, Korea, during the last 6500 years and pathway change of the westerlies over east Asia. *Journal of Geophysical Research: Atmospheres*, 113.
- LIM, J. & MATSUMOTO, E. C. L. (2006) Bimodal grain-size distribution of aeolian quartz in a maar of Cheju Island, Korea, during the last 6500 years: Its flux variation and controlling factor. *Geophysical Research Letters*, 33, n/a-n/a.
- LIU, C., ZHANG, J. & LI, C. (1999) Variations in CaCO₃ content and Sr isotopic composition of loess and records of paleoclimatic fluctuations. *Chinese Science Bulletin*, 44, 1512-1516.

- LIU, H., PROBERT, I., UITZ, J., CLAUSTRE, H., ARIS-BROUSO, S. P., FRADA, M., NOT, F. & DE VARGAS, C. (2009a) Extreme diversity in noncalcifying haptophytes explains a major pigment paradox in open oceans. *Proceedings of the National Academy of Sciences*, 106, 12803-12808.
- LIU, J., CHEN, F., CHEN, J., XIA, D., XU, Q., WANG, Z. & LI, Y. (2011) Humid medieval warm period recorded by magnetic characteristics of sediments from Gonghai Lake, Shanxi, North China. *Chinese Science Bulletin*, 56, 2464-2474.
- LIU, J., CHEN, F., CHEN, J., ZHANG, X., LIU, J. & BLOEMENDAL, J. C. J. D. (2013a) Weakening of the East Asian summer monsoon at 1000-1100 A.D. within the Medieval Climate Anomaly: Possible linkage to changes in the Indian Ocean-western Pacific. *Journal of Geophysical Research: Atmospheres*, 119, 2209-2219.
- LIU, J., CHEN, J., SELVARAJ, K., XU, Q., WANG, Z. & CHEN, F. (2014a) Chemical weathering over the last 1200 years recorded in the sediments of Gonghai Lake, Lvliang Mountains, North China: a high-resolution proxy of past climate. *Boreas*, 43, 914-923.
- LIU, J., LIU, W., AN, Z. & YANG, H. (2016) Different hydrogen isotope fractionations during lipid formation in higher plants: Implications for paleohydrology reconstruction at a global scale. *Scientific reports*, 6.
- LIU, W., LIU, Z., FU, M. & AN, Z. (2008) Distribution of the C37 tetra-unsaturated alkenone in Lake Qinghai, China: A potential lake salinity indicator. *Geochimica et Cosmochimica Acta*, 72, 988-997.
- LIU, W., YANG, H. & LI, L. (2006a) Hydrogen isotopic compositions of n-alkanes from terrestrial plants correlate with their ecological life forms. *Oecologia*, 150, 330-338.
- LIU, X., COLMAN, S., BROWN, E., MINOR, E. & LI, H. (2013b) Estimation of carbonate, total organic carbon, and biogenic silica content by FTIR and XRF techniques in lacustrine sediments. *Journal of Paleolimnology*, 50, 387-398.
- LIU, X., DONG, H., YANG, X., HERZSCHUH, U., ZHANG, E., STUUT, J.-B. W. & WANG, Y. (2009b) Late Holocene forcing of the Asian winter and summer monsoon as evidenced by proxy records from the northern Qinghai-Tibetan Plateau. *Earth and Planetary Science Letters*, 280, 276-284.
- LIU, X., FISHER, T. G., LEPPER, K. & LOWELL, T. V. (2014b) Geochemical characteristics of glacial Lake Agassiz sediments and new ages for the Moorhead Phase at Fargo, North Dakota, USA. *Canadian Journal of Earth Sciences*, 51, 850-861.
- LIU, Y., SUN, L., ZHOU, X., LUO, Y., HUANG, W., YANG, C., WANG, Y. & HUANG, T. (2014c) A 1400-year terrigenous dust record on a coral island in South China Sea. *Sci. Rep.*, 4.
- LIU, Y. H., HENDERSON, G. M., HU, C. Y., MASON, A. J., CHARNLEY, N., JOHNSON, K. R. & XIE, S. C. (2013c) Links between the East Asian monsoon and North Atlantic climate during the 8,200 year event. *Nature Geosci*, 6, 117-120.
- LIU, Z., HENDERSON, A. C. G. & HUANG, Y. (2006b) Alkenone-based reconstruction of late-Holocene surface temperature and salinity changes in Lake Qinghai, China. *Geophys. Res. Lett.*, 33, L09707.
- LIU, Z., WEN, X., BRADY, E. C., OTTO-BLIESNER, B., YU, G., LU, H., CHENG, H., WANG, Y., ZHENG, W., DING, Y., EDWARDS, R. L., CHENG, J., LIU, W. & YANG, H. (2014d) Chinese cave records and the East Asia Summer Monsoon.

- LOTTER, A. F., BIRKS, H. J. B. & ZOLITSCHKA, B. (1995) Late-glacial pollen and diatom changes in response to two different environmental perturbations: volcanic eruption and Younger Dryas cooling. *Journal of Paleolimnology*, 14, 23-47.
- LOWENSTAM, H. (1981) Minerals formed by organisms. *Science*, 211, 1126-1131.
- LOZANO-GARCIA, M. S., ORTEGA-GUERRERO, B., CABALLERO-MIRANDA, M. & URRUTIA-FUCUGAUCHI, J. (1993) Late Pleistocene and Holocene Paleoenvironments of Chalco Lake, Central Mexico. *Quaternary Research*, 40, 332-342.
- LU, R. & KIM, B.-J. (2004) The climatological Rossby wave source over the STCZs in the summer Northern Hemisphere. *J. Meteor. Soc. Japan*, 82, 657-669.
- MACDONALD, G. M. & CASE, R. A. (2005) Variations in the Pacific Decadal Oscillation over the past millennium. *Geophysical Research Letters*, 32, L08703.
- MAN, W., ZHOU, T. & JUNGCLAUS, J. H. (2012) Simulation of the East Asian Summer Monsoon during the Last Millennium with the MPI Earth System Model. *Journal of Climate*. American Meteorological Society.
- MANN, M. E. & JONES, P. D. (2003) Global surface temperatures over the past two millennia. *Geophysical Research Letters*, 30.
- MANN, M. E., ZHANG, Z., RUTHERFORD, S., BRADLEY, R. S., HUGHES, M. K., SHINDELL, D., AMMANN, C., FALUVEGI, G. & NI, F. (2009) Global Signatures and Dynamical Origins of the Little Ice Age and Medieval Climate Anomaly. *Science*, 326, 1256-1260.
- MANTUA, N. & HARE, S. (2002) The Pacific Decadal Oscillation. *Journal of Oceanography*, 58, 35-44.
- MANTUA, N. J., HARE, S. R., ZHANG, Y., WALLACE, J. M. & FRANCIS, R. C. (1997) A Pacific Interdecadal Climate Oscillation with Impacts on Salmon Production. *Bulletin of the American Meteorological Society*. American Meteorological Society.
- MAO, R., HO, C.-H., SHAO, Y., GONG, D.-Y. & KIM, J. (2010) Influence of Arctic Oscillation on dust activity over northeast Asia. *Atmospheric Environment*, 45, 326-337.
- MARLOWE, I. T., GREEN, J. C., NEAL, A. C., BRASSELL, S. C., EGLINTON, G. & COURSE, P. A. (1984) Long chain (n-C37-C39) alkenones in the Prymnesiophyceae. Distribution of alkenones and other lipids and their taxonomic significance. *British Phycological Journal*, 19, 203-216.
- MASSON-DELMOTTE, V. R., JOUZEL, J., LANDAIS, A., STIEVENARD, M., JOHNSEN, S. J., WHITE, J., WERNER, M., SVEINBJORNSDOTTIR, A. & FUHRER, K. (2005) GRIP deuterium excess reveals rapid and orbital-scale changes in Greenland moisture origin. *Science*, 309, 118-121.
- MATSUBAYASHI, J., MORIMOTO, J., MANO, T., ARYAL, A. & NAKAMURA, F. (2014) Using stable isotopes to understand the feeding ecology of the Hokkaido brown bear (*Ursus arctos*) in Japan. *Ursus*, 25, 87-97.
- MEEKER, L. D. & MAYEWSKI, P. A. (2002) A 1400-year high-resolution record of atmospheric circulation over the North Atlantic and Asia. *The Holocene*, 12, 257-266.
- MELLES, M., BRIGHAM-GRETTE, J., MINYUK, P. S., NOWACZYK, N. R., WENNRICH, V., DECONTO, R. M., ANDERSON, P. M., ANDREEV, A. A., COLETTI, A., COOK, T. L., HALTIA-HOVI, E., KUKKONEN, M., LOZHKIN, A. V., ROSÉN, P., TARASOV, P., VOGEL, H. & WAGNER, B. (2012) 2.8 Million Years of Arctic Climate Change from Lake El'gygytgyn, NE Russia. *Science*, 337, 315-320.

- MERLIVAT, L. & JOUZEL, J. (1979) Global climatic interpretation of the deuterium-oxygen 18 relationship for precipitation. *Journal of Geophysical Research: Oceans*, 84, 5029-5033.
- MEYERS, P. A. (1994) Preservation of elemental and isotopic source identification of sedimentary organic matter. *Chemical Geology*, 114, 289-302.
- MEYERS, P. A. (1997) Organic geochemical proxies of paleoceanographic, paleolimnologic, and paleoclimatic processes. *Organic Geochemistry*, 27, 213-250.
- MEYERS, P. A. & ISHIWATARI, R. (1993a) Lacustrine organic geochemistry-- an overview of indicators of organic matter sources and diagenesis in lake sediments. *Organic Geochemistry*, 20, 867-900.
- MEYERS, P. A. & ISHIWATARI, R. (1993b) Lacustrine organic geochemistry--an overview of indicators of organic matter sources and diagenesis in lake sediments. *Organic Geochemistry*, 20, 867-900.
- MIKAMI, M., SHI, G. Y., UNO, I., YABUKI, S., IWASAKA, Y., YASUI, M., AOKI, T., TANAKA, T. Y., KUROSAKI, Y., MASUDA, K., UCHIYAMA, A., MATSUKI, A., SAKAI, T., TAKEMI, T., NAKAWO, M., SEINO, N., ISHIZUKA, M., SATAKE, S., FUJITA, K., HARA, Y., KAI, K., KANAYAMA, S., HAYASHI, M., DU, M., KANAI, Y., YAMADA, Y., ZHANG, X. Y., SHEN, Z., ZHOU, H., ABE, O., NAGAI, T., TSUTSUMI, Y., CHIBA, M. & SUZUKI, J. (2006) Aeolian dust experiment on climate impact: An overview of Japan-China joint project ADEC. *Global and Planetary Change*, 52, 142-172.
- MISCHKE, S., ZHANG, C., BÖRNER, A. & HERZSCHUH, U. (2009) Lateglacial and Holocene variation in aeolian sediment flux over the northeastern Tibetan Plateau recorded by laminated sediments of a saline meromictic lake. *Journal of Quaternary Science*, 25, 162-177.
- MISHIMA, M., SUZUKI, A., NAGAO, M., ISHIMURA, T., INOUE, M. & KAWAHATA, H. (2010) Abrupt shift toward cooler condition in the earliest 20th century detected in a 165 year coral record from Ishigaki Island, southwestern Japan. *Geophysical Research Letters*, 37.
- MISHRA, V., CHERKAUER, K. A., BOWLING, L. C. & HUBER, M. (2011) Lake Ice phenology of small lakes: Impacts of climate variability in the Great Lakes region. *Global and Planetary Change*, 76, 166-185.
- MORRILL, C., OVERPECK, J. T. & COLE, J. E. (2003) A synthesis of abrupt changes in the Asian summer monsoon since the last deglaciation. *The Holocene*, 13, 465-476.
- MUNSELL COLOUR COMPANY (1994) *Munsell Soil Colour Charts*, New Windsor, NY, Macbeth Division of Kollmorgen.
- NAKAMURA, H. & FUKAMACHI, T. (2004) Evolution and dynamics of summertime blocking over the Far East and the associated surface Okhotsk high. *Quarterly Journal of the Royal Meteorological Society*, 130, 1213-1233.
- NOAA CENTRE FOR WEATHER AND CLIMATE PREDICTION (2016) Arctic Oscillation Index.
- NOGAMI, M., FUJISE, T. & FUKUDA, M. (1980) Periglacial environment in Japan: present and past. *GeoJournal*, 4, 125-132.
- NOWACZYK, N. R., MINYUK, P., MELLE, M., BRIGHAM-GRETTE, J., GLUSHKOVA, O., NOLAN, M., LOZHKIN, A. V., STETSENKO, T. V., ANDERSEN, P. & FORMAN, S. L. (2002) Magnetostratigraphic results from impact crater Lake El'gygytgyn, northeastern Siberia: a 300 kyr long high-resolution terrestrial palaeoclimatic record from the Arctic. *Geophysical Journal International*, 150, 109-126.

- NOWLIN, W. H., EVARTS, J. L. & VANNI, M. J. (2005) Release rates and potential fates of nitrogen and phosphorus from sediments in a eutrophic reservoir. *Freshwater Biology*, 50, 301-322.
- OCHIAI, S., NAGAO, S., ITONO, T., SUZUKI, T., KASHIWAYA, K., YONEBAYASHI, K., OKAZAKI, M., KAERIYAMA, M., QIN, Y.-X. & HASEGAWA, T. (2015) Recent eutrophication and environmental changes in the catchment inferred from geochemical properties of Lake Onuma sediments in Japan. *Earth Surface Processes and Environmental Changes in East Asia*. Springer.
- OGI, M., TACHIBANA, Y. & YAMAZAKI, K. (2004) The connectivity of the winter North Atlantic Oscillation (NAO) and the summer Okhotsk High. *Journal of the Meteorological Society of Japan*, 82, 905-913.
- OLSEN, G. J., LANE, D. J., GIOVANNONI, S. J., PACE, N. R. & STAHL, D. A. (1986) Microbial ecology and evolution: a ribosomal RNA approach. *Annual review of microbiology*, 40, 337-365.
- OMOTE, K., NISHIDA, C., TAKENAKA, T., SAITO, K., SHIMURA, R., FUJIMOTO, S., SATO, T. & MASUDA, R. (2015) Recent fragmentation of the endangered Blakiston's fish owl (*Bubo blakistoni*) population on Hokkaido Island, Northern Japan, Revealed by Mitochondrial DNA and Microsatellite Analyses. *Zoological Letters*, 1, 16.
- ONO, Y. & IRINO, T. (2004) Southern migration of westerlies in the Northern Hemisphere PEP II transect during the Last Glacial Maximum. *Quaternary International*, 118, 13-22.
- ONO, Y. & NARUSE, T. (1997) Snowline elevation and eolian dust flux in the Japanese Islands during Isotope Stages 2 and 4. *Quaternary International*, 37, 45-54.
- OPPO, D. W., ROSENTHAL, Y. & LINSLEY, B. K. (2009) 2,000-year-long temperature and hydrology reconstructions from the Indo-Pacific warm pool. *Nature*, 460, 1113-1116.
- ORTEGA, B., CABALLERO, M., LOZANO, S., VILACLARA, G. & RODRÍGUEZ, A. (2006) Rock magnetic and geochemical proxies for iron mineral diagenesis in a tropical lake: Lago Verde, Los Tuxtlas, East-Central Mexico. *Earth and Planetary Science Letters*, 250, 444-458.
- PAGANI, M., PEDENTCHOUK, N., HUBER, M., SLUIJS, A., SCHOUTEN, S., BRINKHUIS, H., DAMSTÉ, J. S. S., DICKENS, G. R., BACKMAN, J. & CLEMENS, S. (2006) Arctic hydrology during global warming at the Palaeocene/Eocene thermal maximum. *Nature*, 442, 671-675.
- PARK, Y. J. & AHN, J. B. (2014) Characteristics of atmospheric circulation over East Asia associated with summer blocking. *Journal of Geophysical Research: Atmospheres*, 119, 726-738.
- PEARSON, E. J., JUGGINS, S. & FARRIMOND, P. (2008) Distribution and significance of long-chain alkenones as salinity and temperature indicators in Spanish saline lake sediments. *Geochimica et Cosmochimica Acta*, 72, 4035-4046.
- PEDENTCHOUK, N., FREEMAN, K. H. & HARRIS, N. B. (2006) Different response of $\delta^{13}C$ values of n-alkanes, isoprenoids, and kerogen during thermal maturation. *Geochimica et Cosmochimica Acta*, 70, 2063-2072.
- PEDENTCHOUK, N., SUMNER, W., TIPPLE, B. & PAGANI, M. (2008) $\delta^{13}C$ and δD compositions of n-alkanes from modern angiosperms and conifers: An experimental set up in central Washington State, USA. *Organic Geochemistry*, 39, 1066-1071.
- PEINERUD, E. K. (2000) Interpretation of Si concentrations in lake sediments: three case studies. *Environmental Geology*, 40, 64-72.

- POND, D. & HARRIS, R. (1996) The lipid composition of the coccolithophore *Emiliana huxleyi* and its possible ecophysiological significance. *Journal of the Marine Biological Association of the United Kingdom*, 76, 579-594.
- PORTER, S. C. & WEIJIAN, Z. (2006) Synchronism of Holocene East Asian monsoon variations and North Atlantic drift-ice tracers. *Quaternary Research*, 65, 443-449.
- PORTER, S. C. & ZHISHENG, A. (1995) Correlation between climate events in the North Atlantic and China during the last glaciation. *Nature*, 375, 305-308.
- POYNTER, J., FARRIMOND, P., ROBINSON, N. & EGLINTON, G. (1989) Aeolian-derived higher plant lipids in the marine sedimentary record: Links with palaeoclimate. *Paleoclimatology and paleometeorology: modern and past patterns of global atmospheric transport*. Springer.
- PRAHL, F. G., MUEHLHAUSEN, L. A. & ZAHNLE, D. L. (1988) Further evaluation of long-chain alkenones as indicators of paleoceanographic conditions. *Geochimica et Cosmochimica Acta*, 52, 2303-2310.
- PRAHL, F. G. & WAKEHAM, S. G. (1987) Calibration of unsaturation patterns in long-chain ketone compositions for palaeotemperature assessment. *Nature*, 330, 367-369.
- PROSPERO, J. M., GINOUX, P., TORRES, O., NICHOLSON, S. E. & GILL, T. E. C. (2002) Environmental characterization of global sources of atmospheric soil dust identified with the Nimbus 7 Total Ozone Mapping Spectrometer (TOMS) absorbing aerosol product *Reviews of Geophysics*, 40, 2-1-2-31.
- QIAN, W., KANG, H.-S. & LEE, D.-K. (2002a) Distribution of seasonal rainfall in the East Asian monsoon region. *Theoretical and Applied Climatology*, 73, 151-168.
- QIAN, W., QUAN, L. & SHI, S. (2002b) Variations of the Dust Storm in China and its Climatic Control. *Journal of Climate*, 15, 1216-1229.
- QIAO, S., YANG, Z., LIU, J., SUN, X., XIANG, R., SHI, X., FAN, D. & SAITO, Y. (2011) Records of late-Holocene East Asian winter monsoon in the East China Sea: Key grain-size component of quartz versus bulk sediments. *Quaternary International*, 230, 106-114.
- QIU, L., WILLIAMS, D. F., GVORZDKOV, A., KARABANOV, E. & SHIMARAEVA, M. (1993) Biogenic silica accumulation and paleoproductivity in the northern basin of Lake Baikal during the Holocene. *Geology*, 21, 25-28.
- RANDLETT, M.-È., COOLEN, M. J. L., STOCKHECKE, M., PICKARSKI, N., LITT, T., BALKEMA, C., KWIECIEN, O., TOMONAGA, Y., WEHRLI, B. & SCHUBERT, C. J. (2014) Alkenone distribution in Lake Van sediment over the last 270 ka: influence of temperature and haptophyte species composition. *Special Issue: Results from the PALEOVAN Drilling Project: a 600,000 year long continental archive in the Near East*.
- REA, D. K., SNOECKX, H. & JOSEPH, L. H. (1998) Late Cenozoic Eolian deposition in the North Pacific: Asian drying, Tibetan uplift, and cooling of the northern hemisphere. *Paleoceanography*, 13, 215-224.
- ROLEDA, M. Y., SLOCOMBE, S. P., LEAKEY, R. J. G., DAY, J. G., BELL, E. M. & STANLEY, M. S. (2013) Effects of temperature and nutrient regimes on biomass and lipid production by six oleaginous microalgae in batch culture employing a two-phase cultivation strategy. *Bioresource Technology*, 129, 439-449.
- ROMMERSKIRCHEN, F., EGLINTON, G., DUPONT, L., GÜNTNER, U., WENZEL, C. & RULLKÖTTER, J. (2003) A north to south transect of Holocene southeast Atlantic continental margin sediments: Relationship between aerosol

- transport and compound-specific $\delta^{13}\text{C}$ land plant biomarker and pollen records. *Geochemistry, Geophysics, Geosystems*, 4, 1101.
- ROSELL-MELÉ, A. (1998) Interhemispheric appraisal of the value of alkenone indices as temperature and salinity proxies in high-latitude locations. *Paleoceanography*, 13, 694-703.
- ROSELL-MELÉ, A., CARTER, J. & EGLINTON, G. (1994) Distributions of long-chain alkenones and alkyl alkenoates in marine surface sediments from the North East Atlantic. *Organic Geochemistry*, 22, 501-509.
- ROSELL-MELÉ, A., JANSEN, E. & WEINELT, M. (2002) Appraisal of a molecular approach to infer variations in surface ocean freshwater inputs into the North Atlantic during the last glacial. *Global and Planetary Change*, 34, 143-152.
- ROTHWELL, R. G. & RACK, F. R. (2006) New techniques in sediment core analysis: an introduction. *Geological Society, London, Special Publications*, 267, 1-29.
- SACHSE, D., BILLAULT, I., J, B. G., CHIKARAISHI, Y., DAWSON, T., E, FEAKINS, S., J, FREEMAN, K., H, MAGILL, C., R, MCINERNEY, F., A, VAN DER MEER, M., T.J, POLISSAR, P., ROBINS, R. J., SACHS, J., P, SCHMIDT, H.-L., SESSIONS, A., L, WHITE, J., W.C, WEST, J., B & ANSGAR, K. (2012) Molecular Paleohydrology: Interpreting the Hydrogen-Isotopic Composition of Lipid Biomarkers from Photosynthesizing Organisms. *Annual Review of Earth and Planetary Sciences*, 40, 221-249.
- SACHSE, D., RADKE, J. & GLEIXNER, G. (2006) δD values of individual n-alkanes from terrestrial plants along a climatic gradient- Implications for the sedimentary biomarker record. *Organic Geochemistry*, 37, 469-483.
- SAGAWA, T., KUWAE, M., TSURUOKA, K., NAKAMURA, Y., IKEHARA, M. & MURAYAMA, M. (2014) Solar forcing of centennial-scale East Asian winter monsoon variability in the mid- to late Holocene.
- SAITO, O. (2010) "Climate and Famine in Historic Japan: A Very Long-Term Perspective". IN KUROSU, S., BENGTSSON, T. AND CAMPBELL, C. (Ed.) *Demographic Responses to Economic and Environmental Crises*, Tokyo. Reitaku University.
- SAKAGUCHI, Y. (1983) Warm and cold stages in the past 7600 years in Japan and their global correlation - Especially on climatic impacts to the global sea level changes and the ancient Japanese history. *Bull. Dept. Geogr. Univ. Tokyo*, 15, 1-31.
- SAMPE, T. & XIE, S.-P. (2010) Large-scale dynamics of the Meiyu-Baiu Rainband: environmental forcing by the westerly jet*. *Journal of Climate*, 23, 113-134.
- SAUER, P. E., EGLINTON, T. I., HAYES, J. M., SCHIMMELMANN, A. & SESSIONS, A. L. (2001) Compound-specific D/H ratios of lipid biomarkers from sediments as a proxy for environmental and climatic conditions. *Geochimica et Cosmochimica Acta*, 65, 213-222.
- SCHEFUß, E., RATMEYER, V., STUUT, J.-B. W., JANSEN, J. H. F. & SINNINGHE DAMSTÉ, J. S. (2003) Carbon isotope analyses of n-alkanes in dust from the lower atmosphere over the central eastern Atlantic. *Geochimica et Cosmochimica Acta*, 67, 1757-1767.
- SCHEFUSS, E., SCHOUTEN, S. & SCHNEIDER, R. R. (2005) Climatic controls on central African hydrology during the past 20,000 years. *Nature*, 437, 1003-1006.
- SCHIMMELMANN, A., LEWAN, M. D. & WINTSCH, R. P. (1999) D/H isotope ratios of kerogen, bitumen, oil, and water in hydrous pyrolysis of source rocks

- containing kerogen types I, II, IIS, and III. *Geochimica et Cosmochimica Acta*, 63, 3751-3766.
- SCHMID, M., HUNZIKER, S. & WÜEST, A. (2014) Lake surface temperatures in a changing climate: a global sensitivity analysis. *Climatic Change*, 124, 301-315.
- SCHMIDT, F., OBERHÄNSLI, H. & WILKES, H. (2014) Biocoenosis response to hydrological variability in Southern Africa during the last 84kaBP: A study of lipid biomarkers and compound-specific stable carbon and hydrogen isotopes from the hypersaline Lake Tswaing. *Global and Planetary Change*, 112, 92-104.
- SCHÖNE, B. R., OSCHMANN, W., TANABE, K., DETTMAN, D., FIEBIG, J., HOUK, S. D. & KANIE, Y. (2004) Holocene seasonal environmental trends at Tokyo Bay, Japan, reconstructed from bivalve mollusk shells—implications for changes in the East Asian monsoon and latitudinal shifts of the Polar Front. *Quaternary Science Reviews*, 23, 1137-1150.
- SCHOUTEN, S., RIJPSTRA, W. I. C., KOK, M., HOPMANS, E. C., SUMMONS, R. E., VOLKMAN, J. K. & SINNINGHE DAMSTÉ, J. S. (2001) Molecular organic tracers of biogeochemical processes in a saline meromictic lake (Ace Lake). *Geochimica et Cosmochimica Acta*, 65, 1629-1640.
- SCHULZ, H.-M., SCHÖNER, A. & EMEIS, K.-C. (2000a) Long-chain alkenone patterns in the Baltic sea—an ocean-freshwater transition. *Geochimica et Cosmochimica Acta*, 64, 469-477.
- SCHULZ, H.-M., SCHÖNER, A. & EMEIS, K.-C. (2000b) Long-chain alkenone patterns in the Baltic sea—an ocean-freshwater transition. *Geochimica et Cosmochimica Acta*, 64, 469-477.
- SCHURER, A. P., TETT, S. F. & HEGERL, G. C. (2014) Small influence of solar variability on climate over the past millennium. *Nature Geoscience*, 7, 104-108.
- SCHWING, F. B., JIANG, J. & MENDELSSOHN, R. (2003) Coherency of multi-scale abrupt changes between the NAO, NPI, and PDO. *Geophysical Research Letters*, 30.
- SEKI, O., KAWAMURA, K. & ISHIWATARI, R. (2012) Assessment of hydrogen isotopic compositions of n-fatty acids as paleoclimate proxies in Lake Biwa sediments. *Journal of Quaternary Science*, 27, 884-890.
- SEKI, O., NAKATSUKA, T., SHIBATA, H. & KAWAMURA, K. (2010) A compound-specific n-alkane $\delta^{13}\text{C}$ and δD approach for assessing source and delivery processes of terrestrial organic matter within a forested watershed in northern Japan. *Geochimica et Cosmochimica Acta*, 74, 599-613.
- SESSIONS, A. L. (2006) Seasonal changes in D/H fractionation accompanying lipid biosynthesis in *Spartina alterniflora*. *Geochimica et Cosmochimica Acta*, 70, 2153-2162.
- SESSIONS, A. L., SYLVA, S. P., SUMMONS, R. E. & HAYES, J. M. (2004) Isotopic exchange of carbon-bound hydrogen over geologic timescales. *Geochimica et Cosmochimica Acta*, 68, 1545-1559.
- SHAO, X., HUANG, L., LIU, H., LIANG, E., FANG, X. & WANG, L. (2005) Reconstruction of precipitation variation from tree rings in recent 1000 years in Delingha, Qinghai.
- SHENG, G., CAI, K., YANG, X., LU, J., JIA, G., PENG, P. A. & FU, J. (1999) Long-chain alkenones in Hotong Qagan Nur Lake sediments and its paleoclimatic implications. *Chinese Science Bulletin*, 44, 259-263.
- SHI, F., GE, Q., YANG, B., LI, J., YANG, F., LJUNGQVIST, F. C., SOLOMINA, O., NAKATSUKA, T., WANG, N., ZHAO, S., XU, C., FANG, K., SANO, M., CHU, G., FAN, Z., GAIRE, N. P. & ZAFAR, M. U. (2015) A multi-proxy

- reconstruction of spatial and temporal variations in Asian summer temperatures over the last millennium. *Climatic Change*, 131, 663-676.
- SHINDELL, D. T., SCHMIDT, G. A., MANN, M. E., RIND, D. & WAPLE, A. (2001) Solar Forcing of Regional Climate Change During the Maunder Minimum. *Science*, 294, 2149-2152.
- SHIOMOTO, A., ASAKUMA, K., HOON, H.-D., SAKAGUCHI, K. & MAEKAWA, K. (2012) An early spring bloom of large diatoms in the ice-covered Saroma-ko Lagoon, Hokkaido, Japan. *Journal of the Marine Biological Association of the United Kingdom*, 92, 29-37.
- SHOUYUN, H., CHENGLONG, D., APPEL, E. & VEROSUB, K. L. (2002) Environmental magnetic studies of lacustrine sediments. *Chinese Science Bulletin*, 47, 613-616.
- SICRE, M.-A., BARD, E., EZAT, U. & ROSTEK, F. (2002) Alkenone distributions in the North Atlantic and Nordic sea surface waters. *Geochemistry, Geophysics, Geosystems*, 3, 1 of 13-13 of 13.
- SIGMAN, D. M. & BOYLE, E. A. (2000) Glacial/interglacial variations in atmospheric carbon dioxide. *Nature*, 407, 859-869.
- SIMONEIT, B. R. T., MAZUREK, M. A., BRENNER, S., CRISP, P. T. & KAPLAN, I. R. (1979) Organic geochemistry of recent sediments from Guaymas Basin, Gulf of California. *Deep Sea Research Part A. Oceanographic Research Papers*, 26, 879-891.
- SMITH, F. A. & FREEMAN, K. H. (2006) Influence of physiology and climate on $\delta^{13}C$ of leaf wax n-alkanes from C3 and C4 grasses. *Geochimica et Cosmochimica Acta*, 70, 1172-1187.
- SOGIN, M. L., ELWOOD, H. J. & GUNDERSON, J. H. (1986) Evolutionary diversity of eukaryotic small-subunit rRNA genes. *Proceedings of the National Academy of Sciences*, 83, 1383-1387.
- SOMAYAJULU, B. L. K., RADHAKRISHNAMURTY, C. & WALSH, T. J. (1978) Susceptibility as a tool for studying magnetic stratigraphy of marine sediments. *Proceedings of the Indian Academy of Sciences - Section A, Earth and Planetary Sciences*, 87, 201-213.
- STOECK, T., BASS, D., NEBEL, M., CHRISTEN, R., JONES, M. D. M., BREINER, H.-W. & RICHARDS, T. A. (2010) Multiple marker parallel tag environmental DNA sequencing reveals a highly complex eukaryotic community in marine anoxic water. *Molecular Ecology*, 19, 21-31.
- SUN, J., WANG, H., YUAN, W. & CHEN, H. C. D. (2010) Spatial-temporal features of intense snowfall events in China and their possible change. *Journal of Geophysical Research: Atmospheres*, 115, n/a-n/a.
- SUN, Q., CHU, G., LI, S., LÜ, C. & ZHENG, M. (2004) Long-chain alkenones in sulfate lakes and its paleoclimatic implications. *Chinese Science Bulletin*, 49, 2082-2086.
- SUN, Q., CHU, G., LIU, G., LI, S. & WANG, X. (2007) Calibration of alkenone unsaturation index with growth temperature for a lacustrine species, *Chrysotila lamellosa* (Haptophyceae). *Organic Geochemistry*, 38, 1226-1234.
- SUN, W., SHEN, J., ZHANG, E., HASEBE, N., KASHIWAYA, K., CHEN, R. & ITONO, T. (2015) Stable nitrogen isotope record of lacustrine sediments in Lake Onuma (Northern Japan) indicates regional hydrological variability during the past four centuries. *Quaternary International*.
- SUN, Y., CLEMENS, S. C., MORRILL, C., LIN, X., WANG, X. & AN, Z. (2012) Influence of Atlantic meridional overturning circulation on the East Asian winter monsoon. *Nature Geosci*, 5, 46-49.

- TAN, M., LIU, T., HOU, J., QIN, X., ZHANG, H. & LI, T. C. (2003) Cyclic rapid warming on centennial-scale revealed by a 2650-year stalagmite record of warm season temperature. *Geophysical Research Letters*, 30, n/a-n/a.
- TAO, F., YOKOZAWA, M., ZHANG, Z., HAYASHI, Y., GRASSL, H. & FU, C. (2004) Variability in climatology and agricultural production in China in association with the East Asian summer monsoon and El Niño Southern Oscillation. *Climate Research*, 28, 23-30.
- TELFORD, R. J., BARKER, P., METCALFE, S. & NEWTON, A. (2004) Lacustrine responses to tephra deposition: examples from Mexico. *Quaternary Science Reviews*, 23, 2337-2353.
- THEISSEN, K. M., ZINNIKER, D. A., MOLDOWAN, J. M., DUNBAR, R. B. & ROWE, H. D. (2005) Pronounced occurrence of long-chain alkenones and dinosterol in a 25,000-year lipid molecular fossil record from Lake Titicaca, South America. *Geochimica et Cosmochimica Acta*, 69, 623-636.
- THEROUX, S., D'ANDREA, W. J., TONEY, J., AMARAL-ZETTLER, L. & HUANG, Y. (2010) Phylogenetic diversity and evolutionary relatedness of alkenone-producing haptophyte algae in lakes: Implications for continental paleotemperature reconstructions. *Earth and Planetary Science Letters*, 300, 311-320.
- THIEL, V., JENISCH, A., LANDMANN, G. N., REIMER, A. & MICHAELIS, W. (1997) Unusual distributions of long-chain alkenones and tetrahymanol from the highly alkaline Lake Van, Turkey. *Geochimica et Cosmochimica Acta*, 61, 2053-2064.
- THOMPSON, D., W.J & WALLACE, J., M (1998) The Arctic Oscillation signature in the wintertime geopotential height and temperature field. *Geophysical Research Letters*, 25, 1297-1300.
- THOMPSON, D., W.J, WALLACE, J., M & HEGERL, G. C. (2000) Annular Modes in the Extratropical Circulation. Part I: Month-to-Month Variability. *Journal of Climate*, 13.
- THOMPSON, L. G., MOSLEY-THOMPSON, E., DAVIS, M., LIN, P., DAI, J., BOLZAN, J. & YAO, T. (1995) A 1000 year climatic ice-core record from the Guliya ice cap, China: its relationship to global climate variability. *Annals of Glaciology*, 21, 175-181.
- THOMPSON, L. G., MOSLEY-THOMPSON, E., DAVIS, M. E., LIN, P.-N., HENDERSON, K. & MASHIOTTA, T. A. (2003) Tropical glacier and ice core evidence of climate change on annual to millennial time scales. *Climate Variability and Change in High Elevation Regions: Past, Present & Future*. Springer.
- TODD, M. C. & MACKAY, A. W. (2003) Large-scale climatic controls on Lake Baikal ice cover. *Journal of Climate*, 16, 3186-3199.
- TOGGWEILER, J. (2009) Shifting westerlies. *Science*, 323, 1434-1435.
- TOMITA, T. & YASUNARI, T. (1996) Role of the Northeast Winter Monsoon on the Biennial Oscillation of the ENSO/Monsoon system. *Journal of the Meteorological Society of Japan*, 74, 399-413.
- TONEY, J. L., HUANG, Y., FRITZ, S. C., BAKER, P. A., GRIMM, E. & NYREN, P. (2010) Climatic and environmental controls on the occurrence and distributions of long chain alkenones in lakes of the interior United States. *Geochimica et Cosmochimica Acta*, 74, 1563-1578.
- TONEY, J. L., LEAVITT, P. R. & HUANG, Y. (2011) Alkenones are common in prairie lakes of interior Canada. *Organic Geochemistry*, 42, 707-712.
- TONEY, J. L., THEROUX, S., ANDERSEN, R. A., COLEMAN, A., AMARAL-ZETTLER, L. & HUANG, Y. (2012) Culturing of the first 37:4 predominant lacustrine haptophyte: Geochemical, biochemical, and genetic implications. *Geochimica et Cosmochimica Acta*, 78, 51-64.

- TROUET, V. R., ESPER, J., GRAHAM, N. E., BAKER, A., SCOURSE, J. D. & FRANK, D. C. (2009) Persistent Positive North Atlantic Oscillation Mode Dominated the Medieval Climate Anomaly. *Science*, 324, 78-80.
- TSUJI, H., NAKATSUKA, T., YAMAZAKI, K. & TAKAGI, K. (2008) Summer relative humidity in northern Japan inferred from $\delta^{18}\text{O}$ values of the tree ring in (1776-2002 A.D.): Influence of the paleoclimate indices of atmospheric circulation. *Journal of Geophysical Research: Atmospheres*, 113, D18103.
- TSUNOGAI, S., KURATA, T., SUZUKI, T. & YOKOTA, K. (1988) Seasonal variation of atmospheric ^{210}Pb and Al in the western North Pacific region. *Journal of Atmospheric Chemistry*, 7, 389-407.
- UEMATSU, M., DUCE, R. A., PROSPERO, J. M., CHEN, L., MERRILL, J. T. & MCDONALD, R. L. (1983) Transport of mineral aerosol from Asia Over the North Pacific Ocean. *Journal of Geophysical Research: Oceans*, 88, 5343-5352.
- VANDENBERGHE, J., LU, H., SUN, D., VAN HUISSTEDEN, J. & KONERT, M. (2004) The late Miocene and Pliocene climate in East Asia as recorded by grain size and magnetic susceptibility of the Red Clay deposits (Chinese Loess Plateau). *Palaeogeography, Palaeoclimatology, Palaeoecology*, 204, 239-255.
- VERARDO, D., FROELICH, P. & MCINTYRE, A. (1990) Determination of organic carbon and nitrogen in marine sediments using the Carlo Erba NA1500 analyzer. *Deep Sea Research Part A. Oceanographic Research Papers*, 37, 157-165.
- VOLKMAN, J. K., BARRERR, S. M., BLACKBURN, S. I. & SIKES, E. L. (1995) Alkenones in *Gephyrocapsa oceanica*: Implications for studies of paleoclimate. *Geochimica et Cosmochimica Acta*, 59, 513-520.
- VOLKMAN, J. K., BARRETT, S. M., BLACKBURN, S. I., MANSOUR, M. P., SIKES, E. L. & GELIN, F. O. (1998) Microalgal biomarkers: A review of recent research developments. *Organic Geochemistry*, 29, 1163-1179.
- VOLKMAN, J. K., EGLINTON, G., CORNER, E. D. S. & FORSBERG, T. E. V. (1980) Long-chain alkenes and alkenones in the marine coccolithophorid *Emiliania huxleyi*. *Phytochemistry*, 19, 2619-2622.
- VON GUNTEN, L., D'ANDREA, W. J., BRADLEY, R. S. & HUANG, Y. (2012) Proxy-to-proxy calibration: Increasing the temporal resolution of quantitative climate reconstructions. *Scientific reports*, 2.
- WANG, B. & CHAN, J. C. (2002) How strong ENSO events affect tropical storm activity over the western North Pacific*. *Journal of Climate*, 15, 1643-1658.
- WANG, B., CLEMENS, S. C. & LIU, P. (2003) Contrasting the Indian and East Asian monsoons: implications on geologic timescales. *Marine Geology*, 201, 5-21.
- WANG, B., WU, R. & FU, X. (2000) Pacific-East Asian teleconnection: how does ENSO affect East Asian climate? *Journal of Climate*, 13, 1517-1536.
- WANG, B., XIANG, B. & LEE, J.-Y. (2013a) Subtropical high predictability establishes a promising way for monsoon and tropical storm predictions. *Proceedings of the National Academy of Sciences*, 110, 2718-2722.
- WANG, H., YU, E. & YANG, S. (2011) An exceptionally heavy snowfall in Northeast china: large-scale circulation anomalies and hindcast of the NCAR WRF model. *Meteorology and Atmospheric Physics*, 113, 11-25.
- WANG, L. & CHEN, W. (2014) An intensity index for the East Asian winter monsoon. *Journal of Climate*, 27, 2361-2374.

- WANG, L., CHEN, W. & HUANG, R. (2008a) Interdecadal modulation of PDO on the impact of ENSO on the East Asian winter monsoon. *Geophysical Research Letters*, 35.
- WANG, L., RIOUAL, P., PANIZZO, V. N., LU, H., GU, Z., CHU, G., YANG, D., HAN, J., LIU, J. & MACKAY, A. W. (2012) A 1000-yr record of environmental change in NE China indicated by diatom assemblages from maar lake Erlongwan. *Quaternary Research*, 78, 24-34.
- WANG, R. & ZHENG, M. (1997) Occurrence and environmental significance of long-chain alkenones in Tibetan Zabuye Salt Lake, S.W. China. *International Journal of Salt Lake Research*, 6, 281-302.
- WANG, T., YAN, C. Z., SONG, X. & LI, S. (2013b) Landsat images reveal trends in the aeolian desertification in a source area for sand and dust storms in China's Alashan Plateau (1975-2007). *Land Degradation & Development*, 24, 422-429.
- WANG, X., LÄ, VLIE, R., SU, P. & FAN, X. (2008b) Magnetic signature of environmental change reflected by Pleistocene lacustrine sediments from the Nihewan Basin, North China. *Palaeogeography, Palaeoclimatology, Palaeoecology*, 260, 452-462.
- WANG, Y., CHENG, H., EDWARDS, R. L., HE, Y., KONG, X., AN, Z., WU, J., KELLY, M. J., DYKOSKI, C. A. & LI, X. (2005) The Holocene Asian Monsoon: Links to Solar Changes and North Atlantic Climate. *Science*, 308, 854-857.
- WANG, Y., CHENG, H., EDWARDS, R. L., KONG, X., SHAO, X., CHEN, S., WU, J., JIANG, X., WANG, X. & AN, Z. (2008c) Millennial- and orbital-scale changes in the East Asian monsoon over the past 224,000 years. *Nature*, 451, 1090-1093.
- WANG, Y., WANG, B. & OH, J.-H. (2001) Impact of the preceding El Niño on the east asian summer monsoon. *Journal of the Meteorological Society of Japan*, 79, 575-588.
- WEN, M., YANG, S., KUMAR, A. & ZHANG, P. (2009) An Analysis of the Large-Scale Climate Anomalies Associated with the Snowstorms Affecting China in January 2008. *Monthly Weather Review*. American Meteorological Society.
- WOESE, C. R. (1987) Bacterial evolution. *Microbiology Review*, 51, 221-271.
- WOODRUFF, J. D., DONNELLY, J. P. & OKUSU, A. (2009) Exploring typhoon variability over the mid-to-late Holocene: evidence of extreme coastal flooding from Kamikoshiki, Japan. *Quaternary Science Reviews*, 28, 1774-1785.
- WU, B. & WANG, J. C. (2002) Winter Arctic Oscillation, Siberian High and East Asian Winter Monsoon. *Geophysical Research Letters*, 29, 3-1-3-4.
- WU, B., ZHANG, R. & D'ARRIGO, R. (2006a) Distinct Modes of the East Asian Winter Monsoon. *Monthly Weather Review*. American Meteorological Society.
- WU, T.-W. & QIAN, Z.-A. (2003) The relation between the Tibetan winter snow and the Asian summer monsoon and rainfall: An observational investigation. *Journal of Climate*, 16, 2038-2051.
- WU, Y., ANDREAS, L. C., JIN, Z., WANG, S., GERHARD H, S., RICHARD W, B. & XIA, W. (2006b) Holocene climate development on the central Tibetan Plateau: A sedimentary record from Cuoe Lake. *Palaeogeography, Palaeoclimatology, Palaeoecology*, 234, 328-340.
- XIAO, J., INOUCHI, Y., KUMAI, H., YOSHIKAWA, S., KONDO, Y., LIU, T. & AN, Z. (1997a) Biogenic Silica Record in Lake Biwa of Central Japan over the Past 145,000 Years. *Quaternary Research*, 47, 277-283.

- XIAO, J., INOUCHI, Y., KUMAI, H., YOSHIKAWA, S., KONDO, Y., LIU, T. & AN, Z. (1997b) Eolian Quartz Flux to Lake Biwa, Central Japan, over the Past 145,000 Years. *Quaternary Research*, 48, 48-57.
- XIAO, J., PORTER, S. C., AN, Z., KUMAI, H. & YOSHIKAWA, S. (1995) Grain Size of Quartz as an Indicator of Winter Monsoon Strength on the Loess Plateau of Central China during the Last 130,000 Yr. *Quaternary Research*, 43, 22-29.
- XIAO, J. L., AN, Z. S., LIU, T. S., INOUCHI, Y., KUMAI, H., YOSHIKAWA, S. & KONDO, Y. (1999) East Asian monsoon variation during the last 130,000 Years: evidence from the Loess Plateau of central China and Lake Biwa of Japan. *Quaternary Science Reviews*, 18, 147-157.
- XIAO, S., LI, A., LIU, J. P., CHEN, M., XIE, Q., JIANG, F., LI, T., XIANG, R. & CHEN, Z. (2006) Coherence between solar activity and the East Asian winter monsoon variability in the past 8000 years from Yangtze River-derived mud in the East China Sea. *Palaeogeography, Palaeoclimatology, Palaeoecology*, 237, 293-304.
- XIE, S.-P., HU, K., HAFNER, J., TOKINAGA, H., DU, Y., HUANG, G. & SAMPE, T. (2009) Indian Ocean capacitor effect on Indo-western Pacific climate during the summer following El Niño. *Journal of Climate*, 22, 730-747.
- XIE, S., GUO, J., HUANG, J., CHEN, F., WANG, H. & FARRIMOND, P. (2004) Restricted utility of $\delta^{13}\text{C}$ of bulk organic matter as a record of paleovegetation in some loess-paleosol sequences in the Chinese Loess Plateau. *Quaternary Research*, 62, 86-93.
- XU, H., LIU, B. & WU, F. (2010a) Spatial and temporal variations of Rb/Sr ratios of the bulk surface sediments in Lake Qinghai. *Geochemical Transactions* C7 - 3, 11, 1-8.
- XU, M., CHANG, C.-P., FU, C., QI, Y., ROBOCK, A., ROBINSON, D. & ZHANG, H.-M. C. D. (2006) Steady decline of east Asian monsoon winds, 1969-2000: Evidence from direct ground measurements of wind speed. *Journal of Geophysical Research: Atmospheres*, 111, n/a-n/a.
- XU, P., ZHU, H., SHAO, X. & YIN, Z. (2012) Tree ring-dated fluctuation history of Midui glacier since the little ice age in the southeastern Tibetan plateau. *Science China Earth Sciences*, 55, 521-529.
- XU, T., BAODE, C., PING, L. & WEIHONG, Q. (2010b) Definition and features of the North edge of the East Asian summer monsoon. *Journal of Meteorological Research*, 24, 43-49.
- YAFEI, W., YASUSHI, F. & KURANOSHIN, K. (2003) A teleconnection pattern related with the development of the Okhotsk high and the northward progress of the subtropical high in East Asian summer. *Advances in Atmospheric Sciences*, 20, 237-244.
- YAMADA, K. (2004) Last 40 ka climate changes as deduced from the lacustrine sediments of Lake Biwa, central Japan *Quaternary International*, 123, 43-50.
- YAMADA, K. & FUKUSAWA, H. (1999) Paleointensity of the Asian winter monsoon and the westerlies since the last glacial period, reconstructed by eolian dust flux in lacustrine sediments of Lake Biwa and Lake Suigetsu, central Japan.
- YAMADA, K. & ISHIWATARI, R. (1999) Carbon isotopic compositions of long-chain n-alkanes in the Japan Sea sediments: implications for paleoenvironmental changes over the past 85 kyr. *Organic Geochemistry*, 30, 367-377.
- YAMADA, K., KAMITE, M., SAITO-KATO, M., OKUNO, M., SHINOZUKA, Y. & YASUDA, Y. (2010) Late Holocene monsoonal-climate change inferred from

- Lakes Ni-no-Megata and San-no-Megata, northeastern Japan. *Quaternary International*, 220, 122-132.
- YAMADA, K., MASUMA, T., SAKAI, S., SETO, K., OGUSA, H. & IRIZUKI, T. (2016) Centennial-scale East Asian summer monsoon intensity based on $\delta^{18}\text{O}$ values in ostracode shells and its relationship to land-ocean air temperature gradients over the past 1700 years. *Geology*, 44, 255-258.
- YAMAMOTO, S., KAWAMURA, K. & SEKI, O. (2011) Long-range atmospheric transport of terrestrial biomarkers by the Asian winter monsoon: Evidence from fresh snow from Sapporo, northern Japan. *Atmospheric Environment*, 45, 3553-3560.
- YAN, H., SUN, L., WANG, Y., HUANG, W., QIU, S. & YANG, C. (2011a) A record of the Southern Oscillation Index for the past 2,000 years from precipitation proxies. *Nature Geosci*, 4, 611-614.
- YAN, H., YANG, H., YUAN, Y. & LI, C. (2011b) Relationship between East Asian winter monsoon and summer monsoon. *Advances in Atmospheric Sciences*, 28, 1345-1356.
- YANCHEVA, G., NOWACZYK, N. R., MINGRAM, J., DULSKI, P., SCHETTLER, G., NEGENDANK, J. F. W., LIU, J., SIGMAN, D. M., PETERSON, L. C. & HAUG, G. H. (2007) Influence of the intertropical convergence zone on the East Asian monsoon. *Nature*, 445, 74-77.
- YANG, B., ACHIM, B., SHI, Y. & CHEN, F. (2004) Evidence for a late Holocene warm and humid climate period and environmental characteristics in the arid zones of northwest China during 2.2 ~ 1.8 kyr BP. *Journal of Geophysical Research: Atmospheres*, 109.
- YANG, B., BRÄUNING, A., ZHANG, Z., DONG, Z. & ESPER, J. (2007) Dust storm frequency and its relation to climate changes in Northern China during the past 1000 years. *Atmospheric Environment*, 41, 9288-9299.
- YANG, X., LIU, J., LIANG, F., YUAN, D., YANG, Y., LU, Y. & CHEN, F. (2014) Holocene stalagmite $\delta^{18}\text{O}$ records in the East Asian monsoon region and their correlation with those in the Indian monsoon region. *The Holocene*.
- YAO, T., JIAO, K., TIAN, L., LI, Z., LI, Y., LIU, J., HUANG, C., XIE, C. & THOMPSON, L. (1995) Climatic and environmental records in Guliya Ice Cap. *Science in China. Series B, Chemistry, life sciences & earth sciences*, 38, 228-237.
- YI, S. (2011) *Holocene vegetation responses to East Asian monsoonal changes in South Korea*, INTECH Open Access Publisher.
- YIN, J. H. (2005) A consistent poleward shift of the storm tracks in simulations of 21st century climate. *Geophysical Research Letters*, 32.
- YOSHINAGA, S. (1996) Variations in rates of accumulation of tropospheric fine quartz in tephra, loess, and associated paleosols since the Last Interglacial stage, Tokachi Plain, northern Japan, and paleoclimatic inferences. *Quaternary International*, 34, 139-146.
- YOSHINO, M. (1978) *Climate change and food production*, Tokyo, University of Tokyo.
- ZENG, Y., CHEN, J., XIAO, J. & QI, L. (2014) Non-residual Sr of the sediments in Daihai Lake as a good indicator of chemical weathering.
- ZHANG, P., CHENG, H., EDWARDS, R. L., CHEN, F., WANG, Y., YANG, X., LIU, J., TAN, M., WANG, X. & LIU, J. (2008) A test of climate, sun, and culture relationships from an 1810-year Chinese cave record. *Science*, 322, 940-942.
- ZHANG, R., SUMI, A. & KIMOTO, M. (1996) Impact of El Niño on the East Asian monsoon : A diagnostic study of the '86/87 and '91/92 events. *Journal of the Meteorological Society of Japan. Ser. II*, 74, 49-62.

- ZHANG, X., SHENG, J. & SHABBAR, A. (1998) Modes of Interannual and Interdecadal Variability of Pacific SST. *Journal of Climate*. American Meteorological Society.
- ZHANG, Y., SPERBER, K. R. & BOYLE, J. S. (1997) Climatology and Interannual Variation of the East Asian Winter Monsoon: Results from the 1979-95 NCEP/NCAR Reanalysis. *Monthly Weather Review*, 125, 2605-2619.
- ZHAO, C., LIU, Z., ROHLING, E. J., YU, Z., LIU, W., HE, Y., ZHAO, Y. & CHEN, F. (2013) Holocene temperature fluctuations in the northern Tibetan Plateau.
- ZHAO, P., ZHANG, X., ZHOU, X., IKEDA, M. & YIN, Y. (2004) The sea ice extent anomaly in the North Pacific and its impact on the East Asian summer monsoon rainfall. *Journal of Climate*, 17, 3434-3447.
- ZHOU, H., GUAN, H. & CHI, B. (2007) Record of winter monsoon strength. *Nature*, 450, E10-1; discussion E11.
- ZHOU, T., GONG, D., LI, J. & LI, B. (2009a) Detecting and understanding the multi-decadal variability of the East Asian Summer Monsoon-Recent progress and state of affairs. *Meteorologische Zeitschrift*, 18, 455-467.
- ZHOU, T., YU, R., ZHANG, J., DRANGE, H., CASSOU, C., DESER, C., HODSON, D. L., SANCHEZ-GOMEZ, E., LI, J. & KEENLYSIDE, N. (2009b) Why the western Pacific subtropical high has extended westward since the late 1970s. *Journal of Climate*, 22, 2199-2215.
- ZHOU, X., ZHAO, P. & LIU, G. (2009c) Asian-Pacific Oscillation index and variation of East Asian summer monsoon over the past millennium. *Chinese Science Bulletin*, 54, 3768-3771.
- ZHOU, X., ZHAO, P., LIU, G. & ZHOU, T. (2011) Characteristics of decadal-centennial-scale changes in East Asian summer monsoon circulation and precipitation during the Medieval Warm Period and Little Ice Age and in the present day. *Chinese Science Bulletin*, 56, 3003-3011.
- ZHU, C., WANG, B., QIAN, W. & ZHANG, B. C. L. (2012) Recent weakening of northern East Asian summer monsoon: A possible response to global warming. *Geophysical Research Letters*, 39, n/a-n/a.
- ZIMMERMAN, A. R. & CANUEL, E. A. (2000) A geochemical record of eutrophication and anoxia in Chesapeake Bay sediments: anthropogenic influence on organic matter composition. *Marine Chemistry*, 69, 117-137.
- ZINK, K.-G., LEYTHAEUSER, D., MELKONIAN, M. & SCHWARK, L. (2001) Temperature dependency of long-chain alkenone distributions in recent to fossil limnic sediments and in lake waters. *Geochimica et Cosmochimica Acta*, 65, 253-265.